

# **Analysis of reduced Neurocalcin delta (NCALD) as a protective modifier in mouse models of Spinal Muscular Atrophy (SMA)**



Inaugural-Dissertation  
zur  
Erlangung des Doktorgrades  
der Mathematisch-Naturwissenschaftlichen Fakultät  
der Universität zu Köln

vorgelegt von  
Anna Kaczmarek  
aus Sucha Beskidzka, Polen

Köln  
2016



The Doctoral Thesis “Analysis of reduced Neurocalcin delta (NCALD) as a protective modifier in mouse models of Spinal Muscular Atrophy (SMA)” was performed at the Institute of Human Genetics, Institute of Genetics and Centre for Molecular Medicine Cologne (CMMC) of the University of Cologne from December 2010 to October 2016.

Berichterstatter: Prof. Dr. rer. nat. Brunhilde Wirth  
Prof. Dr. rer. nat. Aleksandra Trifunovic

Tag der mündlichen Prüfung: 28.11.2016





*It is not the critic who counts; not the man who points out how the strong man stumbles, or where the doer of deeds could have done them better. The credit belongs to the man who is actually in the arena, whose face is marred by dust and sweat and blood; who strives valiantly; who errs, who comes short again and again, because there is no effort without error and shortcoming; but who does actually strive to do the deeds; who knows great enthusiasms, the great devotions; who spends himself in a worthy cause; who at the best knows in the end the triumph of high achievement, and who at the worst, if he fails, at least fails while daring greatly, so that his place shall never be with those cold and timid souls who neither know victory nor defeat.*

Theodore Roosevelt, "Citizenship In A Republic"

Sorbonne, Paris, France on 23<sup>rd</sup> April 1910

Mojej kochanej Rodzinie:

Mamulce, Tatulkowi,

Madziuni i Bartkowi

Z podziękowaniem za nieustanne ogromne wsparcie i wiarę



## Table of content

<b>List of figures .....</b>	<b>IV</b>
<b>List of tables .....</b>	<b>VI</b>
<b>Abbreviations .....</b>	<b>VII</b>
<b>Summary .....</b>	<b>IX</b>
<b>Zusammenfassung .....</b>	<b>XI</b>
<b>1 Introduction .....</b>	<b>1</b>
1.1 SMA: clinical pathology, subtypes and genetics .....	1
1.2 SMN protein .....	5
1.3 Animal models of SMA .....	6
1.4 SMA therapy .....	9
1.4.1 SMN replacement therapy .....	9
1.4.2 Compounds increasing SMN by enhancing protein stability or <i>SMN2</i> transcription .....	10
1.4.3 Correcting <i>SMN2</i> splicing using antisense oligonucleotides (ASOs) .....	11
1.4.4 SMN-independent therapeutics: neuroprotective agents .....	12
1.5 Modifier genes in SMA .....	14
1.5.1 Identification of SMA modifiers in model organisms and biochemical screens .....	14
1.5.2 Identification of SMA modifiers in asymptomatic <i>SMN1</i> -deleted relatives of SMA patients .....	15
1.5.3 Neurocalcin delta – a novel potential modifier for SMA in humans .....	16
<b>2 Preliminary results .....</b>	<b>18</b>
2.1 <i>NCALD</i> is downregulated in asymptomatic <i>SMN1</i> -deleted individuals .....	18
2.2 <i>NCALD</i> reduction rescues SMA phenotype <i>in vitro</i> and <i>in vivo</i> across species .....	19
<b>3 Aim of the study .....</b>	<b>21</b>
<b>4 Materials and methods .....</b>	<b>23</b>
4.1 Materials .....	23
4.1.1 Laboratory equipment .....	23
4.1.2 Mouse work equipment .....	24
4.1.3 Chemicals .....	24
4.1.4 Reagents .....	25
4.1.5 Kits .....	26
4.1.6 Enzymes .....	27

4.1.7	Antibodies .....	27
4.1.8	Secondary antibodies .....	27
4.1.9	Solutions and media .....	27
4.1.10	Primers and oligonucleotides.....	31
4.1.11	Plasmids.....	33
4.1.12	Software packages and internet databases .....	34
4.2	Methods.....	34
4.2.1	Working with nucleic acids .....	34
4.2.2	Working with bacteria .....	41
4.2.3	Working with proteins .....	42
4.2.4	Working with cells.....	44
4.2.5	Working with mice and mouse tissues.....	45
4.2.6	Microscopic image acquisition and analysis .....	56
4.2.7	Statistical analysis .....	57
<b>5</b>	<b>Results.....</b>	<b>58</b>
5.1	SMA mouse model with NCALD reduction – a transgene shRNA approach.....	58
5.1.1	Selection of the efficient shRNA sequences against <i>Ncald</i> .....	60
5.1.2	Stable integration of the shRNA cassette in ES cells.....	63
5.2	Severe SMA mouse model with NCALD reduction – a transgene knock-out approach .....	66
5.2.1	Analysis of NCALD expression in wildtype, <i>Ncald</i> <sup>ko/wt</sup> and <i>Ncald</i> <sup>ko/ko</sup> mice.....	66
5.2.2	Crossing the <i>Ncald</i> <sup>ko</sup> allele in the severe SMA mouse model.....	68
5.2.3	Phenotypic <i>in vivo</i> analysis of SMA- <i>Ncald</i> <sup>ko/wt</sup> mice: survival and weight.....	69
5.2.4	Phenotypic <i>in vivo</i> analysis of SMA- <i>Ncald</i> <sup>ko/wt</sup> mice: motoric skills .....	71
5.2.5	NCALD reduction in motor neurons from SMA mice restored axonal outgrowth <i>in vitro</i> .....	73
5.2.6	Neuromuscular junctions of SMA- <i>Ncald</i> <sup>ko/wt</sup> mice show larger AChR clusters .....	75
5.2.7	Number of glutamatergic inputs on spinal cord motor neurons is increased in SMA- <i>Ncald</i> <sup>ko/wt</sup> mice.....	77
5.2.8	Muscle fiber size is not changed in the EDL of SMA- <i>Ncald</i> <sup>ko/wt</sup> mice .....	80
5.2.9	SMA- <i>Ncald</i> <sup>ko/wt</sup> mice suffer from impairment of peripheral organs outside of CNS .....	81
5.3	Intermediate SMA mouse model with NCALD reduction – an SMN-ASO approach .....	83

5.3.1	SMN-ASO injection increased SMN levels in the liver and spinal cord in SMA+ASO mice .....	83
5.3.2	Phenotypic analysis of SMA- <i>Ncald</i> <sup>ko/wt</sup> +ASO mice: survival and weight .....	85
5.3.3	Phenotypic analysis of SMA- <i>Ncald</i> <sup>ko/wt</sup> +ASO mice: motoric tests .....	86
5.3.4	Neuromuscular junctions of SMA- <i>Ncald</i> <sup>ko/wt</sup> +ASO mice are more mature and have a larger area of AChR clusters .....	87
5.3.5	The number of glutamatergic inputs on MN soma and the MN cell size are increased in SMA- <i>Ncald</i> <sup>ko/wt</sup> +ASO mice .....	89
5.3.6	Muscle fiber size is increased in the EDL muscle of PND21 SMA- <i>Ncald</i> <sup>ko/wt</sup> +ASO mice .....	91
5.3.7	The impairment of the gastrointestinal tract is not rescued by reduced NCALD levels .....	93
5.4	SMA mouse model with NCALD reduction – an <i>Ncald</i> -ASO approach .....	94
<b>6</b>	<b>Discussion .....</b>	<b>100</b>
6.1	Different strategies to reduce NCALD <i>in vivo</i> in SMA mice .....	100
6.2	Effect of NCALD reduction on the motor neurons of SMA animals .....	102
6.3	Effect of NCALD reduction on the NMJs of SMA animals .....	104
6.4	Why did NCALD reduction have no effect on the lifespan of SMA mice? .....	106
6.5	Effect of NCALD reduction on HET animals .....	109
6.6	Clinical relevance of neuronal calcium sensors .....	110
6.7	Two independently identified SMA modifiers: NCALD and PLS3 act on endocytosis as a common pathway which is impaired in SMA .....	112
6.8	Future outlook .....	114
<b>7</b>	<b>References .....</b>	<b>116</b>
<b>8</b>	<b>Appendix .....</b>	<b>135</b>
<b>9</b>	<b>Publications, talks, poster presentations and scholarships .....</b>	<b>176</b>
	<b>Acknowledgements .....</b>	<b>IX</b>
	<b>Erklärung .....</b>	<b>X</b>
	<b>Lebenslauf .....</b>	<b>XI</b>

## List of figures

Fig. 1: The schematic overview of SMA pathology.....	2
Fig. 2: The genetic landscape of SMA. ....	4
Fig. 3: The mechanism of action of SMN-ASO. ....	12
Fig. 4: SMA therapy strategies with their specific target site in an exemplary motor neuron.....	13
Fig. 5: Pedigree of the family with NCALD reduction in asymptomatic individuals. ....	18
Fig. 6: NCALD reduction ameliorated neuronal outgrowth defects mediated by SMN deficiency. ....	20
Fig. 7: Annealing of shRNA oligonucleotides .....	37
Fig. 8: The necessary steps of a mouse generation strategy using an inducible shRNA targeting vector. ....	46
Fig. 9: The breeding scheme to obtain SMA and HET animals with reduced NCALD levels.....	51
Fig. 10: The tube test positions corresponding to the respective values of the hind limb score.....	53
Fig. 11: The shRNA mouse generation strategy .....	59
Fig. 12: Induction of shRNA expression upon Doxycycline induction.....	60
Fig. 13: The longest transcript (3733 bp) of mouse <i>Ncald</i> (NM_134094).....	61
Fig. 14: Analysis of <i>Ncald</i> knock-down on protein and mRNA in NSC34 cells transfected with shRNAs.....	61
Fig. 15: Identification of efficient shRNA sequences in an <i>Ncald</i> -GFP overexpression set-up.....	62
Fig. 16: Efficient knock-down of GFP-NCALD upon Dox-mediated shRNA expression .....	63
Fig. 17: Validation of the successful recombination in individual ES clones.....	64
Fig. 18: Quantification of <i>Ncald</i> in ES clones upon Doxycycline induction.....	65
Fig. 19: Analysis of NCALD expression in wildtype mouse tissue on PND10 .....	67
Fig. 20: Analysis of NCALD expression in mutant mouse tissue on PND10 .....	68
Fig. 21: Survival and weight studies of SMA- <i>Ncald</i> <sup>ko/wt</sup> mice.....	71
Fig. 22: Evaluation of motoric skills of SMA- <i>Ncald</i> <sup>ko/wt</sup> mice.....	72
Fig. 23: Motor neurons from SMA- <i>Ncald</i> <sup>ko/wt</sup> mice show longer axons and increased branching than SMA mice .....	74
Fig. 24: Analysis of NMJ size in the TVA muscle of PND10 mice .....	76
Fig. 25: Analysis of NMJ size in the TVA muscle of PND5 and PND13 mice .....	77

<b>Fig. 26: Evaluation of glutamatergic inputs on spinal motor neuron soma in SMA-<i>Ncald</i><sup>ko/wt</sup> mice .....</b>	<b>79</b>
<b>Fig. 27: Analysis of the muscle fiber size in the EDL of PND10 mice .....</b>	<b>81</b>
<b>Fig. 28: The intestinal impairment in the severe SMA mouse model.....</b>	<b>82</b>
<b>Fig. 29: SMN-ASO mode of action.....</b>	<b>83</b>
<b>Fig. 30: SMN-ASO injection increased SMN levels in liver and spinal cord.....</b>	<b>84</b>
<b>Fig. 31: Survival and weight studies of SMA+ASO and SMA-<i>Ncald</i><sup>ko/wt</sup>+ASO mice</b>	<b>85</b>
<b>Fig. 32: Evaluation of motoric skills of SMA-<i>Ncald</i><sup>ko/wt</sup>+ASO mice .....</b>	<b>87</b>
<b>Fig. 33: NMJ size and maturation are improved in SMA-<i>Ncald</i><sup>ko/wt</sup>+ASO animals ..</b>	<b>89</b>
<b>Fig. 34: Number of VGlut1+ inputs and motor neuron size are increased in SMA-<i>Ncald</i><sup>ko/wt</sup>+ASO animals.....</b>	<b>91</b>
<b>Fig. 35: Analysis of muscle fiber size in the EDL muscle of PND21 mice .....</b>	<b>92</b>
<b>Fig. 36: Intestine impairment is still visible in SMA+ASO mice. ....</b>	<b>93</b>
<b>Fig. 37: A screen of different ASO sequences against <i>Ncald</i> performed by Ionis Pharmaceuticals.....</b>	<b>95</b>
<b>Fig. 38: NCALD knock-down by i.c.v. <i>Ncald</i>-ASO injection in wildtype and SMA mice .....</b>	<b>96</b>
<b>Fig. 39: Efficient NCALD knock-down by combined i.c.v. and s.c. injection of ASO2 against <i>Ncald</i> in SMA mice.....</b>	<b>97</b>
<b>Fig. 40: Increased mortality following the injection of <i>Ncald</i>-ASOs .....</b>	<b>99</b>
<b>Fig. 41: A model of restored neuromuscular homeostasis under concomitant depletion of SMN and NCALD .....</b>	<b>110</b>
<b>Fig. 42: A map of known interaction partners of NCS proteins .....</b>	<b>113</b>
<b>Fig. 43: Proposed mode of NCALD acting on the endocytosis at the synaptic membrane .....</b>	<b>114</b>

## List of tables

Table 1: Primers for cloning Ncald / qRT-PCR / genotyping .....	32
Table 2: Oligonucleotides for cloning shRNA into the pEx-H1-tetO-CAG-teR vector .....	32
Table 3: Antisense oligonucleotides for <i>in vivo</i> injection .....	33
Table 4: List of used and produced plasmids .....	33
Table 5: A standard 20 µl PCR composition .....	36
Table 6: A standard thermocycler PCR program .....	36
Table 7: The composition and conditions of an oligonucleotide annealing reaction .....	38
Table 8: The composition of a standard digestion using restriction enzyme .....	38
Table 9: The composition of a typical ligation reaction (10 µl) .....	39
Table 10: The composition of a typical reverse transcription reaction (10µl) .....	40
Table 11: The composition of a typical qRT-PCR (10µl) .....	41
Table 12: Primary and secondary antibodies used for protein detection .....	44
Table 13: The summary of the characteristics of SMA-Ncald <sup>ko/wt</sup> and HET-Ncald <sup>ko/wt</sup> analyzed in the severe and intermediate SMA mouse model. ....	94



**Abbreviations**

A	adenine
AChR	acetylcholine receptor
ALS	amyloid lateral sclerosis
APS	ammonium persulfate
ASO	antisense oligonucleotide
BBB	blood-brain barrier
bp	base pairs
BSA	bovine serum albumin
BTX	bungarotoxin
C	cytosine
CNS	central nervous system
cDNA	coding DNA
DMEM	Dulbecco's modified Eagle medium
DMSO	dimethyl sulfoxide
DNA	deoxyribonucleic acid
Dox	Doxycycline
E	embryonic day
EDL	<i>Extensor digitorum longus</i>
EDTA	ethylene diamine tetraacetic acid
e.g.	exempli gratia
EGTA	ethylene glycol tetraacetic acid
ESC	embryonic stem cells
et al.	et alii
FCS	fetal calf serum
FDA	Food & Drug Administration
FL	full length
fwd	forward
g	gravitational force
G	guanine
GFP	green fluorescent protein
h	hours
HDAC	histone deacetylase
i.c.v.	intracerebroventricular
kb	kilobases
kDa	kilodalton
ko	knock-out
L	liter
m	mili
μ	micro
M	molar
min	minutes
MN	motor neuron
MOE	methoxyethoxy
mRNA	messenger RNA
n	number
NCS	neuronal calcium sensor

NF	neurofilament
NMJ	neuromuscular junction
NT	neurotransmitter
n.s.	not significant
OMIM	Online Mendelian Inheritance in Man
o.n.	overnight
<i>P</i>	probability
PAA	polyacrylamide
PBS	phosphate buffered saline
PCR	polymerase chain reaction
PD	Parkinson's disease
PFA	paraformaldehyde
pH	power of hydrogen
pmol	picomol
PND	postnatal day
PS	phosphorothioate
RNA	ribonucleic acid
rev	reverse
s.c.	subcutaneous
scAAV	self-complementary adeno-associated virus
SD	standard deviation
SDS	sodium dodecyl sulfate
sec	seconds
SEM	standard error of means
shRNA	short hairpin RNA
siRNA	small interfering RNA
SMA	spinal muscular atrophy
snRNP	small nuclear ribonucleoprotein
T	tyrosine
TVA	Transversus abdominis
TEMED	N,N,N',N'-tetramethylethylenediamine
UTR	untranslated region
wt	wildtype

## Summary

Spinal muscular atrophy (SMA) is a common and devastating genetic disease characterized by degeneration of spinal alpha motor neurons and muscle atrophy. SMA is caused by homozygous deletions or rarely other mutations of the *SMN1* gene, resulting in a functional loss of the Survival of Motor Neuron (SMN) protein. SMA severity is determined by a nearly identical copy gene, *SMN2*, which encodes an identical SMN protein but produces only ~10% correctly spliced transcripts. Rarely, individuals with *SMN1* deletion are fully asymptomatic, suggesting a protection by other modifying genes. Identification of these modifiers would allow us to better understand the cellular pathways affected by SMN deficiency and to develop new therapies.

Here, we report a novel modifier of SMA, *Neurocalcin delta* (*NCALD*), that showed a reduced expression in *SMN1*-deleted asymptomatic individuals as compared to other affected family members or unrelated SMA patients. NCALD is a neuronal calcium sensor mainly expressed in CNS. Further preliminary studies *in vitro* and in non-mammalian SMA animal models (*C. elegans*, zebrafish) have shown that NCALD knock-down ameliorates SMA-related symptoms. Therefore, we proceeded to study the protective effect of NCALD suppression in SMA mouse models. First, we followed a strategy of generating an inducible *Ncald* knock-down mouse. We identified efficient shRNA sequences that suppressed NCALD expression and cloned them into the targeting vector, which was integrated into mouse embryonic stem cells by electroporation. This approach was discontinued when an *Ncald*<sup>ko/ko</sup> mouse line became available at the Jackson Laboratory. Next, we crossed the *Ncald*<sup>ko</sup> allele heterozygously with a severely affected SMA mouse model and performed extensive phenotypic analysis. Reduced NCALD expression improved many characteristics related to SMN deficiency, such as axonal length of cultured motor neurons, size of acetylcholine receptor (AChR) clusters at the neuromuscular junction and spinal motor neuron circuitry as assessed by the number of glutamatergic inputs on motor neuron soma. However, due to very low SMN levels, other internal organs were impaired, which resulted in early death of the SMA mice irrespective of their NCALD levels. Therefore, we hypothesized that increasing peripheral SMN levels is needed for the modifier to fully exert its function. Indeed, in SMA-*Ncald*<sup>ko/wt</sup> mice injected with a suboptimal dose of SMN-ASO (antisense oligonucleotides), all characteristics listed above were reproducibly improved; additionally, also the muscle fiber size was increased. Unexpectedly, also in this intermediate model the survival of the SMA-*Ncald*<sup>ko/wt</sup>+ASO mice was not rescued, presumably because NCALD is mainly expressed in neurons and unable to counteract SMN deficiency in other inner organs. Currently, we are performing further studies of NCALD suppression in an even milder SMA model, which shows only a motoric impairment but without a shortened lifespan; this model resembles better the phenotype

of asymptomatic individuals, who all carry four *SMN2* copies and would hypothetically develop a milder SMA type without compromised survival. Indeed, first results show that mild SMA mice have an improved motoric behavior upon reduced NCALD levels.

Finally, we anticipated that NCALD suppression would be eligible for a combinatorial therapy using a mix of ASOs to increase SMN and simultaneously downregulate NCALD. In collaboration with Ionis Pharmaceuticals (USA), a walk along the *Ncald* gene was performed to identify the most efficient *Ncald*-ASOs. In our laboratory two ASOs were subsequently tested by intracerebroventricular injections in neonatal mice. While we achieved a satisfying NCALD knock-down, we encountered some toxicity issues; therefore, the therapeutic potential of NCALD suppression requires further examination considering its biosafety and clinical efficiency.

## Zusammenfassung

Spinale Muskelatrophie (SMA) ist eine häufige verheerende genetische Erkrankung, die durch die Degenerierung von Alpha-Motoneuronen im Rückenmark sowie die Atrophie von Muskeln gekennzeichnet ist. Die Ursache von SMA sind homozygote Deletionen oder in seltenen Fällen andere Mutationen vom *SMN1*-Gen, die zu einem Funktionsverlust des Survival of Motor Neuron (SMN) Proteins führen. Das Schweregrad der Erkrankung wird durch ein beinahe identisches Kopiegen bestimmt, *SMN2*, jedoch werden nur etwa 10% der *SMN2* Transkripte korrekt gespleißt, die dann ein mit SMN identisches Protein kodieren. Selten zeigen Menschen mit einer *SMN1*-Deletion keine SMA Symptome, was einen Schutzmechanismus durch andere modifizierenden Gene vermuten lässt. Die Identifizierung solcher Modifizergene würde ein besseres Verständnis der zellulären Prozesse ermöglichen, die durch den SMN-Mangel beeinträchtigt sind, sowie die Entwicklung neuer Therapieansätze fördern.

Wir berichten hier von einem neuen SMA-Modifizergen, *Neurocalcin delta* (*NCALD*), das eine reduzierte Expression in *SMN1*-deletierten asymptomatischen Probanden im Vergleich zu den SMA-kranken Familienmitgliedern sowie nicht verwandten SMA Patienten zeigte. Weitere vorläufige Studien in zellulären Systemen und einfacheren Tiermodellen (*C. elegans*, Zebrafisch) haben gezeigt, dass die Reduktion von *NCALD* die Symptome von SMA mildert. Daher haben wir weitere Studien zum protektiven Effekt der *NCALD*-Reduktion in SMA Mausmodellen unternommen. Als Erstes verfolgten wir eine Strategie zur Generierung einer induzierbaren *Ncald*-Knockdown-Mauslinie. Dafür haben wir effiziente shRNA-Sequenzen gegen *Ncald* identifiziert und in einen Zielvektor kloniert, der in embryonale Mausstammzellen mittels Elektroporation integriert wurde. Da jedoch eine *Ncald*<sup>ko/ko</sup> Mauslinie bei dem Jackson Laboratory verfügbar wurde, haben wir diese Strategie eingestellt. Als Nächstes haben wir dann das *Ncald*<sup>ko</sup>-Allel heterozygot mit dem etablierten schwer betroffenen SMA Mausmodell gekreuzt und eine umfangreiche Phänotypanalyse durchgeführt. Die Herunterregulierung von *NCALD* hat mehrere Merkmale des SMN-Mangels verbessert, z. B. die Axonlänge von kultivierten Motoneuronen, die Größe der Acetylcholinrezeptoren (AChR) Cluster an der neuromuskulären Endplatte sowie die spinalen Motoneuronennetzwerke, evaluiert durch die Zahl der glutamatergischen Inputs auf die Zellkörper der Motoneurone. Die geringe SMN-Menge führte jedoch zu Defekten in verschiedenen inneren Organen der SMA-Mäuse, wodurch unabhängig von der *NCALD*-Expression das frühe Sterben der Mäuse verursacht wurde. Wir vermuteten daher, dass die Erhöhung der allgemeinen SMN-Menge nötig wäre, um die vollständige Wirkung des Modifiers zu erlauben. Tatsächlich wurden alle oben aufgeführten Eigenschaften beständig verbessert, wenn die SMA-*Ncald*<sup>ko/wt</sup>

Mäuse mit einer suboptimalen Dosis vom SMN-ASO (Antisense Oligonukleotid) injiziert wurden; zusätzlich ist auch die Größe der Muskelfaser gewachsen. Überraschend hat die Verminderung von NCALD auch in dem intermediären SMA-Mausmodell keine Verlängerung der Lebenserwartung der SMA-*Ncald*<sup>ko/wt</sup>+ASO Mäuse erzielt. Wir vermuten, dass die durch den SMN-Mangel bedingten Defekte in anderen inneren Organen durch das überwiegend in Neuronen exprimierte NCALD Protein korrigiert werden. Es werden zur Zeit Studien von NCALD-Reduktion in einem noch milderen SMA-Modell durchgeführt, das ausschließlich motorische Defekte, aber keine Beeinträchtigung der Lebenserwartung zeigt. Möglicherweise spiegelt dieses Modell besser den Phänotyp der asymptomatischen Probanden wieder, die alle das *SMN2*-Gen in vier Kopien tragen. Hypothetisch würde solch ein genetisches Profil im Menschen zu einem milden SMA Typ ohne Einschränkung der Lebenserwartung führen. Die ersten Ergebnisse zeigen, dass die NCALD-Reduktion das motorische Verhalten der mild betroffenen SMA-Tiere verbessert. Letztlich vermuteten wir, dass die Herunterregulierung von NCALD für eine kombinatorische Therapie geeignet wäre, in der eine Kombination von ASOs einerseits die Menge von SMN erhöhen und andererseits die von NCALD vermindern würde. In einer Kollaboration mit Ionis Pharmaceuticals (USA) wurde ein Screen von dem *Ncald*-Gen durchgeführt, um die effizientesten *Ncald*-ASO Sequenzen zu identifizieren. In unserem Labor wurde dann zwei *Ncald*-ASOs mittels einer intrazerebroventrikulären Injektion in neugeborene Mäuse getestet. Während das Ausmaß der Herunterregulierung von NCALD zufriedenstellend war, erwies sich die Verträglichkeit der ASOs als problematisch. Daher werden weitere Tests benötigt, um das Therapiepotenzial der Herunterregulierung von NCALD unter dem Aspekt der Sicherheit und Effizienz zu untersuchen.

## 1 Introduction

### 1.1 SMA: clinical pathology, subtypes and genetics

The proximal spinal muscular atrophy (SMA) is after cystic fibrosis the second most frequent autosomal recessive disease with the carrier frequency of about 1 in 35-40 and estimated incidence of 1 in 6,000-10,000 (Wirth et al. 2013). First cases of SMA were described in 1890s by an Austrian physician, Guido Werdnig, and a German physician, Johann Hoffmann (Werdnig 1891, Hoffmann 1893). The disease pathology is characterized by progressive neurodegeneration, where the large alpha motor neurons are lost from the ventral horns of the spinal cord. The remaining motor neurons can show swollen appearance as effect of chromatolysis and contain phosphorylated neurofilament, ribosomes or vesicles (Harding et al. 2015).

Neurogenic atrophy of skeletal muscle is another hallmark of the disease that affects proximal muscles more than the distal ones, the lower limbs more than the upper ones and intercostal and axial muscle groups more than the diaphragm (Dubowitz 2009). Muscles of severely affected SMA patients have small, atrophic fibers interspersed with large, hypertrophic ones; some atrophic fibers are immature with central nuclei. Muscles fiber of more mildly affected SMA patients show evidence of repeated de- and re-innervation (Monani and De Vivo 2014).

Muscle wasting was long assumed to be the consequence of motor neuron death, however, many findings originated from autopsies from severe SMA patients and reflected more the endpoint stage of the disease, making it difficult to differentiate between the primary cause and secondary defects. Much insight in the early pathophysiology of SMA was granted by the studies of SMA animal models, particularly in mice (see 1.3). The observation that muscle wasting precedes the loss of motor neuron bodies in the spinal cord led to the discovery of distal defects at the neuromuscular junctions (NMJ) as one of the earliest effects of low SMN (Kariya et al. 2008). These encompass both morphological abnormalities: frequently reported accumulation of phosphorylated neurofilament (Cifuentes-Diaz et al. 2002, Murray et al. 2008), delayed maturation (Kariya et al. 2014), signs of denervation (Ling et al. 2012), as well as functional changes: impaired neurotransmitter release (Kong et al. 2009) and altered calcium homeostasis (Ruiz et al. 2010). This distal phenotype was later confirmed in human samples and established SMA as an axonopathy, where defects begin at the synapse and presumably by a dying-back mechanism eventually lead to cell death in the spinal cord (Harding et al. 2015). Mouse

studies unraveled also defects of the glutamatergic synapses that harbour on the motor neurons in the spinal cord, hinting to an impairment of the entire motor neuron circuitry (Ling et al. 2010, Mentis et al. 2011). These defects are depicted in Fig. 1.

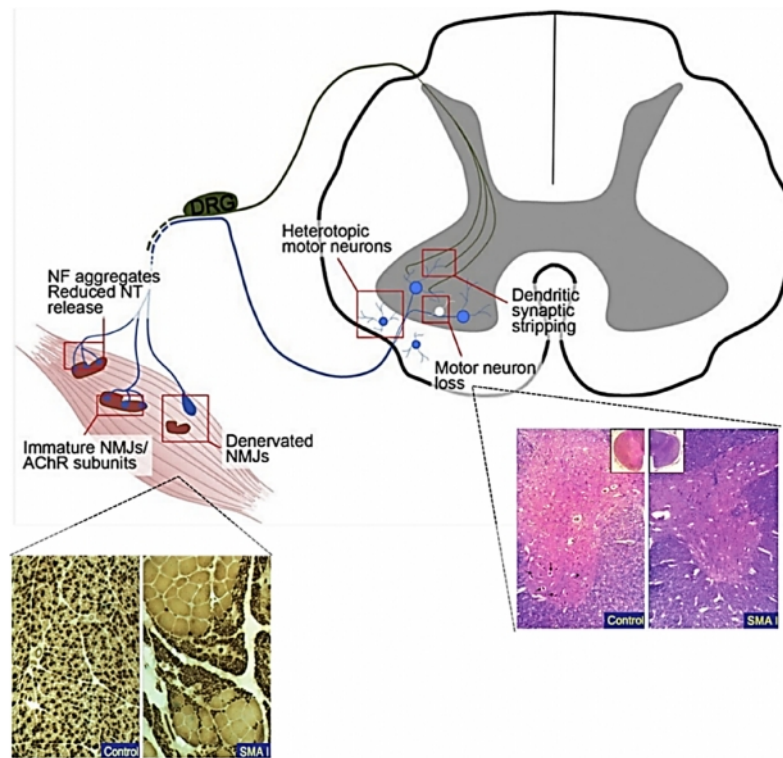


**Fig. 1: The schematic overview of SMA pathology.**

In the spinal cord, the SMA hallmarks are loss of spinal motor neurons in the anterior ventral horns, occasional motor neuron mispositioning (heterotropy) into ventral white matter and reduced number of inputs from proprioceptive neurons. The abnormalities at the neuromuscular junction involve neurofilament aggregation, impaired neurotransmitter release and maturation delay. The skeletal muscle of SMA individuals is affected by muscle fiber atrophy (adapted from (Fallini et al. 2012, Monani and De Vivo 2014).

The clinical presentation of SMA can be highly variable: historically patients were classified into four classes (types) according to the age of onset and motoric milestones achieved (Lunn and Wang 2008). These types will be briefly described herein; however, SMA is nowadays increasingly acknowledged as a clinical continuum, ranging from a very severe form with onset in utero (Dubowitz 1999) to the very mild form with middle and late onset.

The most severe form affecting ~60% of SMA patients is type 1 (MIM #253300), known also as Werdnig-Hoffman disease after the doctors who first described it. It is also the most common genetic cause of infant death (Melki et al. 1994). The patients can be described as non-sitters, as the majority does not acquire the ability to sit unaided. The first symptoms usually observed in the first 6 months of life are poor head control, low muscle tone (hypotonia) resulting in a clinical picture of a “floppy infant”, “frog-leg” position and



bell-shaped chest due to the weak intercostal muscles and areflexia. The muscle weakness is generalized and affects the limb muscles, as well as muscles important for swallowing and respiration. Unfortunately, the progressive nature of the disease results in most SMA type 1 patients in a complete loss of movement (paralysis). Previously, the expected survival did not exceed 2 years, with most patients succumbing to respiratory dysfunction. However, nowadays the standards of care of SMA type 1 patients have prolonged the expected survival due to ventilation and nutritional assistance (Oskoui et al. 2007). Still, the clinical trials set the time of a complete dependency on assisted ventilation as an endpoint equal with the actual death of a patient (Finkel et al. 2014).

In the intermediate type 2 (MIM #253550), affecting ~27% of SMA patients, first symptoms manifest between 6 and 18 months of age. These patients learn to sit unaided but not to stand or walk (sitters), and frequently suffer from scoliosis as a result of weak trunk muscles. They usually reach adulthood but the life expectancy is still reduced (Dubowitz 1964).

Type 3 (MIM #253300), present in ~12% of SMA patients, is a milder form diagnosed >18 months of age. Patients learn to walk independently, though this ability is lost as the disease progresses and they become wheelchair-bound; however, the life expectancy is unaffected (Kugelberg and Welander 1956).

Very rarely (in ~1% of patients), SMA shows adult onset in the fourth to sixth decade, following a normal active early life (Zerres et al. 1995). These individuals are classified as type 4 (MIM #271150); as all types described above, they suffer from progressive muscle weakness and can be in need of a wheelchair, but with normal life expectancy.

The high variability of SMA is a direct result of the genetic background of this disorder. The disease causing gene was mapped to the longer arm of chromosome 5 (Brzustowicz et al. 1990, Gilliam et al. 1990, Melki et al. 1990), and in 1995 the *SMN* (survival of motor neuron) gene was identified as absent or mutated in >98% SMA patients from the study cohort (Lefebvre et al. 1995). Further studies of this genomic region unraveled the presence of a copy number variant (CNV), which is constituted of two ~500kb repeat units arranged in an inverted manner; the number of the repeat units may vary from 0-4 on each chromosome and the entire region is prone to rearrangement and gene conversion. The telomeric repeat unit contains the evolutionary older *SMN1* gene and the centromeric one – its duplication, *SMN2* gene. These genes both encode the same protein, SMN (survival of motor neuron), and are almost identical except for five silent nucleotides located in the 3' end of the genes: one in exon 7 (c.840C>T), one in exon 8 (nt 27869 G>A), one in intron 6 (nt 27092 G>A) and two in intron 7 (nt 27289 A>G and 27404 A>G) (Burglen et al. 1996).

Out of those, the critical change is the c.840C>T transition at position 6 in exon 7 which disrupts an exonic splicing enhancer (ESE) and abolishes the binding of SF2/ASF (Lorson et al. 1999); instead, it creates a novel binding site for hnRNPA1 and thus an exonic splicing silencer (ESS) (Kashima and Manley 2003). As a result, most of the *SMN2* transcripts are alternatively spliced so that they lack exon 7 (Lorson et al. 1999). This *SMN2* mRNA is translated to a truncated SMN protein which does not oligomerize properly and is rapidly degraded (Lorson and Androphy 2000). Only a small proportion of *SMN2* mRNA escapes this defective splicing and gives rise to a functional full-length SMN protein. The scheme of *SMN1* and *SMN2* splicing and translation is depicted in Fig. 2.

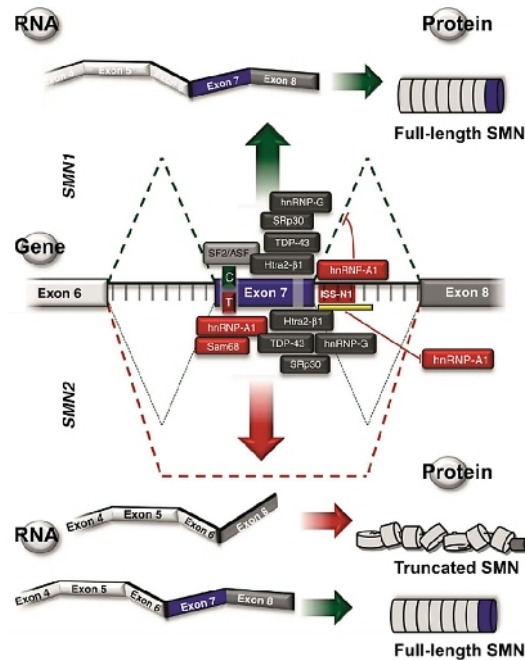


**Fig. 2: The genetic landscape of SMA.**

In SMA patients, *SMN1* gene is absent or mutated, however, all of them retain one or more copies of the *SMN2* gene. *SMN2* differs from *SMN1* by a C>T transition (in exon 7) that leads to a frequent exon 7 skipping during splicing of *SMN2* pre-mRNA. As a result, most transcripts lack exon 7 and encode a truncated, unstable protein that is rapidly degraded. Only small proportion of *SMN2* transcript carries exon 7 and encode the full-length SMN protein. Both genes are subject of complex regulation by many *cis* and *trans* factors: Two exonic splicing enhancers within exon 7 are shaded in light grey. Factors promoting exon 7 inclusion are dark grey boxes, while factors favouring exon 7 skipping are red boxes. The intronic splicing silencer ISS-N1, which is bound by hnRNP-A1, is shaded red in intron 7, and the antisense oligo preventing hnRNP-A1 binding is highlighted in yellow. (adapted from (Wirth et al. 2013)).

For healthy individuals, who carry at least one *SMN1* copy, the majority of their SMN protein comes from *SMN1* and the amount produced from *SMN2* is negligible; indeed, 10-15% of the general population carry no *SMN2* gene at all. Classic SMA patients, however, who lack functional *SMN1*, are solely dependent on the SMN protein produced from *SMN2* gene. Predictably, the *SMN2* copy number is inversely correlated with SMA severity as

are the levels of SMN protein (Feldkotter et al. 2002). Still, this correlation is not sufficient to predict the clinical severity exclusively from the number of *SMN2* copies, especially for the intermediate types, e.g. three *SMN2* copies have been reported for all three types (Feldkotter et al. 2002). The cause for this variability is first, presence of *SMN2* gene variants that produce more full-length SMN protein (Prior et al. 2009, Vezain et al. 2010), and second, action of SMN-independent modifiers, as haploidentical siblings of SMA patients (with the same *SMN2* copy number) can show a phenotype of a different severity, reaching even full rescue (Cobben et al. 1995, Hahnen et al. 1995, Oprea et al. 2008).

## 1.2 SMN protein

*SMN1* and *SMN2* genes both encode an identical survival of motor neuron (SMN) protein which has the length of 294 aminoacids and the molecular weight of 38 kDa. SMN is ubiquitously expressed and localizes both to the nucleus, where it is frequently found in structures called Gems, and to the cytoplasm, commonly as part of a large multiprotein complex together with Gemin2-8 und Unrip2 (Pellizzoni 2007). The housekeeping function of the SMN complex is the assembly of Sm proteins onto small nuclear ribonucleoproteins (snRNPs), crucial factors in pre-mRNA splicing (Pellizzoni et al. 1998). Impairment of snRNP assembly has been shown in SMA mice in correlation to the severity of the phenotype; furthermore, it was suggested that transcripts necessary for motor neurons activity are preferentially affected by deficient snRNP assembly (Gabanella et al. 2007). Numerous attempts have been undertaken to identify these transcripts in order to explain why motor neurons seem particularly susceptible to low SMN level and thus to prove the so called “snRNP theory” of SMA, which deems motor neurons as more sensitive to a global splicing defect: yet, although many splicing changes were detected, it could not be excluded that these are secondary effects from cellular stress (Zhang et al. 2008). Alternatively, low SMN could affect the splicing of one or a subset of important motor neuron-specific genes and thus specifically compromise this cell type: recently, Stasimon was identified as one such potential neuronal transcript which shows specific splicing defect when SMN is low and *in vivo* experiments in *Drosophila* and zebrafish underlined the critical role of Stasimon for motor circuit function (Lotti et al. 2012). Recent technological advances in cell-specific transcriptome analyses combining laser microdissection with deep RNA sequencing (RNA-seq) revealed dysregulation of many neuronal genes, such as complete exon skipping in agrin, which is critical for NMJ maintenance, upregulation of C1, a complement factor promoting synapse pruning, and downregulation of Etv1/ER81, a transcription factor required for establishing sensory-motor, in motor neurons from PND1 SMA mice. These early defects of motor neuron

specific synaptogenesis genes connect the SMN depletion to the hallmark SMA pathology (Zhang et al. 2013). Another comprehensive RNA-seq study covering multiple tissues in an SMA mouse model could identify splicing changes in several  $\text{Ca}^{2+}$  channel genes, which might explain disrupted  $\text{Ca}^{2+}$  homeostasis observed in SMA (Doktor et al. 2016). Also many genes associated with mitochondrial bioenergetics were reported to be dysregulated in SMN deficient motor neurons, which corresponded to increased oxidative stress, impaired mitochondrial mobility and enhanced fragmentation of mitochondrial network in these neurons under SMA disease conditions; intriguingly, these deficiencies occur presymptomatically and may therefore have a role in SMA initiation (Miller et al. 2016).

Other studies found that cytoplasmic SMN localises to axons and growth cones of motor neurons with some components of the nuclear SMN complex, but in the absence of Sm proteins, therefore a non-canonical, motor neuron-specific function of SMN was hypothesized, the “axonal theory”. Evidence for a role of SMN in axons has come from studies in cultured spinal motor neurons from SMA mice and in zebrafish which both showed axonal truncation; moreover, reduced amount of  $\beta$ -actin mRNA and altered distribution of calcium channels were observed in the growth cones of SMA motor neurons (McWhorter et al. 2003, Rossoll et al. 2003, Jablonka et al. 2007). Further studies found reduced axonal localization of other neuronal transcripts in SMA motor neurons (*cpg15*, *GAP43*) and some suggested a general defect of protein synthesis within neuronal growth cones (Akten et al. 2011, Fallini et al. 2016). In the proposed model SMN is necessary for the assembly of ribonucleoproteins (mRNP) responsible for the transport and local translation of axonal mRNAs which are important for axon outgrowth and growth cone dynamics. SMN deficiency would thus contribute to axon degeneration and in a dying-back mode also to muscle denervation and motor neuron cell death (Fallini et al. 2012).

### 1.3 Animal models of SMA

Studies of animal models contributed greatly to the knowledge of SMA pathomechanism, although obviously not all characteristics are common between species, even mammals.

When first attempts were undertaken to model SMA as constitutive deficiency of the SMN protein, soon the human specificity of the disease was revealed: most other species (except for primates) carry only one *Smn* gene indispensable for survival as homozygous whole body knock-out turned out to be embryonic lethal in fly, nematode, zebrafish or mouse (Schrack et al. 1997, Schmid and DiDonato 2007). These models were made available for SMA research by careful reduction of SMN protein, e.g. using RNA

interference or conditional genetic ablation; however, most relevant SMA models for human studies, particularly for testing of potential therapeutics, are transgenic mouse lines. A large number of SMA mouse models have been generated in order to accommodate the variability observed in patients; the most widely used ones will be briefly described herein. Still, interpretation of animal disease models needs to be performed with great care and caution, as the severe SMA phenotype in mice is increasingly acknowledged as a multi-systemic disorder, with involvement of multiple organs, e.g. brain, heart, liver, pancreas (Hamilton and Gillingwater 2013). At the same time, these defects have been only sporadically observed in the most severe SMA patients; it is possible, however, that the full scope of the disease, particularly in the severe type 1 patients, is only beginning to be understood (Shababi et al. 2014).

The mouse genome harbours only a single *Smn* gene and its complete deletion results in early embryonic lethality (E8.5), underlining the housekeeping function of SMN protein (Schränk 2003). Heterozygous *Smn*<sup>ko/wt</sup> animals do not show gross abnormalities (unchanged life expectancy), however some studies used these mice as a mild SMA model of SMA as some neuromuscular changes occur in older animals (Jablonka et al. 2000). To mimic the SMN deficiency in mice, in most models variable numbers of human *SMN2* gene were integrated: two *SMN2* copies rescued the embryonic lethality of *Smn*<sup>ko/ko</sup> and generated a mouse model phenotypically resembling human severe SMA type 1 (*Smn*<sup>ko/ko</sup>; *hSMN2*<sup>tg/tg</sup>) with a reduced survival of 5 days, while eight *SMN2* copies fully rescued the phenotype (Monani et al. 2000). When an additional transgene, *SMN* 7, which lacks exon 7 and therefore encodes exclusively the misspliced transcript, was included, the survival was prolonged to 13-15 days, enabling more detailed phenotypic analysis as well as screening of therapeutics (Le et al. 2005).

Another severe mouse model of SMA (Hsieh-Li et al. 2000) is the so called “Taiwanese” or Hung mice, as it was generated by the research group of professor Hung Li in Taiwan. This model combines the knock-out of the endogenous murine *Smn* gene with a 115 kb transgene that carries the entire coding region and the flanking sequence of the two tandem copies of the human *SMN2* gene. Importantly, the *SMN2* containing transgene is present in tandem as two copies on one allele. Depending on how many copies of the transgene are present in *Smn*<sup>ko/ko</sup> animals, mouse lines of different severity could be obtained, somehow mimicking the SMA spectrum in humans: the most severe line does not develop hairy fur and dies before PND10, the intermediate shows variable phenotype and survives between 2 to 4 weeks and the mildest line reaches adulthood and is fertile, however it has shortened and later in life also necrotic tail. Of note, this SMA mouse model

was initially studied on a mixed genetic background and therefore the offspring showed a large variability in survival.

Our group has established a breeding scheme crossing the mildest line of the Hung mice *Smn*<sup>ko/ko</sup>; *hSMN2*<sup>tg/tg</sup> (importantly, each *hSMN2*<sup>tg</sup> allele carries two tandem copies of the gene, therefore these mice have four *SMN2* copies in total), with heterozygous *Smn*<sup>ko/wt</sup> animals (Riessland et al. 2010). All offspring carry one allele with two *SMN2* copies, and can be either homozygous (SMA) or heterozygous (HET) for the *Smn*<sup>ko</sup> allele. The SMA animals recapitulate many hallmarks observed in humans, such as diminished NMJs, loss of spinal motor neurons and muscle atrophy. Additionally, numerous non-neuronal organs show anatomical abnormalities: heart, lungs and intestine (Schreml et al. 2013). The mean survival is strongly dependent of the genetic background: while SMA mice on FVB background survive on average 9.9 days, on C57BL/6 background it is prolonged to 15.5 days (Riessland et al. 2010, Ackermann et al. 2013). It has been shown that genetic heterogeneity mitigates the severity of the disease phenotype, as crossing mice from two distinct strains (FVB x C57BL/6N) leads to SMA mice with mixed background which survive for 19.2 days, which is longer than the mean survival observed at any pure background (Ackermann et al. 2013).

Being a house-keeping protein involved in a key cellular process, SMN plays an important role in many cell types, not only in the motor neurons, therefore the question remains, which tissues need to be targeted therapeutically. As numerous Cre lines have become available allowing a tissue-specific expression of transgenes, it is now possible to test the need of SMN independently in various tissues have become possible (Nagy et al. 2009). It has been shown in mouse models that selective depletion of SMN either in spinal cord motor neurons or in the skeletal muscle gives rise to SMA symptoms (Cifuentes-Diaz et al. 2002, Park et al. 2010). Interestingly, a motor neuron-specific ablation of SMN induces a milder phenotype than a constitutive one, indicating that also other organs contribute to the overall SMA phenotype. Indeed, also a liver specific SMN deficiency lead to severe developmental defects that resulted in late embryonic lethality (Vitte et al. 2004).

As SMA presents a significant clinical variability in humans, it would be very helpful to represent this with a range of SMA mouse models with variable severity of symptoms. Therefore, numerous attempts to generate genetic intermediate SMA mouse models have been undertaken: when one allele with the human *SMN2* carrying a A2G missense mutation in exon 1 (identified in SMA patients) was crossed onto the severe Monani model (*Smn*<sup>ko/ko</sup>; *hSMN2*<sup>tg/tg</sup>; *hSMN2*<sup>A2G/0</sup>), the survival was prolonged to ~8 months (Monani et al. 2003). Another model helped to determine the critical threshold of SMN levels to prevent the disease symptoms: when an *Smn*<sup>2B</sup> allele with a 3 bp substitution in the exon

7 exonic splicing enhancer (ESE) and 15% of wildtype SMN expression was combined with the *Smn*<sup>ko</sup> allele, resulting mice survived for ~4 weeks, while the homozygous *Smn*<sup>2B/2B</sup> were phenotypically normal (Bowerman et al. 2011). Recently another mouse model was generated that after a survival of ~ 60 days succumbed to sudden cardiac failure, proving the susceptibility of other organs to SMN deficiency (Bogdanik et al. 2015).

Another approach to obtain an intermediate SMA model would be by administration of suboptimal doses of compounds that increase SMN levels but do not achieve a complete rescue: one example of this strategy could prove that the genetic modifier PLS3 is capable of extending lifespan of SMA mice, provided that sufficient SMN levels are present to ameliorate severe defects of peripheral organs, such as heart, lung and intestine (Hosseinibarkooie et al. 2016).

## 1.4 SMA therapy

There is still no approved therapy for SMA, however, since *SMN1* and *SMN2* were identified as the disease causing and modifying genes for SMA, the researchers have not only learned much about SMA biology but also made great advancements towards finding a cure. As in SMA the SMN protein is missing, to elevate SMN levels would be the straightforward therapeutic approach. This requires, however, the establishment of safe and efficient ways of SMN delivery. This has been achieved by development of new viral vectors with clinical potential.

As all SMA patients carry the *SMN2* gene, which produces low levels of SMN protein, another promising approach would be to identify pharmacological compounds which enhance full-length SMN expression from *SMN2*, either by upregulating transcription or correcting splicing towards greater proportion of full-length transcript. Many screens of chemical agents were performed aiming at identification of compounds capable of increasing SMN. Also neuroprotective agents and muscle function enhancers were speculated as potential drugs for SMA. In the following, these four classes will be briefly described; for more detailed review, see (Kaczmarek et al. 2015) .

### 1.4.1 SMN replacement therapy

In gene therapy, a DNA sequence encoding the full-length SMN protein is delivered to the SMA patients packaged into modified viral vectors (so called self-complementary adeno-associated vectors, scAAV) that can reach the target tissues when administered systemically, e.g. intravenously. A caveat of this method is the necessity of the vectors to cross the blood-brain barrier (BBB), therefore, great advantage came from a serotype

scAAV9 that penetrated BBB and transduced effectively spinal motor neurons (Duque et al. 2009). The first proof-of-concept study showed that exogenous administration of scAAV9-SMN results in an almost complete rescue of a severe SMA mouse model; furthermore, the therapeutic window of this intervention was characterized: while the gene delivery on PND1 rescued neuromuscular pathologies and the survival, delaying the intervention till PND5 resulted in a partial phenotype correction, and little improvement was observed when SMN-scAAV9 was administered on PND10 (Foust et al. 2010). This therapeutic approach proceeded fast to clinical trials (ClinicalTrials Identifier: NCT02122952).

#### 1.4.2 Compounds increasing SMN by enhancing protein stability or *SMN2* transcription

First class of drugs extensively studied for SMA therapy were histone deacetylase inhibitors (HDACIs). The acetylation status of histones, core chromatin proteins, is crucial for epigenetic regulation of gene expression: inhibition of histone deacetylation can increase in a non-specific manner the transcription of many genes, also *SMN2*. Numerous HDACIs have been reported to increase full-length *SMN2* transcripts in fibroblasts from SMA patients and SMA mouse models: short-chain fatty acids VPA, sodium butyrate and phenylbutyrate, as well as hydroxamic acids LBH589, SAHA, TSA, JNJ-26481585 and the benzamide M344 (Sumner et al. 2003, Riessland et al. 2006, Avila et al. 2007, Garbes et al. 2009, Riessland et al. 2010, Schreml et al. 2013). Some HDACIs showed motor function and survival improvement in SMA mouse model, however, the transition to human trials was not very successful, as frequently no or at best moderate improvement could be observed (Mercuri et al. 2007, Swoboda et al. 2009, Swoboda et al. 2010). A potential cause for these apparently disappointing results could be variable responsiveness of the treated patients to the HDACIs as those who were classified as responders indeed showed positive impact of the treatment (Garbes et al. 2009).

SMN levels could also be enhanced by increasing the protein stability: as SMN is degraded by ubiquitin proteasome system, its inhibition could potentially increase SMN in SMA patients. Indeed, bortezomib, an FDA-approved proteasome inhibitor, ameliorated motor phenotype in SMA mice (Burnett et al. 2009). Also aminoglycosides, antibiotics that promote the read-through of the stop codon in exon 8 of *SMN2*, were reported to stabilize SMN protein in patients' fibroblasts and moderately improved the phenotype of SMA mice (Mattis et al. 2009). Other non-HDACI compounds that were shown to increase SMN levels were: hydroxyurea, beta-adrenergic agonists albuterol and salbutamol tested in patients cell lines, and quinazoline, prolactin, activators of p38 (celecoxib, BAY 55-9837) and NMDA receptor activators tested in SMA mouse models (Grzeschik et al. 2005, Angelozzi



et al. 2008, Biondi et al. 2010, Farooq et al. 2011, Farooq et al. 2013, Hadwen et al. 2014). Particularly noteworthy are small-molecule splicing modifiers SMN-C1, -C2 and -C3, developed by PTC Therapeutics, that led to an impressive survival rescue in severe SMA mice from 14 days to >6 months (Naryshkin et al. 2014); however, the clinical trials of these substances were suspended as some long-term safety concerns came up in animal studies.

#### 1.4.3 Correcting *SMN2* splicing using antisense oligonucleotides (ASOs)

A strategy that is currently likely the most advanced towards an SMA-specific, FDA approved therapy is splicing correction of *SMN2* by antisense oligonucleotides. These active compounds benefited greatly from the elucidation of the complex *cis* and *trans* regulation of exon 7 inclusion or skipping in *SMN1/2* genes as depicted in Fig. 2. This allowed the identification of a tandem motifs hnRNP A1/A2 in intron 7, which constitute a potent intronic splicing silencer (ISS). Blocking this ISS by sequence-complementary ASOs resulted in enhanced production of full-length SMN in patients' cell lines and in mice carrying the *SMN2* transgene (Hua et al. 2008, Singh et al. 2009). The mechanism of action of these SMN-ASO in order to promote exon 7 inclusion is depicted in Fig. 3.

Once the suitable locus for SMN-ASO treatment was identified, many following studies *in vivo* attempted to optimize the ASO chemistry and delivery route (Porensky et al. 2012, Zhou et al. 2013). Unexpectedly, the greatest survival rescue of a severe SMA mouse model was achieved by systemic administration of SMN-ASO while the positive impact of a CNS-specific intracerebroventricular ASO injection was significantly smaller, suggesting the importance of peripheral SMN restoration for a long-term survival rescue (Hua et al. 2011, Passini et al. 2011). The company Ionis Pharmaceuticals who cooperated with the researchers in the former study launched Phase I (NCT01494701, completed) and numerous Phase II clinical trials of the ASO currently under the name nusinersen (previously ISIS-SMN<sub>Rx</sub>) which brought very promising results, so that Phase III trials soon followed. Very recently, Ionis Pharmaceuticals and their partner Biogen announced that a Phase III trial (NCT02193074) has shown an acceptable safety profile and significant improvement of treatment in type 1 SMA infants and is ready for filing FDA approval, which would make nusinersen the first drug ever approved and developed specifically for SMA (Biogen and Ionis Pharmaceuticals 2016). Understandably, this announcement raised hope and excitement in the community of both researchers and patients.

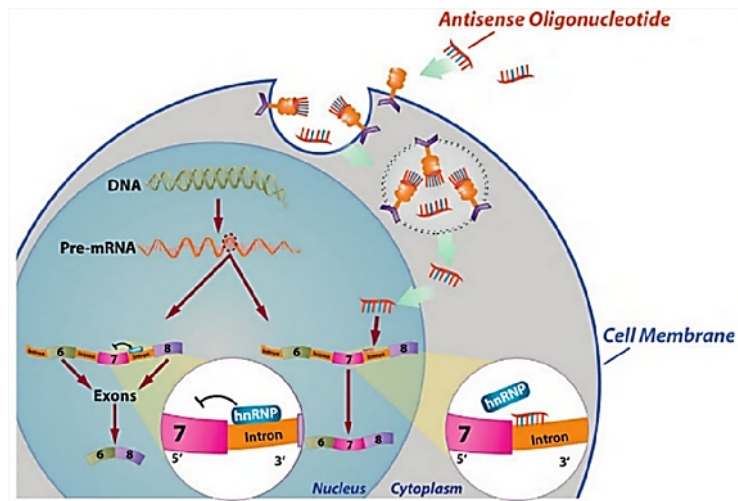


**Fig. 3. The mechanism of action of SMN-ASO.**

Single-stranded ASOs interact with proteins at the cell membrane and are taken up by endocytosis. In the cytoplasm they escape the endosome and enter the nucleus, where they bind to the *SMN2* pre-mRNA and disable the binding of hnRNP, which normally suppresses exon 7 splicing. In the presence of ASO, exon 7 inclusion in the *SMN2* transcript is promoted and subsequently the production of full-length SMN protein is enhanced (courtesy of Frank Bennett, Ionis Pharmaceuticals, Carlsbad, California).

#### 1.4.4 SMN-independent therapeutics: neuroprotective agents

Increasing SMN levels has not been the only therapeutic strategy to counteract SMA: numerous compounds with a neuroprotective mode of action have been tested, building on the research of other neurodegenerative disease, e.g. amyotrophic lateral sclerosis. Olesoxime (TRO01922) has been identified in a screen of rat motor neurons as a compound that most potently promoted the motor neuron survival; the neuroprotective function is presumably mediated by inhibition of mitochondrial permeability transition pore complex (mPTP) at the mitochondrial membrane (Bordet et al. 2007). The positive effect of olesoxime could be recapitulated *in vivo* in a model of motor neuron degeneration and also a Phase II clinical trials in SMA patients (NCT01302600) has shown positive results.

Another neuroprotectant riluzole restored the outgrowth defects in SMN deficient cells, likely through activation of small conductance  $\text{Ca}^{2+}$  activated  $\text{K}^{+}$  channels; furthermore, it improved the phenotype in SMN-deficient *C.elegans* and mouse models (Haddad et al. 2003, Dimitriadi et al. 2013).

Actin cytoskeleton dynamics has emerged as a pathway impaired by SMN deficiency (Oprea et al. 2008, Bowerman et al. 2009, Nolle et al. 2012). One of its hallmark is an aberrant expression profile of the actin stabilizer profilin IIa and an overactivation of the small GTPase protein RhoA, observed in SMN deficient cell lines and in the intermediate

*Smn*<sup>2B/KO</sup> mice (Bowerman et al. 2007). Therefore, compounds that would inhibit RhoA kinase (ROCK) and thus prevent the RhoA overactivation were speculated as SMA drugs: Y-27632 and Fasudil increased the lifespan, improved NMJ maturation and muscle fiber size in the *Smn*<sup>2B/KO</sup> mice (Bowerman et al. 2010, Bowerman et al. 2012). Notably, both compounds also act systemically and could improve not only motor neuron phenotype, but also heart physiology and glucose metabolism (Coque et al. 2014).

All therapeutic strategies for SMA discussed above are depicted in Fig. 4.

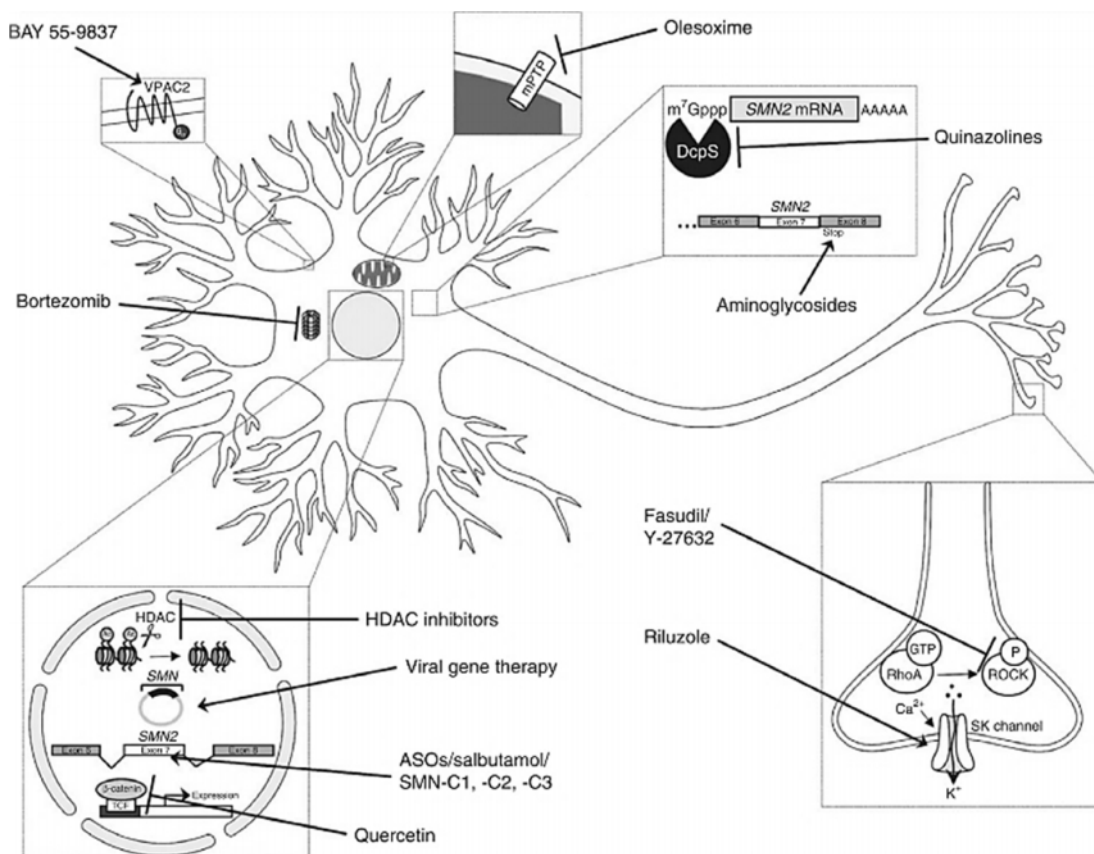


**Fig. 4: SMA therapy strategies with their specific target site in an exemplary motor neuron.**

**BAY 55-9837**, an agonist of the VPAC2 receptor in the plasma membrane, activates the p38 pathway. **Olesoxime** inhibits mPTP opening in mitochondria and acts neuroprotectively. **Quinazolines** prevent SMN2 mRNA decapping by inhibiting the scavenger enzyme DcpS. **Aminoglycosides** increase the probability to read through a stop codon in exon 8 of SMN2. **ROCK inhibitors Fasudil** and **Y-27632** have a neuroprotective effect. **Riluzole** acts neuroprotectively by activating SK (small conductance Ca<sup>2+</sup>-activated K<sup>+</sup>) channels in the cell membrane. **HDAC inhibitors** increase FL-SMN2 levels. **Viral gene therapies** (particularly scAAV9) are able to deliver SMN1 DNA in the cell nucleus. **ASOs, salbutamol** and **PTC SMA C1-C3** act as splicing modulators promoting FL-SMN expression. **Quercetin** prevents accumulation of  $\beta$ -catenin. **Bortezomib** increases SMN levels by inhibiting proteasomal degradation (adapted from (Kaczmarek et al. 2015)).

## 1.5 Modifier genes in SMA

It is meanwhile widely accepted that seemingly simple Mendelian traits which result in genetic disorders can have phenotypes varying in features such as age of onset, severity, etc. One cause of these variable phenotypes, apart from obvious environmental factors, can be modifier genes (Nadeau 2001). SMA itself is a prominent example of such modification by the *SMN2* gene.

Genetic modification occurs when expression of one gene (the modifier) alters the phenotypic manifestation of the target gene. The modification can occur at the level of gene expression (when the modifier induces the up- or downregulation of the target gene) or at any other level: molecular or cellular (when protein interactions or entire signaling pathways are changed), to the end phenotype at the organ, system or whole organism level. Studies of genetic modifiers can be therefore a powerful tool to find both direct and indirect interactions.

As some mechanisms that affect SMN expression were already discussed, this part will focus on SMN-independent genetic modifiers of SMA.

### 1.5.1 Identification of SMA modifiers in model organisms and biochemical screens

For the identification of genetic modifiers, the invertebrate SMA models: nematode *C. elegans* and fruitfly *D. melanogaster* proved particularly useful as many established genetic tools enabled high-throughput screenings which would not be possible in higher organisms. In *Drosophila* a screen with a collection of annotated transposons (Exelixis) uncovered >25 novel modifiers, among them players in conserved signaling pathways: FGF (fibroblast growth factor), NHR (nuclear hormone receptor) and BMP (bone morphogenetic protein) (Chang et al. 2008). A follow-up large-scale screen complemented with protein interaction studies and bioinformatics analysis uncovered an interactome of >300 genes altering the *Smn*-dependent phenotype in vivo (Sen et al. 2013). Another screen in *C. elegans* aimed at the identification of cross-species SMA modifiers by re-testing those found in *Drosophila*, and vice versa (Dimitriadi et al. 2010).

SMA is undoubtedly a disease of SMN deficiency, however, it is still unclear what function (s) of SMN protein are responsible for the major neuromuscular pathology. To better understand the cellular consequences of low SMN levels, biochemical screens have been performed using libraries of annotated compounds and samples from SMA mice were subjected to a proteomic analysis (Makhortova et al. 2011, Wishart et al. 2014).

In summary, the modifiers identified with the aforementioned screens unraveled the following pathways to be dysregulated in SMA: cytoskeleton actin dynamics, synaptic vesicle trafficking and neurotransmission, axonal transport and local translation, and control of gene expression (reviewed in (Wirth et al. 2016)).

#### 1.5.2 Identification of SMA modifiers in asymptomatic *SMN1*-deleted relatives of SMA patients

A rare, but very powerful approach to identify SMA modifying genes are studies of asymptomatic human subjects, when genetic testing of SMA families uncovers relatives who carry homozygous *SMN1* deletion, yet without any disease symptoms. Our hypothesis is that the protective phenotype of these unaffected individuals is mediated by modifier genes, which by different expression levels (up- or downregulation) are able to counteract the SMN deficiency and prevent the disease phenotype. Using this strategy, our group has previously identified *Plastin 3* (*PLS3*) as the first fully protective SMA modifier in six unrelated SMA families with haploidentical patients and their unaffected siblings: an mRNA microarray analysis detected a 40fold *PLS3* upregulation in lymphoblastoid cell lines from the latter. Plastin 3 is an F-actin bundling protein with two EF-hands for Ca<sup>+</sup> binding. Functional studies revealed that *PLS3* overexpression rescued the axonal outgrowth defect both *in vitro* in cultured motor neurons derived from SMA mice and *in vivo* in *Smn*-deficient zebrafish (Oprea et al. 2008). Final proof of the protective effect mediated by high *PLS3* levels came from mouse studies: when *PLS3* was overexpressed in the severe SMA mouse models (Taiwanese and *SMN*<sup>-7</sup>), no survival improvement could be observed, presumably due to dysfunction of multiple organs related to very low SMN levels (Ackermann et al. 2013, McGovern et al. 2015). However, already in a slightly milder SMA mouse model (with a mixed genetic background) *PLS3* overexpression showed a moderate effect on survival, induced a stronger motor performance and improved neuronal connectivity, which was visible both in the morphological and electrophysiological qualities of the NMJs (Ackermann et al. 2013). Notably, when *PLS3* transgene was overexpressed homozygously in an intermediate ASO-mediated SMA model, which showed a mean survival of 28 days, the lifespan was prominently rescued and reached >250 days in 60% of animals (Hosseinibarkooie et al. 2016). This study underlined the importance of intermediate SMA mouse models, which faithfully recapitulate the variable disease severity observed in humans: as all unaffected individuals carried three or four *SMN2* copies, most probably they would not present with the severe SMA type, but rather the intermediate range (type 2 or 3). Mechanistically, *PLS3* and its interaction partner *CORO1C* ameliorate the SMA phenotype by enhancing

endocytosis which has recently emerged as an important cellular process impaired in SMA (Hosseini-barkooie et al. 2016).

### 1.5.3 Neurocalcin delta – a novel potential modifier for SMA in humans

The foundation of the work presented in this thesis was the identification of *Neurocalcin delta* (*NCALD*) as a novel putative modifier gene for SMA (see chapter 2.1). In humans *Neurocalcin delta* (*NCALD*) gene is located on the antisense strand of chromosome 8q22.3 and spans the length of ~437 kb. The *NCALD* mRNA is transcribed from the antisense strand and >30 isoforms of variable length have been reported. The main isoform is 2289 bp long and includes 7 exons, however only 3 exons are protein-coding, as the starting codon is located in exon 5. While the 3'UTR of the transcript is remarkably long (>1500 bp), the coding sequence has the length of only 579 bp and gives yield to a small protein of 193 aminoacids and molecular weight of ~20-22 kDa.

Neurocalcin delta (*NCALD*) belongs to a conserved protein family of neuronal calcium sensors (NCS). Biochemically, the NCS proteins do not possess an intrinsic enzymatic activity but transduce  $\text{Ca}^{2+}$  signals to their downstream effectors. These are likely specific for each NCS protein, which would partially explain the non-overlapping functions of NCS proteins despite a high sequence and structure homology (Burgoyne and Haynes 2015). Other factors which regulate the specificity of NCS proteins are their tissue-specific and subcellular localization,  $\text{Ca}^{2+}$  affinity and kinetics. These characteristics enable the NCS proteins to integrate  $\text{Ca}^{2+}$  signaling spatially, temporally and over a wide range of concentrations (Haynes et al. 2012). Common for all NCS protein is the presence of four calcium-binding EF-hands domains. However, the EF-hand domain 1 is inactive in all NCS proteins and the EF-domain 4 is active only in some of them (Braunewell and Klein-Szanto 2009). Structurally, *NCALD* possesses an N-terminal myristoylation moiety that determines the protein localization. At low intracellular calcium concentration, the myristoyl group is contained within the protein structure and *NCALD* is mainly cytosolic; however, when calcium levels are elevated, the myristoyl group is exposed to the outside and *NCALD* can associate to the membranes, also of the trans-Golgi compartment (Burgoyne 2007). Interestingly, when cytosolic  $\text{Ca}^{2+}$  was elevated by ionomycin treatment, *NCALD* colocalized with clathrin, a key component of the cellular endocytotic machinery, particularly strongly in the trans-Golgi network; as their interaction could be confirmed with biochemical methods, this suggested a possible role of *NCALD* in the regulation of the transport of clathrin-coated vesicles (Ivings et al. 2002).

Functionally, little is known about NCALD: SNPs in *NCALD* were identified in a number of GWAS studies as potentially involved in susceptibility to bipolar disorder and dietary fat intake (Xu et al. 2014, Rudkowska et al. 2015). It has also been linked to few forms of cancer in lung, ovaries and prostate (Isaksson et al. 2014, Roudier et al. 2016, Shi et al. 2016). In humans, a deletion of the *NCALD* region was associated with epilepsy and intellectual disability (Kuroda et al. 2014). Recent studies have also found differential NCALD expression in mice lacking paraoxonase (*Pon1*), a gene linked to the Alzheimer's disease (Suszynska-Zajczyk et al. 2014), as well as in a rat model of schizophrenia (Vercauteren et al. 2007).

Hippocalcin (HCPA) is a more studied member of NCS family that has shown some functional similarity with NCALD: both were implicated as involved in the activation of the slow calcium-activated afterhyperpolarizing current (Villalobos and Andrade 2010). An *Hpca* knock-out mouse line has shown impairment in spatial and associative memory (Kobayashi et al. 2005). Interestingly, recently genetic mutations in *HPCA* in humans were reported to cause autosomal-recessive primary isolated dystonia, a disorder characterized by movement impairment and frequently accompanied by tremor. Functional studies could show that HPCA reduction in cortical neurons and astrocytes severely altered their response to physiological stimuli: the neurons showed no  $\text{Ca}^{2+}$  rise in response to membrane depolarization by KCl and a lower amplitude in response to glutamate, while astrocytes showed a diminished amplitude under ATP stimulus (Charlesworth et al. 2015). The possible interpretations of these results would be that *HPCA* deficiency alters the maintenance of membrane potential and in consequence the cellular response to membrane depolarization, or that it inhibits voltage-dependent  $\text{Ca}^{2+}$  channels. However, also opposing functions of hippocalcin and neurocalcin have been reported: while the reduction of the former had a detrimental effect on neuronal outgrowth (Oh et al. 2008), a similar effect was achieved by NCALD overexpression (Yamatani et al. 2010).

## 2 Preliminary results

### 2.1 *NCALD* is downregulated in asymptomatic *SMN1*-deleted individuals

The indication that Neurocalcin delta may be a novel SMA modifier originated from the diagnostics of a four-generation SMA family from Utah (USA), with two SMA type I patients carrying two *SMN2* copies (pedigree depicted in Fig. 5). Surprisingly, in two generations five relatives were identified who carried homozygous deletion of *SMN1* and four copies of *SMN2*, which would normally predestine a milder SMA type, however, these individuals remain fully asymptomatic. Under the assumption that the protective phenotype stems from a common genetic modifier (as it was inherited across generations), the family was tested using a dual approach combining data from an mRNA expression microarray and an Affymetrix SNP array (Applied Technologies). The SNP analysis showed that regions on chromosomes 1-3, 5, 8, 13 and 18 co-segregated in all five unaffected individuals but not in the SMA patients. Cross-reference to the mRNA expression results showed that *Neurocalcin delta* (*NCALD*) was the single gene identified by both approaches. *NCALD* showed a 4-5fold downregulation in the five unaffected individuals when compared to their two SMA type 1 relatives and to the control group of unrelated SMA patients with the same *SMN2* copy number (Riessland et al. under review).

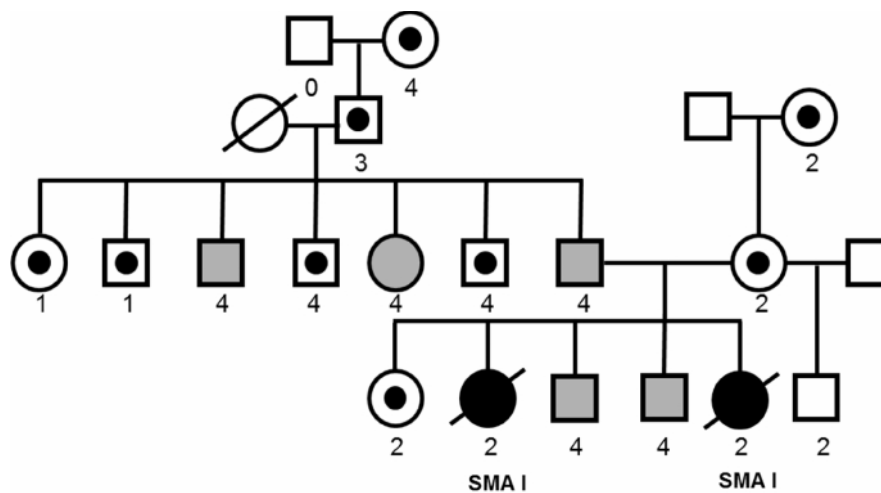


**Fig. 5: Pedigree of the family with *NCALD* reduction in asymptomatic individuals.**

SMA type I patients are marked with black filled symbols, asymptomatic *SMN1*-deleted individuals with grey filled symbols and carriers heterozygous for *SMN1* deletion with dotted symbols. The numbers below the symbols represent the number of *SMN2* copies in the given individual.



As the unaffected members of the Utah family showed a common phenotype of lower NCALD levels, which co-segregated with the asymptomatic phenotype, we hypothesized that NCALD reduction rescues the SMA symptoms. To test the hypothesis, NCALD depletion was first analyzed in various cellular and non-vertebrate animal models.

## **2.2 NCALD reduction rescues SMA phenotype *in vitro* and *in vivo* across species**

The first functional analyses performed by Markus Rießland, a postdoctoral fellow in Wirth lab, showed that NCALD reduction ameliorates SMA symptoms in cellular SMA models and in *smn*-deficient zebrafish. *In vitro* studies were performed in primary motor neurons from SMA mice, which showed shorter axons in comparison to HET controls; concurrent NCALD depletion by siRNA rescued the impaired axonal outgrowth (Fig. 6a). In zebrafish, *smn* deficiency resulted in truncated axons, which were restored by concomitant *ncald* depletion; additionally, enhanced axonal branching was observed (Fig. 6b). In collaboration with Anne C. Hart (Brown University), the effect of *Ncald* depletion in the *Smn*-deficient nematode *C.elegans* was tested: while *Smn* deficiency lead to impaired pharyngeal pumping, concomitant *Ncald* depletion improved this phenotype (Fig. 6c).

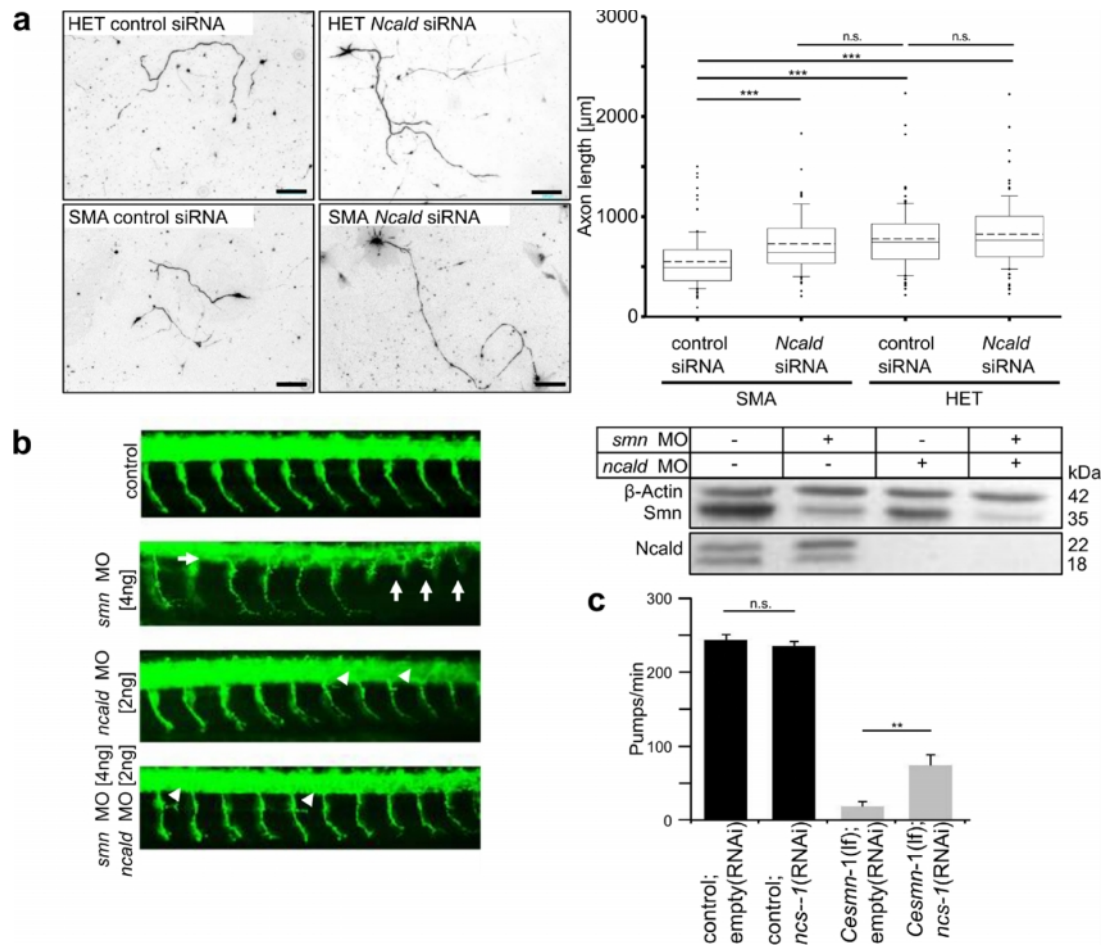


**Fig. 6: NCALD reduction ameliorated neuronal outgrowth defects mediated by SMN deficiency.**

**a)** Primary motor neurons (MNs) from SMA mice show significantly shorter axons than MNs from HET controls. Reduction of NCALD by siRNA mediates a rescue of the axonal outgrowth defects *in vitro*. **b)** In zebrafish morpholino-mediated (MO) *smn* depletion leads to truncation of spinal axons (white arrows). Concomitant *ncald* depletion by *smn+ncald* MO rescues axon truncation and increases branching (white arrowheads). **c)** *ncald* reduction rescued pharyngeal pumping defect in *C. elegans* (Riessland et al. under review).

Significance was determined with the two-tailed student's t-test. n.s. not significant, \*\* $P < 0.01$ , \*\*\* $P < 0.001$ .

### 3 Aim of the study

SMA is a Mendelian genetic disease, inherited in an autosomal recessive manner. SMA is caused by homozygous deletions or rarely other mutations of *SMN1*. In rare cases *SMN1*-deleted individuals remain asymptomatic, despite carrying only three or four *SMN2* copy genes, which in general are insufficient to compensate for the lack of *SMN1* (Hahnen et al. 1995, Cobben et al. 1996). These naturally occurring events suggest a protection through other genetic modifiers. *Plastin 3 (PLS3)* has been identified as a first fully protective SMA modifiers in humans (Oprea et al. 2008). The protection was validated in various SMA animal models: in nematode, fruitfly, zebrafish and mouse (Oprea et al. 2008, Dimitriadi et al. 2010, Ackermann et al. 2013, Hosseinibarkooie et al. 2016).

Preliminary work in our laboratory identified *Neurocalcin delta (NCALD)* as a novel protective SMA modifier. *NCALD* showed reduced expression and linkage to chromosome 8 in five *SMN1*-deleted asymptomatic members of an SMA family. As *NCALD* knock-down showed a positive effect on the SMA-like phenotype in cell lines and in non-mammalian animal models, we aimed to verify the impact of *NCALD* reduction in SMA mouse models. Notably, the SMA mouse models recapitulate many characteristics of the human phenotype, which can be analyzed upon a therapeutic intervention or a genetic modification, as described here. The aims of this thesis were the following:

1. Generation of a new inducible *Ncald* knock-down mouse line using the shRNA strategy proposed in (Kleinhammer et al. 2011) and crossing with the SMA mouse model, followed by a detailed analysis.
2. Since a constitutive *Ncald*<sup>ko/ko</sup> mouse line became available in 2014 at the Jackson Laboratory, we changed our strategy and used the heterozygous *Ncald*<sup>ko/wt</sup> as a model for *NCALD* reduction. As SMA is a clinically variable disorder depending on the genetic constitution of the patient (mainly on the *SMN2* copy number), subsequently we will study the effect of reduced *NCALD* in two SMA models of different severity: one severe (Hsieh-Li et al. 2000) and one intermediate (Hua et al. 2011, Hosseinibarkooie et al. 2016). For the latter, *SMN-ASO* will be injected at a suboptimal dose to moderately prolong survival. Both models will be subjected to a detailed *in vivo* and *ex vivo* analysis to delineate the effect of reduced *NCALD* on the organs primarily affected in SMA. *In vivo* studies will include survival, weight monitoring and motoric tests. *Ex vivo* analysis will include expression analysis, microscopic evaluation of MNs and NMJs as structures impaired in SMA, as well as histochemical studies of skeletal muscles and intestine as peripheral organs with reported defects in SMA mice (Ackermann et al. 2013, Schreml et al. 2013).

Also primary motor neurons from embryonic spinal cord will be cultured and analyzed.

3. Since NCALD reduction is anticipated to have a direct therapeutic potential, in collaboration with Ionis Pharmaceuticals we will generate *Ncal/d*-ASOs and test them *in vivo* in SMA mice.

The findings of these studies will provide first insights into the effect of NCALD suppression in mammalian models of SMA, showing both its advantages and possible caveats. The studies of modifier genes can be of great importance for understanding the molecular mechanism of disorders and especially for designing therapeutic strategies.

## 4 Materials and methods

### 4.1 Materials

#### 4.1.1 Laboratory equipment

Analytical balance	AX2202M	Ohaus
Analytical balance (fine scale)	ARJ 120-4M	Kern
Bacterial incubators	Innova 44	New Brunswick Scientific
	Innova 4230	New Brunswick Scientific
Bioruptor		Diagenode
Cell incubator	Heracell™ 150	Heraeus
Cell culture hood	Herasafe™ KS 12	Heraeus
Centrifuges	AllegraX22-R	Beckmann Coulter
	Avanti J-20XPI	Beckmann Coulter
	5415R	Eppendorf
	5415D	Eppendorf
	5804	Eppendorf
	Concentrator 5301	Eppendorf
	Galaxy Mini	VWR
	CM3050 S	Leica
Cryostat		
Electrophoresis chambers		
Agarose gels	MGV-620T	C.B.S & Scientific
	SGE-020-02	C.B.S & Scientific
	E-H6	Febicon
SDS-PAA gels	Mini-Protean 3 cell	Bio-Rad
Electroporation cuvettes	GP cuvettes, 0.4 cm	Bio-Rad
Electroporation system	Gene pulser Xcell	Bio-Rad
Embedding module	EG1150 H	Leica
Fibre optic light source	KL 1500 LCD	Leica
Gel documentation	ChemiDoc XRS	Bio-Rad
Heating block	HTMR132	HLC Bio Tech
Heating magnetic stirrer	MR 3001	Heidolph
Horizontal shaker	3015	GFL
Homogenizer	Precellys 24	Peqlab
Microplate reader	Safire <sup>2</sup>	Tecan
Microscopes		
Bright field	Axioskop 2	Zeiss
Fluorescent	Axiomager.M2	Zeiss
	Apotome	Zeiss
Inverted	DMIL	Leica
Stereo	S8 AP0	Leica
	VisiScope SBL 350	VWR
Microscope cameras	AxioCam MRm	Zeiss
	AxioCam ICc 1	Zeiss
	AxioCam ERc 5s	Zeiss

Microtome	RM2255	Leica
Microwave	R-898 (AL)-A	Sharp
Neubauer chamber	1100000	LO Laboroptik Ltd
pH meter	inoLab pH level	WTW
Photometer	BioPhotometer	Eppendorf
Photometer	NanoDrop 1000	Peqlab
Pipettes		
Research	2.5/10/20/200/1000 µl	Eppendorf
Automatic	Research Pro (10/100 µl)	Eppendorf
Repetitive	Multipette Plus	Eppendorf
Pipettor	Easypet	Eppendorf
Power supplies	PowerPac™ Basic/HC/1000	Bio-Rad
Real-time thermocycler	7500 RealTimePCR System	Applied Biosystems
Rotating wheel		
Roller mixer	SRT9	Stuart
	RM5	Hartenstein
Thermocyclers	DNAEngine Dyad/Tetrad	MJ Research
	C1000 Touch	Bio-Rad
	S1000	Bio-Rad
Tissue processor	ASP300	Leica
Vacuum pump	PM126040-026.3	Biometra
Vortex	444-1372	VWR
Water bath	1083	GFL
Water bath	FBC 620	Fischer Brand

#### 4.1.2 Mouse work equipment

Ear tag applicator	1005-s1	National Band & Tag Co.
Ear tags	1005-1	National Band & Tag Co.
Forceps	BD047R	Aeskulap
	FM002R	Aeskulap
	Dumont #55	Fine Science Tools
Heating pad	76084	Trixie
Microliter syringe (5 µl)	75 N SYR	Hamilton
Operating scissors	BC 321R	Aeskulap
	BC 341R	Aeskulap
Student Vannas Spring Scissors	FD012R	Fine Science Tool

#### 4.1.3 Chemicals

If available, chemicals used in this work had the purity grade “pro analysis”.

-Mercaptoethanol (99%, p.a)	AppliChem
2-Propanol ( 99.5%)	AppliChem
Acetone	AppliChem

Agarose	Sigma
Ammonium persulfate	AppliChem
Ampicillin	AppliChem
Bacto Agar	AppliChem
Bovine serum albumin (BSA)	Sigma
Bromophenol blue	AppliChem
Coomassie Brilliant Blue R-250	AppliChem
Dimethyl sulfoxide	Sigma
Doxycycline hyclate	Sigma
Eosin Y (acidic)	Sigma
Ethanol ( 99.5%, p.a.)	AppliChem
Ethidium bromide (1% in H <sub>2</sub> O)	AppliChem
Ethylenediaminetetracetic acid (EDTA)	AppliChem
Glycerol (86%, p.a.)	AppliChem
Glycine	AppliChem
Hematoxylin	Sigma
Hydrochloric acid (37%)	AppliChem
Hydroxymethylaminoethane (Tris)	AppliChem
Kanamycin	AppliChem
Methanol ( 99.9%, p.a.)	AppliChem
Milk powder (low fat)	AppliChem
Mowiol	Sigma
Paraformaldehyde	Fluka
Sodium chloride (p.a.)	AppliChem
Sodium dodecyl sulfate (SDS)	AppliChem
Sucrose	AppliChem
TBE buffer (10x)	AppliChem
Tetratmethylenediamine (TEMED)	AppliChem
Triton X-100	AppliChem
Trizma base	Sigma
Tryptone (microbiology base)	AppliChem
Tween-20	AppliChem
Water (HPLC grade)	Sigma
Yeast extract (microbiology grade)	AppliChem

#### 4.1.4 Reagents

##### 4.1.4.1 Reagents for molecular biology

10x PCR master mix	New England Biolabs
AquaPlus Mix 40% (29:1) Acrylamide	AppliChem
Bradford reagent	AppliChem
Complete Mini Protease Inhibitors	Roche
DNA ladder (100bp/1kb)	Life Technologies
dNTPs	Peqlab
Horse serum	Life Technologies

Page Ruler Prestained Protein Ladder  
 PBS (10x)  
 Ponceau S  
 Restore Western Blot Stripping Buffer  
 RIPA buffer  
 Super Signal West Pico ECL Substrate

Thermo Fisher Scientific  
 Roche  
 Sigma  
 Sigma  
 Sigma  
 Thermo Fisher Scientific

#### 4.1.4.2 Cell culture reagents and media

1x PBS Dulbecco, w/o  $\text{Ca}^{2+}$ ,  $\text{Mg}^{2+}$   
 B-27 Supplement (50x) (#17540)  
 -mercaptoethanol 1000x (ME) (#31350-010)  
 Amphotericin B  
 Brain derived neurotrophic factor (BDNF)  
 Ciliary neurotrophic factor (CNTF)  
 DMEM (+ 4.5 g/L D-Glucose, +L-Glutamine)  
 +Pyruvate) (#11995-065)  
 DNase I (2000 U/ml)  
 Fetal Calf Serum (FCS)  
 Gelatin (2%)  
 Geneticin (G418-Sulfate)  
 Glial cell-line derive neurotrophic factor (GDNF)  
 HEPES  
 Leukemia inhibitory factor 1000x (LIF)  
 Lipofectamine® 2000  
 Mitomycin C (MMC)  
 Neurobasal® Medium (1x) (#21103)  
 Non-essential amino acids 100x (NEAA)  
 OptiMEM® (1x) (#31985)  
 Penicillin/Streptomycin  
 Poly-D-Lysine  
 Pansera ES  
 Trypsin/EDTA  
 Trypsin

Life Technologies  
 Life Technologies  
 Life Technologies  
 Promocell  
 Peprotech  
 Peprotech  
 Life Technologies  
  
 New England Biolabs  
 Biochrom AG  
 Sigma  
 Life Technologies  
 Peprotech  
 Life Technologies  
 Millipore  
 Life Technologies  
 Sigma  
 Life Technologies  
 Life Technologies  
 Life Technologies  
 Life Technologies  
 Applichem  
 PAN-Biotech  
 Life Technologies  
 Worthington

#### 4.1.5 Kits

Power SYBR Green Master Mix  
 NucleoSpin Gel and PCR Clean-up  
 PureYield Plasmid Miniprep System  
 PureYield Plasmid Midiprep System  
 QuantiTect Reverse Transcription Kit  
 RNeasy Mini Kit  
 RNase-free DNase I Set  
 pcDNA3.1/CT-GFP-TOPO TA Expression Kit

Thermo Fisher Scientific  
 Macherey Nagel  
 Promega  
 Promega  
 QIAGEN  
 QIAGEN  
 QIAGEN  
 Thermo Fisher Scientific



#### 4.1.6 Enzymes

Ascl	New England Biolabs
BscBI	New England Biolabs
Platinum Taq DNA Polymerase High Fidelity	Life Technologies
RNase A	Life Technologies
RNase-free DNase I	QIAGEN
T4 DNA ligase	Promega

#### 4.1.7 Antibodies

##### 4.1.7.1 Primary antibodies and staining reagents

-Actin beta, HRP-conjugated, mouse	Proteintech
Rhodamine-labeled Bungarotoxin	Thermo Fisher Scientific
-Choline Acetyltransferase (ChAT), goat	Millipore
-GFP, mouse	Biochemistry, University of Cologne
-HB9/HLXB9, rabbit	Abcam
-Neurocalcin delta, rabbit	Proteintech
-Neurofilament M, rabbit	Millipore
-Neurofilament, mouse (2H3-c)	Hybridoma Bank
-Survival Motor Neuron, mouse	BD Transduction Lab.
-Synaptic Vesicle 2, mouse (SV2-c)	Hybridoma Bank
-Tau, mouse	Santa Cruz

#### 4.1.8 Secondary antibodies

HRP-conjugated goat -mouse IgG	Dianova
HRP-conjugated goat -rabbit	Cell Signaling
Goat -mouse Alexa 488 IgG (NMJ staining)	Thermo Fisher Scientific
Donkey -rabbit Alexa 488 (Vglut1, HB9)	Thermo Fisher Scientific
Donkey -goat Alexa 568 IgG (ChAT)	Thermo Fisher Scientific
Goat -mouse Alexa 568 IgG (tau)	Thermo Fisher Scientific

#### 4.1.9 Solutions and media

##### 4.1.9.1 Cell culture media

All cell culture media was stored at 4°C. MMC-solution and Doxycycline solution were aliquoted and stored at -20°C.

##### Common media (for MEF, HEK293T and NSC34 cells)

DMEM	500 ml
FCS	50 ml

Pen/Strep (10 U/ml)	7 ml
Amphotericin B (250 µg/ml)	1.25 ml

Doxycycline solution (10 mg/ml)

Doxycycline	1 g
1x PBS	100 ml

→ aliquot and store at -20°C

Embryonic stem (ES) cell media

DMEM	500ml
Pansera ES	75 ml
HEPES	12 ml
Non-essential aminoacids 100x (NEAA)	6 ml
β-mercaptoethanol	1.2 ml
LIF	90 µl
Pen/Strep	7 ml

Freezing media (10 ml)

FCS sterile filtered	9 ml
DMSO	1 ml

Gelatin (0.1%, for 50 ml)

Gelatin (2%)	2.5 ml
PBS	47.5 ml

Mitomycin C (MMC) medium (100 µg/ml)

Common media w/a antimicrobials	200 ml
MMC	2 mg

→ sterile filtered aliquots stored at -20°C

Motor neuron culture media

Neurobasal®Medium	500 ml
B-27 supplement (50x)	10 ml
L-Glutamine	5 ml
Pen/Strep	7 ml
Amphotericin B	1.25 ml
BDNF	50 ng/ml
CNTF	50 ng/ml
GDNF	50 ng/ml

Motor neuron plating media (for 50 ml)

DMEM	45 ml
FKS	2.5 ml
Glucose (20%)	1.5 ml
Pen/Strep	0.7 ml
Amphotericin B	0.15 ml

→ sterile filtered before use

## 4.1.9.2 Solutions for work with bacteria

LB-media (pH 7.5, for 1 L)

Bacto Trypton	10 g
Yeast extract	5 g
NaCl	5 g
Deionized H <sub>2</sub> O	to 1 L

→ adjust pH to 7.5, autoclave and store at 4°C

LB-Agar (for 500 ml)

LB-media	500 ml
Agar	7.5 g

→ autoclave and store at 4°C

## 4.1.9.3 Solutions for work with DNA

10x annealing buffer (for 10 ml)

Tris/HCl (1 M, pH 7.5)	1 ml
NaCl (5 M)	2 ml
EDTA (0.5 M)	0.2 ml
ddH <sub>2</sub> O	to the final volume of 10 ml

dNTP mix (for 1 ml)

dNTP (100 mM)	12.5 µl of each dNTP
ddH <sub>2</sub> O	to the final volume of 1 ml

Tail lysis buffer (pH 7.4, for 500 ml)

EDTA (0.5 M)	5 ml
NaCl (5 M)	20 ml
SDS (20%)	5 ml
Tris/HCl (1 M, pH 8.5)	50 ml
Deionized H <sub>2</sub> O	to the final volume of 500 ml

→ Proteinase K (200 µg/ml) added freshly before use

TE<sup>-4</sup> buffer (for 100 ml):

Tris (1 M, pH 8.0)	1 ml
EDTA (0.5 M, pH 8.0)	20 µl
Deionized H <sub>2</sub> O	to the final volume of 100 ml

→ RNase A (50 µg/ml) added freshly before use

## 4.1.9.4 Solutions for work with proteins

Ammonium Persulfate (APS) solution (10%, for 10 ml):

APS	1 g
Deionized H <sub>2</sub> O	to the final volume of 10 ml

→ aliquoted and stored at -20°C

Blocking solution (6%, for 100 ml)

Milk powder (low fat)	6 g
TBS Tween buffer	to the final volume of 100 ml

Electrophoresis buffer (10x, for 1 L)

Trizma® base	30.29 g
Glycine	144.13 g
SDS	10 g
Deionized H <sub>2</sub> O	to the final volume of 1 L

Laemmli buffer for SDS page (3x, for 10 ml)

Tris/HCl (1M, pH 6.8)	2.4 ml
Glycerol	3 ml
SDS (20%)	3 ml
Bromophenol blue	6 mg
β-mercaptoethanol	1.6 ml

Separating gel for SDS PAGE (12%, for 10ml)

Deionized H <sub>2</sub> O	4.85 ml
AquaPlus Mix (39:1) Acrylamide	2.55 ml
Tris (1.5 M, pH 8.8)	2.6 ml
SDS (10%)	0.1 ml
APS (10%)	0.1 ml
TEMED	40 µl

Stacking gel for SDS PAGE (for 4 ml)

Deionized H <sub>2</sub> O	2.96 ml
AquaPlus Mix (39:1) Acrylamide	0.52 ml
Tris (1 M, pH 6.8)	0.52 ml
SDS (10%)	40 µl
APS (10%)	40 µl
TEMED	4 µl

TBS Tween buffer (for 5 L)

Tris (20 mM)	12.1 g
NaCl (137 mM)	40 g
Tween-20 (0.5%)	25 ml
Deionized H <sub>2</sub> O	to the final volume of 5 L
→ adjust pH to 7.56	

Transfer buffer (for 5 L)

Trizma® Base	12.1 g
Glycine	56.3 g
Methanol	1 L
Deionized H <sub>2</sub> O	to the final volume of 5 L

Tris-HCl (1 M, pH 6.8, for 100 ml)

Tris-HCl	15 g
Deionized H <sub>2</sub> O	to the final volume of 100 ml
→ adjust pH to 6.8 with 37% HCl	

Tris-HCl (1.5 M, pH 8.8, for 200 ml)

Tris-HCl	45.25 g
Deionized H <sub>2</sub> O	to the final volume of 200 ml
→ adjust pH to 8.8 with 37% HCl	

## 4.1.9.5 Solutions for histo- and immunohistochemical stainings

Blocking solution (motor neuron and NMJ staining, for 10 ml)

BSA (4%)	0.4 g
1% Tween/1x PBS	2 ml
1x PBS	to the final volume of 10 ml

Blocking solution (spinal cord cryosections, for 10 ml)

BSA (4%)	0.4 g
Horse serum (5%)	0.5 ml
1% Tween/1x PBS	2 ml
1x PBS	to the final volume of 10 ml

4% paraformaldehyde (PFA) in PBS (pH 7.3, for 1 L)

PFA	40 g
Deionized H <sub>2</sub> O	to the volume of 900 ml
→ adjust pH to 7.3	
Deionized H <sub>2</sub> O	to the volume of 1 L
→ aliquot and store at -20°C	

## 4.1.10 Primers and oligonucleotides

Sequences for primers and oligonucleotides for shRNA cloning were designed with SeqBuilder software and purchased as lyophilized from Integrated DNA Technologies. Stock solutions at a concentration of 100 pmol/μl were prepared from lyophilized products and subsequently diluted to 10 pmol/μl. The oligonucleotides for shRNA annealing were diluted at a concentration of 50 μM.

**Table 1: Primers for cloning Ncald / qRT-PCR / genotyping**

Application	Name		Sequence	Amplicon length (bp)	Annealing temp (°C)
Cloning	<i>Ncald</i> cDNA	fwd	ATGGGGAAACAGAACAGC	513	58
		rev	TGAACTGGCCGGCACTGCTG		
qRT-PCR	<i>Ncald</i>	fwd	GCTGGAGATTGTACAGGCGATC	130	61
		rev	GAGCTTTCCATCTCTATTGGTATC		
	<i>Gapdh</i>	fwd	GGCTGCCCAGAACATCATCC	169	
		rev	GTCATCATACTTGGCAGGTTTCTC		
Genotyping	Pgk	fwd	CACGCTTCAAAAGCGCACGTCTG	622	65
	Neo	rev	GTTGTGCCAGTCATAGCCGAATAG		
	Hygro	fwd	GAAGAATCTCGTGCTTTCAGCTTCGATG	550	
		rev	AATGACCGCTGTTATGCGGCCATTG		
	<i>Ncald</i> mut	fwd	CGGTCGCTACCATTACCACT	824	60
		rev	GCATGTGTGACAACAGACCC		
	<i>Ncald</i> wt	fwd	AGCATTTCTGCCTTGCTGAT	201	58
		rev	TTTCCCTTACGGGGATGCT		
	<i>Smn</i> KO	rev	AGCCTGAAGAACGAGATCAGC	950	59
		fwd-1	ATAACACCACCACTCTTACTC		
		fwd-2	GTAGCCGTGATGCCATTGTCA	1050	

**Table 2: Oligonucleotides for cloning shRNA into the pEx-H1-tetO-CAG-teR vector**

Name	Target gene	Sense sequence	Original vector	bp
shRNA#1	<i>Ncald</i>	GCCAGGTGATTACCCATTAT	pLKO.1	21
shRNA#2	<i>Ncald</i>	CCTGAAGTCATGCAGGACTTA	pLKO.1	21
shRNA#3	<i>Ncald</i>	GCAAACGGTGATGGGACAATA	pLKO.1	21
shRNA#4	<i>Ncald</i>	CGCCAGATGGATACCAATAGA	pLKO.1	21
shRNA#5	<i>Ncald</i>	GCTTCCAAATTTGCAGAGCAT	pLKO.1	21
shScramble1	none	CCTAAGGTTAAGTCGCCCTCGCTC	pLKO.1	24
shRNA#6	<i>Ncald</i>	GGATGCTTCCAAATTTGCAGAGCATGTCT	pGFP-V-RS	29
shScramble2	none	GGATTTCAAGTCAATGTACACGTTTCGTAC	pGFP-V-RS	29

Antisense oligonucleotides (ASOs) were obtained within a collaboration from Ionis Pharmaceuticals, either already diluted at a given concentration (mg/ml) or lyophilized. In the latter case, the specific ASO was dissolved in sterile PBS and the stock concentration was determined by absorbance measurement at 260 nm (AD260) and calculated with the following equation: ASO concentration [mg/ml] = (AD260 x dilution factor x molecular weight) / (extinction coefficient x path length x 1000). For the injections, a working solution of 10 mg/ml was prepared and controlled photometrically.

**Table 3: Antisense oligonucleotides for *in vivo* injection**

Name	Ionis number	Target gene	Sequence	Chemistry	Delivery route	bp
SMN-ASO	387954	<i>SMN2</i>	ATTCACCTTTCATAATGCTGG	Uniform MOE, PS	s.c.	20
ASO1	673636	<i>Ncald</i>	TGGCATTGGAATATGTGTTT	MOE-gapmer, mixed backbone	i.c.v.	20
ASO2	673672	<i>Ncald</i>	AACACTTAATTTGGTCTGCA	MOE-gapmer, mixed backbone	i.c.v.	20
ASOctrl	676626	scramble	GTTTTCAAATACACCTTCAT	MOE-gapmer, mixed backbone	i.c.v.	20

#### 4.1.11 Plasmids

The following plasmids have been used in the work presented here. The correct cloning of inserts was verified by sequencing.

**Table 4: List of used and produced plasmids**

Name	Vector backbone	Insert	Resistance to antibiotics	Source of original plasmid
CT-GFP- <i>Ncald</i> -TOPO	pcDNA3.1/CT-GFP-TOPO	<i>Ncald</i> cDNA	Ampicillin	Life Technologies
TRC shRNA#1	pLKO.1	shRNA#1 against <i>Ncald</i>	Ampicillin	RNAi Consortium, TRCN0000104695
TRC shRNA#2	pLKO.1	shRNA#2 against <i>Ncald</i>	Ampicillin	RNAi Consortium, TRCN0000104696
TRC shRNA#3	pLKO.1	shRNA#3 against <i>Ncald</i>	Ampicillin	RNAi Consortium, TRCN0000104697
TRC shRNA#4	pLKO.1	shRNA#4 against <i>Ncald</i>	Ampicillin	RNAi Consortium, TRCN0000104698
TRC shRNA#5	pLKO.1	shRNA#5 against <i>Ncald</i>	Ampicillin	RNAi Consortium, TRCN0000104699
TRC control	pLKO.1	scramble shRNA	Ampicillin	Addgene #1864
GFP shRNA#6	pGFP-V-RS	shRNA#6 against <i>Ncald</i>	Kanamycin	Origene
GFP shScramble	pGFP-V-RS	scramble shRNA	Kanamycin	Origene
Dox shRNA#4	pEx-H1-tetO-CAG-tetR	shRNA#4 against <i>Ncald</i>	Ampicillin Geneticin	Dr. Ralf Kühn (MTA)
Dox shRNA#6	pEx-H1-tetO-CAG-tetR	shRNA#6 against <i>Ncald</i>	Ampicillin Geneticin	Dr. Ralf Kühn (MTA)
Dox shScramble	pEx-H1-tetO-CAG-tetR	scramble shRNA	Ampicillin Geneticin	Dr. Ralf Kühn (MTA)
C31 integrase	pCAG-Int (NLS)	C31 integrase ORF	Ampicillin	Dr. Ralf Kühn (MTA)

#### 4.1.12 Software packages and internet databases

– 1D Scan EX (densitometric analysis)	Scanalytics Inc.
– EndNoteX7 (reference organization)	Thomson Research
– Fiji (ImageJ) (image analysis)	Open Source
– GraphPad Prism (graph design, statistical analysis)	GraphPad Software
– Inkscape (figure design)	Inkscape Community
– Lasergene Package (DNA sequence analysis)	DNAstar Inc.
– Office 2013 (text processing, data analysis)	Microsoft
– Quantity One 4.5.1 (image acquisition and analysis)	Bio-Rad
– ZEN (image acquisition and analysis)	Zeiss
– Ensembl	<a href="http://www.ensembl.org/">http://www.ensembl.org/</a>
– GeneCards	<a href="http://www.genecards.org/">http://www.genecards.org/</a>
– Medline	<a href="https://www.ncbi.nlm.nih.gov/pubmed">https://www.ncbi.nlm.nih.gov/pubmed</a>
– NCBI	<a href="http://www.ncbi.nlm.nih.gov/">http://www.ncbi.nlm.nih.gov/</a>
– OMIM	<a href="http://www.ncbi.nlm.nih.gov/omim">http://www.ncbi.nlm.nih.gov/omim</a>
– UCSC	<a href="http://genome.ucsc.edu/">http://genome.ucsc.edu/</a>
– UniProt	<a href="http://www.uniprot.org/">http://www.uniprot.org/</a>

## 4.2 Methods

Unless stated otherwise, all molecular biology methods were adapted from the standard reference work “Molecular Cloning: A Laboratory Manual (volume 1-3)” by Joseph Sambrook and David W. Russell. The culture, transfection and selection of ES cells was performed according to the guidelines from the work “Laboratory protocols for conditional gene targeting” by Raul M. Torres and Ralf Kühn.

### 4.2.1 Working with nucleic acids

#### 4.2.1.1 Isolation of DNA

In order to isolate DNA from mouse tissue for genotyping purposes, a small piece of tissue (mostly a tail tip) was put in 493 µl Tail lysis buffer, freshly supplemented with 7 µl proteinase K (200 µg/ml) and incubated at 55°C under shaking until it was completely dissolved, usually o.n. Fully dissolved tissue suspension was centrifuged for 5 min at



maximum speed (16200 x g) to pellet potential debris. The supernatant was transferred to a new 1.5 ml tube with 500 µl isopropanol and DNA was precipitated with gentle shaking and centrifuged for 10 min at maximum speed. After discarding the supernatant, the pellet was washed with 200 µl 70% ethanol to remove residual salt and centrifuged again for 5 min at maximum speed. The ethanol was removed and the pellet was dried for 10 min in a concentrator centrifuge and subsequently resuspended in 100 µl TE<sup>-4</sup> with RNase for min 1 h at 37°C. 1 µl of the DNA suspension was used for genotyping PCR.

Isolation of DNA from ES cells for genotyping was performed on the 96-well plate, where cells were grown until fully confluent. Each well was washed with 100 µl PBS and 50 µl Tail lysis buffer with 1 mg/ml freshly added proteinase K was added. The plate was wrapped with parafilm and wet towels and placed in a box to prevent evaporation and put in a 55°C incubator o.n. On the following day the plate was cooled down at room temperature for 1 h and 100 µl of cold 96% ethanol was added to each well to precipitate DNA for 2 h. The presence of the precipitate was monitored under the binocular. Then the plate was carefully inverted to dispose of the ethanol so that most DNA remained attached to the bottom and subsequently each well was washed 3x with 100 µl of 70% ethanol. After the last wash, DNA was air dried for 15 min and resuspended in 100µl TE<sup>-4</sup> with RNase and 1 µl of the DNA suspension was used for genotyping PCR.

#### 4.2.1.2 Polymerase chain reaction (PCR)

If a specific genomic fragment was needed for cloning or genotyping purposes, it was amplified using the polymerase chain reaction, which is one of the most important molecular techniques, developed in 1980s by Kary Mullis (Mullis et al. 1986). It is an enzymatic technique that amplifies certain DNA fragments using complementary oligonucleotides (primers) that flank the fragment of interest in order to start the reaction. DNA is amplified by a thermostable DNA polymerase from *Thermophilus aquaticus*, termed Taq polymerase, which synthesizes new DNA starting from the 3' end of a single-strand DNA template. The components of a PCR are: a ribonucleic acid as template (mainly genomic DNA, but also cDNA), primers, Taq polymerase, MgCl<sub>2</sub> as a necessary co-factor, all dNTPs as building blocks, buffer and water. Currently, many manufacturers offer all PCR components (except template DNA and primers) as convenient and inexpensive ready-to-use Master mixes which are optimized for a wide range of annealing temperatures. For genotyping, such a 2x Master mix (New England Biolabs) was routinely used. An exemplary PCR composition with individual components or with a Master mix is given in Table 5.

**Table 5: A standard 20 µl PCR composition****Left side – with individual components, right side – with 2x Master Mix**

Components	Volume [µl]	Components	Volume [µl]
10x PCR buffer	2	2x Master mix	10
100 mM of dNTP	3		
MgCl <sub>2</sub>	0.75		
Taq polymerase	0.15		
ddH <sub>2</sub> O	11.1	ddH <sub>2</sub> O	7
Primer fwd (10 pmol)		1	
Primer fwd (10 pmol)		1	
Template DNA		1	

Each PCR consists of a series of three steps: denaturation, primer annealing and elongation; these three steps together constitute one PCR cycle. Each step requires different temperature conditions: the denaturation is performed at 95°C to separate two strands of the template DNA, the primer annealing depends on the sequence of an individual primer (specifically on its length and CG/AT proportion) and the elongation depends on the amplicon length, as the amplification speed of the Taq polymerase is ~ 1 kb/min. An exemplary PCR program is given in Table 6.

**Table 6: A standard thermocycler PCR program**

Step	Duration	Temperature [°C]
1. Initial denaturation	5 min	95
2. Denaturation	30 sec	95
3. Primer annealing	30 sec	Primer dependent, usually 58-62°C
4. Elongation	1 min per 1 kb	72
Repeat steps 2-4 for 35x		
5. Final elongation	10 min	72
Cooling	-	4

#### 4.2.1.3 Agarose gel electrophoresis

The agarose gel electrophoresis aims to separate DNA fragments depending on their size using an electric field. As DNA has a negative charge, it migrates towards the positively charged pole in the electric field (the anode).

Routinely 1% gels were prepared by solving agarose powder in 1x TBE buffer (e.g. 0.5 g in 50 ml for one gel) by warming up in a microwave. Upon complete dissolving the solution was cooled under stirring and ethidium bromide was added (final concentration 1 µg/ml).

This solution was poured into a gel chamber with well combs and left to solidify. Then the gel was covered with 1x TBE, the combs were removed and PCR samples (with loading dye already included in the master mix or added separately) were carefully pipetted into the wells. The gel was run for 20-30 min at 110-120 V and the separated bands were documented with the ChemiDoc XRS Imaging System (Bio-Rad).

#### 4.2.1.4 Cloning

Cloning involved generation of plasmids (circular DNA fragments) which were further used as molecular tools to express a desired protein or an shRNA sequence in the cells of interest. The plasmids were obtained either commercially or by material-transfer agreement and contained a number of functional sequences, such as promoters (constitutive or inducible), resistance genes for selection in bacteria and tags to mark exogenously expressed proteins. The crucial element of a plasmid is a multiple cloning site, which contains many loci recognized by restriction enzymes, which are site-specific endonucleases of bacterial origin. During incubation with a specific restriction enzyme, a circular plasmid was cut in a locally controlled manner and subsequently a new DNA fragment of choice (e.g. an open reading frame or an shRNA sequence) was built in (ligated) into the plasmid and amplified in bacteria culture. Eventually, the desired plasmid DNA was isolated from bacteria using commercial kits and further transfected into cells.

#### 4.2.1.5 Annealing of shRNA oligonucleotides

For cloning into the Dox-inducible pEx-H1-tetO-CAG-tetR vector, the identified potent shRNAs were ordered as two self-complementary oligonucleotides with the following sequence: 1) oligonucleotide A: 5'-AGATGCC-sense target sequence-GAAGCTTG-antisense target-sequence-CTTTTT-3', 2) oligonucleotide B 5'-CGCGAAAAAAG-sense target sequence-CAAGCTTC-antisense target sequence-GGCATCT-3'. Both oligonucleotides are depicted in Fig. 7. The oligonucleotides were dissolved in ddH<sub>2</sub>O at the concentration of 50 µM and annealed using the annealing mix and temperature conditions given in Table 7. The ready double-strand oligonucleotide was then directly used for ligation into pre-digested pEx-H1tetO-CAG-tetR vector as described in 4.2.1.7.

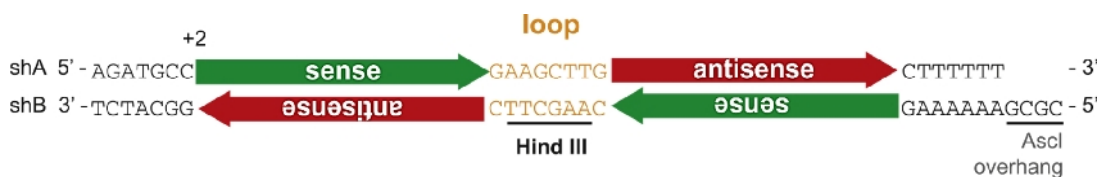


**Fig. 7: Annealing of shRNA oligonucleotides**

Two self-complementary oligonucleotides A and B including the shRNA sequence are designed and annealed resulting in a cloneable DNA fragment (Kleinhammer et al. 2011).

**Table 7: The composition and conditions of an oligonucleotide annealing reaction**

Components	Volume [ $\mu$ l]
oligonucleotide A	2.5
oligonucleotide B	2.5
10x annealing buffer	5
ddH <sub>2</sub> O	45
Incubate at 95°C for 5 min.	
Cool down to 4°C in a thermocycler at a rate 0.5° C/min	

#### 4.2.1.6 Digestion with restriction enzymes

The restriction enzymes are sequence-specific endonucleases of bacterial origin that cut DNA by hydrolyzing phosphodiester bonds between two nucleotides. Digestion with restriction enzymes was used for opening the circular plasmids in order to clone annealed shRNAs. Routinely, 3  $\mu$ g of plasmid DNA was mixed with 10x buffer, 100x BSA and the appropriate enzyme (3 U per 1  $\mu$ g of plasmid DNA) and incubated for 4 h at 37°C. An exemplary composition of a digestion with restriction enzymes is given in Table 8. The digested plasmids were then subjected to gel electrophoresis and the single band of the correct size was cut out and purified using NucleoSpin Gel and PCR Clean-up kit (Macherey Nagel).

**Table 8: The composition of a standard digestion using restriction enzyme**

Component	Amount
Plasmid DNA	5 $\mu$ g
Ascl (10 U/ $\mu$ l)	2 $\mu$ l
BsaBI (10 U/ $\mu$ l)	2 $\mu$ l
100x BSA	0.5 $\mu$ l
10x CutSmart Buffer	5 $\mu$ l
ddH <sub>2</sub> O	35.5 $\mu$ l

#### 4.2.1.7 Ligation of DNA fragments

To ligate DNA fragments (usually linearized plasmids and inserts, e.g. annealed shRNAs), the T4 DNA ligase was used (Promega). This enzyme catalyzes the joining of two DNA strands by creating a new chemical bond between the 5'-phosphate group of one DNA strand and the 3'-hydroxyl group of the second DNA strand. The ligation reaction is facilitated by the presence of complementary “sticky” ends which can be generated by digestion with the same restriction enzyme. A standard ligation requires an excess of insert, therefore the vector and insert were used in a 1:3 molar ratio. The composition and temperature conditions of a standard ligation reaction are given in Table 9. Typically, 2-4

µl of the product of ligation reaction were subsequently used for transformation into chemocompetent bacteria as described in 4.2.2.1.

**Table 9: The composition of a typical ligation reaction (10 µl)**

Component	Amount
10x Ligation buffer	1 µl
T4 DNA ligase	1 µl
Linearized vector	1 µl
Insert	3x amount of vector
ddH <sub>2</sub> O to the final volume of 10 µl	

#### 4.2.1.8 TOPO cloning

TOPO TA cloning method was used to generate the GFP-*Ncald* overexpressing plasmid. This technique uses the enzyme topoisomerase I derived from the *Vaccinia virus* instead of a standard ligase; it further utilizes the terminal transferase activity of the Taq polymerase which adds a single deoxyadenosine (A) to the 3' end of the PCR products. A TOPO vector is linearized with a specific 5'-(C/T)CCTT-3' sequence and a covalently attached topoisomerase at the free 3' ends of both strands. When the TOPO vector is mixed with PCR products, their free 5' ends with the deoxyadenosine overhangs are ligated by the topoisomerase to the complementary 3' deoxythime at the ends of the vector. This reaction proceeds efficiently at room temperature in the presence of necessary salts.

To clone *Ncald* coding sequence in the pcDNA3.1/CT-GFP-TOPO vector, the coding sequence was amplified from cDNA using specific primers and Taq polymerase. The PCR product was purified using NucleoSpin Gel and PCR Clean-up kit (Macherey Nagel) and 4 µl of it was mixed with 1 µl salt solution and 1 µl pcDNA3.1/CT-GFP-TOPO vector. This reaction was incubated at room temperature for 30 min and subsequently 2 µl of the reaction was transformed into TOP10 chemocompetent *E.coli* as described in 4.2.2.1.

#### 4.2.1.9 Isolation of RNA

Total RNA was isolated from cells using the RNeasy Kit (QIAGEN) according to the manufacturer's protocol. In short, the cells were washed with 1x PBS and lysed in RLT buffer supplemented with β-mercaptoethanol to inhibit RNases. Then an equal volume of 70% ethanol was added to the cell lysate and the entire volume was loaded on a silica column. Subsequently, the silica membrane was washed and the digestion with DNase I was performed to eliminate contamination of DNA. Finally, the total RNA was eluted from the column with RNase free water.

The concentration of RNA was determined using the Quant-iT RiboGreen RNA Assay Kit performed in triplicated for each sample and analyzed with the TECAN Safire2 microplate reader.

#### 4.2.1.10 Reverse transcription of RNA into cDNA

As RNA is not suitable as template for quantitative real-time PCR, it requires a reverse transcription to a more stable cDNA. For this purpose, QuantiTect Reverse Transcription Kit (QIAGEN) was used according to the manufacturer's protocol. The DNA wipe-out served as an additional measure to avoid contamination with genomic DNA. For qRT-PCR routinely 300 ng RNA and for samples of the standard series 600 ng RNA was reverse transcribed to cDNA in a 10  $\mu$ l reaction in a thermocycler. The exemplary composition and temperature conditions of the reaction are given in Table 10.

**Table 10: The composition of a typical reverse transcription reaction (10 $\mu$ l)**

Component	Amount
RNA	300 ng
DNA wipe-out	1 $\mu$ l
RNase-free H <sub>2</sub> O	to the final volume of 6 $\mu$ l
Incubate at 42°C for 2 min	
5x RT buffer	2 $\mu$ l
Primer mix	0.5 $\mu$ l
Reverse transcriptase	0.5 $\mu$ l
Incubate at 42°C for 20 min	

#### 4.2.1.11 Quantitative real-time PCR (qRT-PCR)

In order to quantitatively analyze the transcript of interest, quantitative real-time PCR was utilized. qRT-PCR follows the same kinetics as any PCR, only that product amplification can be monitored in real-time by measuring a DNA binding fluorescent dye, SYBRgreen. SYBRgreen dye emits green light when excited and its fluorescent signal is the strongest when bound to double stranded DNA. Therefore, SYBRgreen fluorescence was measured during each elongation stage at 72°C. At this temperature, most double stranded DNA comes from the PCR product; however, as SYBRgreen binds unspecifically to any double stranded DNA irrespective of its sequence, it is crucial for qRT-PCR primers to amplify a single product. In this study, this was verified by melting curve analysis where single peak was visible, as well as by agarose gel electrophoresis.

As the template for qRT-PCR, the reverse transcribed cDNA (4.2.1.10) was diluted in TE<sup>-4</sup> at a 1:4 ratio for the samples and at a 2:3 ratio for the standards. For the qRT-PCR, 2x Power SYBR Green Master mix (ThermoFisher Scientific) was used. The composition of a typical qRT-PCR is shown in Table 11.

**Table 11: The composition of a typical qRT-PCR (10µl)**

Component	Amount
2 x Power SYBR Green Master Mix	5 µl
Primer fwd (10 pmol)	0.5 µl
Primer rev (10 pmol)	0.5 µl
diluted cDNA template	3 µl
RNase-free H <sub>2</sub> O	to the final volume of 10µl

#### 4.2.2 Working with bacteria

Most work in bacteria (propagating the GFP-*Ncald* and shRNA plasmids) was performed in TOP10 chemocompetent *Escherichia coli* (Life Technologies). The propagation of pEx-H1tetO-CAG-tetR plasmid required a bacterial strain free of methylases for the subsequent digestion with methylase-sensitive endonucleases, therefore for this purpose the SCS110 bacteria strain (Agilent) was used.

##### 4.2.2.1 Transformation

Competent bacteria were thawed on ice and 5 µl of the ligation mix (see 4.2.1.7) was added and gently mixed by inverting the tube. The bacteria-DNA mixture was incubated on ice for 1 h. After the incubation step, the heat shock was performed for 45 sec at 42°C. The tube was again put on ice and 250 µl of LB media was added. Next, the tube was placed on a horizontal shaker for 1 h at 37°C. Subsequently, the bacteria-DNA mixture was distributed with a glass spatula on plates containing LB agar supplemented with the correct antibiotics (Ampicilin or Canamycin at the concentration of 50 µg/ml) and the plates were incubated o.n. in an incubator at 37°C.

##### 4.2.2.2 Picking clones and colony PCR for clone identification

Single clones were picked from o.n. incubated LB agar plates with sterile tips and lysed by osmotic shock in 20 µl ddH<sub>2</sub>O: 5 µl of the clone suspension were used for colony PCR and with the rest 15 µl an o.n. culture for plasmid DNA preparation was inoculated. The colony PCR was designed in a way that one primer was located in the plasmid and the other one in the insert to ascertain a successful ligation. This way, only clones carrying a correctly ligated plasmid would yield a PCR product.

##### 4.2.2.3 Preparation of plasmid DNA

Only clones which tested positive in the colony PCR were used for o.n. culture and used for isolation of plasmid DNA with the PureYield Plasmid Miniprep System (Promega) according to manufacturer's instructions. The sequence of the plasmid with the intended insert was validated by Sanger sequencing (GATC Biotech, Konstanz).

To isolate a larger amount of high-purity plasmid DNA for transfection, a large o.n. culture was prepared of plasmids with validated sequence. Routinely, 200 ml o.n. culture was processed with PureYield Plasmid Midiprep System (Promega), which includes an endotoxin removal step, and ~ 500 µl of plasmid DNA at the concentration > 500 ng/ml was obtained. A small volume (0.5 ml) of the o.n. culture was mixed with the same volume of sterile 50% glycerol, snap-frozen and stored as stock at -80°C.

#### 4.2.3 Working with proteins

As proteins are highly sensitive biomolecules which are easily degraded at higher temperatures, all work with proteins was carried out on ice. Additionally, a cocktail of protease inhibitors (Roche) was routinely added to lysis buffer.

##### 4.2.3.1 Isolation of proteins from cells

Cultured cells were washed with 1x PBS and a sufficient amount of RIPA buffer was added so that whole surface of cells was covered. Then the cells were scraped using a cell scraper and cell suspension was collected in 1.5 ml Eppendorf tubes and incubated on ice for 10 minutes. After that step the cell suspension was centrifuged for 20 min at 4°C at the speed of 16200 x g. The supernatant containing proteins was transferred to a fresh tube and the pellets were discarded. Subsequently, protein concentration was determined by Bradford assay. The protein lysates were stored at -80°C.

##### 4.2.3.2 Isolation of proteins from tissues

The tissues for protein isolation were collected during mice dissection and immediately snap-frozen. For protein isolation the tissue samples were homogenized using Precellys24 device (Peqlab): the tissue sample was placed into a 2 ml tube with ceramic beads and a sufficient amount of cold RIPA buffer. The program for homogenization was 25 sec at 5500 rpm. Subsequently, the samples were sonicated for 5 minutes using Bioruptor® Plus device (Diagenova) to fragment DNA and therefore prevent smear during SDS-PAGE. Finally, the tissue suspension was centrifuged for 30 min at 4°C at the speed of 16200 x g. The supernatant was processed exactly as in 4.2.3.1.

##### 4.2.3.3 Bradford assay

The Bradford assay was used to determine the protein concentration (Bradford 1976). Bradford reagent is characterized by a shift in its absorption maximum from 470 to 595 nm upon protein binding, which can be measured photometrically. A photometer was first calibrated for the Bradford assay using a standard curve of BSA dilutions. 1 µl of the lysate



of unknown protein concentration was mixed with 499  $\mu$ l of Bradford solution and incubated for 15 min at room temperature; in parallel, a blank containing 1  $\mu$ l of the lysis buffer (routinely RIPA buffer) with 499  $\mu$ l of the Bradford solution was prepared. First the absorption of the blank, and then of all samples was measured at a wavelength of 595 nm and the protein concentration was calculated from the measured values by comparison to the BSA standard curve.

#### 4.2.3.4 SDS polyacrylamide gel electrophoresis (SDS-PAGE)

The protein lysates were analyzed by SDS-PAGE followed by Western blotting. First, a specific amount of protein lysate (15-20  $\mu$ g) was mixed with 3x Laemmli buffer and denatured for 5 min at 95°C. The addition of the SDS both in the Laemmli buffer and the polyacrylamide (PAA) gel gives the proteins a strong negative charge exceeding their native charge. This allows the separation of all proteins in the lysates according only to their molecular weight, irrespective of their intrinsic charge.

For SDS PAGE, a 12% PAA separating and a stacking gel were prepared between two 0.5 mm glass plates (detailed composition given in 4.1.9.4). These two gel types differ by the PAA concentration and pH. The stacking gel contains less PAA and forms larger pores, so that the proteins can migrate easily and concentrate at the border between both gels. The separating gel contains more PAA and forms smaller pores, so that bigger proteins migrate more slowly and can be identified in the upper part of the gel, while smaller proteins move easily to the bottom part of the gel.

The separating gel was poured first and covered with isopropanol to secure a smooth edge of the gel. After gel polymerization, the isopropanol was washed out and the stacking gel was carefully pipetted on top of the separating gel and well combs were inserted.

The protein lysates with 3x Laemmli loading buffer were loaded into the wells of the stacking gel and separately, a protein ladder PAGE Ruler Plus (Thermo Fisher Scientific) was loaded in order to estimate the size of analyzed proteins. PAA gel electrophoresis was performed in the Mini-Protean 3 cell system (Bio-Rad) at 50-100 V in 1x electrophoresis buffer.

#### 4.2.3.5 Western blot

After the size separation by SDS-PAGE the samples were transferred from the separating gel to a nitrocellulose membrane (Hartenstein) by wet blotting in the transfer system (Bio-Rad). The gel transfer was arranged from the following components (all of them previously equilibrated in the transfer buffer): a sponge pad, a Whatman paper layer, the gel, the nitrocellulose membrane, again a Whatman paper layer and finally a sponge pad. All

components were fixed in a transfer device and transferred to a transfer chamber filled with transfer buffer. The protein transfer was performed for 2 h at 110 V in a cold room. During the transfer negatively charged proteins migrate in the electric field to the positively charged anode and by hydrophobic interaction adhere to the membrane.

#### 4.2.3.6 Immunochemical detection of proteins

After the transfer the membrane was washed with TBS-T to remove residual methanol and stained with the Ponceau solution to assess the quality of the transfer. After washing away the Ponceau dye with TBS-T the membrane was blocked for at least 1 h in 6% milk solution and subsequently incubated overnight at 4°C with the primary antibody diluted in 3% milk solution. After the given incubation time, the membrane was washed 3x 10 min with TBS-T and subsequently incubated with the secondary antibody solution. The primary and secondary antibodies with the respective dilutions and incubation times are listed in Table 12. Finally, the membrane was again washed 3x 10 min with TBS-T and incubated for 5 min in the SuperSignal® Wets Pico Chemiluminescent Substrate (Thermo Fisher Scientific) in order to visualize the proteins stained with the specific antibodies. The visualization was performed using ChemiDoc XRS Imaging System (Bio-Rad).

**Table 12: Primary and secondary antibodies used for protein detection**

Antibody	Dilution	Incubation time
HRP anti- $\beta$ -actin	1:10000	2 h
anti-GFP	1:2500	o.n.
anti-NCALD	1:1000	o.n.
anti-SMN	1:200	o.n.
Secondary antibody		
anti-mouse-HRP	1:5000	1 h
anti-rabbit-HRP	1:5000	1 h

#### 4.2.4 Working with cells

All work with cell lines was performed in sterile conditions in a laminar flow culture hood. Additionally, cell culture media was supplemented with antibiotics and anti-fungal agents to prevent contamination. All cells were kept in sterile cell incubators at 37°C with 5% CO<sub>2</sub>.

##### 4.2.4.1 Culturing cell lines

The adherent cell lines HEK293T and NSC34 as well as human and murine fibroblasts were grown as monolayers in the standard DMEM medium with 10% fetal calf serum (FCS) and split upon reaching 70-80% confluence. The splitting of a cell line occurred in the

following steps: first, the old medium was removed and the cells were washed briefly with 1x PBS. Then, dependent of the culture dish or flask used, a sufficient volume of Trypsin-EDTA was added to cover the entire monolayer and incubated for 5 min at 37°C, when the trypsinization was stopped by equal volume of fresh culture medium and cell were split into new flasks at a variable ratio depending on the growth pace of the respective cell line.

#### 4.2.4.2 Freezing cells

The solution of trypsinized cells was centrifuged at 1200 x g for 10 min. The cell pellet was briefly washed with 1x PBS and then resuspended in the freezing medium (sterile filtered solution of 90% FCS and 10% DMSO) and frozen at a -1°C/min rate using a cryo container. The frozen cells were first stored in -80°C freezer and transferred for long-time storage to the liquid nitrogen tank.

#### 4.2.4.3 Transfection of cells

The knock-down potential of the shRNAs against *Ncald* was tested by transfecting the shRNA vectors into NSC34 cells. For transfection, 90% confluent NSC34 cells on a 6-well plate were used, with  $2.5 \times 10^5$  cell per well. For each well 2 µg of the shRNA plasmid was transfected using the Lipofectamine® 2000 reagent. The transfection mix was prepared in two 1.5 ml tubes: the first tube contained 10 µl Lipofectamine® 2000 and 500 µl OptiMEM, the second tube contained 2 µg of shRNA plasmid DNA and 500 µl OptiMEM. After 5 min incubation at room temperature, the content of both tubes was mixed and again incubated for 20 min at room temperature. Meanwhile each well with the NSC34 was supplemented with 2 ml of fresh standard medium without antibiotics and after the incubation time the transfection mix was added in droplets to the cells. After 4 h the medium containing the transfection mix was replaced with standard medium with antibiotics. The transfected cells were lysed 48 h after transfection for protein or RNA analysis.

The HEK293T cells were transfected in the same manner, with the only difference that 250 ng DNA of the GFP-*Ncald* overexpressing vector was co-transfected with 2 µg of the shRNA plasmid DNA per well. When Doxycycline-inducible shRNA plasmid was transfected, the standard media was supplemented with 4 µg/ml Doxycycline.

### 4.2.5 Working with mice and mouse tissues

#### 4.2.5.1 Generating a new *Ncald* knock-down mouse line

In order to study the effect of NCALD reduction *in vivo* in a mammalian model, we planned to generate a new *Ncald* knock-down mouse line along the strategy proposed in

(Kleinhammer et al. 2011). The necessary steps are outlined in the Fig. 8 and the methodology is described in more detail in the following paragraphs and in the chapter 5.1. Within this project, steps 1 to 5 were completed; however, as we decided to apply the recently available *Ncald*<sup>ko/wt</sup> mouse line (see 4.2.5.7.2) as a model of NCALD reduction, the steps 6 to 9, which would require the assistance of the Centre for Mouse Genetics of the University of Cologne in order to produce living transgene animals, were discontinued.

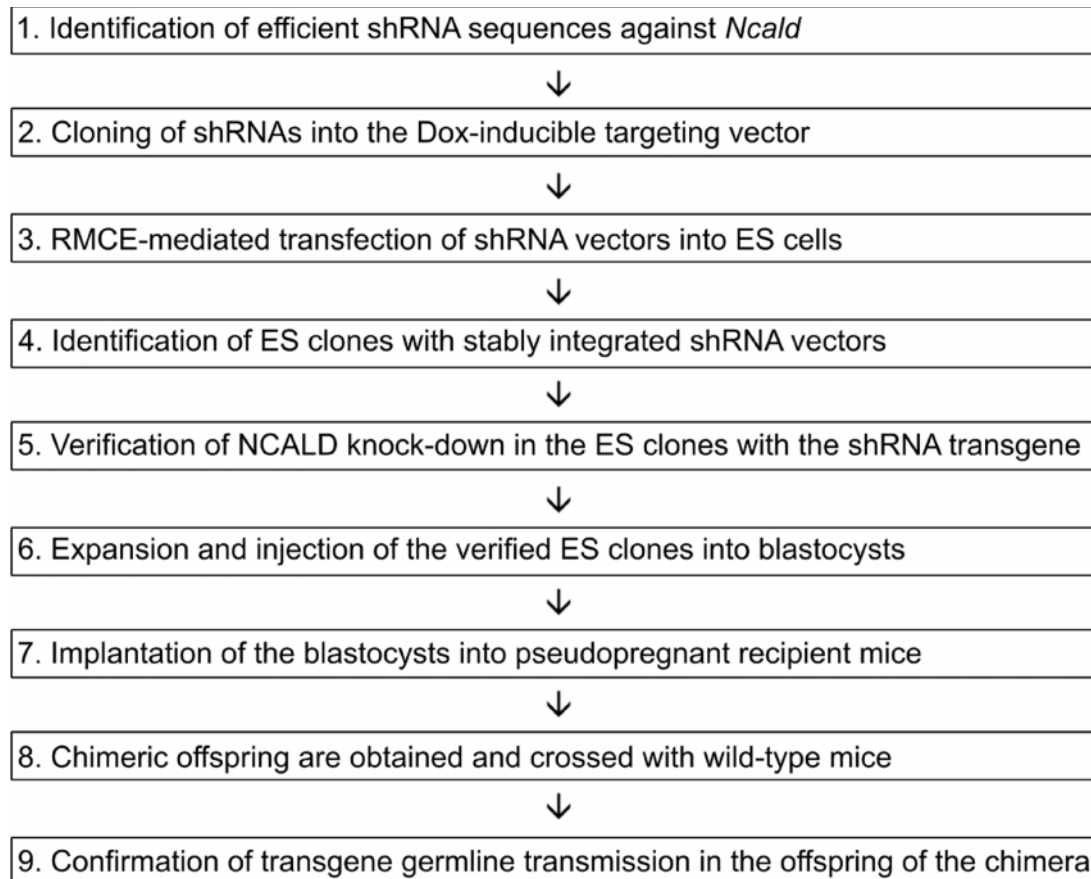


**Fig. 8: The necessary steps of a mouse generation strategy using an inducible shRNA targeting vector.** Steps 1 to 5 were performed according to the guidelines proposed in (Torres and Kuhn 1997, Kleinhammer et al. 2011).

#### 4.2.5.2 Culturing embryonic stem (ES) cells

Mouse embryonic stem (ES) cells are pluripotent cell lines derived from blastocysts of an early stage embryo (around 3 days post fertilization). ES cells retain the capacity to develop into all lineages and are able to contribute to a newly developing embryo. Targeted manipulations of the genome of ES cells have made it possible for researchers to generate transgene animals, particularly mice, either by removing a specific DNA fragment or – in

most cases – by an integration of desired DNA fragments either randomly or into defined loci in the genome of the ES cells (Thomas and Capecchi 1987). The cultivation of ES requires certain conditions in order to prevent differentiation and sustain their pluripotent state: the cells are routinely cultured on mitotically inactivated murine embryonic fibroblasts (MEFs), so called feeders, which secrete differentiation preventing leukemia inhibitory factor (LIF), and allow the ES cells to keep their rounded morphology (Evans and Kaufman 1981). Additionally, recombinant LIF is added to the ES medium.

The ES cell line used here was the IDG26.10-3 cell line with a modified Rosa26 locus (see 5.1). As mentioned above, the ES cells were routinely cultured on feeders, except when they were harvested for DNA or mRNA analysis, when they were cultured on gelatinized plates instead. The ES cells were fed daily with fresh ES medium and grown only until 60-70% confluence; accordingly, they were split at least every second day as described in 4.2.4.1.

#### 4.2.5.3 Preparation of feeder cells

The feeder cells are mitotically inactivated murine embryonic fibroblasts (MEFs), derived from Neomycin-resistant mice. MEFs are generated from E13.5 embryos; in order to assess the embryonic age, it is necessary to determine the start of the pregnancy, which is achieved by a plug check. A female mouse is housed with a male and daily monitored for the presence of the vaginal plug which indicates the mating. The day when a plug has been observed is considered E0.5 and weight progression of the presumably pregnant female is monitored. If the female has gained weight, it was sacrificed on E13.5 and the embryos were carefully released out of the uterus. The head and liver of the embryo were removed and a small fragment of the head was used for genotyping. The remaining tissue was transferred to a Petri dish and rinsed twice in 1x PBS, whereupon the tissue was incubated in 25 ml Trypsin-EDTA at 37°C for 30 min. The trypsinization was stopped using 25 ml of the standard medium and cells were centrifuged at 200 x g for 5 min. The cell pellet was resuspended in standard medium prior to cell counting and  $2.5 \times 10^6$  cells were plated on a 15 cm Petri dish. MEFs were grown till confluent and split three times at a 1:3 ratio, yielding in the end 27 plates of MEFs at passage 3. These MEFs were then subjected to mitotic inactivation by Mitomycin C (MMC) treatment. MMC was dissolved in standard medium without antibiotics at a final concentration of 10 µg/ml and sterile filtered. A 15 cm Petri dish with confluent MEFs was rinsed once with 1x PBS and 15 ml of MMC medium was added for 2-4 h at 37°C in a sterile incubator. After the incubation, the MMC medium was removed and cells were washed twice with 1x PBS, trypsinized and counted and aliquots of  $1 \times 10^6$  cells were frozen. One aliquot was sufficient for one 10 cm pre-

gelatinized dish (30 min incubation with 0.1% gelatin in 1x PBS at 37°C). The feeders were routinely thawed one day before splitting the ES cells.

#### 4.2.5.4 Electroporation of the vector DNA into ES cells

In order to manipulate the genome of ES cells, vector DNA carrying the desired transgene needs to be stably integrated. This is best achieved by electroporation as the electric current leads to a temporary permeabilization of the cell and the nuclear membrane and the exogenous DNA can insert the nucleus. Traditionally, the integration of the transgene depended on a rare event of homologous recombination where the homology arms of the targeting vectors would align to complementary regions in the genome of the acceptor cell and become integrated during mitosis. However, the frequency of such a genomic integration is very low, so that many clones required screening in order to identify the successfully recombined ones. Our strategy utilized an enzyme, C31 integrase, which would be electroporated together with the targeting vector and upon expression by the ES cell would mediate the recombination (the mechanism is described in detail in 5.1).

The ES cells were fed with fresh ES medium 3-4 h prior to the electroporation. 15 µg of the targeting vector and 15 µg of the C31 integrase plasmid were diluted in 1x PBS at a final concentration of 0.5 µg/µl. Each 10 cm plate of ES cells was washed with 1x PBS and trypsinized with 2 ml Trypsin-EDTA for 3-5 min at 37°C, whereupon 2 ml of standard medium were added to stop the trypsinization. The ES cell suspension was thoroughly pipetted to singularize the cells and subsequently centrifuged for 5 min at 1000 x g. The cells were resuspended in 1x PBS and counted using the cell-counting chamber; subsequently, the cells were again centrifuged and dissolved at a concentration of  $1.25 \times 10^6$  cells/ml. 0.8 ml of the ES cell suspension was mixed with the 15 µg + 15 µg DNA of both plasmids and electroporated with a single pulse of 230 µV at 500 F. The electroporation mix was supplemented with 30 ml of fresh ES medium and distributed onto three 10 cm feeder plates. 24 h after electroporation, the medium was exchanged to the selection medium with 140 µg/ml G418 (Geneticin).

#### 4.2.5.5 Selection and isolation of ES clones

After single resistant ES clones have become visible after 7-8 days under G418 selection, they were grown for 2-3 more days until reaching the suitable size for isolation. Again, the ES clones were fed with fresh ES medium 3-4 h before the procedure. A U-shaped 96-well plate with 50 µl Trypsin in each well was prepared for clone collection and kept on ice to block the enzyme activity. The plates with ES clones are washed once and then covered with 1x PBS and single ES clones are gently pipetted off the feeder plate with <20 µm of 1x PBS and transferred to the Trypsin-EDTA plate. After the complete 96-well plate has

been filled with ES clones, it is incubated for 5 min at 37°C, whereupon the trypsinization is stopped with 100 µl of ES medium per well. Each ES clone is singularized by energetic pipetting and the entire volume of ES clone suspension is transferred into a bottom-shaped 96-well plate with feeders. The single ES clones on 96-well plates are cultured in G418 selection media until reaching 50-60% confluence, upon which each plate was split onto three fresh 96-well plates with feeders. When these have reached 50-60% confluence, two of them were frozen (see 4.2.5.6) and one was split onto three gelatinized 96-well plates, which were cultured for 3 more days and used for DNA analysis.

#### 4.2.5.6 Freezing of 96-well plates with ES clones

The 96-well feeder plates with ES clones were frozen, so that after DNA analysis the ES clones with the correctly integrated transgene could be reclaimed by thawing and expansion. A 50-60% confluent 96-well plate with ES clones was washed with 1x PBS and trypsinized by adding 50 µl Trypsin/EDTA to each well and incubating for 5 min at 37°C, whereupon the trypsinization was stopped with 50 µl of the freezing medium (80% Pan-Sera ES, 20% DMSO). Each ES clone was singularized by pipetting, whereupon 100 µl mineral oil were added to each well. The plate was sealed with parafilm and stored at -80°C.

#### 4.2.5.7 Mouse strains

As the genetic background of a mouse strain has been shown to affect the gene expression and therefore the phenotypic outcome, most animal studies utilize inbred mouse strains that are highly homozygous (Linder 2006). The experiments in this work were performed on the genetically pure background, either C57BL/6N (for the studies of the *Ncal*<sup>ko/wt</sup> allele in SMA mice, both severe and ASO-injected intermediate ones) or FVB (for the preclinical testing of the *Ncal*-ASOs). All mice were housed in the mouse facility of the Institute of Genetics, Cologne. The experiments have been described in an animal experimental protocol that was permitted by the local animal protection committee under the reference number 84-02.04.2014.A126. All mice were humanly euthanized according to protocols approved by the Landesamt für Natur, Umwelt und Verbraucherschutz of Northrhine Westfalia (LANUV NRW).

In the following paragraphs details are given for the two strains used in this study: SMA mice and *Ncal*<sup>ko/ko</sup> mice.

##### 4.2.5.7.1 SMA mice

The FVB.Cg-Tg(*hSMN2*)2Hung *Smn1*<sup>tm1Hung</sup>/J mice were obtained from The Jackson Laboratory (Stock number #005058) (Hsieh-Li et al. 2000). These mice carry a targeted insertion of a hypoxanthine phosphoribosyl transferase (HPRT) cassette instead of exon

7 of *Smn*. If this transgene is bred homozygously, it results in early embryonic lethality. Therefore, in order to obtain viable mice with an SMA phenotype, another transgene carrying tandem *hSMN2* copies was crossed onto the *Smn*<sup>ko/ko</sup> background. If both transgenes are present homozygously, *Smn*<sup>ko/ko</sup>; *hSMN2*<sup>tg/tg</sup> mice have no survival or fertility impairment (Hsieh-Li et al. 2000). In our breeding scheme adapted from (Riessland et al. 2010), *Smn*<sup>ko/ko</sup>; *hSMN2*<sup>tg/tg</sup> mice are crossed with heterozygous *Smn*<sup>ko/wt</sup>; *Ncald*<sup>ko/wt</sup> animals and the resulting offspring can have one of four genotypes (see Fig. 9): half of the animals are homozygously lacking the *Smn* gene and show the disease phenotype (termed here SMA and SMA-*Ncald*<sup>ko/wt</sup>), while another half with only heterozygous *Smn*<sup>ko/wt</sup> show a normal phenotype (termed here HET and HET-*Ncald*<sup>ko/wt</sup>). Originally, the purchased SMA mice were on a pure FVB background; however, the line used in this worked has been previously backcrossed for >7 generations with C57BL/6N wildtype to obtain a pure C57BL/6N background (Ackermann et al. 2013).

#### 4.2.5.7.2 *Ncald*<sup>ko/ko</sup> mice

The B6N.Cg-*Ncald*<sup>tm1.1(KOMP)Vlcr/J</sup> mice were also obtained from the Jackson Laboratory (Stock number #018575). These mice were generated by the Knockout Mouse Phenotyping Program (KOMP<sup>2</sup>) using the VelociGene strategy developed by the Regeneron company to target most difficult genes. The insertion of VelociGene cassette ZEN-Ub1 created a 28620 bp deletion between positions 37298567-37327186 of chromosome 15 (Genome Build37); the neomycin cassette used for selection was subsequently excised by Cre expression. The *Ncald*<sup>ko/ko</sup> mice were viable and fertile, but in our observation the fertility of homozygous knock-out mice was diminished compared to wildtype. The phenotypic analysis revealed a number of abnormalities, particularly concerning body weight and size, skeleton and adipose tissue, cardiovascular and vision systems, as well as some neurological and behavioral changes (Jackson Laboratory 2016). We crossed the *Ncald*<sup>ko</sup> allele with *Smn*<sup>ko/wt</sup> animals and used the resulting *Ncald*<sup>ko/wt</sup>; *Smn*<sup>ko/wt</sup> animals (preferably male due to a compromised maternal behavior of the females) for breeding with the *Smn*<sup>ko/ko</sup>; *hSMN2*<sup>tg/tg</sup> mice to obtain SMA-*Ncald*<sup>ko/wt</sup> and HET-*Ncald*<sup>ko/wt</sup> offspring for analysis (Fig. 9).



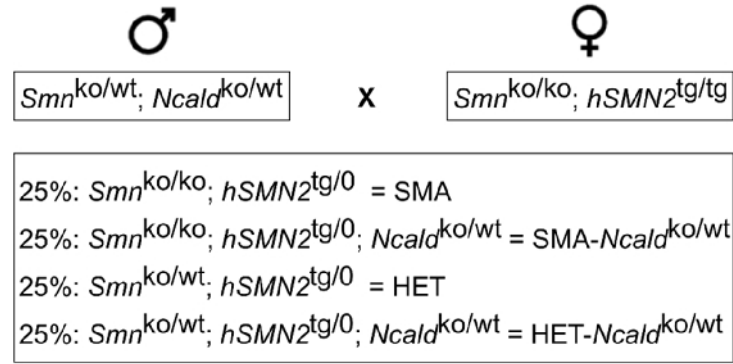


**Fig. 9: The breeding scheme to obtain SMA and HET animals with reduced NCALD levels**

Preferably, male animals carrying the allele were used for breeding as the breeding performance and paternal care of mothers was inferior to wildtype.

#### 4.2.5.8 Generation of primary motor neurons

Primary motor neurons were prepared from spinal cords of E13.5 of embryos; similar to the MEF isolation, the start of the pregnancy needed to be determined by plug check. On E13.5, the pregnant female was sacrificed and embryos were carefully released from the uterus. Subsequently, the embryo was placed on a Sylgard-filled Petri dish and covered in 1x PBS. In order to open the embryo dorsally, it was fixed ventrally with fine minuten pins using forceps and the skin of the embryo above the spinal cord was carefully removed. The spine was released by scraping out along the vertebrae with sharp pins and the surrounding meninges membrane and glial cells were removed as thoroughly as possible. The clean spinal cord tissue was placed in 500  $\mu$ l 1x PBS in a 1.5 ml tube and centrifuged for 10 min at 4°C and 1000 x g. Then the 1x PBS was pipetted off and the spinal cord was resuspended in 500  $\mu$ l of 1% Trypsin in 1x PBS and centrifuged again for 7 min at 4°C and 1000 x g. The Trypsin solution was removed and 500  $\mu$ l of motor neuron plating medium with DNase I (100 U/ml) was added and the tissue was completely dissolved by pipetting. After 2 min incubation for the undissolved debris to sediment, the cell suspension was transferred to a fresh 1.5 ml tube and the cells were counted using the Neubauer chamber. For immunofluorescent staining to determine axonal length, 75.000 cells/well were plated on poly-D-lysine (PDL) coated coverslips in a 12-well plate containing 2 ml of plating medium. For protein analysis,  $2 \times 10^5$  cells/well were plated on PDL-coated 6-well plates with 2 ml of plating medium. On the following day, the plating medium was replaced with Neurobasal® medium with growth factors. For the staining, the motor neurons were cultured for 6 days and for the protein analysis for 7 days.

#### 4.2.5.9 Immunofluorescent staining of motor neurons

In immunofluorescent stainings (of cells or tissues, see 4.2.5.14), the proteins of interest are specifically detected using a primary antibody, which is subsequently visualized by the binding of a fluorophore-conjugated secondary antibody.

For immunofluorescent staining, cells were seeded out and cultured on coverslips. After they have grown in the cell culture incubator for a given time, cells were washed with 1x PBS and fixed with 4% PFA supplemented with 4% sucrose for 15 min. After the fixation cells were washed again and permeabilized for 5 minutes with 1% Triton detergent in 1x PBS. Subsequently, cells were blocked with 4% BSA in PBS with 0.2% Triton for 1 h at room temperature. Primary antibodies (rabbit anti-HB9 1:250, mouse anti-Tau 1:500) were diluted in the blocking solution and applied to the cells after blocking for o.n. incubation at 4°C. On the following day, the cells were washed 3x for 5 min with 1x PBS and then incubated in a dark chamber with secondary antibodies (Alexa 488 anti-mouse and Alexa 568 anti-rabbit, both 1:250) diluted in 1x PBS for 1 h at room temperature. Then the cells were again washed 3x with 1x PBS and 1x with ddH<sub>2</sub>O to remove residual salts. Finally, the coverslips were mounted on glass slides with Mowiol and stored at 4°C for microscope analysis.

#### 4.2.5.10 Motoric tests

To assess the motoric fitness of mice, an array of tests suitable for neonatal mice (till PND14) was developed and we applied two of the suggested tests: the tube test and the righting reflex test were recruited (El-Khodori et al. 2008).

##### 4.2.5.10.1 The tube test

In the tube test the animal is placed with its head downwards in a softly bedded 50 ml Falcon tube and holds on to the tube edge by its hind limbs. Based on the positioning of the hind limbs towards each other, the so called hind limb score (HLS) was evaluated: 4 for fully spread hind limbs and upright tail, 3 for hind limbs parallel to each other, 2 for hind limbs occasionally clasping together and lowering the tail to support the hold, 1 for hind limbs permanently clasped together and 0 for no hold and falling into the tube. The positions reflecting the respective scores are presented in Fig. 10.

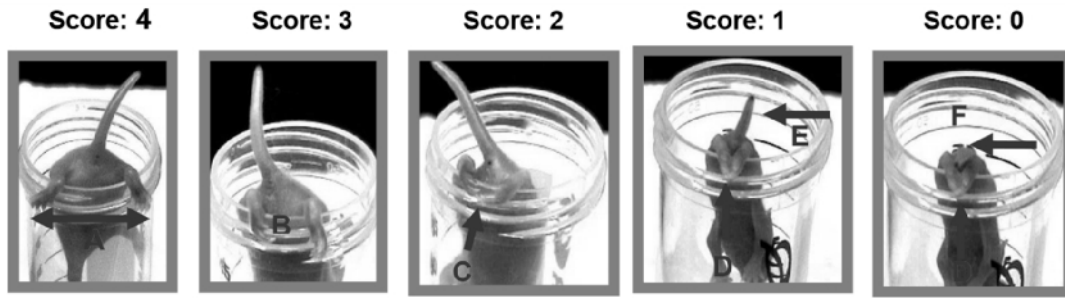


**Fig. 10: The tube test positions corresponding to the respective values of the hind limb score**

Following features were highlighted: A) normal separation of hind limbs; B) hind limbs are closer together reflecting the weakness; C) hind limbs are touching each other; D) hind limbs are clasped together; E) the tail remains raised; F) the tail is lowered (adapted from (El-Khodori et al. 2008)).

#### 4.2.5.10.2 The righting reflex test

For the righting reflex, the animals were placed on their back on a flat surface and the time to reposition themselves was measured over a 10 sec period. The time to right was replaced with a score value in the following manner: >1 sec = 0, 1-2 sec = 1, 3-4 sec = 2, 5-6 sec = 3, 7-8 sec = 4, 9-10 sec = 5, <10 sec = 6.

#### 4.2.5.10.3 Weight measurement

To monitor the weight progression, the analyzed animals were weighted daily for the first 14 days and then weekly (the longer living HET and HET-*Ncal/d*<sup>ko/wt</sup> animals) on a bench scale. The average was calculated separately for male and female animals to account for sex-related weight differences and a mean of these two values was considered.

#### 4.2.5.11 The injection of antisense oligonucleotides

The SMN-ASO (Hua et al. 2008) was dissolved in sterile 1x PBS at a concentration of 10 µg/µl and stored at -20°C; repeated thaw-and-freeze cycles were avoided. The subcutaneous injection (in the skin fold of the neck) at a dose of 30 µg (3 µl) was performed twice, on PND1 and 2.

The *Ncal/d*-ASOs (ASO1, ASO2 and ASOctrl, manufactured by Ionis Pharmaceuticals) were dissolved in sterile 1x PBS at concentrations of 30 and 60 µg/µl and stored at -20°C. The detailed injections regimens and doses are described separately for each experiment in the results section in chapter 5.4.

#### 4.2.5.12 Preparation of mouse tissues and organs

In order to prepare mouse tissues and organs, a mouse was sacrificed by decapitation (till PND13) or carbon dioxide euthanasia. The mouse body was placed dorsally on a preparation tray and the forelimbs and hind limbs were fixed with needles. The animal was opened with a central cut of the abdominal skin which was gently detached from the

muscle and removed above ribs to expose the whole abdomen. Routinely, first the TVA muscle was prepared (see 4.2.5.15). Next, the inner organs such as heart, lungs, liver and intestine were carefully isolated using ligature scissors and dissecting forceps and either snap frozen in liquid nitrogen (for subsequent protein analysis) or placed in embedding chambers for further procedures.

#### 4.2.5.13 Isolation of mouse spinal cord

The mouse spinal cord was routinely isolated from sacrificed mice as the last tissue and thus cut out of the body cavity, otherwise the fur and skin on the dorsal side of the animals was removed, the head and the tail were cut off and the vertebral column was carefully detached excised from the surrounding ventral connective tissue. Then the backbone was fixed with minuten pins to a Sylgard-plate and using forceps and microscissors, all vertebrae were individually removed to visualize the spinal cord beneath. The spinal cord was released and the upper half was snap frozen in a 1.5 ml tube for protein analysis, while the lower lumbar part was fixed in 4% PFA for subsequent sectioning.

#### 4.2.5.14 Immunohistochemical staining of spinal cord sections

For immunofluorescent staining, lumbar parts of mouse spinal cords were fixed with 4% PFA o.n. at 4°C. On the following day, the spinal cords were briefly washed with 1x PBS and then incubated at 4°C for two subsequent nights with sucrose (20% and 30%, respectively) for cryoprotection. The cryoprotected tissue samples were embedded in OptiTec medium and then sectioned using the cryotome device (Leica). The sections were collected in 1.5ml Eppendorf tubes containing 1x PBS for further processing. Then sections were briefly centrifuged at 4200 x g, washed with 1x PBS and permeabilized with 2% Triton in 1x PBS at room temperature for 30 min on a rotating wheel. Subsequently the sections were blocked for 1 h at room temperature in 4% BSA and 5% Horse serum in 1% Triton in 1x PBS. After that the sections were incubated with primary antibodies dissolved in the blocking solution at 4°C overnight. The motor neurons were visualized by anti-ChAT antibody and the glutamatergic synapses on the motor neuron soma by anti-VGlu1 antibody. On the following day, the spinal cord sections were washed 5x 10 min with 1x PBS and then incubated in the dark chamber with secondary antibodies diluted in 1x PBS for 2 h at room temperature. Then the sections were again washed 5x 10 min with 1x PBS and 1x with ddH<sub>2</sub>O. Finally, the sections were mounted on glass slides with Mowiol and stored at 4°C for microscope analysis.

#### 4.2.5.15 Preparation of mouse muscle tissue: *Transversus abdominis* (TVA) and *Extensor digitorum longus* (EDL)

The isolation of the proximal *Transversus abdominis* (TVA) muscle was performed as described in (Murray et al. 2014). The decapitated body of the sacrificed mouse was prepared as described in 4.2.5.12 and then the complete fur and skin covering the upper trunk were removed over the head. The exposed abdominal wall was carefully cut above the bladder and on both sides laterally toward the spinal cord. Then a cut was made on the dorsal side of the animal along the spine towards the neck through the dorsal part of the ribcage using micro scissors. With the final section on both sides through the diaphragm, the whole ribcage and the abdominal muscles were released and placed on a Sylgard-filled Petri dish with 1x PBS. The abdominal wall was stretched with forceps and pinned with fine minuten pins. The muscle was fixed for 20 min with 4% PFA and upon kept in 1x PBS. Under the stereomicroscope two upper muscle layers (external oblique muscle and internal oblique muscle) were gently removed with forceps to expose the TVA muscle. A triangular piece of the TVA muscle was cut out and stored in 1x PBS for subsequent immunohistochemical staining.

To isolate the *Extensor digitorum longus* (EDL), the hind limb was cut off the euthanized animal and the fur and skin were removed. The hind limb was pinned to the Sylgard plate at the feet and the knee and the dissection was performed under the stereomicroscope. First the fleshy *Tibialis anterior* muscle located directly under the skin had to be sectioned off at the tendons, then the visually available EDL muscle was gently separated from the tibia bone with the forceps and sectioned off at the tendons using microscissors. As the EDL muscle was exclusively used for muscle fiber size determination, it was fixed in 4% PFA o.n. at 4°C, dehydrated and embedded in paraffin in an automated tissue processor (Leica) and subsequently sectioned using a microtome (Leica).

#### 4.2.5.16 Immunohistochemical staining of the TVA muscle

The TVA muscle samples were immunohistochemically stained in order to visualize the neuromuscular junctions. After processed as described in 4.2.5.15, the muscle fragments were washed 3x 10 min in 1x PBS and subsequently permeabilized in 2% Triton X in 1x PBS for 30 min and blocked in the blocking solution (see 4.1.9.5) for 1 h; both permeabilization and blocking were conducted at room temperature on a rocking platform. The primary antibodies (mouse anti-SV2, 1:100, rabbit anti-NF, 1:250 or only mouse anti-NF, 1:250) were diluted in the blocking solution and 200 µl of the antibody solution was added per TVA fragment for an o.n. incubation at 4°C. On the following day, the TVA fragments were washed 6x 10 min with 1x PBS to prevent a high background from the primary antibodies. Subsequently, TVA fragments were stained for 10 min with rhodamine-

conjugated Bungarotoxin diluted in 1x PBS (0.5 µg/ml) in order to visualize the AChR clusters at the endplates. Next, the samples were incubated with secondary antibody (Alexa 488 anti-mouse, 1:250) in 1x PBS for 1 h in the dark. After this incubation, final washing steps were carried out: 2x 5 min with 1% Triton/1x PBS, 2x 10 min with 1x PBS and 1x 10 min in ddH<sub>2</sub>O. TVA fragments were mounted in Mowiol on glass slides and stored at 4°C for microscopic analysis.

#### 4.2.5.17 Hematoxylin and eosin staining of paraffin sections

In this study H&E stainings were performed to stain muscle tissue for subsequent fiber size measurements as well as to perform a gross histological analysis of the intestine as a non-neuronal organ affected in SMA. Upon o.n. fixation in 4% PFA the tissue specimens were prepared for sectioning by dehydration and paraffin-embedding using an automated tissue processor (Leica) and subsequently sectioned using a microtome (Leica).

In order to stain with H&E, the 7 µm sections were deparaffinized by incubation in Xylol for 30 min and rehydrated in a series of decreasing EtOH concentrations (100%, 96%, 70%, 50 %, 3 min each). Sections were quickly washed in 1x PBS and then in H<sub>2</sub>O for 1 min. Next, sections were incubated in Hematoxylin for 6 min, shortly rinsed with H<sub>2</sub>O and afterwards washed in H<sub>2</sub>O for 15 min. Afterwards the sections were rinsed quickly in fresh H<sub>2</sub>O to remove excess dye and placed into Eosin solution for 1 min. Finally, the sections were rinsed in H<sub>2</sub>O 6-7 times and then dehydrated in increasing EtOH concentrations (50%, 70%, 96% and 100%, 1 min each). Finally, sections were air dried and embedded in Eukitt mounting medium.

#### 4.2.6 Microscopic image acquisition and analysis

All fluorescent images were acquired with a fully motorized fluorescence microscope AxioImager.M2 equipped with an AxioCam MRm camera and an ApoTome device for optical sectioning (Zeiss). For the NMJ and spinal cord images, Z stacks of 30-50 images at a 0.5 µm interval were acquired. The images included in this thesis represent the maximum intensity projections of the Z stacks. The image analysis was performed with the ZEN (Zeiss) or Fiji software (Open Source).

For the analysis of VGlut1+ inputs on motor neuron soma, a custom macro developed by Peter Zentis (CECAD imaging facility) with Fiji 3D Viewer extension was applied. The macro segmented each image into two channels: one for ChAT+ motor neuron soma and another for VGlut1+ inputs and ensured that voxels were isometric. Subsequently, both single-channel images were smoothed: in the motor neuron soma image each pixel was replaced with the median of its 6x6x4 neighborhood and an optional automatic background

removal was performed by Li's Minimum Cross Entropy thresholding method (Li and Tam 1998). In the VGlut1+ image each pixel was replaced with the median of its 16x16x16 neighborhood. In the smoothed VGlut1+ image the inputs were automatically segmented using the 3D simple segmentation function of the 3D ImageJ Suite (Ollion et al. 2013) under the following criteria: the intensity threshold was obtained from Otsu's threshold clustering algorithm applied to the stack histogram (Otsu 1979) and 20 voxel was used as a minimum size criterion. In smoothed ChAT+ image the experimenter draws the smallest possible cuboids around non-overlapping motor neuron soma. Within the cuboid further segmentation was performed automatically using the Otsu method to obtain input values for a 3D hysteresis thresholding (3D ImageJ suite). The resulting mask was dilated by 4 voxels and finally holes in the mask were filled. Once all suitable motor neurons soma within an image were selected, the macro processed each 3D selection, again using functions of the 3D ImageJ suite, so that it first quantified all VGlut1 inputs within the selection and then calculated only those relevant for a given motor neuron soma within 2  $\mu\text{m}$  distance. Additionally, the volume of each motor neuron soma was determined. All bright field images were acquired with a Axioskop2 microscope with an AxioCam ICc 1 camera (Zeiss) and processed with the ZEN (Zeiss) or Fiji software (Open Source).

#### 4.2.7 Statistical analysis

Statistical analysis was performed with the GraphPad Prism 6 software. To test the significance of RNA expression or protein levels, two-tailed unpaired student's tests were applied. Significance of in the phenotypic analyses *in vivo* was determined with two-way ANOVA with Tukey's correction for multiple comparisons. The survival was analyzed with the Kaplan-Meier log rank method. Significance of histological analyses assessing the NMJ and muscle fiber area, motor axon length and glutamatergic inputs on motor neurons was determined with two-tailed unpaired student's tests.

Values of  $P < 0.05$  were considered significant and three levels of statistical significance were distinguished: \* $P < 0.05$ , \*\* $P < 0.01$  and \*\*\* $P < 0.001$ .

## 5 Results

### 5.1 SMA mouse model with NCALD reduction – a transgene shRNA approach

As other *in vitro* and *in vivo* studies performed in our group as well as in collaboration with the group of Anne C. Hart (Brown University) pointed strongly towards a rescuing potential of NCALD downregulation on the SMA phenotype, ultimately we wanted to test this hypothesis in a mammalian model of SMA, and the best studied model for that purpose is the mouse. However, at that time no *Ncald* knock-out or inducible *Ncald* knock-down mouse was available, so to analyze the effect of NCALD ablation on the SMA *in vivo*, we needed to generate a new mouse line. To optimally model the phenotype present in the Utah family members, who do not show complete loss-of-function but rather a reduction of NCALD, we decided to apply a strategy of inducible gene knock-down in the mouse using RNAi (Kleinhammer et al. 2011), which is making use of two molecular tools described herein.

First, a modified line of mouse embryonic stem cells, IDG26.10-3, enables a more efficient integrase-assisted recombination. In this line, a hygromycin resistance gene, driven from a pgk promoter, has been inserted in the Rosa26 locus (Hitz et al. 2007) and is flanked by a pair of attP sites, which are recognized by the C31 integrase, a site-specific bacteriophage which catalyzes unidirectional recombination between attachment motifs found in phage and bacterial genomes, termed attP and attB (Thyagarajan et al. 2001). The targeting vector is carrying the knock-in cassette flanked by attB; when it is delivered to the cells together with the C31 integrase expressing plasmid, the cassette will be inserted in the genome specifically as a single copy into the attP-modified Rosa26 locus, with simultaneous excision of hygromycin gene. Therefore, both the genomic localization and the number of transgenes integrated can be tightly monitored. The Rosa26 locus is commonly used for transgene recombination as an integration of a single vector copy in this locus is sufficient to induce body-wide expression transgene (Nyabi et al. 2009).

Second, the downregulation of the gene of interest can be achieved by a knock-in of a gene-specific shRNA sequence, which can be expressed constitutively or in a cell type specific manner (using Cre recombinase system). Its expression can also be induced by Doxycycline administration. We utilized the latter approach, where shRNA is expressed from a Tet off/on H1 promoter, as best suited for our purpose as we could not exclude the possibility that NCALD depletion impairs the development of the mice. The system proposed by the group of Ralf Kühn had the advantage that all components necessary for Dox-inducible shRNA expression were incorporated into a single vector: the shRNA



sequence under the Doxycyclin-inducible H1 promoter, tet repressor (tetR) expressed from a strong CAG promoter and neomycin resistance gene for later selection. When both C31 integrase and shRNA plasmids are delivered together to the ES cells by electroporation, the C31 integrase recognizes attP and attB sites, excises both cassettes flanked by them: the hygromycin gene in the ES cells genome and the transgene cassette (containing shRNA sequence and all regulatory components) and integrates the latter into the host genome. The structure of the targeting vector and the modified Rosa26 locus are schematically showed in Fig. 11.

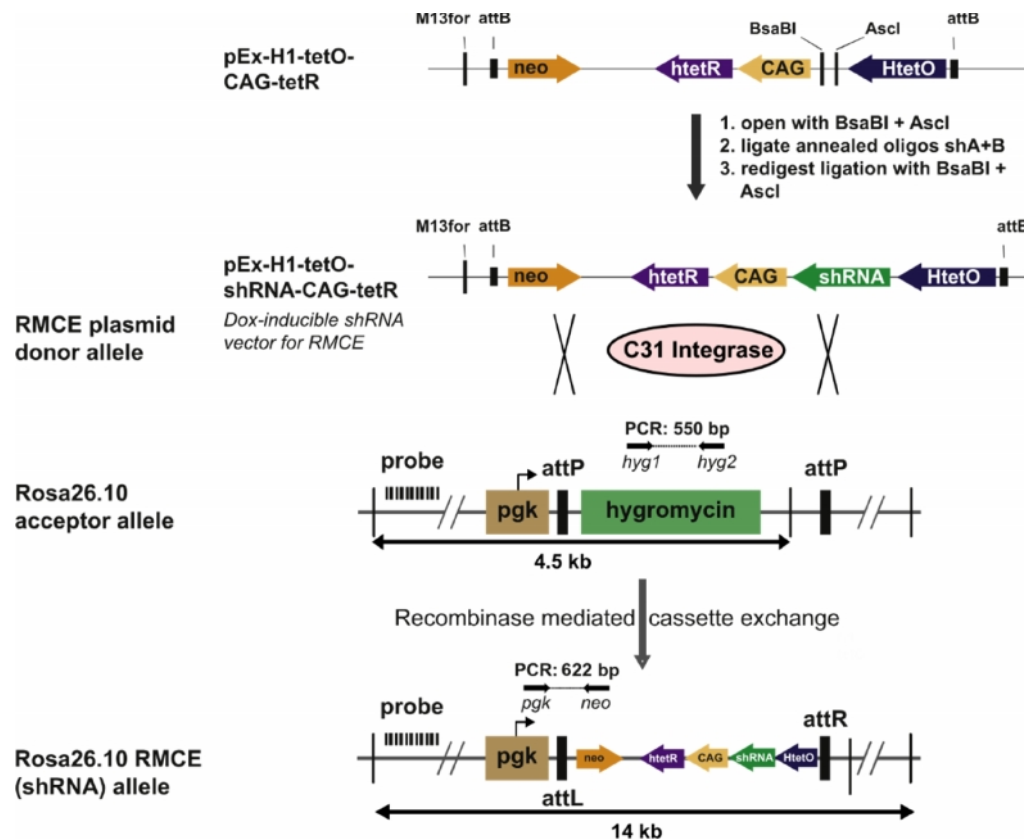


**Fig. 11: The shRNA mouse generation strategy**

An shRNA against the gene of interest is cloned in the Dox-inducible targeting vector (pEx-H1-tetO-shRNA-CAG-tetR) and by a recombinase-mediated cassette exchange (RMCE) mediated by the C31 integrase it is integrated in the modified Rosa26.10 locus of murine ES cells. The transgene integration can be verified by PCR (adapted from (Kleinhammer et al. 2011)).

The ES clones that underwent successful RMCE can be selected in cell culture via their Neomycin resistance: upon excision of the hygromycin, the Neomycin gene is expressed from the pgk promoter. Further details to the verification of transgene integration in the ES are included in 5.1.2.

The schematic mode of action of the H1-tetO-shRNA-TetR cassette within the targeting vector is depicted in Fig. 12.

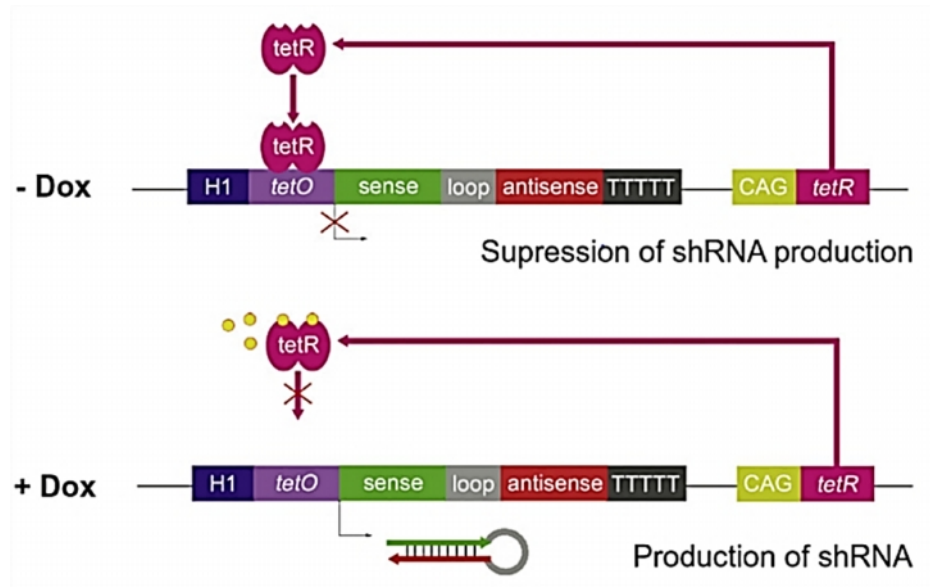


**Fig. 12: Induction of shRNA expression upon Doxycycline induction.**

In the absence of the inducer (Doxycycline), the constitutively expressed tetR binds to the tet-responsive element within the H1 promoter and by steric hindrance prevents shRNA expression. When Doxycycline (depicted as small circles) is applied, it would bind tightly to tetR and block its binding to the H1 promoter, enabling shRNA expression (Wiederschain et al. 2009) (adapted from (Kleinhammer et al. 2011)).

#### 5.1.1 Selection of the efficient shRNA sequences against *Ncal*

The crucial step and a prerequisite for generation of a functional knock-down mouse model is the selection of the most efficient shRNA sequence. Despite the progress in the algorithm development for *in silico* prediction of effective si- and shRNAs, it is still necessary to validate the sequences experimentally. Therefore, we obtained a commercially available collection of lentiviral pLKO.1 vectors carrying five different shRNA sequences directed against mouse *Ncal* (ThermoFisher Scientific). Fig. 13 shows the localization of the shRNAs in the mouse *Ncal* gene and their sequences are listed in Table 2.

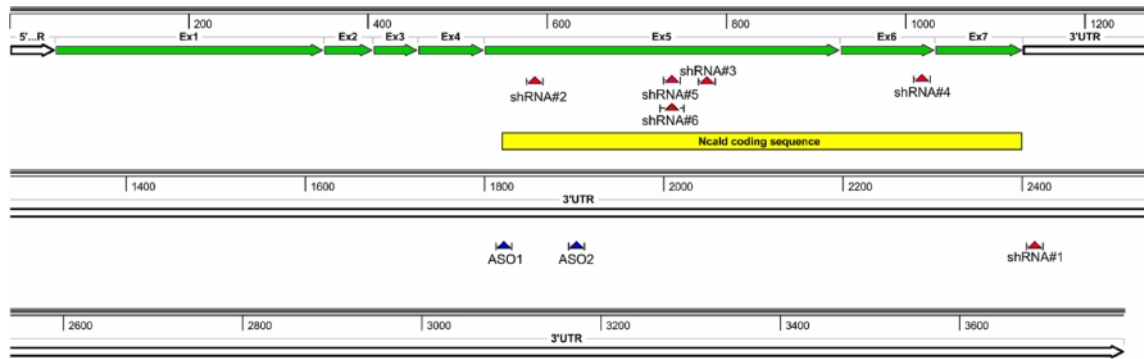


**Fig. 13: The longest transcript (3733 bp) of mouse *Ncald* (NM\_134094)**

All 7 exons are depicted as green arrows and the coding sequence with the start codon in exon 5 and the stop codon in exon 7 is highlighted as a yellow box. The sites targeted by the tested shRNAs are marked by red triangles. Additionally, two ASO sequences described in chapter 5.3 are marked by blue triangles in the 3'UTR of *Ncald* (5' and 3' UTR are depicted as black arrows upstream and downstream of the *Ncald* exons).

We transfected the *Ncald*-shRNA plasmids into mouse NSC34 cells and evaluated the knock-down of endogenous NCALD by Western blot and by qRT-PCR (Fig. 14). However, with this approach we were not able to determine the most potent shRNA sequence as all vectors yielded low levels of silencing, possibly because of poor transfection efficiency of lentiviral plasmids, which are originally designed for packaging and transduction of lentiviral particles (Moffat et al. 2006). Also the results of replicate experiments remained inconsistent, for example shRNA#2 was the least efficient in experiment 1 and the most efficient in experiment 3 (Fig. 14a).

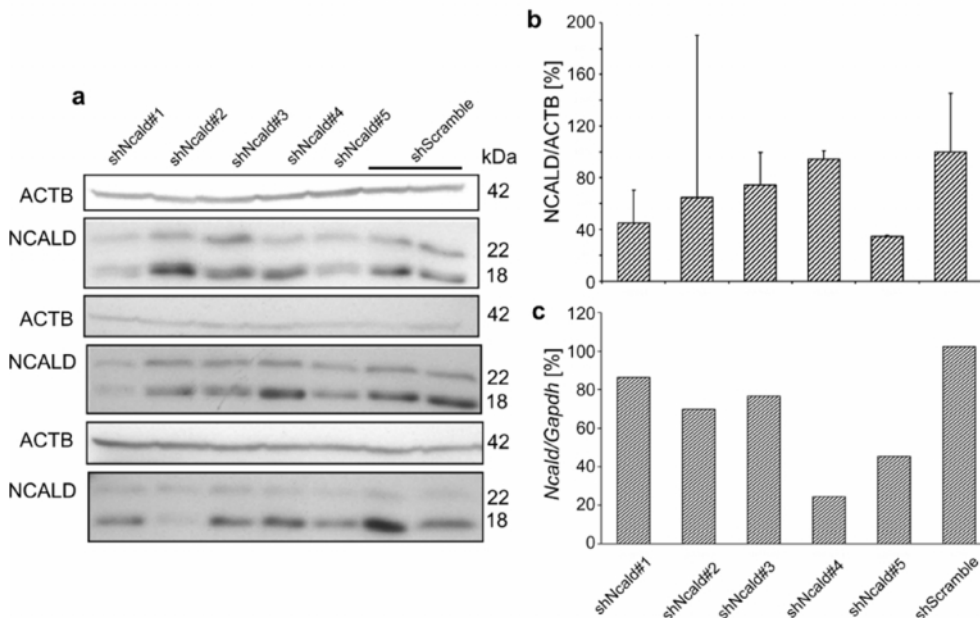


**Fig. 14: Analysis of *Ncald* knock-down on protein and mRNA in NSC34 cells transfected with shRNAs**  
**a)** Western blots of cell lysates and **b)** quantification of NCALD knock-down efficiency from three independent shRNA transfection experiments in NSC34 cells. Beta-actin (ACTB) was used as loading control. **c)** Quantification of qRT-PCR of *Ncald* levels. *Gapdh* was used as housekeeping gene.

Therefore, we decided to optimize the shRNA testing by applying an improved design of longer shRNAs (29bp) in an EGFP-vector to better monitor the transfection efficiency (Origene). Additionally, as the NSC34 cells were apparently not an optimal system for shRNA screening, we developed an alternative, albeit more artificial, experimental set-up using HEK293T cells. This cell line guarantees excellent transfection efficiency but due to its kidney origin it does not express endogenous NCALD. Therefore, we co-expressed in this cellular system a plasmid encoding *Ncald*-GFP (recognized by an anti-GFP antibody) and shRNA vectors and by that we were able to identify two potent shRNA sequences: one 21bp-sequence (shNcald#4) located in the exon 6 of *Ncald* led to ~90% knock-down, and second 29bp-sequence (shNcald#6), which targeted exon 5 of *Ncald*, was the most efficient one and achieved >95% knock-down (when compared to scramble shRNA). The blots and knock-down quantification are depicted in Fig. 15. The limitation of this method was that we could only validate shRNA sequences which targeted the coding sequence of *Ncald* as the *Ncald*-GFP overexpressing vector contained only the minimal cDNA ranging from the start to the stop codon, without any intronic regions or 5' and 3'UTR, therefore shRNA#1 had to be excluded from these tests.

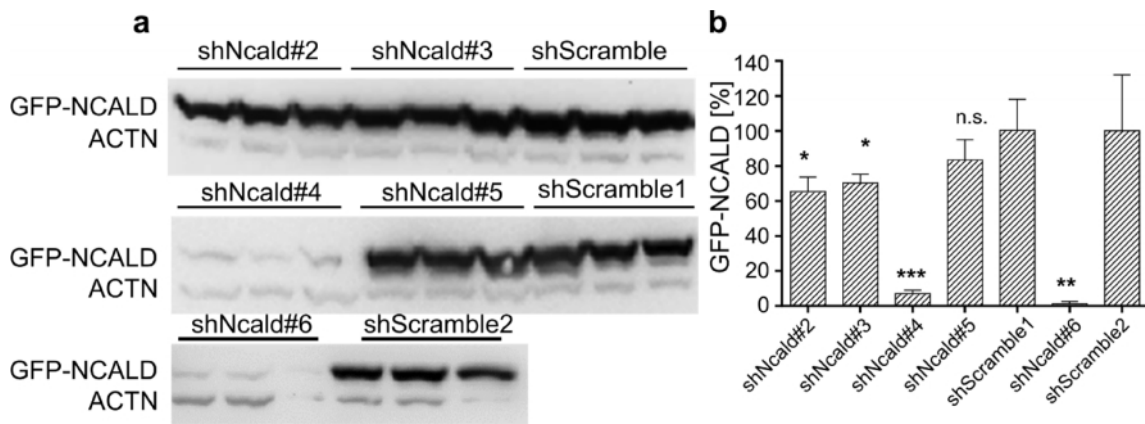


**Fig. 15: Identification of efficient shRNA sequences in an *Ncald*-GFP overexpression set-up**

**a)** Blots of HEK293T cells co-transfected with *Ncald*-GFP plasmid and shRNA plasmids against *Ncald* coding sequence. Transfection was performed in triplicates. **b)** Quantification of GFP-NCALD levels upon co-transfection with respective shRNA plasmids: shNcald#4 and shNcald#6 were most potent in reducing GFP-NCALD.

Statistical analysis was performed using two-tailed student's t-test. n.s. not significant, \* $P < 0.05$ , \*\* $P < 0.01$ , \*\*\* $P < 0.001$ .

The two shRNA sequences: shNcald#4 and shNcald#6 were subcloned to the targeting vector which carried all necessary elements for Tet off/on regulation and their knock-down efficiency was again confirmed under Doxycycline administration (Fig. 16).

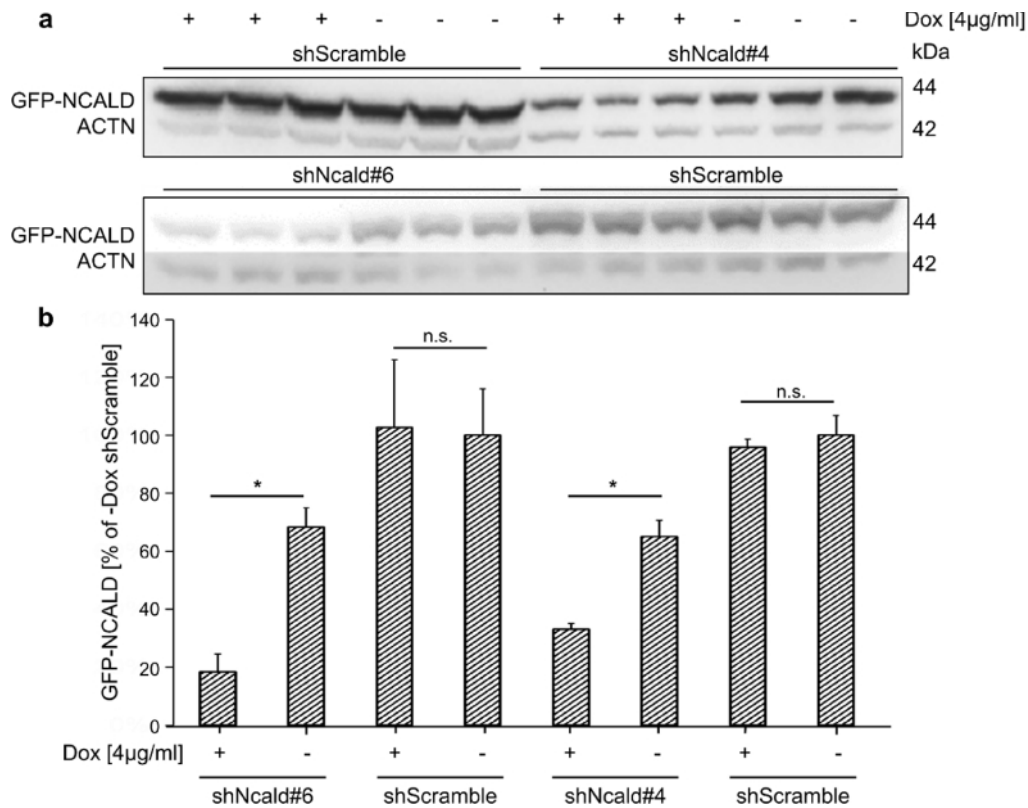


**Fig. 16: Efficient knock-down of GFP-NCALD upon Dox-mediated shRNA expression**

**a)** Western blot and **b)** quantification of GFP-NCALD knock-down in HEK293T cells co-transfected with *Ncald*-GFP and Dox-inducible shRNA#4 and shRNA#6. Addition of Doxycycline reduced GFP-NCALD to 33% (shRNA#4) and 18% (shRNA#6) of control levels. GFP-NCALD was not changed upon Doxycycline administration in HEK293T cells transfected with scramble shRNA.

The experiment was performed in triplicates. Statistical analysis was performed using two-tailed student's t-test. n.s. not significant, \* $P < 0.05$ .

### 5.1.2 Stable integration of the shRNA cassette in ES cells

Finally, we electroporated the targeting *Ncald*-shRNA vectors in combination with a vector expressing the C31 integrase, a protein needed for directional recombination into the Rosa26 locus of IDG26.10-3 murine embryonic stem (ES) cells. Following electroporation, the ES cells were cultured in selection conditions for ~10 days in the presence of G418 antibiotic to specifically select clones with integrated neomycin resistance cassette which would be a hallmark of successful recombination. Then individual clones were picked and expanded on two types of 96-well plates until confluence when they were treated as following: the feeder-coated plates were frozen and stored in -80°C for future expansion, whereas gelatin-coated plates were processed for DNA analysis.

The DNA analysis consisted of two PCR reactions:

- PCR Nr.1, where the forward primer was located in the pgk-promoter and the reverse in the neomycin gene, therefore the PCR product spanned the boundary between the Rosa26 locus and the integrated transgene and was obtained only when successful RMCE occurred (positive control of recombination);
- PCR Nr.2, where both primers aligned to the hygromycin gene, therefore the PCR product was obtained in ES clones with unchanged Rosa26 locus, suggesting an incomplete recombination, as the hygromycin gene was intended to be excised in the course of the RMCE (negative control of recombination) (see Fig. 11).

For clones that scored positive for PCR Nr.1 and negative for PCR Nr.2 a successful and complete recombination was anticipated. An exemplary agarose gel showing products of both PCRs for the screened ES clones is shown in Fig. 17.



**Fig. 17: Validation of the successful recombination in individual ES clones.**

PCR results of 12 first clones (A1-B4) from one 96-well plate are depicted: P stands for PCR Nr.1 (pgk-promoter), H stands for PCR Nr.2 (hygromycin) and M is the 100bp DNA ladder. All clones have undergone recombination (positive for PCR Nr.1) but in clones A2, A7, A8 and B2 (positive for PCR Nr. 2) the recombination was not complete as the hygromycin gene is still present.

Four ES clones with verified integration of the shRNA transgene were thawed and cultured in the presence of 4 µg/ml of Doxycycline. The degree of *Ncal*d knock-down was validated by qRT-PCR. All clones showed efficient *Ncal*d depletion following Dox induction, while no such effect was observed in the unrecombined IDG26.10-3 cell line without the shRNA transgene. The results of the qRT-PCR are depicted in Fig. 18.

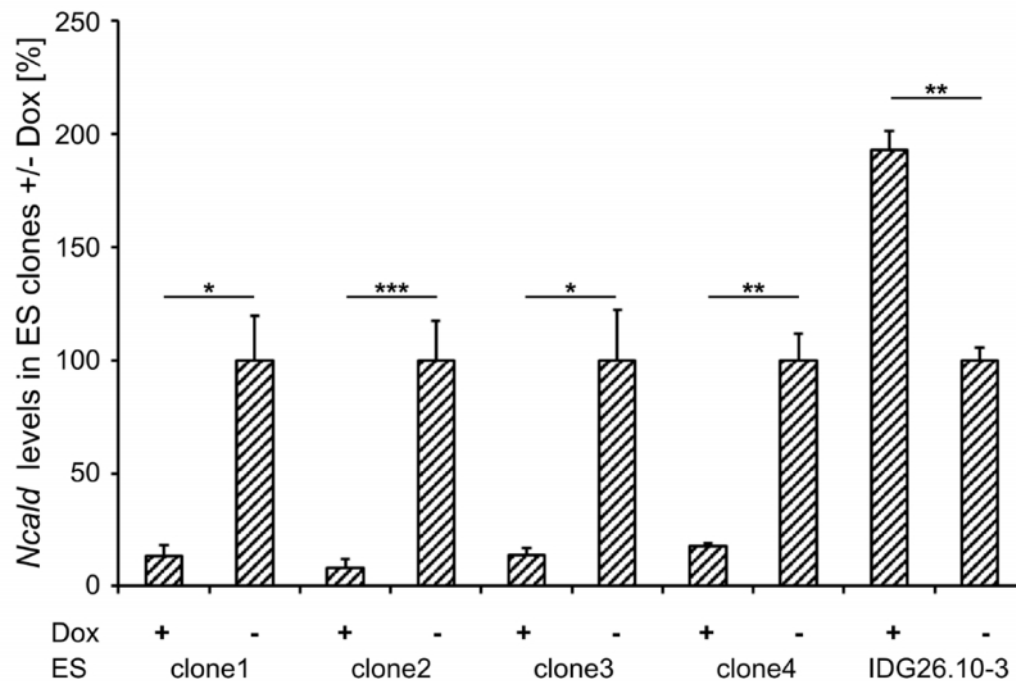


**Fig. 18: Quantification of *Ncald* in ES clones upon Doxycycline induction**

Clones 1-4 tested positive for the presence of the shRNA transgene and the unrecombined ES cell line IDG26.10-3 were cultured in the presence or absence of Doxycycline [4 µg/ml] for 120 h and subsequently the levels of *Ncald* were determined by qRT-PCR. For each clone the levels of the untreated sample were set to 100%. *Gapdh* was used as the housekeeping gene.

The experiment was performed in triplicates. Mean ± SEM. Statistical analysis was performed using the two-tailed student's t-test. n.s. not significant, \* $P < 0.05$ , \*\* $P < 0.01$ , \*\*\* $P < 0.001$ .

In the next steps the correctly integrated ES clones were supposed to be thawed, expanded and injected into blastocysts, which would then be implanted into pseudopregnant female mice to generate animals chimeric for the shRNA transgene. However, at this stage of our mouse generation project we learned that a *Ncald* knock-out mouse line is available at Jackson Laboratory (from April 2014, stock number #018575). As this mouse model was both viable and fertile in the homozygous state, we decided to stop the generation of the inducible *Ncald* knock-down mouse line and instead continue with a stronger genetic model to unequivocally determine the potential of NCALD reduction to improve the SMA phenotype.

## 5.2 Severe SMA mouse model with NCALD reduction – a transgene knock-out approach

The female and male *Ncald*<sup>ko/wt</sup> mice purchased from the Jackson Laboratory were on a pure C57BL6/N background (backcrossed for min. 7 generations) and therefore could be directly crossed with the SMA model used in our group.

The knock-out of mouse *Ncald* was achieved using the VelociGene strategy developed by the Regeneron company (for further details see also 4.2.5.7.2). This first targeting pipeline for mouse ES cells utilized bacterial artificial chromosome (BAC)-based targeting vectors to replace the coding sequence of the target gene with a *lacZ* reporter and promoter-driven neo selection cassette (Valenzuela et al. 2003). For the construction of targeting vectors, cDNA sequences surrounding the translation initiation and termination signals of each target gene were used, and in a single recombination, modified BAC ES clones were generated with gene deletion of up to 70 kb size. This strategy was therefore particularly suitable for targeting the large *Ncald* gene (> 426 kb).

As reported by the Jackson Laboratory, *Ncald*<sup>ko/ko</sup> mice were viable and fertile, but in our observation the fertility of homozygous knock-out mice was severely diminished compared to wildtype. Especially female *Ncald*<sup>ko/ko</sup> animals were not suited for breeding purposes: although they gave birth to living pups, in most cases they did not feed their offspring sufficiently and only very rarely litters of *Ncald*<sup>ko/ko</sup> dams survived to weaning. This phenotype was less exacerbated in *Ncald*<sup>ko/wt</sup> females, although also here the interval between pregnancies was noticeably longer than for wildtype. Surprisingly, *Smn*<sup>ko/wt</sup>; *Ncald*<sup>ko/wt</sup> females also showed a compromised maternal behavior, therefore, in order to obtain consistent conditions for the *in vivo* analysis of SMA pups, only *Smn*<sup>ko/wt</sup>; *Ncald*<sup>ko/wt</sup> males were used for breedings (see also Fig. 9). Another striking characteristic of *Ncald*<sup>ko/wt</sup> and *Ncald*<sup>ko/ko</sup> mice was a prominent weight reduction in comparison to wildtype.

### 5.2.1 Analysis of NCALD expression in wildtype, *Ncald*<sup>ko/wt</sup> and *Ncald*<sup>ko/ko</sup> mice

The protein analysis of diverse regions of CNS (hippocampus, cortex, cerebellum, spinal cord) as well as peripheral organs (various muscles: TVA, EDL, Gastrocnemius, Tibialis, as well as lung, kidney, liver and heart) confirmed the reported predominantly neuronal expression profile of NCALD, with strongest expression in the hippocampus and cortex. To a lesser degree NCALD could also be detected in peripheral organs: lung, liver and kidney. At comparable exposure time and equal amount of protein, very weak NCALD signal could be observed in muscle tissue or in the heart (Fig. 19a). Compared to SMN, NCALD showed overall much lower expression levels (Fig. 19b).



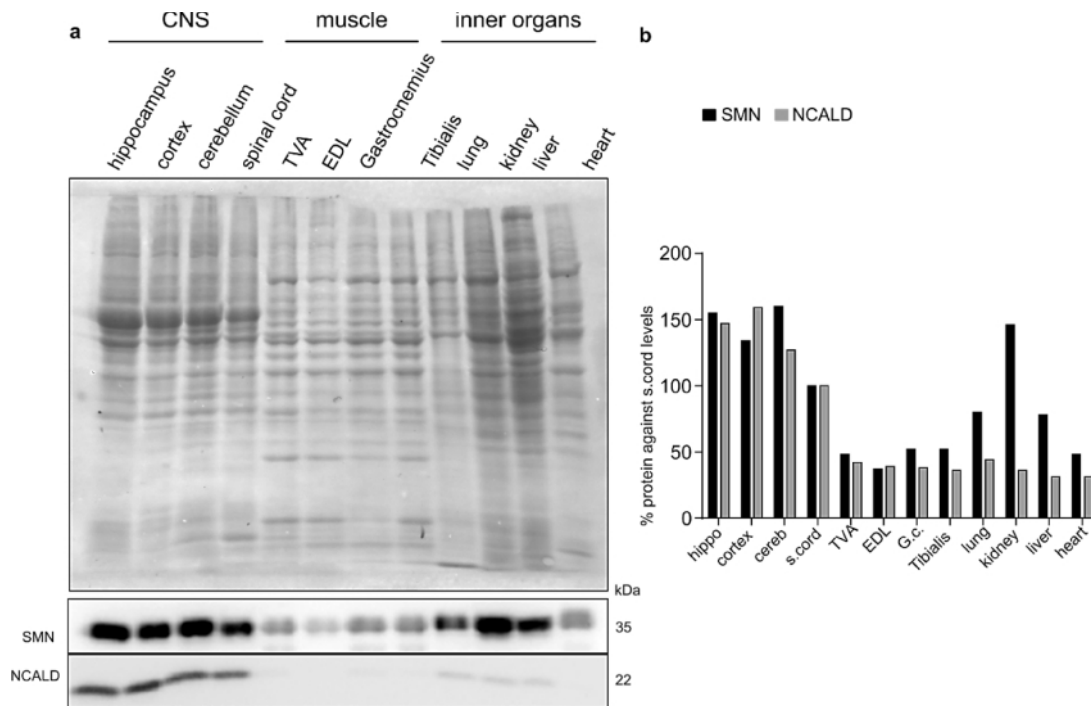


**Fig. 19: Analysis of NCALD expression in wildtype mouse tissue on PND10**

**a)** NCALD expression in different organs: CNS, skeletal muscles and peripheral organs. Stain-free gel was used to determine total protein level. Membrane was also probed with an anti-SMN antibody as a ubiquitous protein. **b)** Quantification of NCALD and SMN in various organs.

We analyzed the spinal cord and hippocampus samples of the *Ncald*<sup>ko</sup> mouse line by Western blotting. As expected, we could see that NCALD signal had reduced intensity in *Ncald*<sup>ko/wt</sup> mice and the band was completely absent in samples from *Ncald*<sup>ko/ko</sup> animals, confirming the specificity of the antibody and the complete knock-out of *Ncald* (Fig. 20).

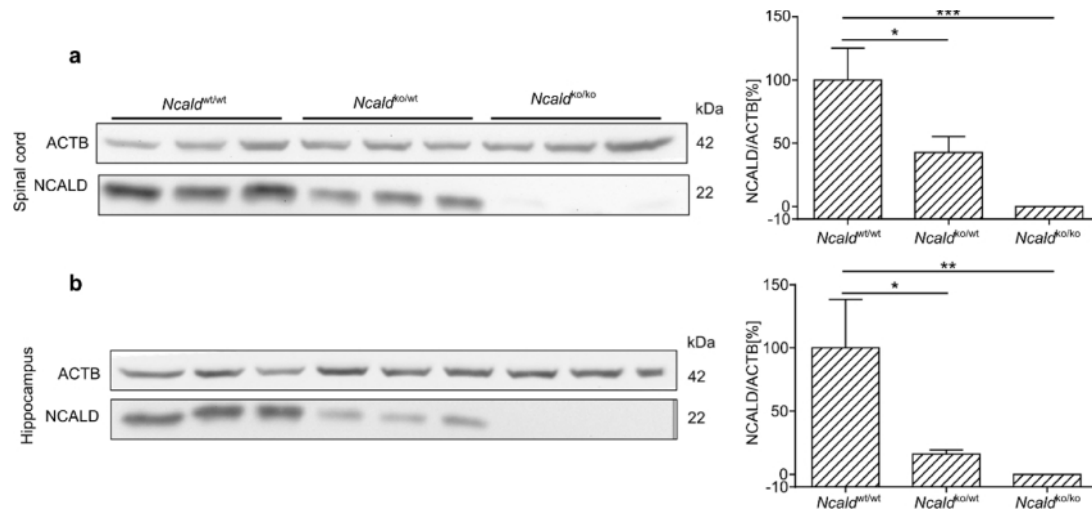


**Fig. 20: Analysis of NCALD expression in mutant mouse tissue on PND10**

**a)** Western blot of spinal cord and **b)** hippocampus lysates obtained from PND10 *Ncald*<sup>wt/wt</sup>, *Ncald*<sup>ko/wt</sup> and *Ncald*<sup>ko/ko</sup> mice. Already one *Ncald*<sup>ko</sup> allele decreased the NCALD levels to ~40% in spinal cord and ~20% in hippocampus. The NCALD specific band was absent in *Ncald*<sup>ko/ko</sup> animals.

The experiment was performed in triplicates. Mean ± SD. Statistical analysis was performed using the two-tailed student's t-test. \**P* < 0.05.

### 5.2.2 Crossing the *Ncald*<sup>ko</sup> allele in the severe SMA mouse model

In our group, the Taiwanese SMA mouse model has been used for *in vivo* studies (Hsieh-Li et al. 2000). In this model, to obtain offspring with SMA symptoms, the following two parental lines are crossed (Riessland et al. 2010):

- 1) *Smn*<sup>ko/wt</sup> – the mouse line is maintained in a heterozygous state as a complete *Smn* knock-out is embryonic lethal.
- 2) *Smn*<sup>ko/ko</sup>, *hSMN2*<sup>tg/tg</sup> – here the homozygous knock-out of mouse *Smn* is compensated by two transgene alleles, of which each carries two tandem copies of human *SMN2*. The animals survive till adulthood and are fertile; their only remaining phenotype common with severely affected SMA animals is the tail and ear necrosis.

Crossing these two parental lines gives rise to two possible genotypes as offspring:

- 1) *Smn*<sup>ko/ko</sup>, *hSMN2*<sup>tg/0</sup> – In short referred to as SMA mice, these mice are severely affected with motor neuronal and muscular defects as well as a multi-organ impairment. They show poor weight gain (after the disease symptoms start, they show gradually a substantial weight loss) and frequently develop diarrhea; depending on the genetic background, the mean survival ranges from 9.9 days (FVB) to 15.5 days (C57BL6/N) and 19.2 days (mixed

background 50% FVB:50% C57BL6/N) (Riessland et al. 2010, Ackermann et al. 2013, Schreml et al. 2013).

2) *Smn*<sup>ko/wt</sup>, *hSMN2*<sup>tg/0</sup> – In short referred to as HET mice and used as controls. These mice present generally an asymptomatic phenotype: their survival is not decreased and they reach adulthood. Their motor performance and their weight progression are normal (Ackermann et al. 2013).

As the generation of SMA animals carrying complete *Ncald* knock-out required a mouse line with three transgenes, we first pursued the analysis of heterozygous *Ncald* knock-out in SMA animals, particularly as this would better model the human phenotype of NCALD depletion and not a complete absence. For that, the following breeding scheme was used (see also Fig. 9):

*Ncald*<sup>wt/wt</sup>, *Smn*<sup>ko/ko</sup>, *hSMN2*<sup>tg/tg</sup> x *Ncald*<sup>ko/wt</sup>, *Smn*<sup>ko/wt</sup>, *hSMN2*<sup>0/0</sup>

The resulting offspring carried one of the four genotypes:

- 1) *Ncald*<sup>wt/wt</sup>, *Smn*<sup>ko/ko</sup>, *hSMN2*<sup>tg/0</sup> – identical with the SMA mice described above.
- 2) *Ncald*<sup>wt/wt</sup>, *Smn*<sup>ko/wt</sup>, *hSMN2*<sup>tg/0</sup> – identical with the HET mice described above.
- 3) *Ncald*<sup>ko/wt</sup>, *Smn*<sup>ko/ko</sup>, *hSMN2*<sup>tg/0</sup> – SMA mice with reduced NCALD levels due to the presence of one *Ncald*<sup>ko</sup> allele, in short referred to as SMA-*Ncald*<sup>ko/wt</sup> mice.
- 4) *Ncald*<sup>ko/wt</sup>, *Smn*<sup>ko/wt</sup>, *hSMN2*<sup>tg/0</sup> – HET mice with reduced NCALD levels, in short referred to as HET-*Ncald*<sup>ko/wt</sup> mice.

Animals of all four genotypes listed above were subjected to *in vivo* analyses concerning their survival, weight progression and motoric performance. In parallel, the effect of NCALD reduction on SMA phenotype was studied in motor neurons derived from E13 embryos, as well as in the spinal cord, muscle tissue and intestine obtained from PND10 mice of the four genotypes under study.

### 5.2.3 Phenotypic *in vivo* analysis of SMA-*Ncald*<sup>ko/wt</sup> mice: survival and weight

First, we monitored the survival and weight progression for all four genotypes (Fig. 21). Although NCALD reduction could rescue the effects of SMN reduction in other models (particularly those related to neuronal outgrowth and differentiation, e.g. neurite length in cells and axon length in zebrafish), in a severe SMA mouse model we did not observe any difference in mean survival between SMA and SMA-*Ncald*<sup>ko/wt</sup> mice (Fig. 21a). In parallel also the weight progression was monitored and the onset of SMA symptoms in this mouse

model started on PND5, as from this time point the weight between SMA and HET animals differed significantly and the difference increased, confirming the progressive nature of the disease (Fig. 21b). At all time points the weight of SMA and SMA-*Ncald*<sup>ko/wt</sup> animals was not statistically different. For both genotypes the death corresponded to a prior period of noticeable weight loss or stagnation (as opposed to a significant weight gain in HET littermates) and frequent diarrhea which underlines the involvement of gastrointestinal tract in the disease phenotype of the severe SMA mice (Sintusek et al. 2016).

While weight monitoring was only possible for up to 2 weeks on average for SMA animals, we were able to perform long time studies of HET and HET-*Ncald*<sup>ko/wt</sup> animals (Fig. 21c). Interestingly, the weight of HET and HET-*Ncald*<sup>ko/wt</sup> mice differed significantly onwards from 8 weeks of age. Most strikingly, upon reaching the adulthood at ~ 8 weeks of age the HET-*Ncald*<sup>ko/wt</sup> animals have reached almost their final weight while their HET counterparts continued to gain weight. The difference in mean body weight was irrespective of the sex but more pronounced in male mice (significant difference between HET and HET-*Ncald*<sup>ko/wt</sup> male started already from week 8<sup>th</sup>). Upon dissection the decreased body weight manifested itself at the level of adipose tissue, which was abundant in HET animals subcutaneously, peritoneally and epigonadally, but present at a strikingly lower amount in HET-*Ncald*<sup>ko/wt</sup> animals. Already the absence of one *Ncald* gene copy was sufficient to trigger the lower body weight, which was not exasperated by the complete loss of NCALD as the weight of HET-*Ncald*<sup>ko/wt</sup> and HET-*Ncald*<sup>ko/ko</sup> animals was not significantly different at any time point observed, despite the latter showing a trend to lower values (Fig. 21c). This observation suggested that NCALD plays a crucial role in regulating body weight, particularly concerning the body composition and the amount of adipose tissue. In SMA-*Ncald*<sup>ko/wt</sup> animals this effect of NCALD reduction on body weight was not pronounced, presumably because it did not yet manifest during their shortened lifespan. In conclusion, elucidating the mechanism how NCALD affects body weight should be the subject of future studies.

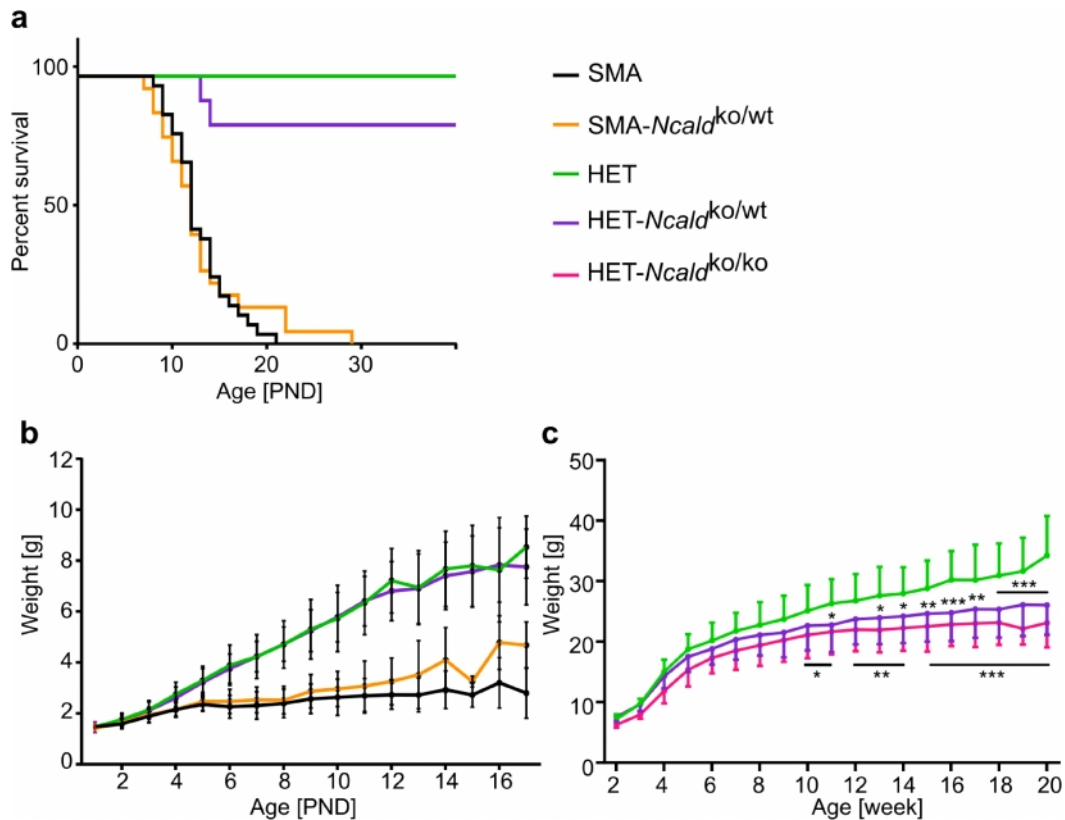


**Fig. 21. Survival and weight studies of SMA-*Ncalcd*<sup>ko/wt</sup> mice**

**a**) Mean survival was not changed between SMA ( $12.9 \pm 3.2$  days,  $n=28$ ) and SMA-*Ncalcd*<sup>ko/wt</sup> mice ( $13.1 \pm 5.3$  days,  $n=22$ ). Survival of both genotypes was not different from each other but highly significantly different from HET controls. Significance of the survival curves was assessed with the Mantel-Kox log-rank test. **b**) During the time period represented on the graph mean body weight did not differ significantly between of SMA and SMA-*Ncalcd*<sup>ko/wt</sup> mice; at the same time, body weight of both SMA groups was significantly smaller from both HET groups, starting from PND5. SMA  $n=18$ , SMA-*Ncalcd*<sup>ko/wt</sup>  $n=25$ , HET:  $n=30$ , HET-*Ncalcd*<sup>ko/wt</sup>:  $n=34$ . **c**) Mean body weight of HET-*Ncalcd*<sup>ko/wt</sup> mice was significantly reduced when HET-*Ncalcd*<sup>ko/wt</sup> to HET littermates from the 11<sup>th</sup> week of life onward. HET:  $n=14$ , HET-*Ncalcd*<sup>ko/wt</sup>:  $n=28$ , HET-*Ncalcd*<sup>ko/ko</sup>:  $n=11$ . The significance calculated against HET controls is indicated above the line for HET-*Ncalcd*<sup>ko/wt</sup> mice and below the line for HET-*Ncalcd*<sup>ko/ko</sup> mice. Mean  $\pm$  SD.

For statistical analysis of the weight studies two-way ANOVA with Tukey correction for multiple comparison was applied. \* $P < 0.05$ , \*\* $P < 0.01$ , \*\*\* $P < 0.001$ .

#### 5.2.4 Phenotypic *in vivo* analysis of SMA-*Ncalcd*<sup>ko/wt</sup> mice: motoric skills

Previous studies by our and other groups reported affected motoric skills in SMA animals as compared to HET littermates. As the SMA mice die usually in the first two weeks of age, the motoric tests have to be suitable for neonatal mice, while still reflecting the muscle strength and performance. The SMA research community has been applying various tests to address this issue: tail-suspension test (self-clasping), negative geotaxis, righting reflex (scored proportionally to the time needed to right) and hind-limb suspension test (also known as the tube test). The last assay was specially developed to assess the muscle

strength of proximal hind limbs in neonatal rodents (between PND2 and 12) and following parameters can be evaluated: the latency to fall (in seconds), the number of pulls and the hind-limb position (El-Khodori et al. 2008). In our group the last two assays have previously been used for studies of modifier genes as well as therapeutic treatments (Garbes et al. 2009, Riessland et al. 2010, Ackermann et al. 2013, Schreml et al. 2013). Therefore, we used both the righting reflex test and the tube test to analyze the motoric skills of the four genotypes under study.

The results of the righting reflex test showed that except for very early time point, SMA-*Ncalcd<sup>ko/wt</sup>* animals needed on average more time to right themselves than SMA littermates, and this difference was significant on PND6 and PND9 (Fig. 22a). SMA-*Ncalcd<sup>ko/wt</sup>* mice performed also significantly worse than HET animals through the symptomatic period (from PND6 till PND11).

The tube test was less sensitive than the righting reflex test, although to guarantee consistency it was in > 90% performed by the same operator (Fig. 22b). We saw that SMA animals performed on average better than SMA-*Ncalcd<sup>ko/wt</sup>* mice and this difference was significant on PND12.

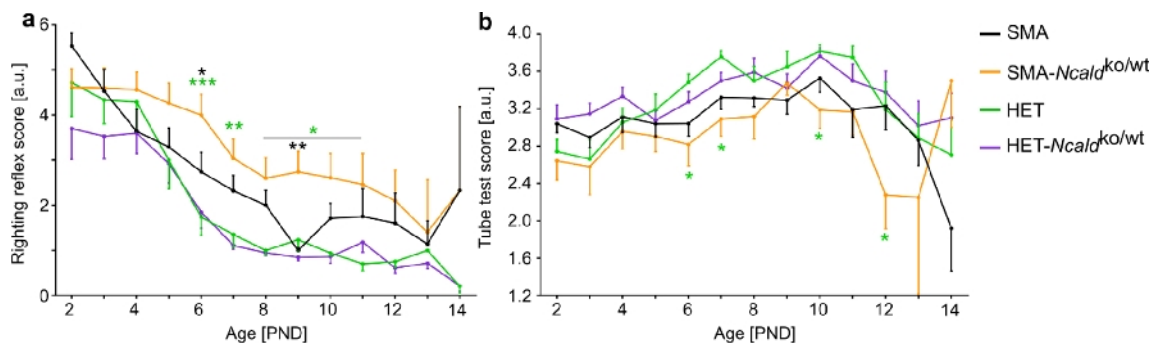


**Fig. 22. Evaluation of motoric skills of SMA-*Ncalcd<sup>ko/wt</sup>* mice**

NCALD reduction did not improve motoric performance of SMA-*Ncalcd<sup>ko/wt</sup>* mice in comparison to SMA littermates as assessed by **a)** righting reflex test or **b)** tube test. The mean number of animals evaluated for motoric performance per day: SMA: n=20, SMA-*Ncalcd<sup>ko/wt</sup>*: n=17, HET: n=27, HET-*Ncalcd<sup>ko/wt</sup>*: n=30.

For both motoric tests two-way ANOVA with Tukey correction for multiple comparisons was applied. \* $P < 0.05$ , \*\* $P < 0.01$ , \*\*\* $P < 0.001$ . The significance is indicated for SMA-*Ncalcd<sup>ko/wt</sup>* mice in comparison to SMA (black stars) or HET (green stars) littermates.

In conclusion, the tests evaluating motoric skills need to be improved in order to detect apparently subtle differences in the motoric skills of SMA-*Ncalcd<sup>ko/wt</sup>* mice: in the righting reflex test, the time of observation could be extended to 30 seconds (instead of 10) and in the tube test, latency to fall could be added as a second parameter.

Parallel to our *in vivo* phenotypic studies, we set out to analyze the effect of NCALD reduction on the neuromuscular system, which is known to be primarily affected in SMA. First, we cultured spinal motor neurons *in vitro* and evaluated the axonal length under reduce NCALD. Then we performed multiple morphological analyses in tissues obtained from PND10 mice: we quantified the glutamatergic inputs on motor neurons, the cell size of spinal motor neurons *in vivo*, the neuromuscular junction area in the *Transversus abdominis* (TVA) muscle and the muscle fiber size in (EDL) muscle. Eventually, we evaluated histologically the intestine as a representative non-neuronal organ, where defects have been also reported in severe SMA mouse models (Sintusek et al. 2016). In these analyses all four genotypes were included (SMA, SMA-*Ncald*<sup>ko/wt</sup>, HET, HET-*Ncald*<sup>ko/wt</sup>), with minimum three animals of each genotype. All analyses were performed in a blinded manner, i.e. the genotypes of the animals were encrypted before the actual analysis and decoded only after the final data have been collected.

#### 5.2.5 NCALD reduction in motor neurons from SMA mice restored axonal outgrowth *in vitro*

To analyze the effect of NCALD reduction on the primary tissue affected in SMA, we cultured spinal motor neurons from E13 embryos of the four genotypes listed above. We confirmed that NCALD levels were reduced in SMA-*Ncald*<sup>ko/wt</sup> and HET-*Ncald*<sup>ko/wt</sup> motor neurons by Western blotting (Fig. 23a).

The motor neurons were fixed at DIV6 and the total axonal length, length of the longest axon and the number of branches were evaluated. The quantification results as well as representative images of all four genotypes are depicted in Fig. 23b-e.

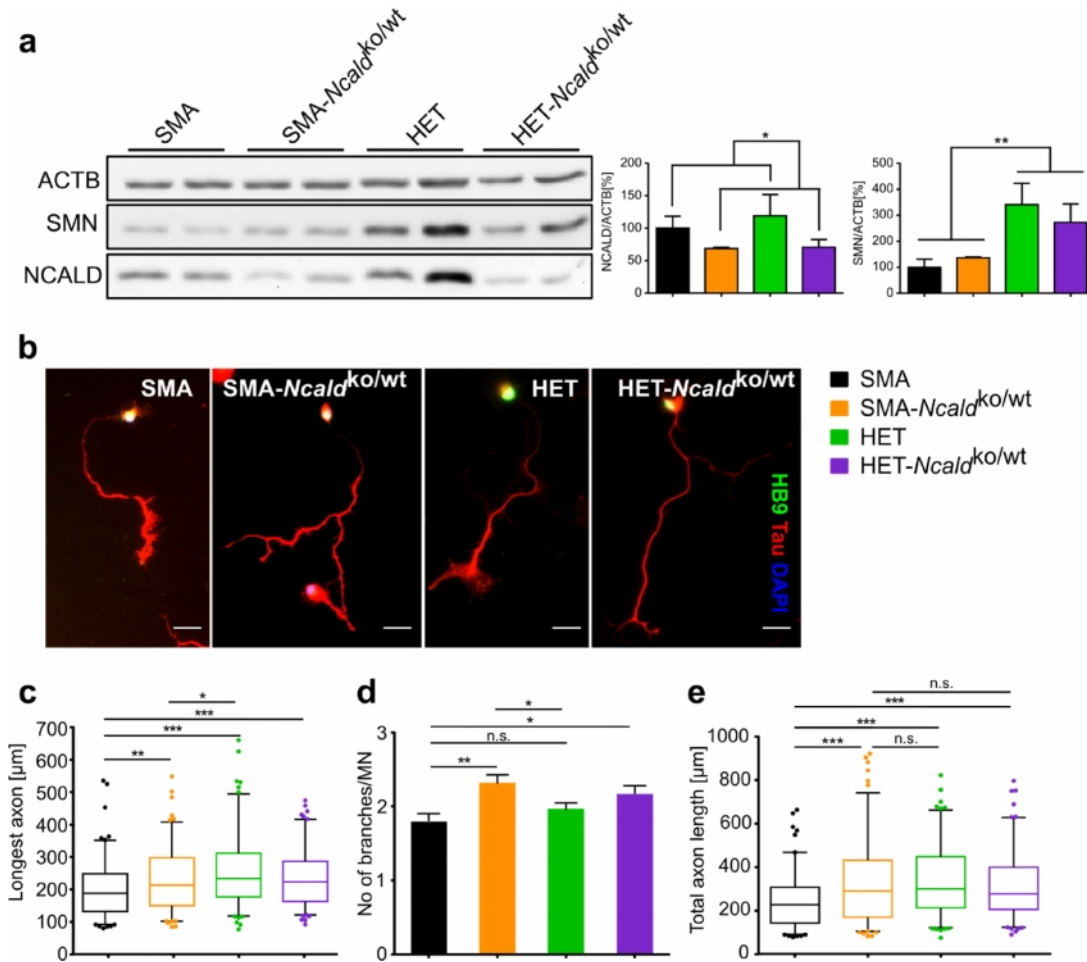


**Fig. 23: Motor neurons from SMA-*Ncald*<sup>ko/wt</sup> mice show longer axons and increased branching than SMA mice**

**a)** Western blot and quantification of NCALD and SMN expression in lysates from motor neurons of indicated genotypes. N = 2 samples per genotype. Mean  $\pm$ SD. **b)** Representative images of motor neurons of all genotypes analyzed stained with antibodies against HB9 (green, motor neuron soma) and Tau (red, axons) and DAPI (blue, nucleus). Scale bar, 25  $\mu$ m. **c)** The mean length of the longest axon was determined for all genotypes. Motor neurons from SMA-*Ncald*<sup>ko/wt</sup> embryos developed *in vitro* longer axons than from SMA littermates, although the rescue did not reach HET levels. **d)** The mean number of branches per MN was determined. NCALD reduction resulted in an increased branching both in SMA-*Ncald*<sup>ko/wt</sup> and HET-*Ncald*<sup>ko/wt</sup> MNs. **e)** The cumulative length of the longest axon and its branches was determined for all genotypes. This total axon length was highly significantly improved in SMA-*Ncald*<sup>ko/wt</sup> MNs when compared to SMA ones and did not differ between SMA-*Ncald*<sup>ko/wt</sup>, HET and HET-*Ncald*<sup>ko/wt</sup> MNs.

For all genotypes at least 120 MNs in total were evaluated, from three embryos from three different litters. The analysis was performed double-blinded (the genotypes were disguised during the image acquisition and the data analysis). Statistical analysis was performed using two-tailed student's t-test. n.s. not significant, \* $P < 0.05$ , \*\* $P < 0.01$ , \*\*\* $P < 0.001$ .

As predicted from previous experiments, where NCALD reduction by RNAi rescued the axon length of SMA motor neurons (Riessland et al. under review), also genetic ablation of NCALD resulted in longer axons in motor neurons derived from SMA-*Ncald*<sup>ko/wt</sup> embryos. This effect could be already observed when only the longest axons were measured (Fig.



23b). Moreover, we noticed an enhanced branching both in SMA-*Ncal*<sup>ko/wt</sup> and HET-*Ncal*<sup>ko/wt</sup> motor neurons, which was in line with the phenotype observed in *smn+ncald* MO zebrafish.

#### 5.2.6 Neuromuscular junctions of SMA-*Ncal*<sup>ko/wt</sup> mice show larger AChR clusters

As SMA is primarily a disease of neuromuscular system, we focused our attention on the synapse which is crucial for this system, namely at the neuromuscular junction (NMJ). It is known that NMJs in SMA mice show the following abnormalities: smaller area covered by acetylcholine receptors (AChR), which can be visualized with fluorescently labeled Bungarotoxin, delayed maturation both on a morphological level (as determined by the structural complexity of the endplate) (Gogliotti et al. 2012) and molecular level (retention of fetal Z-agrin) (Kong et al. 2009), as well as prolonged polyinnervation (Torres-Benito et al. 2011).

As not all muscles are equally affected by the SMA-related atrophy, with the more proximal muscles showing a more severe impairment, we selected for analysis *Transversus abdominis* (TVA), a muscle of the anterior and lateral abdominal wall which has been widely studied in the context of SMA (Murray et al. 2008). TVA is crucial for compressing ribs and viscera as well as involved in expiration. The muscle samples were prepared as in 4.2.5.15 and subsequently the size of the Bungarotoxin-positive endplates was assessed (Fig. 24).

The area occupied by AChR as visualized by rhodamine-labelled bungarotoxin (BTX) was significantly smaller in SMA animals than in HET controls. At the same time, the AChR area was significantly increased in SMA-*Ncal*<sup>ko/wt</sup> animals when compared to SMA littermates, yet it did not reach the levels of HET animals (SMA:  $140.5 \pm 22.8 \mu\text{m}^2$ , SMA-*Ncal*<sup>ko/wt</sup>:  $174.1 \pm 9.2 \mu\text{m}^2$ , HET:  $246.5 \pm 18.9 \mu\text{m}^2$ . Mean  $\pm$  SEM). This finding was the first indication that NCALD suppression in a mammalian SMA model might actually improve structures known to be affected in SMA. This is of particular importance, as NMJ is increasingly acknowledged as the structure where the SMA pathogenesis is initiated (Boido and Vercelli 2016), underlining the axonopathic character of this disease. Recent findings highlight the contribution of skeletal muscle to the SMA phenotype (Fayzullina and Martin 2014) and neuromuscular junction is the synapse which requires the proper cross-talk of axon and muscle fiber to be formed and maintained.

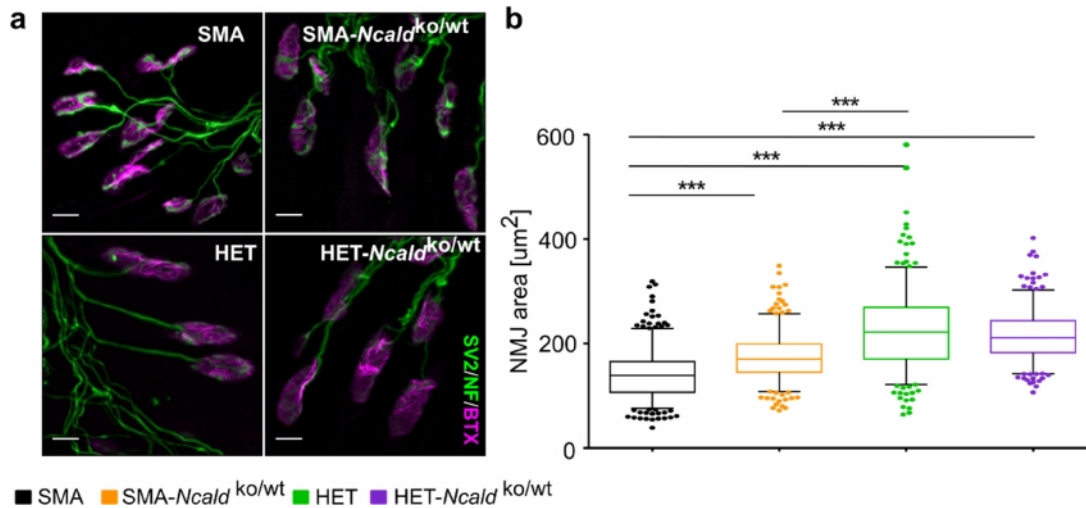


**Fig. 24: Analysis of NMJ size in the TVA muscle of PND10 mice**

a) Representative images and b) quantification of mean Bungarotoxin-positive NMJ area in the TVA of PND10 animals of all four genotypes under study, stained with antibodies against SV2 and NF (green) and Bungarotoxin (BTX, magenta) to visualize the AChR clusters. The mean NMJ area of SMA-*Ncald*<sup>ko/wt</sup> mice is significantly larger than in SMA littermates but does not reach the levels of HET animals. Scale bar, 10 μm. Bars depict the values within the 25-75% range, whiskers cover the 5-95% range.

For all genotypes at least three animals were analyzed, 100-120 NMJs were measured per animal. The analysis was performed double-blinded. Statistical analysis was performed using two-tailed student's t-test. \*\*\*  $P < 0.001$ .

We extended our initial analysis with two further time points to include a presymptomatic stage at PND5 and a late symptomatic stage at PND13. At PND5 the difference in the NMJ area was already significant between SMA and HET animals, which is in line with the NMJ defect being one of the earliest SMA defects (Ling et al. 2012, Yoshida et al. 2015). The NMJ area in the TVA of SMA-*Ncald*<sup>ko/wt</sup> animals was not significantly different from SMA littermates (SMA:  $126.5 \pm 14.6 \mu\text{m}^2$ , SMA-*Ncald*<sup>ko/wt</sup>:  $125.2 \pm 28.4 \mu\text{m}^2$ . Mean  $\pm$  SEM); however, for all genotypes except for SMA mice, the NMJ area increased between PND5 and PND13 (Fig. 25a). These results indicate that NCALD reduction counteracts the developmental impairment of the NMJ synapse in SMA mice.

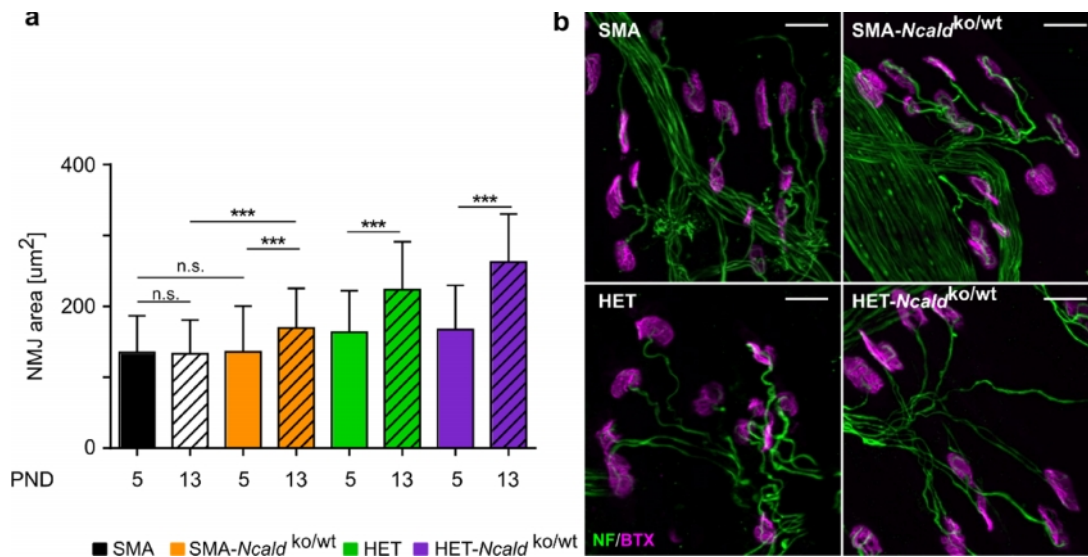


**Fig. 25: Analysis of NMJ size in the TVA muscle of PND5 and PND13 mice**

**a)** Quantification of mean Bungarotoxin-positive NMJ area in the TVA of PND5 and PND13 animals of all four genotypes under study. Mean SD. **b)** Representative images of NMJs in the TVA muscle on PND13 stained with an antibody against NF (green) and Bungarotoxin (BTX, magenta) to visualize the AChR clusters. No denervation was observed in PND13 SMA mice, confirming that in this mouse model denervation is not a prominent phenotype, even at the late stage of the disease. Scale bar, 25 μm. For all genotypes and time points at least three animals were analyzed, 100-120 NMJs were measured per animal. Mean ± SD. Statistical analysis was performed using two-tailed student's t-test. n.s. not significant, \*\*\* $P < 0.001$ .

We observed that practically all endplates in the TVA muscles received axonal inputs, even at the late disease stage on PND13 (Fig. 25b), which is in line with a recent study reporting only very limited denervation in the Taiwanese SMA model (Lin et al. 2016).

### 5.2.7 Number of glutamatergic inputs on spinal cord motor neurons is increased in SMA-*Ncald*<sup>ko/wt</sup> mice

The motor neurons are the cell type most severely affected in SMA both in their number and size (Monani et al. 2000), with specifically alpha motor neurons degenerating and gamma motor neurons being spared in the spinal cord of SMA mice (Powis and Gillingwater 2016). It was reported that additionally to the actual atrophy of motor neurons an impairment in their neuronal circuitry is visible as assessed by the number of glutamatergic inputs from interneurons signaling on motor neurons, although whether this is the cause or rather the consequence of motor neuron soma impairment is under debate (Mentis et al. 2011, Gogliotti et al. 2012). We studied the effect of NCALD reduction on spinal motor neuronal circuitry in PND10 mice by determining the average number of VGlut1 positive inputs per motor neuron soma in lumbar spinal cord sections (Fig. 26). We confirmed that SMA motor neurons had significantly less VGlut1+ inputs than HET controls, particularly those neurons with soma volume greater than 5000 μm<sup>3</sup>. Although our

analysis did not involve a systematic motor neuron counting, we observed in the analyzed population that in SMA animals the average motor neuron volume was smaller than in HET due to a higher proportion of smaller neurons ( $<5000\mu\text{m}^3$ ). NCALD reduction did not increase the average motor neuron volume in SMA-*Ncald*<sup>ko/wt</sup> animals, rather the opposite, as the proportion of smaller motor neurons increased (SMA:  $3445 \pm 1803 \mu\text{m}^3$ , SMA-*Ncald*<sup>ko/wt</sup>:  $3096 \pm 1453 \mu\text{m}^3$ , HET:  $4173 \pm 1996 \mu\text{m}^3$ . Mean  $\pm$  SD) (Fig. 26b). However, NCALD reduction resulted in a significant increase of the mean number of VGlut1+ inputs number per motor neuron soma, suggesting an improvement to the motor neuronal circuitry (Fig. 26a). This effect correlated with the NCALD reduction independently of SMN deficiency, as in the HET-*Ncald*<sup>ko/wt</sup> animals the number of VGlut+ inputs was the highest and was significantly increased in comparison to HET littermates (SMA:  $14.3 \pm 0.4$ , SMA-*Ncald*<sup>ko/wt</sup>:  $17.6 \pm 0.5$ , HET:  $19.2 \pm 0.9$ , HET-*Ncald*<sup>ko/wt</sup>:  $27 \pm 0.9$ . Mean  $\pm$  SEM). It is possible that the effect of NCALD reduction is even stronger in sensory neurons as NCALD expression is supposedly higher in those neurons. As we observed that lower NCALD levels are associated with increased branching in zebrafish, it is possible that also the axons of sensory neurons show this phenotype, resulting in more synaptic contacts on the motor neuron soma.

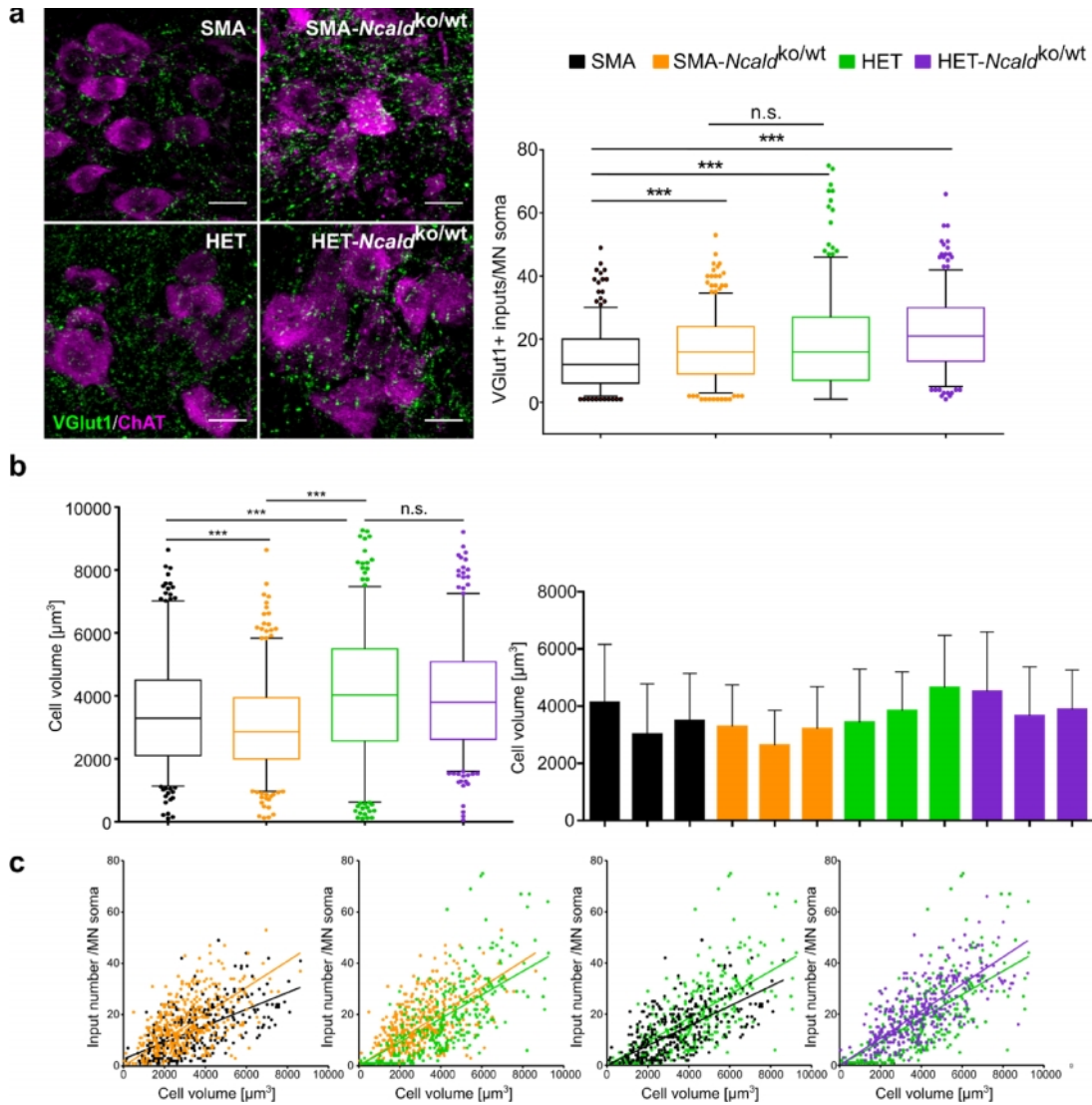


**Fig. 26: Evaluation of glutamatergic inputs on spinal motor neuron soma in SMA-*Ncald*<sup>ko/wt</sup> mice**

**a)** Representative images and quantification of glutamatergic inputs on motor neuron soma. Mean number of VGlut1+ inputs pro motor neuron was increased in spinal cords derived from PND10 SMA-*Ncald*<sup>ko/wt</sup> mice (SMA =  $14.3 \pm 10$ , SMA-*Ncald*<sup>ko/wt</sup> =  $17.6 \pm 9$ . Mean  $\pm$  SD). Spinal cord sections were stained with antibodies against ChAT (magenta) to visualize motor neuron soma and VGlut1 (green) to visualize glutamatergic inputs. Scale bar, 25 μm. **b)** The distribution of cell volume values within a genotype (left panel) and mean values for individual animals (right panel). The motor neuron volume is smaller in SMA animals that in HET controls and is not increased by NCALD reduction, on the contrary, it is further decreased. Bars depict the values within the 25-75% range, whiskers cover the 5-95% range. **c)** Despite smaller volume of motor neuron soma, the higher number of VGlut1+ inputs per motor neurons translated to a steep increase in the input/μm<sup>3</sup> ratio in SMA-*Ncald*<sup>ko/wt</sup> mice.

For each genotype, three animals were analyzed and 100 motor neurons were analyzed per animal. The analysis was performed double-blinded (the genotypes were disguised during the image acquisition and the data analysis). Statistical analysis was performed using two-tailed student's t-test. n.s. not significant, \*\*\* $P < 0.001$ .

### 5.2.8 Muscle fiber size is not changed in the EDL of SMA-*Ncal*<sup>ko/wt</sup> mice

Historically, in SMA the motor neuron degeneration was acknowledged as the primary disease mechanism and the target for treatment, while muscle weakness and paralysis in SMA were viewed as secondary effects (Dubowitz 2009, Hamilton and Gillingwater 2013, Simone et al. 2016). Recent decades, however, have advanced the knowledge of the intricate interaction between motor neurons and the muscles they innervate. Therefore, many studies attempted to elucidate whether the severe reduction of muscle fiber size observed in SMA mice is indeed secondary to defective neuromuscular transmission or possibly the result of intrinsic muscle abnormalities (Ruiz et al. 2010, Lee et al. 2011). Cellular and molecular analyses unraveled a number of abnormalities in myofibers from SMA patients and mouse models: enhanced degeneration, altered expression of myogenic genes crucial for muscle development (MyoD and myogenin) and myotube formation deficits (Braun et al. 1995, Boyer et al. 2014, Bricceno et al. 2014). Recent studies addressed also the question about the temporal relation between muscular and motoneuronal defects and found quite unexpectedly that SMA-related muscle defects occur early in the disease progression and independently of motor neuron cell death: when the extent of cell death was assessed by the degree of apoptosis (evaluated histologically by H&E stainings and TUNEL assays) and DNA fragmentation, in the muscle the damage was visible already at birth (on PND0) and increased till PND8, while on PND5 no loss of motor neurons or any other pathologies in the ventral horns of the spinal cord could be observed and only on PND8 DNA fragmentation was visible in spinal cord (Fayzullina and Martin 2014).

The debate about muscle-intrinsic defects in SMA was based largely on an early study which showed that SMN restoration specifically in muscle tissue did not ameliorate the SMA phenotype as assessed by lifespan and motor performance, in contrast to neuronal SMN expression (Gavrilina et al. 2008). However, the SMN expression in muscle was controlled by the human actin promoter that is not active in satellite cells and myoblasts, which were both reported to show impairment upon low SMN levels (Nicole et al. 2003, Shafey et al. 2005).

To test whether NCALD reduction exert a positive effect on the muscle, we analyzed the diameter of muscle fibers in *Extensor digitorum longus* (EDL), a hind limb muscle which was reported to be affected in the SMA mice and importantly, to respond to therapy (Naryshkin et al. 2014) (Fig. 27).

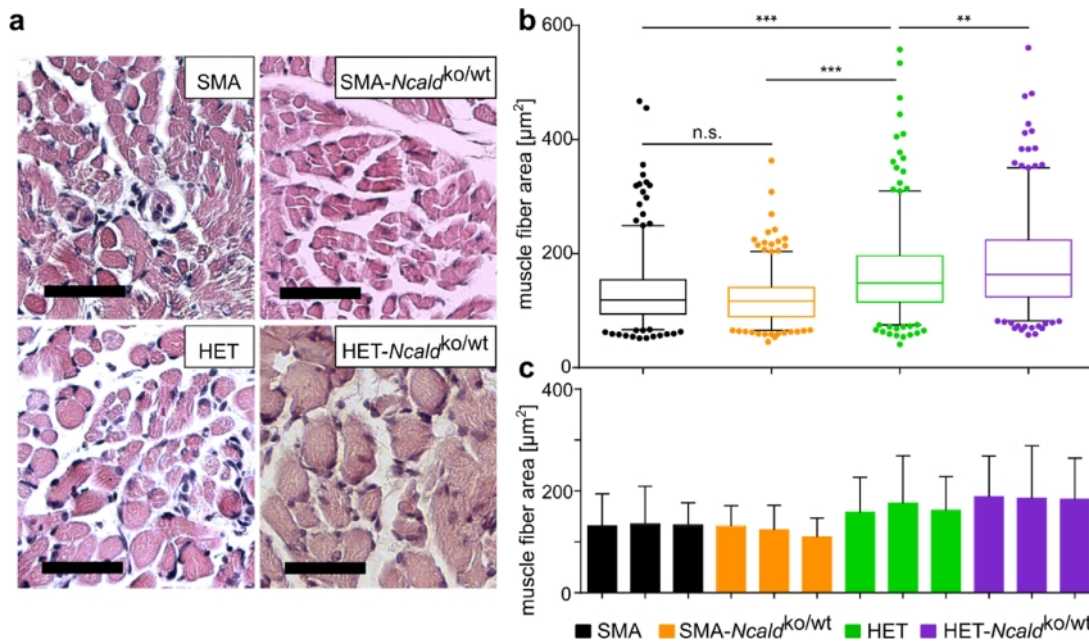


**Fig. 27: Analysis of the muscle fiber size in the EDL of PND10 mice**

a) Representative images of H&E stainings of 7 μm paraffin sections of the EDL muscle. The difference in muscle fiber size is clearly visible between SMA and HET animals. Scale bar, 50 μm. b) The quantification of muscle fiber size shows no difference between SMA and SMA-*Ncald*<sup>ko/wt</sup> mice which both showed lower values than HET animals. Interestingly, the muscle fiber size was significantly increased in HET-*Ncald*<sup>ko/wt</sup> compared to HET littermates. c) Mean values presented as bars for individual mice show little degree of variability within genotype. Mean ± SD.

For each genotype three animals were analyzed and 100 muscle fiber were measured per animal. The analysis was performed double-blinded (the genotypes were disguised during the image acquisition and the data analysis). Statistical analysis was performed using two-tailed student's t-test. n.s. not significant, \*\* $P < 0.01$ , \*\*\* $P < 0.001$ .

The fact that in no improvement could be observed in muscle fiber size can be explained by extremely low NCALD expression in this tissue, as we could not detect NCALD by Western blotting in various muscles (see Fig. 19). Moreover, in the severe SMA model under study the skeletal muscle is affected early in the disease, as some abnormalities were reported already at birth (Fayzullina and Martin 2014). Another hypothesis is that SMN levels in the muscle are too low and the resulting muscle-specific defects too severe so that the *Ncald*<sup>ko/wt</sup>-mediated improvement at the MN soma and the NMJ does not translate to the muscle in the severe SMA animals. This hypothesis was further tested in 5.3.6.

#### 5.2.9 SMA-*Ncald*<sup>ko/wt</sup> mice suffer from impairment of peripheral organs outside of CNS

The fact that we could see improvement of some motor neuronal characteristics of the SMA phenotype upon NCALD reduction, but not of the overall phenotype as monitored by



survival and weight, is partially explained by the fact that this SMA model is known to be severely affected and shows impairment of multiple organs apart from the neuromuscular system, particularly heart, lungs and intestine, as well as liver, pancreas and kidneys (Ackermann et al. 2013, Schreml et al. 2013, Bowerman et al. 2014). Histological sections of the intestine confirmed this hypothesis, showing for both SMA and SMA-*Ncalcd*<sup>ko/wt</sup> mice reduced number and frequently changed shape of villi (many were blunt-ended), edema in the lamina propria and occasional dilation of the lacteals (Fig. 28), which were all reported abnormalities in SMA animals, and absent in the HET littermates (Schreml et al. 2013). In line with these intestinal defects, diarrhea was frequently observed in SMA and SMA-*Ncalcd*<sup>ko/wt</sup> animals.

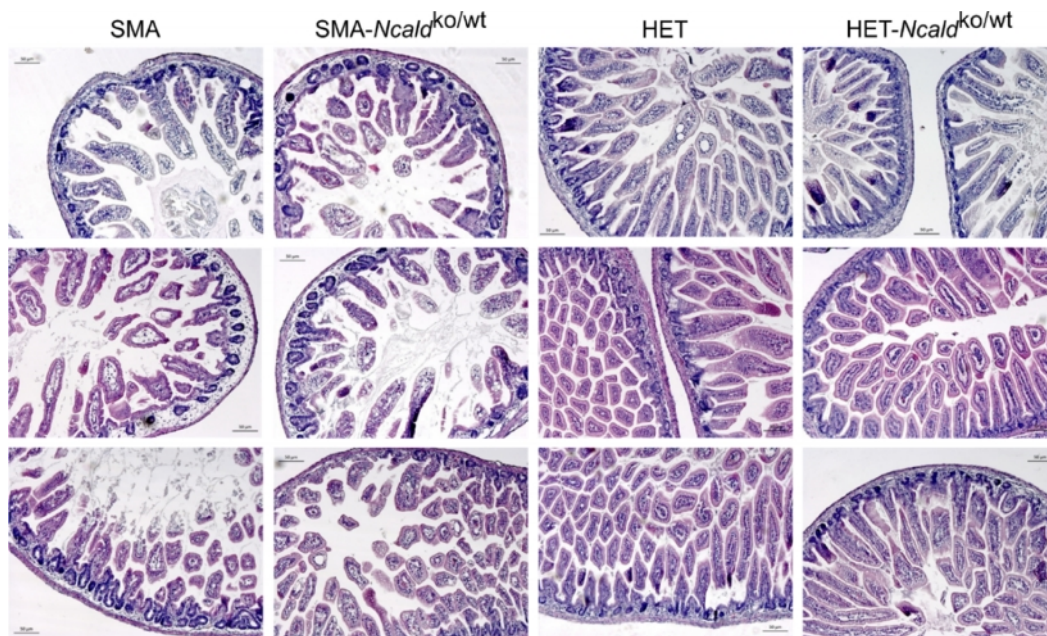


**Fig. 28: The intestinal impairment in the severe SMA mouse model**

Representative images of H&E stainings of 7  $\mu$ m paraffin sections from the small intestine of PND10 SMA, SMA-*Ncalcd*<sup>ko/wt</sup>, HET and HET-*Ncalcd*<sup>ko/wt</sup> animals. The intestine of both SMA and SMA-*Ncalcd*<sup>ko/wt</sup> mice shows abnormalities such as decreased number of villi and edema in the lamina propria (marked by black arrowheads). Scale bar, 50  $\mu$ m. Three animals per each genotype were analyzed.

Another cause of this selective phenotype improvement might be the predominantly neuronal specificity of NCALD expression, which likely does not extend to other tissues affected in SMA (see Fig. 19). Therefore, we decided to analyze how NCALD reduction affects SMA phenotype in an intermediate mouse model where the impairment of most organs is at least moderately ameliorated and the survival is prolonged to 3-4 weeks.



### 5.3 Intermediate SMA mouse model with NCALD reduction – an SMN-ASO approach

As other work performed in our group proved that protective modifiers identified in humans have the potential to improve survival of an intermediate SMA model (Hosseinibarkooie 2016), we applied this model to test whether the protective effect of NCALD reduction is possibly greater provided that SMN levels are sufficiently increased. Importantly, also in the *SMN1*-deleted asymptomatic individuals (see Fig. 5) there are four *SMN2* copies present, and not only two as in the severe SMA model.

The model we used is generated by a treatment with subphenotypic doses of an antisense oligonucleotide (SMN-ASO) (Hua et al. 2011). The SMN-ASO (in the following chapters referred to as ASO) is directed against an intronic splicing silencer (ISS) present in intron 7 of *SMN2* and by masking this ISS it leads to an increase of SMN expression from *SMN2* transgene in the mice (Fig. 29).

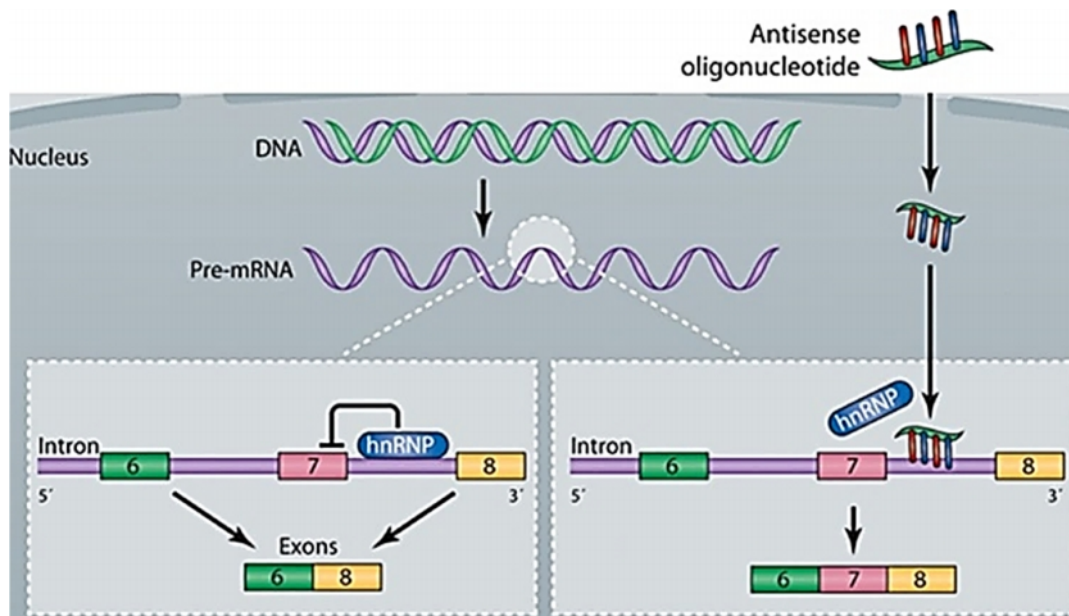


**Fig. 29: SMN-ASO mode of action**

The SMN-ASO targets the 10-27 bp of *SMN2* intron 7 and blocks the binding of the hnRNP to the ISS. As a result, exon 7 is not skipped during splicing but gets included in the *SMN2* transcript, eventually giving rise to more full-length SMN protein (adapted from SMA center at the University Medical Center Utrecht).

#### 5.3.1 SMN-ASO injection increased SMN levels in the liver and spinal cord in SMA+ASO mice

We injected the SMN-ASO subcutaneously twice on two consecutive days to neonatal mice (on PND1 and 2). Each injection consisted of the same dose of 30  $\mu$ g of SMN-ASO at a concentration of 10  $\mu$ g/ $\mu$ l. We confirmed by Western blot of tissues from PND10 mice

that ASO injection elevated SMN levels, particularly strongly in the liver, in comparison to uninjected mice of the same genotype. The effect of ASO injection was also visible in spinal cord, albeit to a lesser degree. Importantly, the SMN-ASO exerted a comparable effect on the SMN levels in both tested genotypes (Fig. 30).

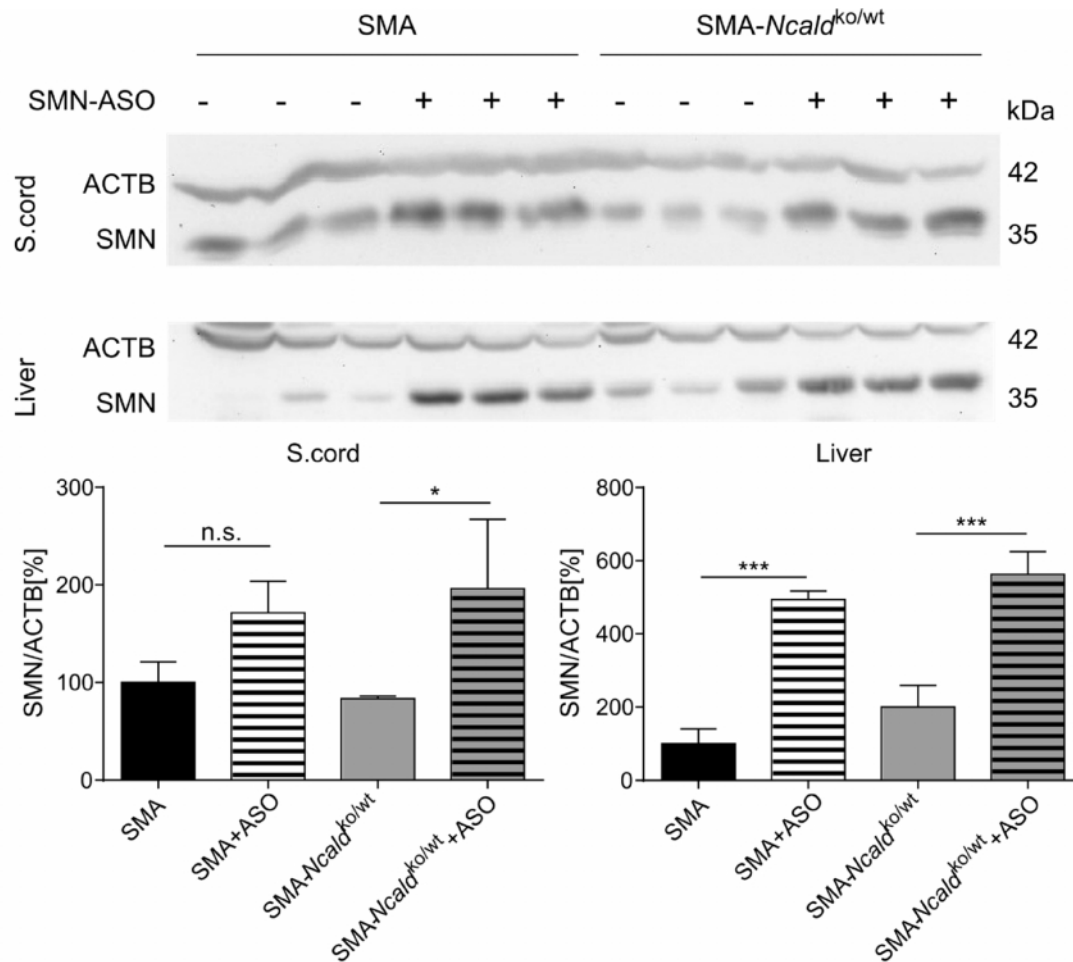


**Fig. 30: SMN-ASO injection increased SMN levels in liver and spinal cord**

Tissue lysates were prepared from three animals per genotype. The SMN levels increased ~2fold in the spinal cord and up to 5fold in the liver which is in line with previous studies that reported an accumulation of SMN-ASO in the liver (Hua et al. 2011, Hosseinibarkooie et al. 2016).

Statistical analysis was performed using two-tailed student's t-test. n.s. not significant, \* $P < 0.05$ , \*\*\* $P < 0.001$ .

Next, the injected animals of all four genotypes were subjected to identical analyses as the uninjected ones: their lifespan and weight progression were evaluated as well as the motoric performance with the tube test and righting reflex test. The anatomical analyses of spinal motor neurons, NMJs in the TVA muscle and muscle fibers in the EDL muscle, as well as the intestinal sections were conducted on PND21 as this represented a symptomatic time point, similar to the PND10 in the uninjected mice.

### 5.3.2 Phenotypic analysis of SMA-*Ncald*<sup>ko/wt</sup>+ASO mice: survival and weight

As expected, the SMN-ASO injection prolonged the mean survival of SMA animals irrespective of the *Ncald* genotype (Fig. 31). However, there was a rather huge variability between as well as within litters: the survival ranged from 8-9 days (and therefore not improved in comparison to uninjected) to >200 days. This broad distribution reflects the variability visible in the uninjected SMA mice as the weakest with confirmed genotype died on PND8 and the strongest survived to PND 21-22 without ASO injection. Another feasible factors accounting for this variability are presumably some variation in ASO administration (despite preparation of larger batches of ASO solution of photometrically confirmed concentration) as well as variable quality of maternal care, possibly also affected by the number of animals in a litter.

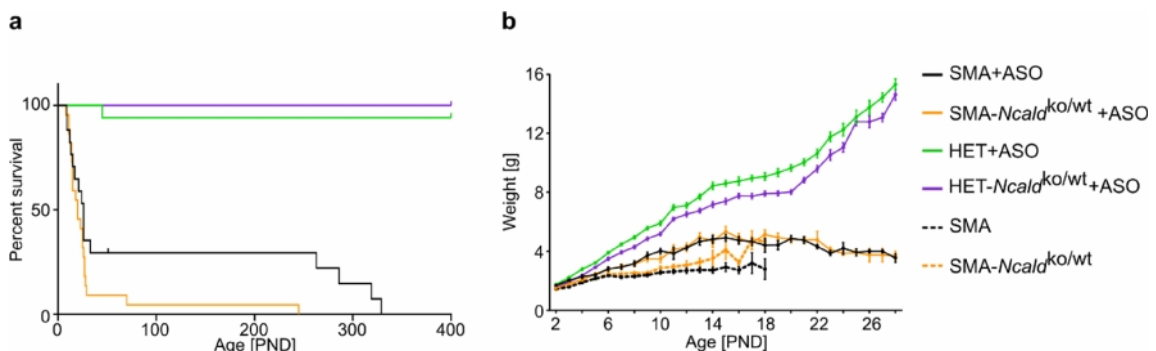


**Fig. 31: Survival and weight studies of SMA+ASO and SMA-*Ncald*<sup>ko/wt</sup>+ASO mice**

**a)** Most SMA+ASO and SMA-*Ncald*<sup>ko/wt</sup>+ASO mice survived 3-4 weeks, however, some animals which survived post weaning showed a much longer lifespan (20% of SMA+ASO and 8% of SMA-*Ncald*<sup>ko/wt</sup>+ASO). The mean survival of short-living SMA+ASO mice was  $19.2 \pm 7.8$  d,  $n=16$ , and of shorter-living SMA-*Ncald*<sup>ko/wt</sup>+ASO mice was  $19.1 \pm 6.7$  d,  $n=22$ . The mean survival of long-living mice SMA+ASO mice was  $269.6 \pm 92.9$  d,  $n=6$ ; the small population of long-living SMA-*Ncald*<sup>ko/wt</sup>+ASO mice survived on average  $177.5 \pm 152$  d,  $n=2$ . Mean  $\pm$  SD. **b)** Body weight did not differ significantly between of SMA+ASO and SMA-*Ncald*<sup>ko/wt</sup>+ASO mice and body weight of both groups was significantly smaller from both HET+ASO groups, but increased in comparison to uninjected animals. The peak of the body weight was reached around PND15.

Significance of the survival curves was assessed with the Mantel-Kox log-rank test.

For statistical analysis of the weight studies two-way ANOVA with Tukey correction for multiple comparison was applied. \* $P < 0.05$ , \*\* $P < 0.01$ , \*\*\* $P < 0.001$ .

### 5.3.3 Phenotypic analysis of SMA-*Ncal*<sup>ko/wt</sup>+ASO mice: motoric tests

The motoric tests described in 4.2.5.9-10 were also applied to assess the motoric performance of SMA+ASO and SMA-*Ncal*<sup>ko/wt</sup>+ASO mice. Similar to the results obtained in uninjected SMA, the differences between genotypes were not very pronounced. Still, some relations observed in the uninjected mice could be recapitulated under SMN-ASO injection.

The results of the righting reflex test showed that except for very early time point (PND2), SMA-*Ncal*<sup>ko/wt</sup>+ASO animals needed on average more time to right themselves than SMA+ASO littermates, though this difference reached significance only on PND7 (Fig. 32a). Again, the motoric performance of SMA-*Ncal*<sup>ko/wt</sup>+ASO mice was significantly worse than of HET+ASO animals starting from PND6 till PND10. The overall tendency shown by the righting reflex test was in agreement with results from uninjected mice (see Fig. 22a).

In the tube test (Fig. 32b) we could not observe any significant difference between the performance of SMA+ASO and SMA-*Ncal*<sup>ko/wt</sup>+ASO mice, except on PND2, which is not a representative time point, as neonatal pups do not show much movement or muscle strength at this age. Notably, animals of both genotypes showed a steep decline in the tube test score from PND10, likely as the muscle weakness was combined with heavier body weight than in uninjected animals (see Fig. 31b). On the PND13 the difference to HET controls was highly significant in SMA+ASO mice ( $P < 0.001$ ) and on PND14 this significance was given for both SMA+ASO and SMA-*Ncal*<sup>ko/wt</sup>+ASO mice.

As these results could be potentially biased by the fact that in the SMA+ASO group some animals ( $n=6$ ) survived significantly longer than 4 weeks, as opposed to SMA-*Ncal*<sup>ko/wt</sup>+ASO mice, where only two animals showed longer survival, we re-analyzed the results in subgroups: short-living SMA+ASO / long-living SMA+ASO / short-living SMA-*Ncal*<sup>ko/wt</sup>+ASO / HET+ASO. In the righting reflex test (Fig. 32c), the long-living SMA+ASO mice showed a tendency towards better performance than the short-living ones, although the results did not reach statistical significance, likely because of a small group size. When only short-living animals were compared, there was no significant difference between SMA+ASO and SMA-*Ncal*<sup>ko/wt</sup>+ASO mice. In the tube test (Fig. 32d), the long-living SMA+ASO mice performed better only till PND7, but again, these results were not statistically significant.

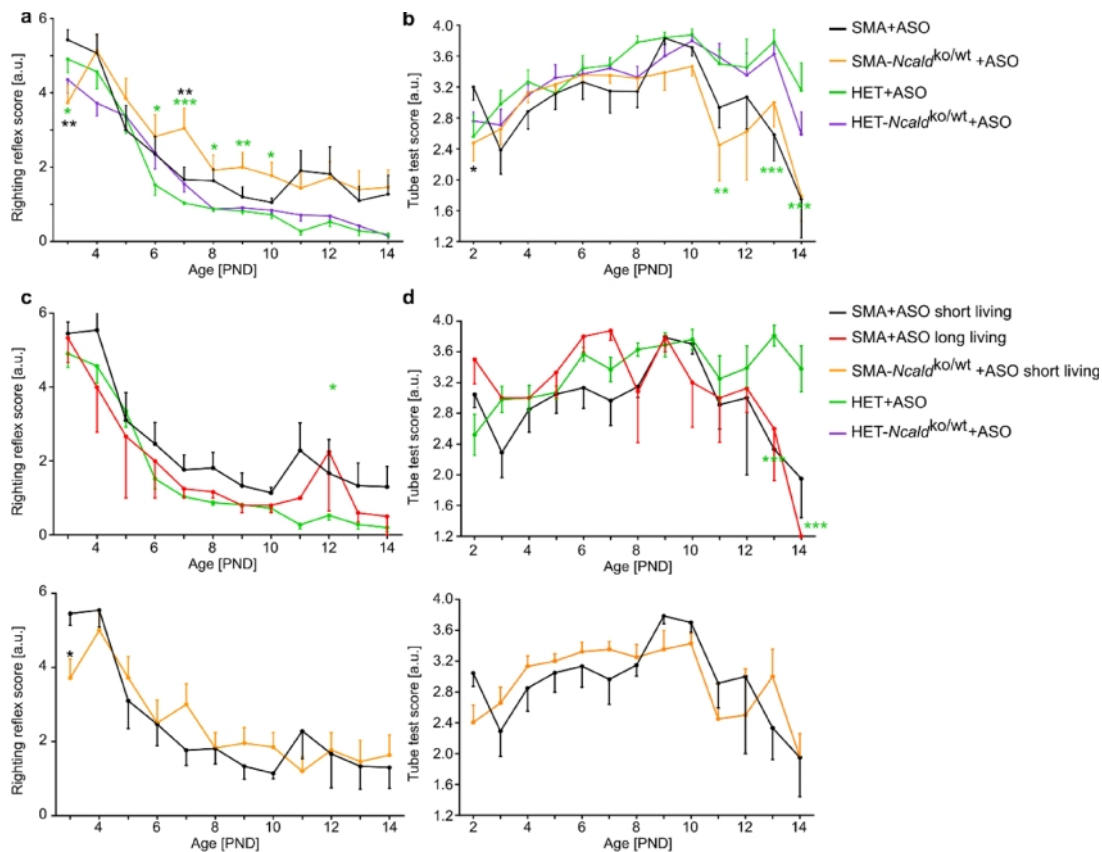


**Fig. 32: Evaluation of motoric skills of SMA-*Ncalcd*<sup>ko/wt</sup>+ASO mice**

**a)** The righting reflex test showed a similar trend as observed for uninjected SMA-*Ncalcd*<sup>ko/wt</sup> mice. **b)** The results of the tube test were not different between SMA+ASO and SMA-*Ncalcd*<sup>ko/wt</sup>+ASO mice. The significance is indicated for SMA-*Ncalcd*<sup>ko/wt</sup>+ASO mice in comparison to SMA+ASO (black stars) or HET+ASO (green stars) littermates, except PND13 in the tube test, which represents SMA+ASO mice in comparison to HET+ASO. SMA+ASO, n= 23, SMA-*Ncalcd*<sup>ko/wt</sup>+ASO, n=23, HET+ASO, n= 34, HET-*Ncalcd*<sup>ko/wt</sup>+ASO, n=34. **c)** The re-analyzed results of the righting reflex test were for short-living and long-living SMA+ASO animals. Short-living SMA+ASO, n=17, short-living SMA+ASO, n=6, short-living SMA-*Ncalcd*<sup>ko/wt</sup>+ASO, n=21. The two long-living SMA-*Ncalcd*<sup>ko/wt</sup>+ASO animals were excluded. **d)**

For both motoric tests two-way ANOVA with Tukey correction for multiple comparisons was applied. \**P*<0.05, \*\**P*<0.01, \*\*\**P*<0.001. The significance is indicated for SMA-*Ncalcd*<sup>ko/wt</sup> mice in comparison to SMA (black stars) or HET (green stars) littermates.

### 5.3.4 Neuromuscular junctions of SMA-*Ncalcd*<sup>ko/wt</sup>+ASO mice are more mature and have a larger area of AChR clusters

The first structure evaluated histologically in SMA-*Ncalcd*<sup>ko/wt</sup>+ASO mice was the neuromuscular junction, as defects of this synapse were reported to be the key SMA associated phenotype in severe and intermediate mouse models (Murray et al. 2010, Bogdanik et al. 2015, Hosseinibarkooie et al. 2016). First, we quantified the area covered by AChR clusters (recognized by Bungarotoxin) in the TVA muscle of ASO-injected PND21 mice: the AChR area was increased in the SMA-*Ncalcd*<sup>ko/wt</sup>+ASO mice compared

to SMA+ASO (Fig. 33b), recapitulating the effect observed in uninjected SMA-*Ncal*<sup>ko/wt</sup> mice (see Fig. 24). This effect was visible only on the SMA background as there was no difference between HET+ASO and HET-*Ncal*<sup>ko/wt</sup>+ASO mice (Fig. 33b). Furthermore, on PND21 we were able to assess not only the area of AChR clusters but also the NMJ maturation. In the first three weeks of postnatal development, the NMJ structure changes from a uniformly stained plaque through an intermediate stage when some folded regions are stained more intensively suggesting a more complex three-dimensional architecture of the endplate up to a fully mature “pretzel” form with clearly visible perforations (Tintignac et al. 2015). We assessed the maturation of NMJs in PND21 animals along recently published criteria where NMJs with three or more perforations were qualified as mature and those with less than three perforations as immature (Bogdanik et al. 2015). Analysis of NMJ maturation showed a significant improvement in SMA-*Ncal*<sup>ko/wt</sup>+ASO animals when compared to SMA+ASO. This effect of NCALD knock-down was also prominent between the groups of HET+ASO and HET-*Ncal*<sup>ko/wt</sup>+ASO animals (see Fig. 33c). Therefore, NCALD knock-down leads not only to an increased area of AChR, but facilitates the NMJ development as well. These findings strengthen the role of NCALD as a negative regulator of neuromuscular system and support the hypothesis that suppressing NCALD might be advantageous in diseases where the neuromuscular system is impaired in its development or maturation. Further studies of NCALD suppression in other disease models, e.g. in ALS mice, could elucidate the potential of NCALD as a cross-disease modifier.

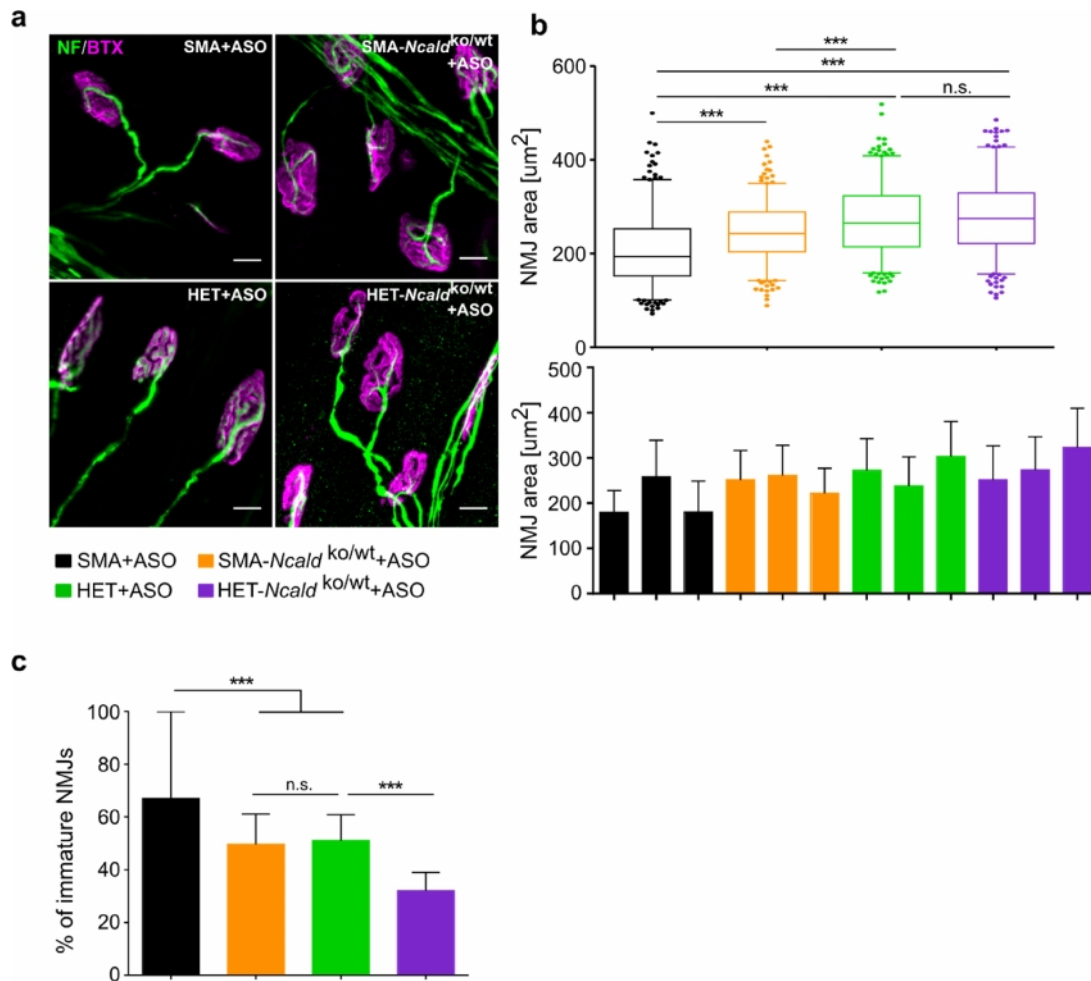


**Fig. 33: NMJ size and maturation are improved in SMA-*Ncalcd*<sup>ko/wt</sup>+ASO animals**

**a)** Representative images and **b)** quantification of mean Bungarotoxin-positive NMJ area in the TVA of PND21 animals of all four genotypes under study, stained with an antibody against NF (green) and Bungarotoxin (BTX, magenta) to visualize the AChR clusters. Scale bar, 10 μm. In the quantification all values per genotype are presented as whisker bars (upper part) and additionally, all values per animal are presented in a bar graph (lower part). The mean NMJ area of SMA-*Ncalcd*<sup>ko/wt</sup>+ASO mice is significantly larger than in SMA+ASO littermates but does not reach the levels of HET+ASO animals. **c)** The maturation of NMJs in PND21 injected animals was evaluated by the number of perforations per endplate: SMA+ASO mice showed the highest and HET-*Ncalcd*<sup>ko/wt</sup>+ASO mice the lowest proportion of immature endplates. The NMJ maturation in SMA-*Ncalcd*<sup>ko/wt</sup>+ASO mice was not significantly different from that of HET+ASO animals.

For all genotypes at least three animals were analyzed, 100-120 NMJs were measured per animal. The analysis was performed double-blinded. Statistical analysis was performed using two-tailed student's t-test. \*\*\* $P < 0.001$ .

### 5.3.5 The number of glutamatergic inputs on MN soma and the MN cell size are increased in SMA-*Ncalcd*<sup>ko/wt</sup>+ASO mice

As NCALD reduction increased the number of glutamatergic synapses on spinal motor neurons, but not the cell soma in the uninjected mice, it was of interest whether by elevating SMN levels in the spinal cord the positive effect of lower NCALD gets enhanced.

Therefore, we performed similar analysis of the VGlut1+ inputs on motor neuron soma as in 5.2.7. As expected, the motor neurons from SMA+ASO received significantly less inputs than those from HET+ASO mice. We could recapitulate the positive effect of NCALD reduction as observed in the severe SMA mice as the number of glutamatergic inputs on motor neurons from the SMA-*Ncald*<sup>ko/wt</sup>+ASO mice was significantly higher in comparison to SMA+ASO littermates (Fig. 34b). However, as the number of VGlut1+ inputs in HET+ASO animals doubled from PND10 to PND21 (from ~19 on PND10 to ~40 on PND21+ASO), possibly augmented by the ASO injection, the SMA-*Ncald*<sup>ko/wt</sup>+ASO mice did not reach the levels of HET+ASO. Notably, in this intermediate SMA model reducing NCALD also resulted in a significant increase in the cell volume of motor neurons (Fig. 34c). The greater phenotypic variability of the intermediate ASO-mediated SMA model was reflected in the huge distribution of mean motor neuron cell volumes between individual animals (Fig. 34d).



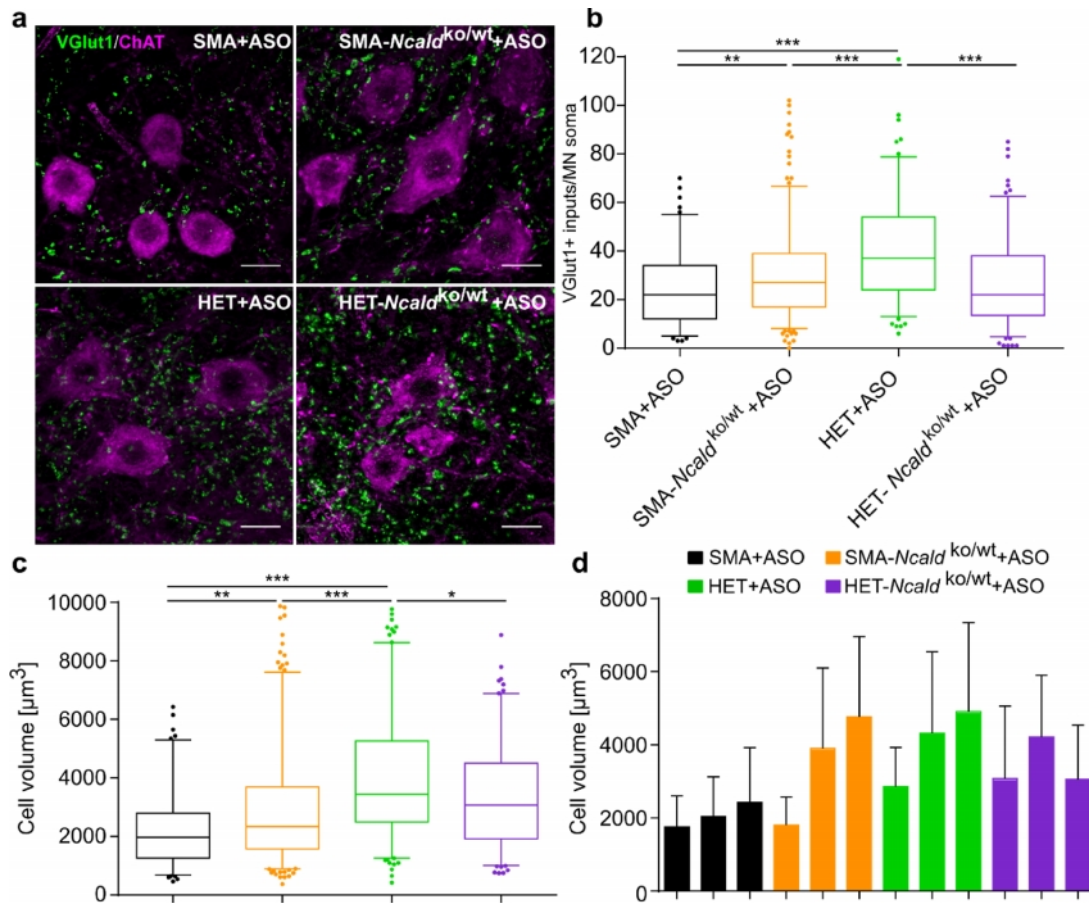


**Fig. 34: Number of VGlut1+ inputs and motor neuron size are increased in SMA-*Ncald*<sup>ko/wt</sup>+ASO animals**

**a)** Representative images and **b)** quantification of glutamatergic inputs on motor neuron soma in PND21 ASO-injected mice. Spinal cord sections were stained with antibodies against ChAT (magenta) to visualize motor neuron soma and VGlut1 (green) to visualize glutamatergic inputs. Scale bar, 20  $\mu$ m. Mean number of VGlut1+ inputs per motor neuron was increased in spinal cords derived from SMA-*Ncald*<sup>ko/wt</sup>+ASO mice (SMA+ASO= 24.0 $\pm$ 14.9, SMA-*Ncald*<sup>ko/wt</sup>+ASO =30.3 $\pm$ 18.4, HET+ASO= 40.9 $\pm$ 21.2, HET-*Ncald*<sup>ko/wt</sup>+ASO =27.3 $\pm$ 18.2). Mean $\pm$ SD. **c)** The distribution of cell volume values within a genotype and **d)** mean values for individual animals. The motor neuron volume is smaller in SMA+ASO animals than in HET+ASO controls and is increased by NCALD reduction. Mean  $\pm$ SD.

For each genotype, three animals were analyzed and 50 motor neurons were analyzed per animal. The analysis was performed double-blinded (the genotypes were disguised during the image acquisition and the data analysis). Statistical analysis was performed using two-tailed student's t-test. \* $P$ <0.05, \*\* $P$ <0.01, \*\*\* $P$ <0.001.

### 5.3.6 Muscle fiber size is increased in the EDL muscle of PND21 SMA-*Ncald*<sup>ko/wt</sup>+ASO mice

In uninjected SMA-*Ncald*<sup>ko/wt</sup> mice, NCALD reduction increased the NMJ Bungarotoxin-positive area in the TVA muscle as well as the number of glutamatergic inputs on motor neuron soma in the spinal cord, showing that structurally both the central as well as distal synapses were enhanced (see Fig. 24 and 26). The structural improvement, however, did

not involve the muscle tissue, as the muscle fiber size remained strongly reduced in SMA-*Ncald*<sup>ko/wt</sup> mice (see Fig. 27). The possible reason could be the intrinsic, motor neuron independent defects of muscle tissue caused by low SMN levels (Fayzullina and Martin 2014). Hypothetically, if SMN levels were elevated in the muscle by a systemic SMN-ASO injection, then the positive impact of NCALD reduction visible at the neuronal site might potentially advance to the muscle tissue. We tested this hypothesis by evaluating the muscle fiber size in the EDL muscle of PND21 SMN+ASO injected mice (Fig. 35).

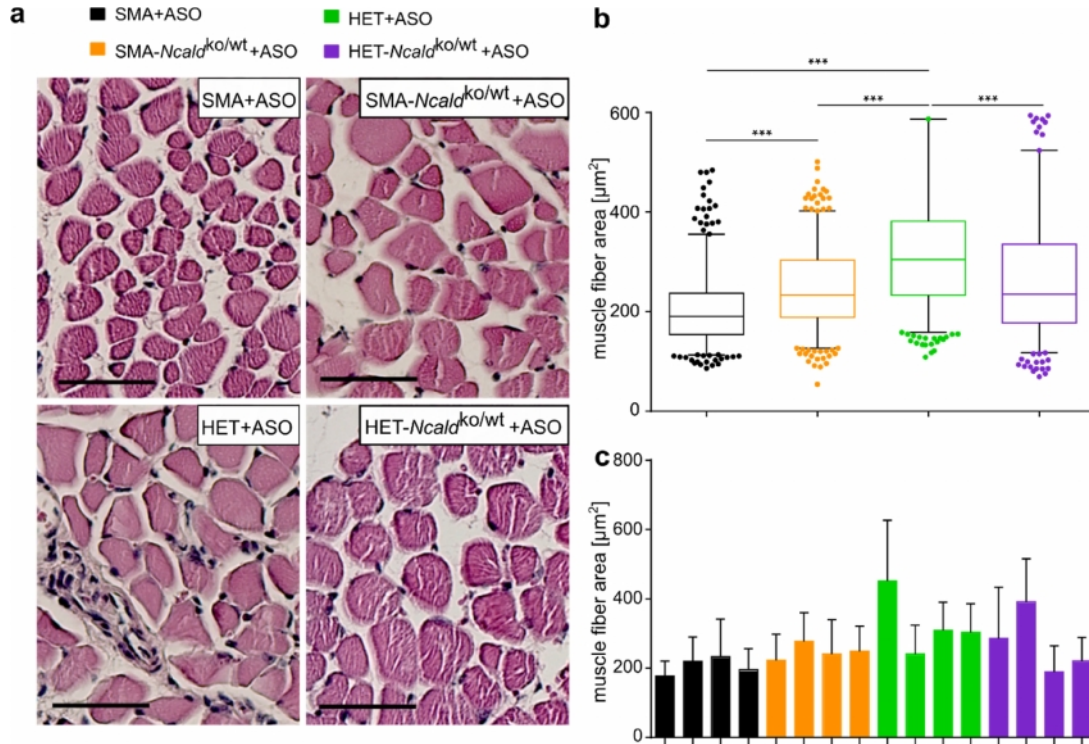


**Fig. 35: Analysis of muscle fiber size in the EDL muscle of PND21 mice**

**a)** Representative images of H&E stainings of 7  $\mu\text{m}$  paraffin sections of the EDL muscle. The difference in muscle fiber size is prominent between SMA+ASO and HET+ASO animals. Scale bar, 50  $\mu\text{m}$ . **b)** The quantification of muscle fiber size shows an increase in SMA-*Ncald*<sup>ko/wt</sup>+ASO mice in comparison to SMA+ASO littermates. Unexpectedly, the muscle fiber size was significantly decreased in HET-*Ncald*<sup>ko/wt</sup>+ASO compared to HET+ASO littermates. **c)** Mean values presented as bars for individual mice show higher variability within the ASO-injected heterozygous animals. Mean  $\pm$  SD.

For each genotype four animals were analyzed and 100 muscle fiber were measured per animal. The analysis was performed double-blinded (the genotypes were disguised during the image acquisition and the data analysis). Statistical analysis was performed using two-tailed student's t-test. \*\*\* $P < 0.001$ .

The mean muscle fiber size was highly significantly reduced in SMN+ASO mice when compared to HET+ASO littermates. Notably, it was increased in SMA-*Ncald*<sup>ko/wt</sup>+ASO in comparison to the SMN+ASO mice, although it did not reach the HET-ASO mice levels. This observation highlights the importance of peripheral SMN restoration for the protective

modifiers to fully exert their function: while in the severe uninjected SMA-*Ncald*<sup>ko/wt</sup> mice the muscle fiber size was unchanged compared to SMA, elevating SMN was sufficient for the structural improvement of the NMJ size (see Fig. 33) to manifest itself also in the target tissue.

### 5.3.7 The impairment of the gastrointestinal tract is not rescued by reduced NCALD levels

Although numerous SMA hallmarks were improved in SMA-*Ncald*<sup>ko/wt</sup>+ASO, their survival and body weight remained reduced. The reason for this could be that NCALD reduction affects predominantly the neuromuscular system, but fails to rescue non-neuronal defects. As previously, the morphology of the small intestine was studied as tantamount for the general phenotype of the mice. As PND21 represented a late stage of the disease in the intermediate model, severe changes were visible in SMA+ASO mice: reduced villi number, edema of the lamina propria and frequent intracytoplasmatic vacuoles at the tips of the villi (Fig. 36).

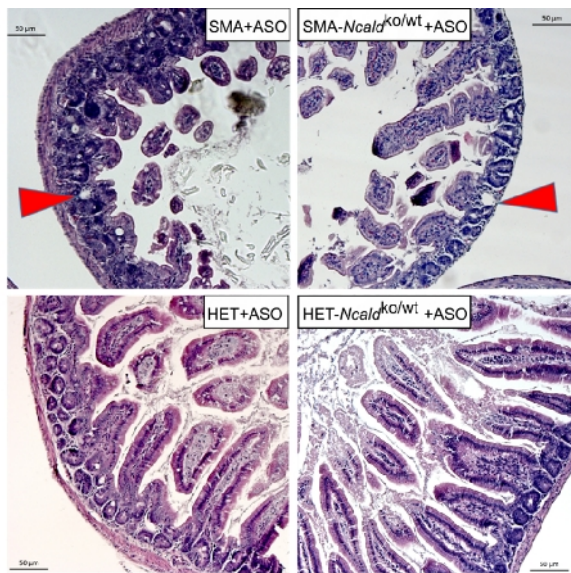


**Fig. 36: Intestine impairment is still visible in SMA+ASO mice.**

Representative images of H&E stainings of 7  $\mu$ m paraffin sections from the intestine of PND21 SMA+ASO, SMA-*Ncald*<sup>ko/wt</sup>+ASO, HET+ASO and HET-*Ncald*<sup>ko/wt</sup>+ASO animals. In the intestine of both SMA and SMA-*Ncald*<sup>ko/wt</sup> mice the villi are less abundant and show a blunt morphology, in contrast to the longitudinal shape of villi in HET+ASO and HET-*Ncald*<sup>ko/wt</sup>+ASO animals. The red arrowheads mark the edema in the lamina propria absent in HET+ASO littermates. Scale bar, 50  $\mu$ m. Three animals per each genotype were analyzed.

The observed phenotypic characteristics of the SMA-*Ncald*<sup>ko/wt</sup> and HET-*Ncald*<sup>ko/wt</sup> mice, analyzed in the severe SMA mouse model on PND10 and in the intermediate SMN-ASO

mediated model on PND21 analyzed, are summarized in Table 13; a group defined in a column by genotype and treatment has always been compared to identically treated littermates carrying the same genetic composition of *Smn* and *SMN2*, but lacking the allele: SMA-*Ncald*<sup>ko/wt</sup> against SMA and HET-*Ncald*<sup>ko/wt</sup> against HET. Overall, independently of the severity of the SMA model, NCALD reduction ameliorated many defects mediated by SMN deficiency: when the SMN levels were elevated by SMN-ASO injection, all analyzed neuromuscular structures showed an improvement. Surprisingly, the effect of NCALD reduction on HET animals was more complex and will be discussed in detail in chapter 6.4.

**Table 13: The summary of the characteristics of SMA-*Ncald*<sup>ko/wt</sup> and HET-*Ncald*<sup>ko/wt</sup> analyzed in the severe and intermediate SMA mouse model.**

Upwards arrows indicate an increase, downwards arrows – a decrease and right-bound arrows – no significant change.

	SMA- <i>Ncald</i> <sup>ko/wt</sup>		HET- <i>Ncald</i> <sup>ko/wt</sup>	
	uninjected PND10	+SMN-ASO PND21	uninjected PND10	+SMN-ASO PND21
1. Motor neuron volume	↓	↑	→	↓
2. Number of VGlut1+ inputs	↑	↑	↑	↓
3. NMJ size	↑	↑	→	→
4. Muscle fiber size	→	↑	↑	↓
5. Motoric skills	→	→	→	→
6. Inner organ impairment	→	→	→	→

#### 5.4 SMA mouse model with NCALD reduction – an *Ncald*-ASO approach

As we anticipated that NCALD reduction might be have some translational potential for SMA therapy, we intended to reduce NCALD by an exogenously administered compound. To achieve an *in vivo* knock-down of genes in model organisms and ultimately in patients, the technology of antisense oligonucleotides (ASOs) has proved very suitable and is already advanced in therapies against SMA and other diseases (Aartsma-Rus and van Ommen 2010, Chiriboga et al. 2016). The antisense oligonucleotides against *Ncald* were developed in close cooperation with an industrial partner, Ionis Pharmaceuticals (Carlsbad, California), who has a vast expertise in developing therapeutic ASOs, with SMA as the most prominent example (Hua et al. 2008, Hua et al. 2010, Hua et al. 2011, Rigo et al. 2012). As the targeted tissue was central nervous system, Ionis Pharmaceuticals

developed ASOs with the mixed 2' MOE chemistry, where the center residues are phosphorothioate oligodeoxyribonucleotides and the several terminal residues carry a methoxyethoxy substitution on the 2' position of ribose, as this provides better tolerability and uptake into CNS (Chery and Naar 2016). Different ASO sequences were tested in adult wildtype mice by bolus injection and the knock-down efficiency was evaluated by qRT-PCR (Fig. 37b,c).

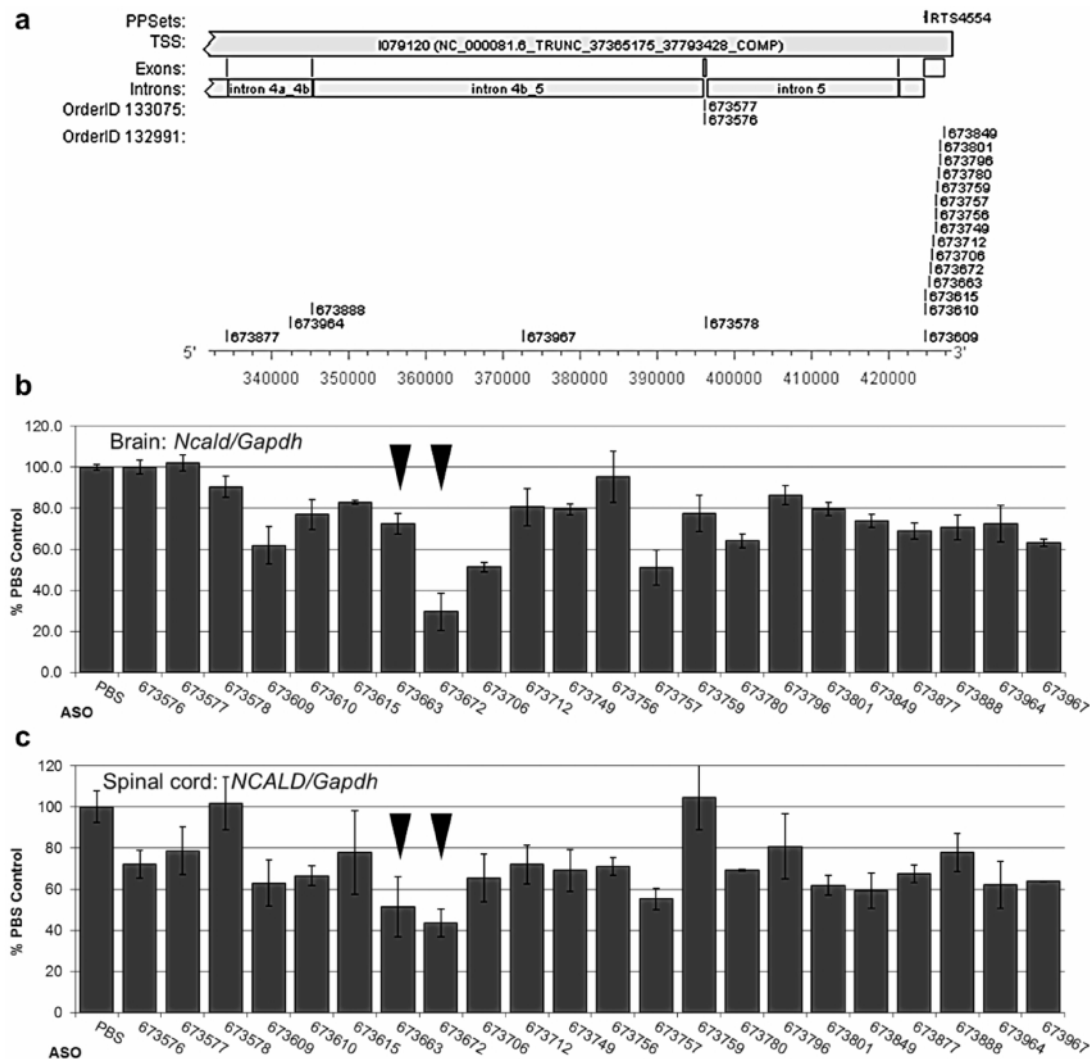


**Fig. 37: A screen of different ASO sequences against *Ncald* performed by Ionis Pharmaceuticals**

**a)** 22 ASO sequences have been tested by administering 500 µg ASO via an i.c.v. bolus to adult wildtype mice. Except for six, all ASOs were targeting the 3'UTR of *Ncald* gene. The mice were sacrificed 2 weeks after injection. *Ncald* knock-down in the brain **b)** and spinal cord **c)** was evaluated by qRT-PCR. The two ASOs which achieved the highest *Ncald* knock-down were ASO673663 and ASO673672 (highlighted with black arrowheads), the latter giving a strong knock-down in both organs tested.

The two ASOs which achieved the greatest NCALD reduction in brain and spinal cord were selected for further tests in neonatal mice, as any interventions against SMA have the greatest chance of improving the phenotype when undertaken early in life, preferentially

before the onset of symptoms. The tests should assess ASO tolerability and efficiency, as well as determine the optimal amount of ASO, the best injection protocol and the right time point of injection.

First, we injected two litters of wild-type pups intracerebroventricularly (i.c.v.) with different doses of two independent ASOs (673663 and 673672, further referred to as ASO1 and ASO2, respectively) and assessed the degree of NCALD knock-down in the brain and the spinal cord (Fig. 38a). As it was crucial that *Ncald*-ASOs are well tolerated when injected into neonatal SMA mice, in the next step we i.c.v. injected two larger litters (n=8 for ASO1 and n=10 for ASO2) of SMA and HET mice, each litter with variable doses of respective ASO (at least 2 animals per dose), and we evaluated the NCALD knock-down by Western blots. Of the 8 mice injected with ASO1, two injected with the higher doses (30 µg and 60 µg) died immediately post injection, while all 10 pups injected with ASO2 survived till PND8. In line with the preliminary tests performed by Ionis Pharmaceuticals, ASO2 achieved a stronger NCALD knock-down in brain and also in the spinal cord (Fig. 38c).

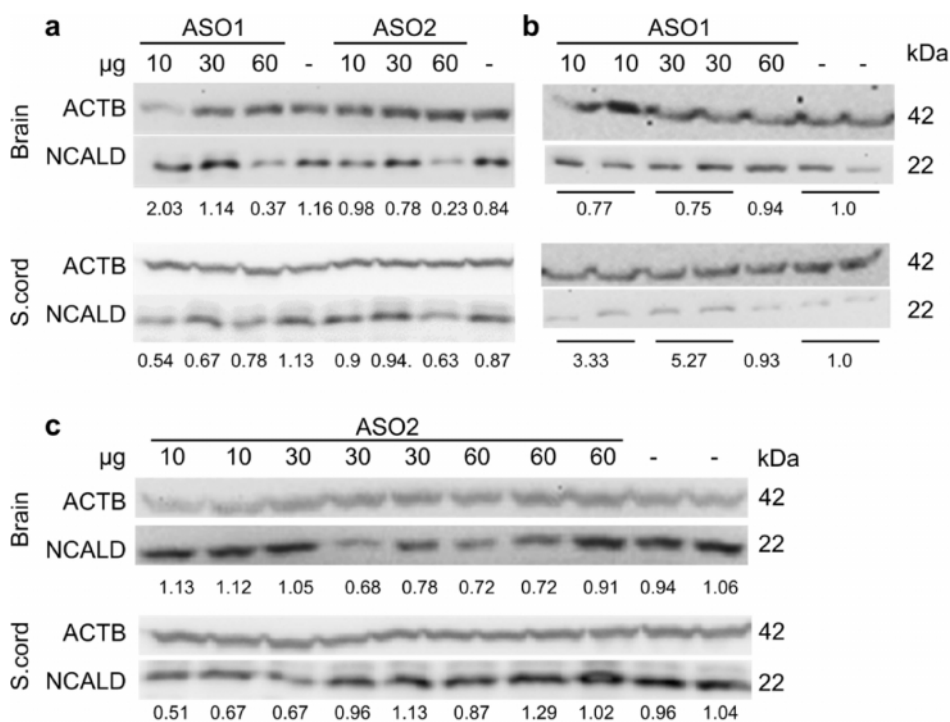


**Fig. 38: NCALD knock-down by i.c.v. *Ncald*-ASO injection in wildtype and SMA mice**

**a)** Western blot of brain and spinal cord lysates of wildtype mice i.c.v. injected with *Ncald*-ASO1 or 2 on PND1 and sacrificed on PND8. For both ASO sequences, the highest dose (60µg) reduced NCALD in the brain and also, although to a lesser degree, in the spinal cord. The quantification of NCALD knock-down is indicated for each sample as proportion to uninjected control on the same blot. **b)** Western blot of brain and spinal cord lysates of SMA mice i.c.v. injected with different doses of ASO1 on PND1 and sacrificed on PND8. Two mice died within 24h after injection. **c)** Western blot of brain and spinal cord lysates of SMA mice i.c.v. injected with different doses of ASO2 on PND1 and sacrificed on PND8 showed NCALD knock-down in the brain at higher doses and in the spinal cord at lower doses. All mice survived ASO2 injection.



As generally NCALD knock-down in the spinal cord after single injection was not very pronounced irrespective of the injected dose, we attempted to maximize the effect by injecting ASO2 on two consecutive days. We injected SMA and HET neonatal mice on days PND1 and 2 and tested different double injection regimens (detailed description in Fig. 39): two i.c.v. injections, two s.c. injections and one i.c.v. plus one s.c. We reasoned that in the neonatal mice the permeability of the blood-brain barrier might allow the ASO to reach the target tissue even if injected subcutaneously. Double intracerebroventricular injection was too invasive as even mice injected with control ASO (676226, further referred to as ASOctrl) succumbed to the intervention. However, one pup injected with 2x i.c.v. ASO2 survived and could be dissected on PND10. Unexpectedly, the combined 1x i.c.v. plus 1x s.c. injection regimen mediated a stronger NCALD knock-down than 2x i.c.v. (Fig. 39a), which was confirmed in a bigger number of animals (Fig. 39b).

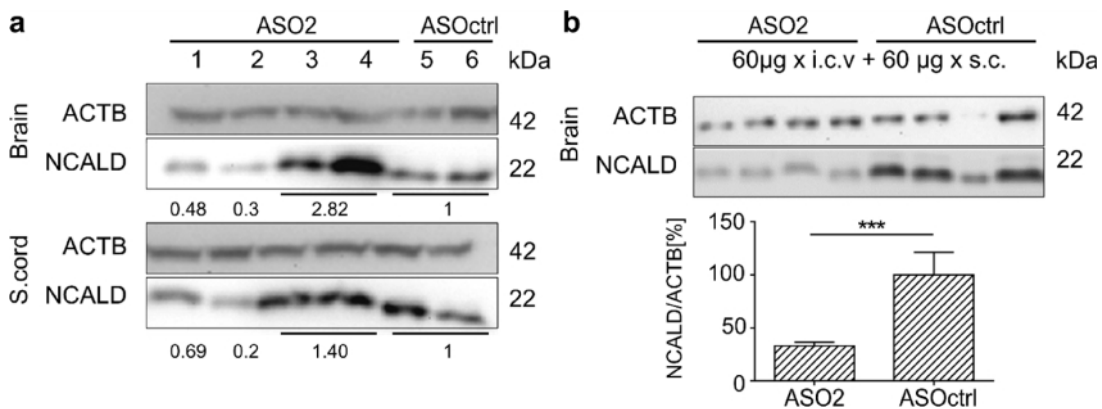


**Fig. 39: Efficient NCALD knock-down by combined i.c.v. and s.c. injection of ASO2 against *Ncald* in SMA mice**

**a)** Western blots of brain and spinal cord lysates of SMA mice injected twice with 60µg *Ncald*-ASO2 on PND1 and 2 and sacrificed on PND10. Each of the following ASO2 injection regimens was tested on two pups: 2x i.c.v. (lane 1), 1x i.c.v. + 1x s.c. (lane 2), 2x s.c. (lanes 3 and 4). Additionally, two mice were injected 2x i.c.v. with 60µg of ASOctrl. From each of the first two regimens one pup died post injection and both mice injected 2x i.c.v. with 60µg of ASOctrl died, therefore lysates from 1x i.c.v. ASOctrl injected mice were used as controls (lanes 5 and 6). The quantification of NCALD knock-down is indicated for each sample as proportion to uninjected control on the same blot. **b)** Western blot of brain lysates from four mice injected with 2x 60 µg ASO2 or ASOctrl, 1x i.c.v. on PND2 and 1x s.c. on PND3. ASO2 mediated > 60% NCALD knock-down in comparison to ASOctrl.

Statistical analysis was performed using two-tailed student's t-test. \*\*\* $P < 0.001$ .

Therefore, we continued with the 1x i.c.v. + 1x s.c. ASO2 injection strategy in next litters. Unfortunately, we observed a relatively high toxicity of the active compound which resulted in death within the 24 hours post injection in >30% of mice, where the more efficient ASO2 exerted also a more toxic effect (Fig. 40a). The toxicity occurred in a dose dependent way,

while the maximal tested amount of 60 µg ASO was also the most toxic. However, we did not observe this increased mortality for animals injected in the same manner with ASOctrl, so that the injection *per se* could be excluded as the death cause. As the ASOctrl of the same chemistry and injected in the same manner did not show a lethal effect, and complete *Ncald*<sup>ko/ko</sup> mice do not show an increased perinatal mortality, it is possible that *Ncald*-ASOs have some off-target effects on a crucial neuronal gene. In an extreme case of a 10-pup-litter all 8 injected with the active compound were dead on the following day, while the two ASOctrl injected pups survived till PND10. It is also unlikely that NCALD reduction alone would have such an extreme effect as complete *Ncald*<sup>ko/ko</sup> mice are viable to adulthood.

We reasoned that possibly the ASO2 dosis is too high and may be toxic for the neonatal mice, therefore we tested a series of ASO2 concentrations; NCALD reduction was ASO2 dose-dependent and visible only at doses 2x 50 µg (Fig. 40b).

As i.c.v. injection of ASO2 too appeared to be the reason of the lethality, we decided to inject ASO2 only subcutaneously and instead inject ASO1 intracerebroventricularly. In the spinal cord the injection of ASO cocktail achieved a knock-down of NCALD up to 30%; surprisingly, there was no advantage of injecting both ASOs compared to injecting only ASO1 (Fig. 40c). Therefore, we decided to continue injecting with ASO1 only; unfortunately, also ASO1 injection was associated with increased mortality, as 30% mice injected i.c.v. with ASO1 died shortly afterwards (Fig. 40a).



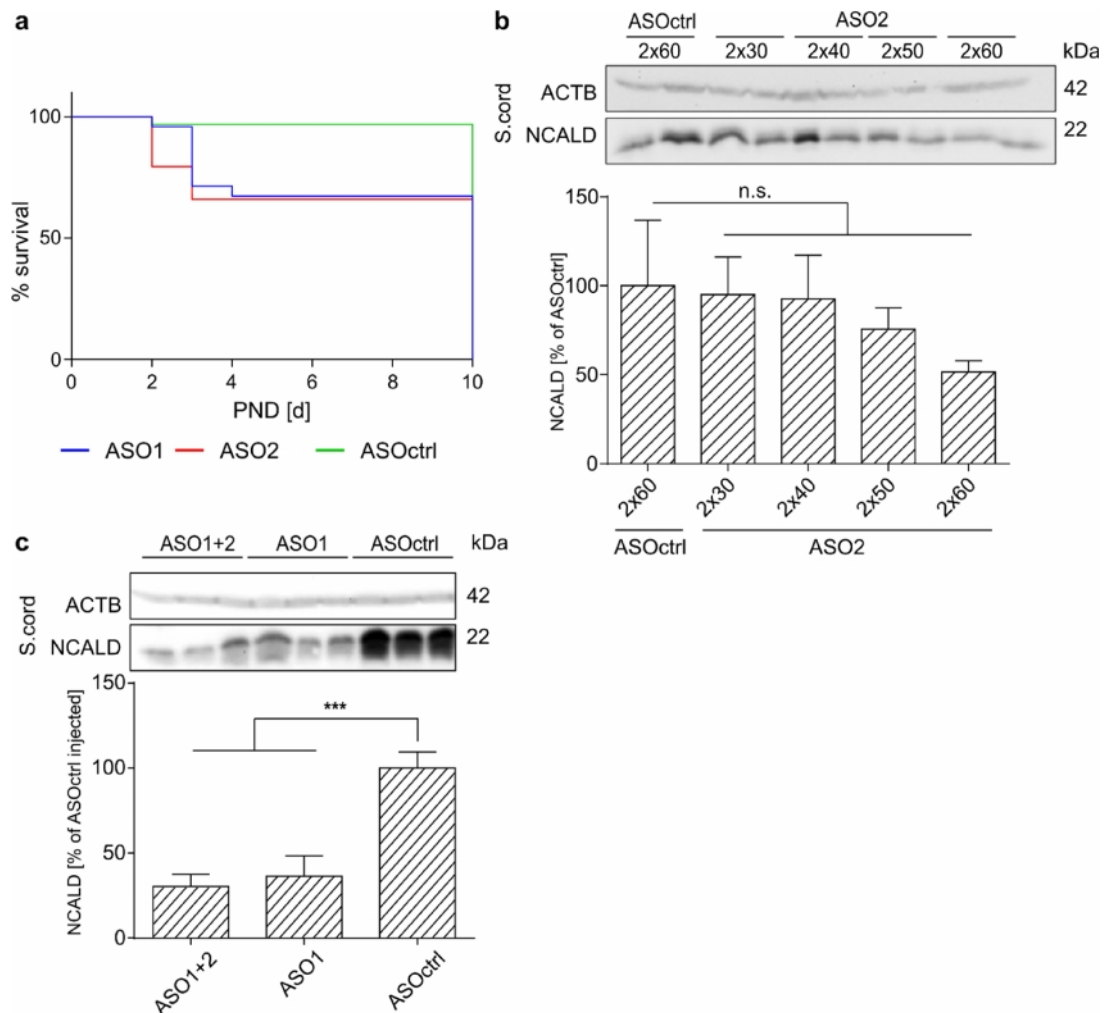


**Fig. 40: Increased mortality following the injection of *Ncald*-ASOs**

**a)** Survival curve of mice injected i.c.v. and s.c. with *Ncald*-ASOs. Both ASOs increased the mortality directly post injection (15 mice out of 50 injected with ASO1 and 17 mice out of 57 injected with ASO2 died before PND10). PND10 was set as cut-off, as the surviving animals were dissected at this age to evaluate the NCALD knock-down. **b)** Western blot and quantification of spinal cord lysates from mice injected with a series of ASO2 concentrations (i.c.v. on PND2 and s.c. on PND3). **c)** Western blot and quantification of spinal cord lysates from mice injected with ASO cocktail (s.c. ASO2 + i.c.v. ASO1), ASO1 or ASOctrl (s.c. on PND1 + i.c.v. on PND3).

Two (**b**) or three animals (**c**) were injected identically for one Western blot experiment. Mean  $\pm$  SEM. Statistical analysis was performed using two-tailed student's t-test.

All in all, we could show a satisfactory NCALD knock-down using ASO compounds, however, their therapeutic potential requires great caution due to observed high toxicity; the safety profile and clinical effect need to be assessed in more detail.

## 6 Discussion

### 6.1 Different strategies to reduce NCALD *in vivo* in SMA mice

*Neurocalcin delta* (NCALD) was identified as a protective SMA modifier in humans. Preliminary work in cellular and non-mammalian models showed that reducing NCALD ameliorated defects mediated by SMN deficiency: particularly, the neuronal outgrowth which is strongly reduced in SMN-deficient cells and zebrafish (McWhorter et al. 2003, Kwon et al. 2011) was restored to control levels when NCALD was concomitantly downregulated. The work presented here attempted to answer the question whether NCALD reduction can rescue the SMA phenotype in mice. Studies of SMA mouse models contributed enormously to the understanding of the disease pathology: by unraveling NMJ defects as one of the earliest SMA symptoms (Kariya et al. 2008), the developmental synaptopathy of the neuromuscular junctions has been identified as the primary pathology both in severe and mild SMA mouse models and, most importantly, in SMA patients (Murray et al. 2008, Bogdanik et al. 2015, Harding et al. 2015). SMA mice serve also as a platform to test potential therapeutics against this devastating disorder which are reviewed in (Kaczmarek et al. 2015). By studying the effect of NCALD reduction in SMA mice we aimed at answering two questions: first, which SMA symptoms are potentially rescued by NCALD reduction, and second, to explore the therapeutic potential of NCALD knock-down. In order to do so, we had to find the optimal method to reduce NCALD *in vivo*: in the scope of this work, three different approaches have been tested and each has shown certain advantages but also some caveats.

Our first strategy to reduce NCALD involved generating a novel mouse line carrying an shRNA that by RNA interference would likely promote the degradation of *Ncald* transcript (Kleinhammer et al. 2011). The shRNA would be expressed only upon induction, while the inducer (Doxycycline) can be either added to the medium *in vitro* or conveniently administered *in vivo* in food or drinking water. This strategy of inducible and incomplete depletion of a gene product is particularly suitable when a gene knock-out would result in embryonic death (McJunkin et al. 2011). Moreover, by merely reducing the levels of a protein of interest the human phenotype can be recapitulated more faithfully, as is the case in the asymptomatic individuals, where NCALD is not completely absent, but expressed at lower levels. The greatest challenge of this approach lies in the identification of potent shRNA sequences, and indeed, we had difficulties identifying an shRNA sequence that would strongly downregulate endogenous NCALD in a mouse cell line. Only when we overexpressed *Ncald* cDNA in a cell line that does not express NCALD endogenously, we could find two efficient shRNA sequences. As also identification of a strong siRNA for

transient NCALD knock-down in mouse cell lines proved difficult, it is feasible that *Ncald* mRNA takes on a secondary structure which is not easily targeted by RNAi (Gutschner et al. 2011).

Second, as the complete *Ncald*<sup>ko/ko</sup> mouse line has become available and turned out to be both viable and fertile, we decided to adapt our strategy accordingly and instead of the shRNA transgene to use the heterozygous *Ncald*<sup>ko/wt</sup> mice as a model of NCALD depletion, which we crossed with the SMA mice. The great advantage of a genetic knock-out model is a consistent degree of protein reduction between individual animals while an exogenous treatment inevitably introduces additional variability. A genetic model is best suited for initial assessment of candidate modifier genes for a disease, however, it has obviously little translational potential. Moreover, most likely virtually any knock-out mouse line has its own phenotype arising from the disruption of the cellular homeostasis. In the case of the *Ncald*<sup>ko/ko</sup> mice, their phenotypical analysis has revealed numerous changes of mainly neurological and metabolic nature (Jackson Laboratory 2016). It remains unclear how many of these changes are already present in the *Ncald*<sup>ko/wt</sup> animals and have an effect on the SMA-*Ncald*<sup>ko/wt</sup> mice that is independent of SMN deficiency. NCALD reduction had a readily noticeable impact on the adipose tissue and body weight (5.2.3), still further analysis of the *Ncald*<sup>ko/wt</sup> and *Ncald*<sup>ko/ko</sup> animals is required to fully comprehend the function of NCALD.

Third, we attempted to deplete NCALD using exogenous compounds with a direct therapeutic potential, antisense oligonucleotides (ASOs). ASOs have the ability to target RNA in a sequence-specific way and depending on the locus they bind to, they can either silence gene expression by a variety of mechanisms or alter the splicing (Bennett and Swayze 2010). The ASOs we used here represent the second generation of antisense compounds with the mixed 2' MOE chemistry: the center residues are phosphorothioate oligodeoxyribonucleotides, while the several terminal residues carry a methoxyethoxy substitution on the 2' position of ribose. This combination increased hybridization affinity and potency, as well as resistance to nuclease cleavage; it also improved the tolerability profile by decreasing the proinflammatory effects (Chery and Naar 2016). Due to their large molecular weight and size, ASOs do not cross the blood brain barrier, therefore targeting ASO to neuronal tissue involves intrathecal or intracerebroventricular administration. In our tests of *Ncald*-ASO we observed that the 2'MOE chemistry (assessed from control ASO) was well tolerated despite the invasive nature of i.c.v. injection. When *Ncald*-ASOs were administered i.c.v., they mediated an NCALD knock-down in the CNS even up to 30% of control level (5.4). Unfortunately, an apparent sequence-related toxicity of *Ncald*-ASOs resulted in increased mortality. One possible way

to overcome this drawback would be to test yet another ASO sequence; this approach is currently in progress. Another way to achieve a milder injection would be the use of a fine glass capillary needle in order to minimize the damage to the sensitive brain tissue (Glascocock et al. 2011); also this refinement is under investigation.

Testing modifier genes in SMA mouse models has previously required laborious generation of new mouse lines carrying the modifying variants. Conveniently, a growing number of knock-out lines has become available for the scientific community to study the functional basis of human diseases (Rosen et al. 2015). In the future, functional genomic screens in mammalian animal models, e.g. in mouse, might be facilitated by the breakthrough gene editing technique using the endonuclease CRISPR/Cas9, especially as the libraries of verified guide RNA sequence are already being generated for many common laboratory species (Hsu et al. 2014). The advantages of the CRISPR/Cas9 mediated gene editing are its specificity, as specific gene variants can be tested instead of disease models only phenocopying a particular disorder, and rapidness, through bypassing the typical ES cell targeting step and directly targeting zygotes to generate transgenic lines (Paquet et al. 2016). This technique has already proven helpful in targeting difficult genes that failed in previous attempts (Schick et al. 2016). It harbors also a therapeutic potential for treating genetic disorders by correcting (even postnatally) the causative mutations while the gene remains expressed in its natural context which is an advantage in comparison to viral gene delivery (Long et al. 2016).

## **6.2 Effect of NCALD reduction on the motor neurons of SMA animals**

The motor neurons are widely accepted as the primary cell type affected by SMN deficiency, although the reason of their susceptibility to low SMN levels is not fully clear and remains the subject of many studies in the SMA research (Saal et al. 2014, Fallini et al. 2016). One possible explanation could be that motor neurons express lower SMN from *SMN2* than other cell populations in the spinal cord due to a particularly inefficient splicing of exon 7 (Ruggiu et al. 2012). Other hypotheses view the high energy demand of neurons as critical for their vulnerability, especially as mitochondrial dysfunction has been reported in SMA (Malkki 2016), as well as the polarity of neurons which is coupled with their high demand of local translation (Liu-Yesucevitz et al. 2011, Fallini et al. 2016).

NCALD was previously identified as localizing to axons of sensory and hippocampal neurons (Yamatani et al. 2010); additionally, our group could pinpoint the localization of NCALD to the soma and growth cones of motor neurons (Svenja Schneider, unpublished data). With this important indication that NCALD may play a role in the tissue of interest, we studied two characteristics of motor neurons that are impaired under low SMN levels:

axonal length and number of glutamatergic inputs on the motor neuron soma as a component of spinal motoneuronal circuitry (Rossoll et al. 2003, Mentis et al. 2011).

Yamanati and colleagues identified NCALD and another protein of the NCS family – VILIP1 – in a proteomic screen as highly upregulated during axon development, which suggested a prominent function of neuronal calcium sensors in the growing axon. Furthermore, both NCALD and VILIP1 localized to the growth cone which is a dynamic structure orchestrating the axonal growth (Tamariz and Varela-Echavarria 2015). Overexpression studies showed detrimental effect of excessive NCALD on neurite outgrowth – thus highlighting that an alteration of NCALD levels is able to affect the homeostasis of axon development (Yamatani et al. 2010). We showed that NCALD suppression counteracts the axonal outgrowth impairment in SMA, strengthening the evidence of NCALD as an important regulator of axonal growth (5.2.5). The mechanism how this happens remains elusive; it is feasible, however, that the reported interaction of NCALD with tubulin and actin, two key components of the cytoskeleton, plays a role as the growth cone and axonal growth are directly dependent on the dynamics of the cytoskeleton (Gordon-Weeks and Fournier 2014). Another hypothesis would involve a possible restoration of  $\text{Ca}^{2+}$  homeostasis, which is known to be altered in SMA, by altering the  $\text{Ca}^{2+}$  sensing (Ruiz et al. 2010). The precise nature of  $\text{Ca}^{2+}$  disturbance in SMA is still under discussion, as human and mouse studies yield incongruous results (McGivern et al. 2013), therefore intensive research would be required to verify this hypothesis.

Recently, disturbed neuronal circuits are increasingly recognized as contributing to and potentially even initiating various neurodegenerative disorders, e.g. Parkinson's and Huntington's disease (Palop et al. 2006). Importantly, as also other cell types directly interacting with motor neurons, such as interneurons and astrocytes, were reported to show alterations when SMN is depleted, not only cell-autonomous effects, but the entire neuronal network needs to be taken into consideration in SMA research (Zhou et al. 2016). This is particularly relevant for motor neurons, as their function is not only dependent on intrinsic qualities, but also reflects the excitatory and inhibitory inputs that the motor neurons receive: when the overall numbers or firing frequency of these inputs or the ratio of excitatory to inhibitory ones are changed, this directly affects the activity of the target neuron and ultimately its output – in this case the activation of skeletal muscle (Kitzmann 2010). In SMA, it has been shown that specifically the excitatory, but not the inhibitory inputs are reduced (Simon 2016). The excitatory inputs are prevalently of glutamatergic nature and provide the motor neuron with sensory information with respect to touch, proprioception, mechanoreception and nociception as well as integrate information from different levels of CNS (cortex, brain stem and spinal cord). We analyzed the glutamatergic

inputs on spinal motor neurons by immunohistochemical staining of spinal cord sections and in both SMA models under study: the severe and the intermediate one, we could observe that reducing NCALD lead to the increase of the number of glutamatergic inputs on motor neuron soma (see 5.2.7 and 5.3.5), implicating that the positive effect of lower NCALD levels is not limited to motor neurons but is capable of modifying the spinal circuitry. Other studies found that the loss of excitatory inputs accompanied by a block in their synaptic transmission leads to hyperexcitability of motor neurons (Simon et al. 2016). This manifested in an alteration of two intrinsic membrane properties: input resistance and time constant, that were reported to be increased in SMA motor neurons. As other neuronal sensor proteins have been shown to play a role in membrane trafficking and calcium channel regulation (Burgoyne and Haynes 2010, Weiss et al. 2010), and defective clustering of calcium channels has been reported to disturb the excitability of SMA motor neurons (Jablonka et al. 2007), one could envisage that reducing NCALD possibly interferes with these SMA defects and restores some provisory balance at the membrane.

The limitation of the anatomical studies is that when an increase in excitatory inputs to motor neurons is detected by immunolabeling, this does not necessarily implicate an actual increase in glutamate release. Therefore, electrophysiological analysis of the properties of SMA motor neurons along the methodology presented in (Mentis et al. 2011, Gogliotti et al. 2012) would be technically challenging, yet highly interesting in order to make a conclusive statement about the functional impact of NCALD reduction.

### **6.3 Effect of NCALD reduction on the NMJs of SMA animals**

Traditionally, SMA was perceived as motor neuron disorder, however since the identification of *SMN1* as the disease determining gene and *SMN2* as the main modifying gene (Lefebvre et al. 1995), our understanding of the nature of this disease has vastly increased, largely due to *in vivo* studies conducted in SMA mouse models. In particular, defects of the neuromuscular junction have been identified as an early pathology, preceding the death of motor neuron (Ling et al. 2012). The pathological alterations of NMJs in SMA are both of structural and functional nature and include impaired maturation (Kariya et al. 2008), neurofilament aggregation (Cifuentes-Diaz et al. 2002), disturbance of calcium homeostasis (Ruiz et al. 2010) and impaired neurotransmitter release (Kong et al. 2009). The axonal degeneration and resulting impairment of neurotransmission happen long before motor neuron cell death: even at end stage of the disease only 25-30% motor neurons in spinal cord are lost (Cifuentes-Diaz et al. 2002). Although muscle weakness and finally paralysis are prominent SMA symptoms, NMJ denervation is rather moderate and varies strongly between muscles: specific muscles in the head, neck and trunk have

been shown to be more affected than those of distal extremities (Ling et al. 2012). This phenotype appears also to vary between mouse models as the Taiwanese SMA mice show a different profile of muscles affected by denervation: a vast majority of analyzed muscles showed minimal levels of denervation in SMA animals when compared to HET and exclusively *Flexor digitorum brevis* 2 and 3 (FDB-2/3) muscles showed severe and progressive denervation (Lin et al. 2016).

The development of NMJ is dependent on motor nerves reaching the muscle fibers; interestingly, some AChR clusters are formed already before the neuronal contact in a process termed “prepatternning” (Lin et al. 2008). However, aneural AChR disappear before birth and only the innervated ones remain and grow in size (Yang et al. 2001). At this stage of development, most AChR are of the “fetal” subtype (Mishina et al. 1986); furthermore, they show a high degree of polyinnervation as in neonatal muscle a single AChR cluster can be contacted by ~10 motor axons (Tapia et al. 2012). The final formation of NMJ occurs in rodents in the first three weeks of life when multiple innervation is reduced to a single motor axon, fetal AChRs are replaced with the adult form, the subsynaptic foldings of the membrane are formed and the size and density of AChR cluster increased and changes shape from a uniform plaque to an elaborate pretzel (Tintignac et al. 2015).

For the reliable transmission of the nerve impulse, the postsynaptic membrane must be organized with the help of numerous proteins. The master organizer of postsynaptic differentiation is the agrin-MusK pathway, where agrin, a heparan sulfate proteoglycan derived from the innervating motor axon, activates the muscle-specific kinase (MuSK) via a coreceptor low-density lipoprotein receptor-related protein 4 (Lrp4); furthermore, also downstream of tyrosine kinases-7 (Dok-7) and 43 kDa receptor-associated protein of the synapse (rapsyn) are necessary for NMJ formation (Zong et al. 2012). Mutations in genes encoding these key structural proteins result in congenital myasthenic syndromes (Ferraro et al. 2012). Importantly, splicing of agrin has been reported to be misregulated when SMN is depleted and thus may contribute to the initiation of NMJ pathology in SMA (Zhang et al. 2013). Although the NMJ development has been extensively studied, still not much is known about how SMN depletion affects the development of this intricately regulated synapse as most studies are limited to anatomical assessment (Goulet et al. 2013).

In our analysis of SMA-*Ncal*<sup>ko/wt</sup> mice, whether in the severe model or upon SMN-ASO injection, we assessed the effect of NCALD reduction by evaluating merely the size of NMJ in the TVA muscle. In both SMA models of variable severity NCALD reduction resulted in an increased NMJ area, however, not reaching the levels observed in HET littermates (5.2.6 and 5.3.4). Furthermore, when we evaluated the maturity in SMN-ASO injected animals, we could see that also this hallmark was improved upon decreased NCALD

levels. Especially the time-course study of NMJ size offered interesting conclusions: while in SMA mice no NMJ growth over time could be observed, reducing NCALD enabled the NMJ structure to grow and (at least partially) mature. It would be highly interesting to investigate the molecular basis of this structural amelioration, e.g. by studying the expression of synaptogenesis genes which were reported to be dysregulated in SMA (Zhang et al. 2013). Indeed, a recent study reported that downregulation of synaptic proteins such as synaptotagmin-1 and -2 and synaptic vesicle protein 2B corresponded to defects in neurotransmission, such as highly reduced evoked release, altered short-term plasticity and inability to modulate normally the number of functional release sites; notable, the reduction of these synaptic protein was correlated to the vulnerability of a given muscle and is potentially determinant for the selective sensitivity of muscles in SMA (Tejero et al. 2016). Also examining the functional consequences of the observed morphological alterations using electrophysiological methods would give us more insight into the protective mechanism of NCALD reduction (Arnold et al. 2014). In this way, we could analyze the effect of NCALD reduction on whole motor units, i.e. axon and its innervated muscle fibers: either by the compound muscle action potential (CMAP), which summates the electrical activity of all motor units in one muscle, or by motor unit number estimation (MUNE).

Due to its peripheral location NMJ is speculated as an attractive target for therapeutic agents (Boido and Vercelli 2016). As NMJs showed a consistent improvement upon genetic reduction of NCALD, it is worthwhile testing whether the same effect can be achieved by exogenous agents, such as *Ncald*-ASOs (5.4); in particular, determining whether the intervention requires a systemic or a CNS administration would potentially enhance the therapeutic value of this novel strategy.

#### **6.4 Why did NCALD reduction have no effect on the lifespan of SMA mice?**

While initially SMA was viewed as a disease of motor neurons, studies of mouse models revealed that other types of neurons (e.g. excitatory interneurons) but also various peripheral organs and systems were affected by SMN deficiency, e.g. bone, heart, intestine, liver, pancreas and vascular system (Khatri et al. 2008, Bevan et al. 2010, Mentis et al. 2011, Sahashi et al. 2013, Schreml et al. 2013, Bowerman et al. 2014, Simon et al. 2016, Somers et al. 2016). The fact that motor neurons are particularly, but not exclusively susceptible to low SMN gave rise to the so called threshold theory: in mouse studies it was observed that with decreasing SMN levels, motor neurons show defects as the first tissue, but once SMN deficiency has passed a certain threshold, heart and other susceptible organs start to develop a disease phenotype, until finally all tissues are affected (Sleigh et



al. 2011). However, this inner organ impairment has been observed mainly in severe SMA mouse models and in humans impairment of internal organs has been reported only for severely affected, so called type 0 patients who often have only one *SMN2* copy (Hamilton and Gillingwater 2013). Due to its housekeeping function, SMN deficiency has been reported to disrupt many essential cellular processes, such as apoptosis, autophagy and recently endocytosis (Anderton et al. 2013, Custer and Androphy 2014, Hosseinibarkooie et al. 2016). Therefore, the positive impact of NCALD reduction that was visible in the motor neurons, their glutamatergic inputs and at the NMJ level in severe SMA mice could not translate to an overall phenotypic improvement, when SMN deficiency continued to impair peripheral tissues (5.2.9 and 5.3.7). The importance of peripheral SMN delivery is highlighted by studies which reported that increasing SMN exclusively in the periphery is sufficient to extend the lifespan of severe SMA mice (Hua et al. 2015, Hammond et al. 2016).

The fact that NCALD reduction did not increase survival in the severe SMA mice is in concordance with similar studies of other SMA modifiers: stathmin and chondrolectin, which showed promising effect *in vitro* and in lower model organisms but failed to achieve a rescue *in vivo* (Wen et al. 2013, Sleight et al. 2014). Another study reported an improved survival by reducing IGF-1R, however, this was mediated by increasing SMN levels (Biondi et al. 2015). Also when SMN levels were increased exogenously by SMN-ASO injection, additionally overexpressing PLS3 has mediated significant survival rescue (Hosseinibarkooie et al. 2016). So far, only one study reported an SMN-independent survival of a severe SMA mouse model upon genetic inhibition of JNK3, a neuron-specific kinase implicated in neurodegeneration which was shown to be activated in spinal cords from SMA patients and mice: complete knock-out of *Jnk3* in SMA 7 mice lead to a systemic rescue of SMA phenotype including lifespan without changing SMN levels (Genabai et al. 2015).

As NCALD reduction ameliorated specifically neuronal pathologies in the severe SMA mice, but without a rescue of muscular and peripheral defects (5.2.8-9), we hypothesized that the positive effect of reduced NCALD is visible above a certain high threshold of SMN, similarly to the levels observed in asymptomatic individuals from Utah family. However, when SMN was increased by low-dose SMN-ASO injection, we observed no survival increase upon concomitant NCALD reduction (5.3.2). Histological studies of gastrointestinal tract revealed defects (although presumably of variable severity due to different SMN levels) in both the severe and the intermediate SMA model under study (5.2.9 and 5.3.7), therefore we concluded that likely this multi-organ impairment accounts for the reduced lifespan. This is contrary to another modifier studied in our group, PLS3, which, when overexpressed, could extend the lifespan of the intermediate model precisely

by ameliorating the disease phenotype in peripheral organs: intestine, heart and lung (HosseiniBarkooie et al. 2016). However, the PLS3 overexpression was driven by a ubiquitous transgene and positively affected the actin dynamics (Ackermann et al. 2013), whereas NCALD expression is mainly restricted to neuronal tissue (see 5.2.1).

The fact that heterozygous knock-out of *Ncald* did not prolong the survival of SMA mice raises the question whether the mouse models we used are good representation of the phenotype observed in *SMN1*-deleted asymptomatic individuals. Notably, these individuals all carry four *SMN2* copies which would theoretically associate with a mild SMA phenotype without a reduced life expectancy (SMA type 3 or 4), as opposed to the mouse models under study, which both showed reduced survival. Whether there is a threshold of SMN levels that still shows reduced survival which could be rescued by reducing NCALD remains unclear but is rather unlikely as it has been shown that increasing SMN levels above a certain threshold has dramatic and not gradual effect on survival (Osborne et al. 2012). Similarly, when only half of SMN-ASO dosis (1x 30 µg) was injected to SMA animals on the mixed background, the decreased survival was completely rescued but these mild SMA mice still displayed motoric impairment (Riessland et al. under review). Importantly, when NCALD was reduced in the mild SMA model, a clear improvement of the motoric phenotype was visible, which likely resembles better the situation of the asymptomatic individuals.

The observation that NCALD downregulation coincided with the asymptomatic phenotype was made in lymphoblastoid cell lines, however, it is not possible to determine the NCALD level in the spinal motor neurons, which are the actual tissue of interest, in living human subjects. This impediment could be overcome with technique of inducible pluripotent stem cell, which can be generated from available fibroblasts and subsequently differentiated into motor neurons; our group has already successfully applied this method to study the SMA modifier PLS3 (Heesen et al. 2016).

While considering potential therapeutic approaches for SMA, a differentiation must be made between severe and milder types. For severe SMA mouse models and for SMA type 1 patients, the survival rescue is crucial as death (or long-term dependence on ventilator support) presents the endpoint in clinical studies and for these groups, an increase of SMN levels seems to be an indispensable therapeutic step. While defects in peripheral organs have a major contribution to the mortality in SMA mouse models (with the sudden cardiac arrest being a likely cause of death), in SMA patients impairment of inner organs is a rare event observed only in the most severe cases (Palladino et al. 2011, Hamilton and Gillingwater 2013), which implicates the limitations of animal models of human diseases. Studies of SMN-independent modifiers that act downstream of SMN might be highly relevant for therapy development, in case the approach to supplement SMN protein does

not bring the desired full rescue in all patients; this is particularly important for therapies that rely on the *SMN2* expression, e.g. ASO that correct the *SMN2* splicing. Therefore, it is feasible that agents which specifically improve the neuromuscular system of the SMA mice might be useful as potential therapeutics in human patients, particularly as candidates for combinatorial therapies. Recent proof-of-principle study showed that once SMN levels were elevated early in the disease progression, modifiers such as PLS3 can mediate a long-term survival rescue (Hosseini et al. 2016). This view is favorable for NCALD reduction as a potential SMA therapy, especially for patients with slower disease progression but with significant motor dysfunction, who are in need of therapies enhancing the regeneration of the neuromuscular system (Iacone et al. 2015).

### 6.5 Effect of NCALD reduction on HET animals

Our studies of NCALD reduction in two SMA mouse models of variable severity quite clearly showed that by decreasing NCALD levels some, although not a complete, phenotypic rescue can be achieved. Paradoxically, the effect of NCALD reduction in HET animals was not unequivocally positive. As we observed in zebrafish studies, reducing *Ncald* resulted in increased EPSP amplitude and frequency and in enhanced neuronal branching (Riessland et al. under review); the latter could be recapitulated in mouse motor neurons (5.2.5). It is feasible that abnormally increased branching translates to a higher synaptic drive on motor neurons which might potentially disturb their normal development. In turn, aberrant motor neuronal signaling might impair the development of the endplate and the muscle as the target tissue (Favero et al. 2015).

In uninjected HET-*Ncald*<sup>ko/wt</sup> mice we observed the following alterations in comparison to HET littermates: the average number of glutamatergic inputs on motor neuron soma was increased without an effect of cell volume, which resulted in a higher ratio of inputs per  $\mu\text{m}^3$  (5.2.7). Interestingly, while the NMJ size was not changed, an increase in muscle fiber size was visible (5.2.6 and 8). Strikingly, in HET-*Ncald*<sup>ko/wt</sup>+ASO animals analyzed at an older age (on PND21), the reverse phenotype was observed: both the number of VGlut1+ inputs and the mean muscle fiber size were decreased when compared to HET+ASO littermates (5.3.5 and 6). It is feasible that excessive glutamatergic inputs disturb the homeostasis between excitatory and inhibitory signaling at the motor neuron soma and eventually results in a defect at the target tissue.

Taken together, these results strongly suggest that reducing NCALD in a healthy setting disrupts the fine balance of the neuromuscular system, which positions NCALD as an important regulator of the transmission of the signal from the nerve to the muscle. Interestingly, in HET-*Ncald*<sup>ko/wt</sup> mice the size of NMJ was not altered either in uninjected

PND10 or in SMN-ASO injected PND21 animals, implicating that under sufficient levels of SMN the effect of NCALD reduction is mediated not by increasing NMJ size, but likely by modifying the neurotransmission as shown in zebrafish (Riessland et al. under review); further electrophysiological studies in mice are needed to conclusively delineate this mechanism.

The possible explanation of the neuromuscular alterations observed in HET-*Ncald*<sup>ko/wt</sup> would be that if HET animals are viewed as representing a physiologically normal neuromuscular system, then by abrogating NCALD, a protein which is anticipated as relevant for neuronal functioning, whether through neurotransmission, synaptic vesicle recycling or neuronal activity, a disturbance of the homeostasis is to be expected. However, as SMN depletion causes a major imbalance in multiple cellular processes, concomitant NCALD reduction is able to restore some provisional balance, particularly in the neuromuscular system (Fig. 41).

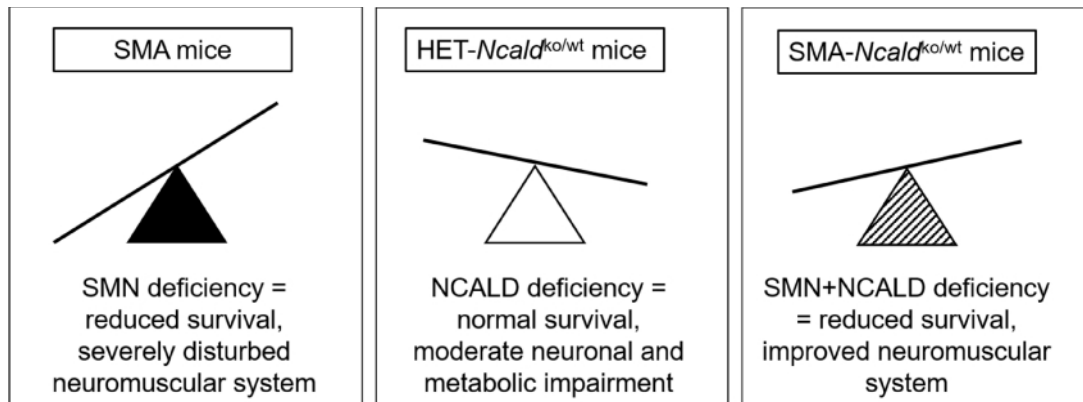


**Fig. 41: A model of restored neuromuscular homeostasis under concomitant depletion of SMN and NCALD**

The consequences of SMN deficiency are widely studied in SMA patients and SMA mouse models (Burghes and Beattie 2009). So far, little is known about the consequences of NCALD reduction. Our results show that many characteristics of the neuromuscular system which are defective in SMA can be partially corrected by concomitant NCALD reduction.

## 6.6 Clinical relevance of neuronal calcium sensors

Changes in intracellular calcium have an enormous impact on neuronal cells: they are essential to trigger neurotransmitter release (Sudhof 2012) but also for other processes such as synaptic plasticity and activity-dependent transcription (Berridge 1998).

Importantly, dysregulation of  $\text{Ca}^{2+}$  has been long implicated as a key contributor to neurodegeneration, e.g. an increase in intracellular  $\text{Ca}^{2+}$  can induce a change in mitochondrial  $\text{Ca}^{2+}$  and subsequently enhance oxidative stress by production of reactive

oxygen species and ultimately activate apoptotic cascade and trigger cell death (Naia et al. 2016).

In order to translate the changes of this single ion into such a plethora of cellular effects, a special class of neuronal calcium sensors (NCS) has evolved (Burgoyne 2007). The NCS proteins do not possess an intrinsic enzymatic activity; instead, upon an increase of  $\text{Ca}^{2+}$  levels they undergo conformational change and are then able to interact with their specific target proteins which allows processing subtle  $\text{Ca}^{2+}$  changes into cellular function (Burgoyne and Haynes 2015). The functions of these proteins are only beginning to be understood and so is their clinical relevance. Our finding that targeting NCALD is able to modify the SMA phenotype is in line with previous reports linking other NCS proteins to various neurodegenerative disorders which will be discussed in the following.

Many NCS proteins have been implicated in the etiology of Alzheimer's disease (AD) as potentially linked to the  $\text{Ca}^{2+}$ -hypothesis of AD where the abnormal metabolism of amyloid beta ( $\text{A}\beta$ ) induces a change in  $\text{Ca}^{2+}$  homeostasis, which initiates first the decline in memory and then massive changes in  $\text{Ca}^{2+}$ -levels and finally increased neuronal cell death (Popugaeva et al. 2016). The  $\text{A}\beta$ -mediated rise in intracellular  $\text{Ca}^{2+}$  has been shown to regulate the binding of calsenilin, a KChIP subfamily of NCS, to presenilin-2, which in turn leads to increase apoptosis and APP production (Jang et al. 2011). Additionally, the NCS protein VILIP1 has been shown to associate with amyloid plaques and to enhance tau phosphorylation which is a well-known hallmark of AD brains (Schnurra et al. 2001); VILIP1 protein levels were increased in the cerebrospinal fluid of AD patients although paradoxically, *VILIP1* mRNA was down-regulated in AD and correlated to the degree of cognitive impairment (Lee et al. 2008). In conclusion of numerous studies, neurons expressing VILIP1 seem to be particularly vulnerable against  $\text{A}\beta$ -induced disturbances of  $\text{Ca}^{2+}$ -homeostasis and die early on in the disease (Braunewell 2012). Notably, NCALD has been reported to be differentially expressed in mice lacking Bleomycin hydrolase (BLMH), a protein involved in the metabolism of homocysteine and linked to AD (Suszynska-Zajczyk et al. 2014).

The work of Dragisevic and colleagues has linked NCS-1, the evolutionary oldest member of the NCS family, to the Parkinson's disease (PD) as it is upregulated in the substantia nigra of PD patients. NCS1 is constitutively membrane-bound and in a complex with  $\text{Ca}_v1.3$  L-type- $\text{Ca}^{2+}$  channel and the dopamine D2 autoreceptor has been shown to tune the adaptive response of substantia nigra neurons dopaminergic agonists. This lead to the suggestion that targeting NCS1 might be a way to modify the vulnerability of substantia nigra neurons to neurodegeneration (Dragicevic et al. 2014).

## 6.7 Two independently identified SMA modifiers: NCALD and PLS3 act on endocytosis as a common pathway which is impaired in SMA

The fact that NCALD reduction ameliorated the SMA phenotype across species: in nematode, zebrafish and mouse, provided a hint towards an evolutionary conserved mechanism (Riessland et al. under review). Presumably, the protective effect of NCALD reduction is mediated by an interaction partner of NCALD; however, so far only few proteins interacting with NCALD have been identified (Fig. 42). We focused our attention on the reported NCALD interaction with clathrin (Ivings et al. 2002), as clathrin has been widely studied in the context of clathrin-mediated endocytosis (Rodemer and Haucke 2008) and NCALD was also identified within synaptic vesicles (Wilhelm et al. 2014). Furthermore, the  $\text{Ca}^{2+}$  dynamics at the presynaptic terminals is crucial for the regulation of endo- and exocytosis of neurotransmitters (Sudhof 2012). We showed that the NCALD-clathrin interaction is  $\text{Ca}^{2+}$  dependent; specifically, the binding occurred only when  $\text{Ca}^{2+}$  was absent (Riessland et al. under review).

The examination of the effect of NCALD reduction on the endocytic uptake in the context of SMA was performed in the NMJs of the TVA muscle in PND10 animals identical with those analyzed in 5.2: SMA, SMA-*Ncald*<sup>ko/wt</sup>, HET and HET-*Ncald*<sup>ko/wt</sup>, using a FM1-43 dye as recently described in (Hosseinibarkooie et al. 2016). When the nerve was stimulated under conditions simulating clathrin-mediated endocytosis, in the NMJs of SMA animals the dye uptake was significantly reduced in comparison to HET littermates, but concomitant NCALD reduction restored the uptake to control levels (Riessland et al. under review).

The importance of endocytosis impairment in SMA is further underlined by the fact that also overexpression of PLS3, which has been identified as protective modifier for SMA in humans (Oprea et al. 2008), could rescue the deficient endocytosis in SMA mice (Hosseinibarkooie et al. 2016). Notably, other proteins acting directly in endocytosis have been reported in a screen for SMA modifiers in *C. elegans* (Dimitriadi et al. 2016). Taken together, these findings recognize endocytosis as a common pathway impacted by both SMA modifiers: NCALD and PLS3.

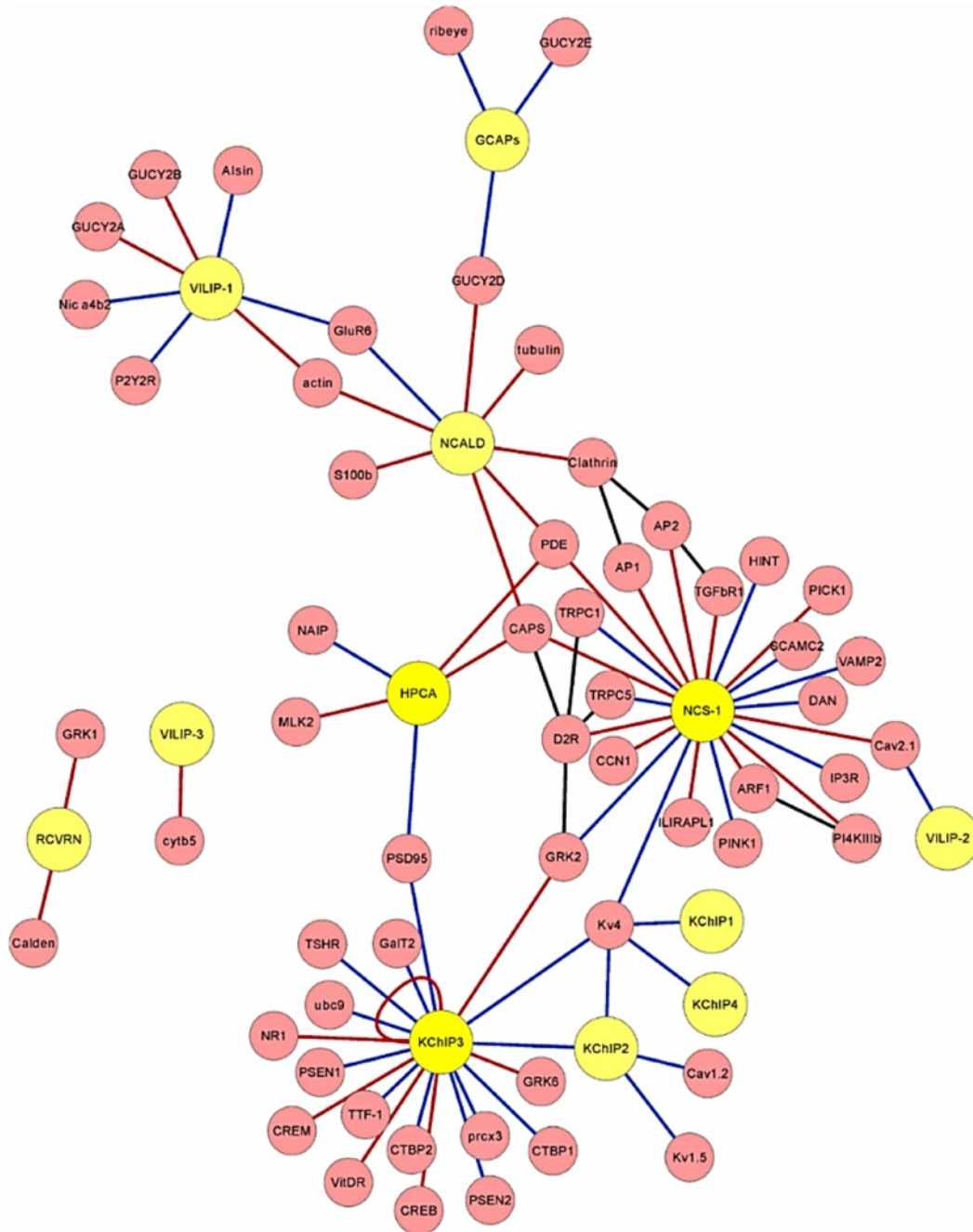


**Fig. 42: A map of known interaction partners of NCS proteins**

NCALD has been shown to interact with the following proteins: NCS-1, clathrin, tubulin and actin, CAPS (Ca<sup>2+</sup>-dependent activator protein for secretion), GluR6 (glutamate receptor 6), GUCY2D (guanylate cyclase 2D), S100b (S100 protein beta) and PDE (phosphodiesterase 1A); detailed information to other NCS proteins can be found in (Ivings et al. 2002, Burgoyne and Haynes 2012).

Interestingly, other NCS proteins have been demonstrated to play a role in a very specific kind of endocytosis indispensable for synaptic plasticity, namely the receptor endocytosis (Kerrigan et al. 2012). The hippocalcin together with calmodulin regulates the trafficking of NMDA receptors (Jo et al. 2010), while NCS-1 interacts with protein C kinase 1 (PICK1)

and IP3 in order to control the synaptic removal of the AMPA receptors by endocytosis (Jo et al. 2008). Interestingly, hippocalcin, which shares 91% homology with NCALD (Braunewell and Klein-Szanto 2009), has been shown to interact with the AP2 adaptor complex subunit to promote the clathrin-mediated endocytosis of AMPA receptors (Palmer et al. 2005). The recruitment of clathrin displaced hippocalcin, suggesting a similar antagonistic interaction between hippocalcin and clathrin as we hypothesize for NCALD in the context of SMA. In normal physiological conditions, after neurotransmitter release clathrin binds to synaptic membrane to participate in vesicle recycling (Takei and Haucke 2001, Soykan et al. 2016). As local  $\text{Ca}^{2+}$  is elevated after vesicle release, this induces conformational change of NCALD and release of clathrin to perform its endocytic function. In SMA, voltage-dependent  $\text{Ca}^{2+}$  influx is reduced and prevents the clathrin release, thus inhibiting clathrin from vesicle coating. However, when NCALD is reduced (as in asymptomatic individuals), even at low intracellular  $\text{Ca}^{2+}$  more clathrin is released to mediate efficient endocytosis (Fig. 43) (Riessland et al. under review).

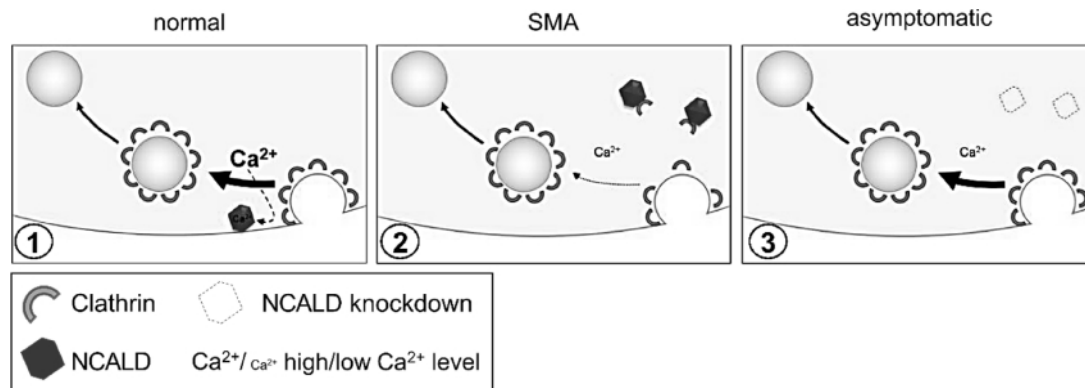


**Fig. 43: Proposed mode of NCALD acting on the endocytosis at the synaptic membrane**

Under normal physiological conditions of  $\text{Ca}^{2+}$  homeostasis, NCALD does not impair the clathrin-mediated endocytosis (CME). In SMA, however, the  $\text{Ca}^{2+}$  homeostasis and subsequently the CME are disturbed, but can be restored to normal function when NCALD is depleted, as in asymptomatic individuals (Riessland et al. under review).

## 6.8 Future outlook

While we succeeded in verifying the positive effect of reduced NCALD levels in various cellular systems and across species (nematode, zebrafish and mouse) and identified endocytosis as the key mechanism how NCALD reduction ameliorates SMA phenotype, the studies have opened new research avenues to follow:

- 1) as the *Ncald*<sup>ko/ko</sup> mouse line is readily available, an unbiased interactome study using proteomics approach with neuronal tissue can be conducted in order to see



the possible effect of *Ncald* knock-out on the binding partners, their stability and function;

- 2) since NCALD has three active EF-hand motifs with calcium binding ability, it is still possible that the calcium signaling is modified in the *Ncald*<sup>ko/ko</sup> animals; further studies including calcium imaging or investigation of the downstream signaling pathways would shed more light on this process;
- 3) considering the weight loss phenotype in the HET-*Ncald*<sup>ko/wt</sup> and HET-*Ncald*<sup>ko/ko</sup>, presumably the lipid metabolism is changed; further characterization of lipid and glucose profile in the blood of *Ncald*<sup>ko/ko</sup> mice can be a starting point to elucidate the role of NCALD in lipid metabolism;
- 4) it is worthwhile to investigate a possible effect of *Ncald* knock-out on the signaling of other closely related member of NCS family like VILIP1-3 and hippocalcin;
- 5) since NCALD has been shown to be upregulated in a mouse model of Alzheimer's disease (Suszynska-Zajczyk et al. 2014), *Ncald*<sup>ko/ko</sup> mouse model might be applied to study the effect of NCALD reduction on AD and on other neurodegenerative diseases;
- 6) so far, our analysis of genetic NCALD reduction was restricted to the neuromuscular system; considering apparent behavioral abnormalities, studies of other neuron populations, particularly in the brain, are presently performed to better understand the neuronal consequences of NCALD depletion;
- 7) a milder model of SMA which does not show a reduced survival but merely a motor phenotype is currently analyzed using electrophysiological recordings (CMAP) in order to investigate the long-term effect of NCALD reduction under lower SMN levels;
- 8) utilizing *Ncald*-ASOs as potential SMA therapeutics needs further optimization, especially to improve the safety profile;
- 9) as both NCALD and PLS3 were shown to improve the SMA phenotype, combining their protective potential in a new *Ncald*<sup>ko/wt</sup>; *PLS3*<sup>tg/tg</sup> mouse line is an exciting opportunity to study a potential synergistic effect of both modifiers *in vivo*.

## 7 References

1. Aartsma-Rus, A. and G. J. van Ommen (2010). "Progress in therapeutic antisense applications for neuromuscular disorders." *Eur J Hum Genet* 18(2): 146-153.
2. Ackermann, B., S. Krober, L. Torres-Benito, A. Borgmann, M. Peters, S. M. Hosseini Barkooie, R. Tejero, M. Jakubik, J. Schreml, J. Milbradt, T. F. Wunderlich, M. Riessland, L. Tabares and B. Wirth (2013). "Plastin 3 ameliorates spinal muscular atrophy via delayed axon pruning and improves neuromuscular junction functionality." *Hum Mol Genet* 22(7): 1328-1347.
3. Akten, B., M. J. Kye, T. Hao le, M. H. Wertz, S. Singh, D. Nie, J. Huang, T. T. Merianda, J. L. Twiss, C. E. Beattie, J. A. Steen and M. Sahin (2011). "Interaction of survival of motor neuron (SMN) and HuD proteins with mRNA cpg15 rescues motor neuron axonal deficits." *Proc Natl Acad Sci U S A* 108(25): 10337-10342.
4. Anderton, R. S., B. P. Meloni, F. L. Mastaglia and S. Boulos (2013). "Spinal muscular atrophy and the antiapoptotic role of survival of motor neuron (SMN) protein." *Mol Neurobiol* 47(2): 821-832.
5. Angelozzi, C., F. Borgo, F. D. Tiziano, A. Martella, G. Neri and C. Brahe (2008). "Salbutamol increases SMN mRNA and protein levels in spinal muscular atrophy cells." *J Med Genet* 45(1): 29-31.
6. Arkblad, E., M. Tulinius, A. K. Kroksmark, M. Henricsson and N. Darin (2009). "A population-based study of genotypic and phenotypic variability in children with spinal muscular atrophy." *Acta Paediatr* 98(5): 865-872.
7. Armstrong, C. M. and F. Bezanilla (1974). "Charge movement associated with the opening and closing of the activation gates of the Na channels." *J Gen Physiol* 63(5): 533-552.
8. Arnold, W. D., P. N. Porensky, V. L. McGovern, C. C. Iyer, S. Duque, X. Li, K. Meyer, L. Schmelzer, B. K. Kaspar, S. J. Kolb, J. T. Kissel and A. H. Burghes (2014). "Electrophysiological Biomarkers in Spinal Muscular Atrophy: Preclinical Proof of Concept." *Ann Clin Transl Neurol* 1(1): 34-44.
9. Avila, A. M., B. G. Burnett, A. A. Taye, F. Gabanella, M. A. Knight, P. Hartenstein, Z. Cizman, N. A. Di Prospero, L. Pellizzoni, K. H. Fischbeck and C. J. Sumner (2007). "Trichostatin A increases SMN expression and survival in a mouse model of spinal muscular atrophy." *J Clin Invest* 117(3): 659-671.
10. Benjamini, Y. and Y. Hochberg (1995). "Controlling the False Discovery Rate: A Practical and Powerful Approach to Multiple Testing " [*Royal Statistical Society, Wiley*] 57(1): 289-300.
11. Bennett, C. F. and E. E. Swayze (2010). "RNA targeting therapeutics: molecular mechanisms of antisense oligonucleotides as a therapeutic platform." *Annu Rev Pharmacol Toxicol* 50: 259-293.
12. Berridge, M. J. (1998). "Neuronal calcium signaling." *Neuron* 21(1): 13-26.
13. Bevan, A. K., K. R. Hutchinson, K. D. Foust, L. Braun, V. L. McGovern, L. Schmelzer, J. G. Ward, J. C. Petruska, P. A. Lucchesi, A. H. Burghes and B. K. Kaspar (2010). "Early heart failure in the SMN $\Delta$ 7 model of spinal muscular atrophy and correction by postnatal scAAV9-SMN delivery." *Hum Mol Genet* 19(20): 3895-3905.
14. Biogen and Ionis Pharmaceuticals (2016). Biogen and Ionis Pharmaceuticals Report Nusinersen Meets Primary Endpoint at Interim Analysis of Phase 3 ENDEAR Study in Infantile-Onset Spinal Muscular Atrophy CAMBRIDGE, Mass. & CARLSBAD, Calif. , Biogen Media.
15. Biondi, O., J. Branchu, A. Ben Salah, L. Houdebine, L. Bertin, F. Chali, C. Desseille, L. Weill, G. Sanchez, C. Lancelin, S. Aid, P. Lopes, C. Pariset, S. Lecolle, J. Cote, M. Holzenberger, C.

- Chanoine, C. Massaad and F. Charbonnier (2015). "IGF-1R Reduction Triggers Neuroprotective Signaling Pathways in Spinal Muscular Atrophy Mice." *J Neurosci* 35(34): 12063-12079.
16. Biondi, O., J. Branchu, G. Sanchez, C. Lancelin, S. Deforges, P. Lopes, C. Pariset, S. Lecolle, J. Cote, C. Chanoine and F. Charbonnier (2010). "In vivo NMDA receptor activation accelerates motor unit maturation, protects spinal motor neurons, and enhances SMN2 gene expression in severe spinal muscular atrophy mice." *J Neurosci* 30(34): 11288-11299.
17. Bogdanik, L. P., M. A. Osborne, C. Davis, W. P. Martin, A. Austin, F. Rigo, C. F. Bennett and C. M. Lutz (2015). "Systemic, postsymptomatic antisense oligonucleotide rescues motor unit maturation delay in a new mouse model for type II/III spinal muscular atrophy." *Proc Natl Acad Sci U S A* 112(43): E5863-5872.
18. Boido, M. and A. Vercelli (2016). "Neuromuscular Junctions as Key Contributors and Therapeutic Targets in Spinal Muscular Atrophy." *Front Neuroanat* 10: 6.
19. Bordet, T., B. Buisson, M. Michaud, C. Drouot, P. Galea, P. Delaage, N. P. Akentieva, A. S. Evers, D. F. Covey, M. A. Ostuni, J. J. Lacapere, C. Massaad, M. Schumacher, E. M. Steidl, D. Maux, M. Delaage, C. E. Henderson and R. M. Pruss (2007). "Identification and characterization of cholest-4-en-3-one, oxime (TRO19622), a novel drug candidate for amyotrophic lateral sclerosis." *J Pharmacol Exp Ther* 322(2): 709-720.
20. Bowerman, M., C. L. Anderson, A. Beauvais, P. P. Boyl, W. Witke and R. Kothary (2009). "SMN, profilin IIa and plastin 3: a link between the deregulation of actin dynamics and SMA pathogenesis." *Mol Cell Neurosci* 42(1): 66-74.
21. Bowerman, M., A. Beauvais, C. L. Anderson and R. Kothary (2010). "Rho-kinase inactivation prolongs survival of an intermediate SMA mouse model." *Hum Mol Genet* 19(8): 1468-1478.
22. Bowerman, M., J. P. Michalski, A. Beauvais, L. M. Murray, Y. DeRepentigny and R. Kothary (2014). "Defects in pancreatic development and glucose metabolism in SMN-depleted mice independent of canonical spinal muscular atrophy neuromuscular pathology." *Hum Mol Genet* 23(13): 3432-3444.
23. Bowerman, M., L. M. Murray, A. Beauvais, B. Pinheiro and R. Kothary (2011). "A critical smn threshold in mice dictates onset of an intermediate spinal muscular atrophy phenotype associated with a distinct neuromuscular junction pathology." *Neuromuscul Disord* 22(3): 263-276.
24. Bowerman, M., L. M. Murray, J. G. Boyer, C. L. Anderson and R. Kothary (2012). "Fasudil improves survival and promotes skeletal muscle development in a mouse model of spinal muscular atrophy." *BMC Med* 10: 24.
25. Bowerman, M., D. Shafey and R. Kothary (2007). "Smn depletion alters profilin II expression and leads to upregulation of the RhoA/ROCK pathway and defects in neuronal integrity." *J Mol Neurosci* 32(2): 120-131.
26. Boyer, J. G., M. O. Deguise, L. M. Murray, A. Yazdani, Y. De Repentigny, C. Boudreau-Lariviere and R. Kothary (2014). "Myogenic program dysregulation is contributory to disease pathogenesis in spinal muscular atrophy." *Hum Mol Genet* 23(16): 4249-4259.
27. Bradford, M. M. (1976). "A rapid and sensitive method for the quantitation of microgram quantities of protein utilizing the principle of protein-dye binding." *Anal Biochem* 72: 248-254.
28. Braun, S., B. Croizat, M. C. Lagrange, J. M. Warter and P. Poindron (1995). "Constitutive muscular abnormalities in culture in spinal muscular atrophy." *Lancet* 345(8951): 694-695.
29. Braunewell, K. H. (2012). "The visinin-like proteins VILIP-1 and VILIP-3 in Alzheimer's disease-old wine in new bottles." *Front Mol Neurosci* 5: 20.

30. Braunewell, K. H. and A. J. Klein-Szanto (2009). "Visinin-like proteins (VSNLs): interaction partners and emerging functions in signal transduction of a subfamily of neuronal Ca<sup>2+</sup> -sensor proteins." *Cell Tissue Res* 335(2): 301-316.
31. Bricceno, K. V., T. Martinez, E. Leikina, S. Duguez, T. A. Partridge, L. V. Chernomordik, K. H. Fischbeck, C. J. Sumner and B. G. Burnett (2014). "Survival motor neuron protein deficiency impairs myotube formation by altering myogenic gene expression and focal adhesion dynamics." *Hum Mol Genet* 23(18): 4745-4757.
32. Briesse, M., B. Esmaeili, S. Fraboulet, E. C. Burt, S. Christodoulou, P. R. Towers, K. E. Davies and D. B. Sattelle (2009). "Deletion of *smn-1*, the *Caenorhabditis elegans* ortholog of the spinal muscular atrophy gene, results in locomotor dysfunction and reduced lifespan." *Hum Mol Genet* 18(1): 97-104.
33. Brzustowicz, L. M., T. Lehner, L. H. Castilla, G. K. Penchaszadeh, K. C. Wilhelmsen, R. Daniels, K. E. Davies, M. Leppert, F. Ziter, D. Wood and et al. (1990). "Genetic mapping of chronic childhood-onset spinal muscular atrophy to chromosome 5q11.2-13.3." *Nature* 344(6266): 540-541.
34. Burghes, A. H. and C. E. Beattie (2009). "Spinal muscular atrophy: why do low levels of survival motor neuron protein make motor neurons sick?" *Nat Rev Neurosci* 10(8): 597-609.
35. Burglen, L., S. Lefebvre, O. Clermont, P. Burlet, L. Violette, C. Cruaud, A. Munnich and J. Melki (1996). "Structure and organization of the human survival motor neurone (SMN) gene." *Genomics* 32(3): 479-482.
36. Burgoyne, R. D. (2007). "Neuronal calcium sensor proteins: generating diversity in neuronal Ca<sup>2+</sup> signalling." *Nat Rev Neurosci* 8(3): 182-193.
37. Burgoyne, R. D. and L. P. Haynes (2010). "Neuronal calcium sensor proteins: emerging roles in membrane traffic and synaptic plasticity." *F1000 Biol Rep* 2.
38. Burgoyne, R. D. and L. P. Haynes (2012). "Understanding the physiological roles of the neuronal calcium sensor proteins." *Mol Brain* 5(1): 2.
39. Burgoyne, R. D. and L. P. Haynes (2015). "Sense and specificity in neuronal calcium signalling." *Biochim Biophys Acta* 1853(9): 1921-1932.
40. Burnett, B. G., E. Munoz, A. Tandon, D. Y. Kwon, C. J. Sumner and K. H. Fischbeck (2009). "Regulation of SMN protein stability." *Mol Cell Biol* 29(5): 1107-1115.
41. Calixto, A., D. Chelur, I. Topalidou, X. Chen and M. Chalfie (2010). "Enhanced neuronal RNAi in *C. elegans* using SID-1." *Nat Methods* 7(7): 554-559.
42. Cashman, N. R., H. D. Durham, J. K. Blusztajn, K. Oda, T. Tabira, I. T. Shaw, S. Dahrouge and J. P. Antel (1992). "Neuroblastoma x spinal cord (NSC) hybrid cell lines resemble developing motor neurons." *Dev Dyn* 194(3): 209-221.
43. Chang, H. C., D. N. Dimlich, T. Yokokura, A. Mukherjee, M. W. Kankel, A. Sen, V. Sridhar, T. A. Fulga, A. C. Hart, D. Van Vactor and S. Artavanis-Tsakonas (2008). "Modeling spinal muscular atrophy in *Drosophila*." *PLoS One* 3(9): e3209.
44. Charlesworth, G., P. R. Angelova, F. Bartolome-Robledo, M. Ryten, D. Trabzuni, M. Stamelou, A. Y. Abramov, K. P. Bhatia and N. W. Wood (2015). "Mutations in HPCA cause autosomal-recessive primary isolated dystonia." *Am J Hum Genet* 96(4): 657-665.
45. Chery, J. and A. Naar (2016). "RNA therapeutics: RNAi and antisense mechanisms and clinical applications." *Postdoc J* 4(7): 35-50.

46. Chiriboga, C. A., K. J. Swoboda, B. T. Darras, S. T. Iannaccone, J. Montes, D. C. De Vivo, D. A. Norris, C. F. Bennett and K. M. Bishop (2016). "Results from a phase 1 study of nusinersen (ISIS-SMN(Rx)) in children with spinal muscular atrophy." *Neurology* 86(10): 890-897.
47. Cifuentes-Diaz, C., S. Nicole, M. E. Velasco, C. Borra-Cebrian, C. Panozzo, T. Frugier, G. Millet, N. Roblot, V. Joshi and J. Melki (2002). "Neurofilament accumulation at the motor endplate and lack of axonal sprouting in a spinal muscular atrophy mouse model." *Hum Mol Genet* 11(12): 1439-1447.
48. Cobben, J. M., H. Scheffer, M. De Visser, G. Van der Steege, J. B. Verhey, J. Osinga, M. Burton, R. G. Mensink, P. M. Grootsholten, L. P. Ten Kate and C. H. Buys (1996). "Prenatal prediction of spinal muscular atrophy. Experience with linkage studies and consequences of present SMN deletion analysis." *Eur J Hum Genet* 4(4): 231-236.
49. Cobben, J. M., G. van der Steege, P. Grootsholten, M. de Visser, H. Scheffer and C. H. Buys (1995). "Deletions of the survival motor neuron gene in unaffected siblings of patients with spinal muscular atrophy." *Am J Hum Genet* 57(4): 805-808.
50. Coque, E., C. Raoul and M. Bowerman (2014). "ROCK inhibition as a therapy for spinal muscular atrophy: understanding the repercussions on multiple cellular targets." *Front Neurosci* 8: 271.
51. Custer, S. K. and E. J. Androphy (2014). "Autophagy dysregulation in cell culture and animals models of spinal muscular atrophy." *Mol Cell Neurosci* 61: 133-140.
52. Di Sole, F., K. Vadnagara, O. W. Moe and V. Babich (2012). "Calcineurin homologous protein: a multifunctional Ca<sup>2+</sup>-binding protein family." *Am J Physiol Renal Physiol* 303(2): F165-179.
53. Dimitriadi, M., A. Derdowski, G. Kalloo, M. S. Maginnis, P. O'Hern, B. Bliska, A. Sorkac, K. C. Nguyen, S. J. Cook, G. Poulogiannis, W. J. Atwood, D. H. Hall and A. C. Hart (2016). "Decreased function of survival motor neuron protein impairs endocytic pathways." *Proc Natl Acad Sci U S A* 113(30): E4377-4386.
54. Dimitriadi, M., A. Derdowski, G. Kalloo, M. S. Maginnis, P. O'Hern, B. Bliska, A. Sorkac, K. C. Nguyen, S. J. Cook, G. Poulogiannis, W. J. Atwood, D. H. Hall and A. C. Hart (2016). "Decreased function of survival motor neuron protein impairs endocytic pathways." *Proc Natl Acad Sci U S A*.
55. Dimitriadi, M., M. J. Kye, G. Kalloo, J. M. Yersak, M. Sahin and A. C. Hart (2013). "The neuroprotective drug riluzole acts via small conductance Ca<sup>2+</sup>-activated K<sup>+</sup> channels to ameliorate defects in spinal muscular atrophy models." *J Neurosci* 33(15): 6557-6562.
56. Dimitriadi, M., J. N. Sleight, A. Walker, H. C. Chang, A. Sen, G. Kalloo, J. Harris, T. Barsby, M. B. Walsh, J. S. Satterlee, C. Li, D. Van Vactor, S. Artavanis-Tsakonas and A. C. Hart (2010). "Conserved genes act as modifiers of invertebrate SMN loss of function defects." *PLoS Genet* 6(10): e1001172.
57. Doktor, T. K., Y. Hua, H. S. Andersen, S. Broner, Y. H. Liu, A. Wieckowska, M. Dembic, G. H. Bruun, A. R. Krainer and B. S. Andresen (2016). "RNA-sequencing of a mouse-model of spinal muscular atrophy reveals tissue-wide changes in splicing of U12-dependent introns." *Nucleic Acids Res.*
58. Dragicevic, E., C. Poetschke, J. Duda, F. Schlaudraff, S. Lammel, J. Schiemann, M. Fauler, A. Hetzel, M. Watanabe, R. Lujan, R. C. Malenka, J. Striessnig and B. Liss (2014). "Cav1.3 channels control D2-autoreceptor responses via NCS-1 in substantia nigra dopamine neurons." *Brain* 137(Pt 8): 2287-2302.
59. Drapeau, P., R. R. Buss, D. W. Ali, P. Legendre and R. L. Rotundo (2001). "Limits to the development of fast neuromuscular transmission in zebrafish." *J Neurophysiol* 86(6): 2951-2956.

60. Dubowitz, V. (1964). "Infantile Muscular Atrophy. A Prospective Study with Particular Reference to a Slowly Progressive Variety." *Brain* 87: 707-718.
61. Dubowitz, V. (1999). "Very severe spinal muscular atrophy (SMA type 0): an expanding clinical phenotype." *Eur J Paediatr Neurol* 3(2): 49-51.
62. Dubowitz, V. (2009). "Ramblings in the history of spinal muscular atrophy." *Neuromuscul Disord* 19(1): 69-73.
63. Dunning, M. J., N. L. Barbosa-Morais, A. G. Lynch, S. Tavare and M. E. Ritchie (2008). "Statistical issues in the analysis of Illumina data." *BMC Bioinformatics* 9: 85.
64. Duque, S., B. Joussemet, C. Riviere, T. Marais, L. Dubreil, A. M. Douar, J. Fyfe, P. Moullier, M. A. Colle and M. Barkats (2009). "Intravenous administration of self-complementary AAV9 enables transgene delivery to adult motor neurons." *Mol Ther* 17(7): 1187-1196.
65. El-Khodori, B. F., N. Edgar, A. Chen, M. L. Winberg, C. Joyce, D. Brunner, M. Suarez-Farinas and M. P. Heyes (2008). "Identification of a battery of tests for drug candidate evaluation in the SMNDelta7 neonate model of spinal muscular atrophy." *Exp Neurol* 212(1): 29-43.
66. Evans, M. J. and M. H. Kaufman (1981). "Establishment in culture of pluripotential cells from mouse embryos." *Nature* 292(5819): 154-156.
67. Fallini, C., G. J. Bassell and W. Rossoll (2012). "Spinal muscular atrophy: the role of SMN in axonal mRNA regulation." *Brain Res* 1462: 81-92.
68. Fallini, C., P. G. Donlin-Asp, J. P. Rouanet, G. J. Bassell and W. Rossoll (2016). "Deficiency of the Survival of Motor Neuron Protein Impairs mRNA Localization and Local Translation in the Growth Cone of Motor Neurons." *J Neurosci* 36(13): 3811-3820.
69. Farooq, F., F. Abadia-Molina, D. MacKenzie, J. Hadwen, F. Shamim, S. O'Reilly, M. Holcik and A. MacKenzie (2013). "Celecoxib increases SMN and survival in a severe spinal muscular atrophy mouse model via p38 pathway activation." *Hum Mol Genet* 22(17): 3415-3424.
70. Farooq, F., F. A. Molina, J. Hadwen, D. MacKenzie, L. Witherspoon, M. Osmond, M. Holcik and A. MacKenzie (2011). "Prolactin increases SMN expression and survival in a mouse model of severe spinal muscular atrophy via the STAT5 pathway." *J Clin Invest* 121(8): 3042-3050.
71. Fatt, P. and B. Katz (1951). "An analysis of the end-plate potential recorded with an intracellular electrode." *J Physiol* 115(3): 320-370.
72. Favero, M., A. Cangiano and G. Busetto (2015). "Lesson from the neuromuscular junction: role of pattern and timing of nerve activity in synaptic development." *Neural Regen Res* 10(5): 686-688.
73. Fayzullina, S. and L. J. Martin (2014). "Skeletal muscle DNA damage precedes spinal motor neuron DNA damage in a mouse model of Spinal Muscular Atrophy (SMA)." *PLoS One* 9(3): e93329.
74. Feldkotter, M., V. Schwarzer, R. Wirth, T. F. Wienker and B. Wirth (2002). "Quantitative analyses of SMN1 and SMN2 based on real-time lightCycler PCR: fast and highly reliable carrier testing and prediction of severity of spinal muscular atrophy." *Am J Hum Genet* 70(2): 358-368.
75. Ferraro, E., F. Molinari and L. Berghella (2012). "Molecular control of neuromuscular junction development." *J Cachexia Sarcopenia Muscle* 3(1): 13-23.
76. Finkel, R. S., M. P. McDermott, P. Kaufmann, B. T. Darras, W. K. Chung, D. M. Sproule, P. B. Kang, A. R. Foley, M. L. Yang, W. B. Martens, M. Oskoui, A. M. Glanzman, J. Flickinger, J. Montes, S. Dunaway, J. O'Hagen, J. Quigley, S. Riley, M. Benton, P. A. Ryan, M. Montgomery, J. Marra, C.

- Gooch and D. C. De Vivo (2014). "Observational study of spinal muscular atrophy type I and implications for clinical trials." *Neurology* 83(9): 810-817.
77. Fischer, U., Q. Liu and G. Dreyfuss (1997). "The SMN-SIP1 complex has an essential role in spliceosomal snRNP biogenesis." *Cell* 90(6): 1023-1029.
78. Flanagan-Steet, H., M. A. Fox, D. Meyer and J. R. Sanes (2005). "Neuromuscular synapses can form in vivo by incorporation of initially aneural postsynaptic specializations." *Development* 132(20): 4471-4481.
79. Foust, K. D., X. Wang, V. L. McGovern, L. Braun, A. K. Bevan, A. M. Haidet, T. T. Le, P. R. Morales, M. M. Rich, A. H. Burghes and B. K. Kaspar (2010). "Rescue of the spinal muscular atrophy phenotype in a mouse model by early postnatal delivery of SMN." *Nat Biotechnol* 28(3): 271-274.
80. Gabanella, F., M. E. Butchbach, L. Saieva, C. Carissimi, A. H. Burghes and L. Pellizzoni (2007). "Ribonucleoprotein assembly defects correlate with spinal muscular atrophy severity and preferentially affect a subset of spliceosomal snRNPs." *PLoS One* 2(9): e921.
81. Garbes, L., M. Riessland, I. Holker, R. Heller, J. Hauke, C. Trankle, R. Coras, I. Blumcke, E. Hahnen and B. Wirth (2009). "LBH589 induces up to 10-fold SMN protein levels by several independent mechanisms and is effective even in cells from SMA patients non-responsive to valproate." *Hum Mol Genet* 18(19): 3645-3658.
82. Gavrilina, T. O., V. L. McGovern, E. Workman, T. O. Crawford, R. G. Gogliotti, C. J. DiDonato, U. R. Monani, G. E. Morris and A. H. Burghes (2008). "Neuronal SMN expression corrects spinal muscular atrophy in severe SMA mice while muscle-specific SMN expression has no phenotypic effect." *Hum Mol Genet* 17(8): 1063-1075.
83. Genabai, N. K., S. Ahmad, Z. Zhang, X. Jiang, C. A. Gabaldon and L. Gangwani (2015). "Genetic inhibition of JNK3 ameliorates spinal muscular atrophy." *Hum Mol Genet* 24(24): 6986-7004.
84. Gilliam, T. C., L. M. Brzustowicz, L. H. Castilla, T. Lehner, G. K. Penchaszadeh, R. J. Daniels, B. C. Byth, J. Knowles, J. E. Hislop, Y. Shapira and et al. (1990). "Genetic homogeneity between acute and chronic forms of spinal muscular atrophy." *Nature* 345(6278): 823-825.
85. Glascock, J. J., E. Y. Osman, T. H. Coady, F. F. Rose, M. Shababi and C. L. Lorson (2011). "Delivery of therapeutic agents through intracerebroventricular (ICV) and intravenous (IV) injection in mice." *J Vis Exp*(56).
86. Gogliotti, R. G., K. A. Quinlan, C. B. Barlow, C. R. Heier, C. J. Heckman and C. J. DiDonato (2012). "Motor neuron rescue in spinal muscular atrophy mice demonstrates that sensory-motor defects are a consequence, not a cause, of motor neuron dysfunction." *J Neurosci* 32(11): 3818-3829.
87. Gomez, M., E. De Castro, E. Guarin, H. Sasakura, A. Kuhara, I. Mori, T. Bartfai, C. I. Bargmann and P. Nef (2001). "Ca<sup>2+</sup> signaling via the neuronal calcium sensor-1 regulates associative learning and memory in *C. elegans*." *Neuron* 30(1): 241-248.
88. Gordon-Weeks, P. R. and A. E. Fournier (2014). "Neuronal cytoskeleton in synaptic plasticity and regeneration." *J Neurochem* 129(2): 206-212.
89. Goulet, B. B., R. Kothary and R. J. Parks (2013). "At the 'junction' of spinal muscular atrophy pathogenesis: the role of neuromuscular junction dysfunction in SMA disease progression." *Curr Mol Med* 13(7): 1160-1174.
90. Greene, L. A. and A. S. Tischler (1976). "Establishment of a noradrenergic clonal line of rat adrenal pheochromocytoma cells which respond to nerve growth factor." *Proc Natl Acad Sci U S A* 73(7): 2424-2428.

91. Grzeschik, S. M., M. Ganta, T. W. Prior, W. D. Heavlin and C. H. Wang (2005). "Hydroxyurea enhances SMN2 gene expression in spinal muscular atrophy cells." *Ann Neurol* 58(2): 194-202.
92. Gutschner, T., M. Baas and S. Diederichs (2011). "Noncoding RNA gene silencing through genomic integration of RNA destabilizing elements using zinc finger nucleases." *Genome Res* 21(11): 1944-1954.
93. Haddad, H., C. Cifuentes-Diaz, A. Miroglio, N. Roblot, V. Joshi and J. Melki (2003). "Riluzole attenuates spinal muscular atrophy disease progression in a mouse model." *Muscle Nerve* 28(4): 432-437.
94. Hadwen, J., D. MacKenzie, F. Shamim, K. Mongeon, M. Holcik, A. MacKenzie and F. Farooq (2014). "VPAC2 receptor agonist BAY 55-9837 increases SMN protein levels and moderates disease phenotype in severe spinal muscular atrophy mouse models." *Orphanet J Rare Dis* 9: 4.
95. Hahnen, E., R. Forkert, C. Marke, S. Rudnik-Schoneborn, J. Schonling, K. Zerres and B. Wirth (1995). "Molecular analysis of candidate genes on chromosome 5q13 in autosomal recessive spinal muscular atrophy: evidence of homozygous deletions of the SMN gene in unaffected individuals." *Hum Mol Genet* 4(10): 1927-1933.
96. Hamilton, G. and T. H. Gillingwater (2013). "Spinal muscular atrophy: going beyond the motor neuron." *Trends Mol Med* 19(1): 40-50.
97. Hammond, S. M., G. Hazell, F. Shabanpoor, A. F. Saleh, M. Bowerman, J. N. Sleight, K. E. Meijboom, H. Zhou, F. Muntoni, K. Talbot, M. J. Gait and M. J. Wood (2016). "Systemic peptide-mediated oligonucleotide therapy improves long-term survival in spinal muscular atrophy." *Proc Natl Acad Sci U S A* 113(39): 10962-10967.
98. Harding, B. N., S. Kariya, U. R. Monani, W. K. Chung, M. Benton, S. W. Yum, G. Tennekoon and R. S. Finkel (2015). "Spectrum of neuropathophysiology in spinal muscular atrophy type I." *J Neuropathol Exp Neurol* 74(1): 15-24.
99. Haucke, V., E. Neher and S. J. Sigrist (2011). "Protein scaffolds in the coupling of synaptic exocytosis and endocytosis." *Nat Rev Neurosci* 12(3): 127-138.
100. Haynes, L. P., H. V. McCue and R. D. Burgoyne (2012). "Evolution and functional diversity of the Calcium Binding Proteins (CaBPs)." *Front Mol Neurosci* 5: 9.
101. Heesen, L., M. Peitz, L. Torres-Benito, I. Holker, K. Hupperich, K. Dobrindt, J. Jungverdorben, S. Ritzenhofen, B. Weykopf, D. Eckert, S. M. Hosseini-Barkooie, M. Storbeck, N. Fusaki, R. Lonigro, R. Heller, M. J. Kye, O. Brustle and B. Wirth (2016). "Plastin 3 is upregulated in iPSC-derived motoneurons from asymptomatic SMN1-deleted individuals." *Cell Mol Life Sci* 73(10): 2089-2104.
102. Hidaka, H. and K. Okazaki (1993). "Neurocalcin family: a novel calcium-binding protein abundant in bovine central nervous system." *Neurosci Res* 16(2): 73-77.
103. Hitz, C., W. Wurst and R. Kuhn (2007). "Conditional brain-specific knockdown of MAPK using Cre/loxP regulated RNA interference." *Nucleic Acids Res* 35(12): e90.
104. Hoffmann, J. (1893). "Über chronische spinale Muskelatrophie im Kindesalter, auf familiärer Basis." *Dtsch Z Nervenheilk* 3: 427-470.
105. Hosseinibarkooie, S., M. Peters, L. Torres-Benito, R. H. Rastetter, K. Hupperich, A. Hoffmann, N. Mendoza-Ferreira, A. Kaczmarek, E. Janzen, J. Milbradt, T. Lamkemeyer, F. Rigo, C. F. Bennett, C. Guschlbauer, A. Buschges, M. Hammerschmidt, M. Riessland, M. J. Kye, C. S. Clemen and B. Wirth (2016). "The Power of Human Protective Modifiers: PLS3 and CORO1C Unravel Impaired Endocytosis in Spinal Muscular Atrophy and Rescue SMA Phenotype." *Am J Hum Genet* 99(3): 647-665.



106. Hsieh-Li, H. M., J. G. Chang, Y. J. Jong, M. H. Wu, N. M. Wang, C. H. Tsai and H. Li (2000). "A mouse model for spinal muscular atrophy." *Nat Genet* 24(1): 66-70.
107. Hsu, P. D., E. S. Lander and F. Zhang (2014). "Development and applications of CRISPR-Cas9 for genome engineering." *Cell* 157(6): 1262-1278.
108. Hua, Y., Y. H. Liu, K. Sahashi, F. Rigo, C. F. Bennett and A. R. Krainer (2015). "Motor neuron cell-nonautonomous rescue of spinal muscular atrophy phenotypes in mild and severe transgenic mouse models." *Genes Dev* 29(3): 288-297.
109. Hua, Y., K. Sahashi, G. Hung, F. Rigo, M. A. Passini, C. F. Bennett and A. R. Krainer (2010). "Antisense correction of SMN2 splicing in the CNS rescues necrosis in a type III SMA mouse model." *Genes Dev* 24(15): 1634-1644.
110. Hua, Y., K. Sahashi, F. Rigo, G. Hung, G. Horev, C. F. Bennett and A. R. Krainer (2011). "Peripheral SMN restoration is essential for long-term rescue of a severe spinal muscular atrophy mouse model." *Nature* 478(7367): 123-126.
111. Hua, Y., T. A. Vickers, H. L. Okunola, C. F. Bennett and A. R. Krainer (2008). "Antisense masking of an hnRNP A1/A2 intronic splicing silencer corrects SMN2 splicing in transgenic mice." *Am J Hum Genet* 82(4): 834-848.
112. Iascone, D. M., C. E. Henderson and J. C. Lee (2015). "Spinal muscular atrophy: from tissue specificity to therapeutic strategies." *F1000Prime Rep* 7: 04.
113. Iino, S., S. Kobayashi and H. Hidaka (1998). "Neurocalcin-immunopositive nerve terminals in the muscle spindle, Golgi tendon organ and motor endplate." *Brain Res* 808(2): 294-299.
114. Isaksson, H. S., B. Sorbe and T. K. Nilsson (2014). "Whole genome expression profiling of blood cells in ovarian cancer patients -prognostic impact of the CYP1B1, MTSS1, NCALD, and NOP14." *Oncotarget* 5(12): 4040-4049.
115. Ivings, L., S. R. Pennington, R. Jenkins, J. L. Weiss and R. D. Burgoyne (2002). "Identification of Ca<sup>2+</sup>-dependent binding partners for the neuronal calcium sensor protein neurocalcin delta: interaction with actin, clathrin and tubulin." *Biochem J* 363(Pt 3): 599-608.
116. Jablonka, S., M. Beck, B. D. Lechner, C. Mayer and M. Sendtner (2007). "Defective Ca<sup>2+</sup>-channel clustering in axon terminals disturbs excitability in motoneurons in spinal muscular atrophy." *J Cell Biol* 179(1): 139-149.
117. Jablonka, S., B. Schrank, M. Kralewski, W. Rossoll and M. Sendtner (2000). "Reduced survival motor neuron (Smn) gene dose in mice leads to motor neuron degeneration: an animal model for spinal muscular atrophy type III." *Hum Mol Genet* 9(3): 341-346.
118. Jackson Laboratory (2016, 27.09.2016). "Ncaldtm1.1(KOMP)Vlbg." <http://www.informatics.jax.org/allele/key/827975#phenotypes> Retrieved 05.10.2016, 2016.
119. Jang, C., J. K. Choi, Y. J. Na, B. Jang, W. Wasco, J. D. Buxbaum, Y. S. Kim and E. K. Choi (2011). "Calsenilin regulates presenilin 1/gamma-secretase-mediated N-cadherin epsilon-cleavage and beta-catenin signaling." *FASEB J* 25(12): 4174-4183.
120. Jo, J., S. Heon, M. J. Kim, G. H. Son, Y. Park, J. M. Henley, J. L. Weiss, M. Sheng, G. L. Collingridge and K. Cho (2008). "Metabotropic glutamate receptor-mediated LTD involves two interacting Ca(2+) sensors, NCS-1 and PICK1." *Neuron* 60(6): 1095-1111.
121. Jo, J., G. H. Son, B. L. Winters, M. J. Kim, D. J. Whitcomb, B. A. Dickinson, Y. B. Lee, K. Futai, M. Amici, M. Sheng, G. L. Collingridge and K. Cho (2010). "Muscarinic receptors induce LTD of NMDAR EPSCs via a mechanism involving hippocalcin, AP2 and PSD-95." *Nat Neurosci* 13(10): 1216-1224.

122. Kaczmarek, A., S. Schneider, B. Wirth and M. Riessland (2015). "Investigational therapies for the treatment of spinal muscular atrophy." *Expert Opin Investig Drugs* 24(7): 867-881.
123. Kariya, S., T. Obis, C. Garone, T. Akay, F. Sera, S. Iwata, S. Homma and U. R. Monani (2014). "Requirement of enhanced Survival Motoneuron protein imposed during neuromuscular junction maturation." *J Clin Invest* 124(2): 785-800.
124. Kariya, S., G. H. Park, Y. Maeno-Hikichi, O. Leykekhman, C. Lutz, M. S. Arkovitz, L. T. Landmesser and U. R. Monani (2008). "Reduced SMN protein impairs maturation of the neuromuscular junctions in mouse models of spinal muscular atrophy." *Hum Mol Genet* 17(16): 2552-2569.
125. Kashima, T. and J. L. Manley (2003). "A negative element in SMN2 exon 7 inhibits splicing in spinal muscular atrophy." *Nat Genet* 34(4): 460-463.
126. Kerrigan, T. L., J. W. Daniel, P. L. Regan and K. Cho (2012). "The role of neuronal calcium sensors in balancing synaptic plasticity and synaptic dysfunction." *Front Mol Neurosci* 5: 57.
127. Khatri, I. A., U. S. Chaudhry, M. G. Seikaly, R. H. Browne and S. T. Iannaccone (2008). "Low bone mineral density in spinal muscular atrophy." *J Clin Neuromuscul Dis* 10(1): 11-17.
128. Kitzmann, P. H. (2010). Animal Models of Spasticity. . Spasticity: Diagnosis and Management. A. E. E. P. Brashear, Demos Medical Publishing: 419-437.
129. Kleinhammer, A., J. Deussing, W. Wurst and R. Kuhn (2011). "Conditional RNAi in mice." *Methods* 53(2): 142-150.
130. Kleinhammer, A., W. Wurst and R. Kuhn (2011). "Constitutive and conditional RNAi transgenesis in mice." *Methods* 53(4): 430-436.
131. Kobayashi, M., T. Masaki, K. Hori, Y. Masuo, M. Miyamoto, H. Tsubokawa, H. Noguchi, M. Nomura and K. Takamatsu (2005). "Hippocalcin-deficient mice display a defect in cAMP response element-binding protein activation associated with impaired spatial and associative memory." *Neuroscience* 133(2): 471-484.
132. Kong, L., X. Wang, D. W. Choe, M. Polley, B. G. Burnett, M. Bosch-Marce, J. W. Griffin, M. M. Rich and C. J. Sumner (2009). "Impaired synaptic vesicle release and immaturity of neuromuscular junctions in spinal muscular atrophy mice." *J Neurosci* 29(3): 842-851.
133. Kubler, E. and H. Riezman (1993). "Actin and fimbrin are required for the internalization step of endocytosis in yeast." *Embo J* 12(7): 2855-2862.
134. Kugelberg, E. and L. Welander (1956). "Heredofamilial juvenile muscular atrophy simulating muscular dystrophy." *AMA Arch Neurol Psychiatry* 75(5): 500-509.
135. Kuroda, Y., I. Ohashi, T. Saito, J. Nagai, K. Ida, T. Naruto, M. Iai and K. Kurosawa (2014). "Refinement of the deletion in 8q22.2-q22.3: the minimum deletion size at 8q22.3 related to intellectual disability and epilepsy." *Am J Med Genet A* 164A(8): 2104-2108.
136. Kwon, J. E., E. K. Kim and E. J. Choi (2011). "Stabilization of the survival motor neuron protein by ASK1." *FEBS Lett* 585(9): 1287-1292.
137. Ladant, D. (1995). "Calcium and membrane binding properties of bovine neurocalcin delta expressed in Escherichia coli." *J Biol Chem* 270(7): 3179-3185.
138. Le, T. T., L. T. Pham, M. E. Butchbach, H. L. Zhang, U. R. Monani, D. D. Covert, T. O. Gavriliina, L. Xing, G. J. Bassell and A. H. Burghes (2005). "SMNDelta7, the major product of the centromeric survival motor neuron (SMN2) gene, extends survival in mice with spinal muscular atrophy and associates with full-length SMN." *Hum Mol Genet* 14(6): 845-857.

139. Lee, J. M., K. Blennow, N. Andreasen, O. Laterza, V. Modur, J. Olander, F. Gao, M. Ohlendorf and J. H. Ladenson (2008). "The brain injury biomarker VLP-1 is increased in the cerebrospinal fluid of Alzheimer disease patients." *Clin Chem* 54(10): 1617-1623.
140. Lee, Y. I., M. Mikesch, I. Smith, M. Rimer and W. Thompson (2011). "Muscles in a mouse model of spinal muscular atrophy show profound defects in neuromuscular development even in the absence of failure in neuromuscular transmission or loss of motor neurons." *Dev Biol* 356(2): 432-444.
141. Lefebvre, S., L. Burglen, S. Reboullet, O. Clermont, P. Burlet, L. Viollet, B. Benichou, C. Cruaud, P. Millasseau, M. Zeviani and et al. (1995). "Identification and characterization of a spinal muscular atrophy-determining gene." *Cell* 80(1): 155-165.
142. Li, C. H. and P. K. S. Tam (1998). "An iterative algorithm for minimum cross entropy thresholding." *Pattern Recognition Letters* 19: 771-776.
143. Lin, S., L. Landmann, M. A. Ruegg and H. R. Brenner (2008). "The role of nerve- versus muscle-derived factors in mammalian neuromuscular junction formation." *J Neurosci* 28(13): 3333-3340.
144. Lin, T. L., T. H. Chen, Y. Y. Hsu, Y. H. Cheng, B. T. Juang and Y. J. Jong (2016). "Selective Neuromuscular Denervation in Taiwanese Severe SMA Mouse Can Be Reversed by Morpholino Antisense Oligonucleotides." *PLoS One* 11(4): e0154723.
145. Linder, C. C. (2006). "Genetic variables that influence phenotype." *ILAR J* 47(2): 132-140.
146. Ling, K. K., R. M. Gibbs, Z. Feng and C. P. Ko (2012). "Severe neuromuscular denervation of clinically relevant muscles in a mouse model of spinal muscular atrophy." *Hum Mol Genet* 21(1): 185-195.
147. Ling, K. K., M. Y. Lin, B. Zingg, Z. Feng and C. P. Ko (2010). "Synaptic defects in the spinal and neuromuscular circuitry in a mouse model of spinal muscular atrophy." *PLoS One* 5(11): e15457.
148. Liu-Yesucevitz, L., G. J. Bassell, A. D. Gitler, A. C. Hart, E. Klann, J. D. Richter, S. T. Warren and B. Wolozin (2011). "Local RNA translation at the synapse and in disease." *J Neurosci* 31(45): 16086-16093.
149. Long, C., L. Amoasii, A. A. Mireault, J. R. McAnally, H. Li, E. Sanchez-Ortiz, S. Bhattacharyya, J. M. Shelton, R. Bassell-Duby and E. N. Olson (2016). "Postnatal genome editing partially restores dystrophin expression in a mouse model of muscular dystrophy." *Science* 351(6271): 400-403.
150. Lorson, C. L. and E. J. Androphy (2000). "An exonic enhancer is required for inclusion of an essential exon in the SMA-determining gene SMN." *Hum Mol Genet* 9(2): 259-265.
151. Lorson, C. L., E. Hahnen, E. J. Androphy and B. Wirth (1999). "A single nucleotide in the SMN gene regulates splicing and is responsible for spinal muscular atrophy." *Proc Natl Acad Sci U S A* 96(11): 6307-6311.
152. Lotti, F., W. L. Imlach, L. Saieva, E. S. Beck, T. Hao le, D. K. Li, W. Jiao, G. Z. Mentis, C. E. Beattie, B. D. McCabe and L. Pellizzoni (2012). "An SMN-dependent U12 splicing event essential for motor circuit function." *Cell* 151(2): 440-454.
153. Lunn, M. R. and C. H. Wang (2008). "Spinal muscular atrophy." *Lancet* 371(9630): 2120-2133.
154. Macia, E., M. Ehrlich, R. Massol, E. Boucrot, C. Brunner and T. Kirchhausen (2006). "Dynasore, a cell-permeable inhibitor of dynamin." *Dev Cell* 10(6): 839-850.

155. Makhortova, N. R., M. Hayhurst, A. Cerqueira, A. D. Sinor-Anderson, W. N. Zhao, P. W. Heiser, A. C. Arvanites, L. S. Davidow, Z. O. Waldon, J. A. Steen, K. Lam, H. D. Ngo and L. L. Rubin (2011). "A screen for regulators of survival of motor neuron protein levels." *Nat Chem Biol* 7(8): 544-552.
156. Malkki, H. (2016). "Neuromuscular disease: Mitochondrial dysfunction could precipitate motor neuron loss in spinal muscular atrophy." *Nat Rev Neurol* 12(10): 556.
157. Mattis, V. B., A. D. Ebert, M. Y. Fosso, C. W. Chang and C. L. Lorson (2009). "Delivery of a read-through inducing compound, TC007, lessens the severity of a spinal muscular atrophy animal model." *Hum Mol Genet* 18(20): 3906-3913.
158. McGivern, J. V., T. N. Patitucci, J. A. Nord, M. E. Barabas, C. L. Stucky and A. D. Ebert (2013). "Spinal muscular atrophy astrocytes exhibit abnormal calcium regulation and reduced growth factor production." *Glia* 61(9): 1418-1428.
159. McGovern, V. L., A. Massoni-Laporte, X. Wang, T. T. Le, H. T. Le, C. E. Beattie, M. M. Rich and A. H. Burghes (2015). "Plastin 3 Expression Does Not Modify Spinal Muscular Atrophy Severity in the 7 SMA Mouse." *PLoS One* 10(7): e0132364.
160. McJunkin, K., A. Mazurek, P. K. Premsrirut, J. Zuber, L. E. Dow, J. Simon, B. Stillman and S. W. Lowe (2011). "Reversible suppression of an essential gene in adult mice using transgenic RNA interference." *Proc Natl Acad Sci U S A* 108(17): 7113-7118.
161. McWhorter, M. L., U. R. Monani, A. H. Burghes and C. E. Beattie (2003). "Knockdown of the survival motor neuron (Smn) protein in zebrafish causes defects in motor axon outgrowth and pathfinding." *J Cell Biol* 162(5): 919-931.
162. Melki, J., S. Abdelhak, P. Sheth, M. F. Bachelot, P. Burlet, A. Marcadet, J. Aicardi, A. Barois, J. P. Carriere, M. Fardeau and et al. (1990). "Gene for chronic proximal spinal muscular atrophies maps to chromosome 5q." *Nature* 344(6268): 767-768.
163. Melki, J., S. Lefebvre, L. Burglen, P. Burlet, O. Clermont, P. Millasseau, S. Reboullet, B. Benichou, M. Zeviani, D. Le Paslier and et al. (1994). "De novo and inherited deletions of the 5q13 region in spinal muscular atrophies." *Science* 264(5164): 1474-1477.
164. Mentis, G. Z., D. Blivis, W. Liu, E. Drobac, M. E. Crowder, L. Kong, F. J. Alvarez, C. J. Sumner and M. J. O'Donovan (2011). "Early functional impairment of sensory-motor connectivity in a mouse model of spinal muscular atrophy." *Neuron* 69(3): 453-467.
165. Mercuri, E., E. Bertini, S. Messina, A. Solari, A. D'Amico, C. Angelozzi, R. Battini, A. Berardinelli, P. Boffi, C. Bruno, C. Cini, F. Colitto, M. Kinali, C. Minetti, T. Mongini, L. Morandi, G. Neri, S. Orcesi, M. Pane, M. Pelliccioni, A. Pini, F. D. Tiziano, M. Villanova, G. Vita and C. Brahe (2007). "Randomized, double-blind, placebo-controlled trial of phenylbutyrate in spinal muscular atrophy." *Neurology* 68(1): 51-55.
166. Miller, N., H. Shi, A. S. Zelikovich and Y. C. Ma (2016). "Motor Neuron Mitochondrial Dysfunction in Spinal Muscular Atrophy." *Hum Mol Genet*.
167. Mishina, M., T. Takai, K. Imoto, M. Noda, T. Takahashi, S. Numa, C. Methfessel and B. Sakmann (1986). "Molecular distinction between fetal and adult forms of muscle acetylcholine receptor." *Nature* 321(6068): 406-411.
168. Moffat, J., D. A. Grueneberg, X. Yang, S. Y. Kim, A. M. Kloepper, G. Hinkle, B. Piqani, T. M. Eisenhaure, B. Luo, J. K. Grenier, A. E. Carpenter, S. Y. Foo, S. A. Stewart, B. R. Stockwell, N. Hacohen, W. C. Hahn, E. S. Lander, D. M. Sabatini and D. E. Root (2006). "A lentiviral RNAi library for human and mouse genes applied to an arrayed viral high-content screen." *Cell* 124(6): 1283-1298.

169. Monani, U. R. and D. C. De Vivo (2014). "Neurodegeneration in spinal muscular atrophy: from disease phenotype and animal models to therapeutic strategies and beyond." *Future Neurol* 9(1): 49-65.
170. Monani, U. R., M. T. Pastore, T. O. Gavrilina, S. Jablonka, T. T. Le, C. Andreassi, J. M. DiCocco, C. Lorson, E. J. Androphy, M. Sendtner, M. Podell and A. H. Burghes (2003). "A transgene carrying an A2G missense mutation in the SMN gene modulates phenotypic severity in mice with severe (type I) spinal muscular atrophy." *J Cell Biol* 160(1): 41-52.
171. Monani, U. R., M. Sendtner, D. D. Covert, D. W. Parsons, C. Andreassi, T. T. Le, S. Jablonka, B. Schrank, W. Rossoll, T. W. Prior, G. E. Morris and A. H. Burghes (2000). "The human centromeric survival motor neuron gene (SMN2) rescues embryonic lethality in *Smn*(<sup>-/-</sup>) mice and results in a mouse with spinal muscular atrophy." *Hum Mol Genet* 9(3): 333-339.
172. Mullis, K., F. Faloona, S. Scharf, R. Saiki, G. Horn and H. Erlich (1986). "Specific enzymatic amplification of DNA in vitro: the polymerase chain reaction." *Cold Spring Harb Symp Quant Biol* 51 Pt 1: 263-273.
173. Murray, L., T. H. Gillingwater and R. Kothary (2014). "Dissection of the transversus abdominis muscle for whole-mount neuromuscular junction analysis." *J Vis Exp*(83): e51162.
174. Murray, L. M., L. H. Comley, D. Thomson, N. Parkinson, K. Talbot and T. H. Gillingwater (2008). "Selective vulnerability of motor neurons and dissociation of pre- and post-synaptic pathology at the neuromuscular junction in mouse models of spinal muscular atrophy." *Hum Mol Genet* 17(7): 949-962.
175. Murray, L. M., K. Talbot and T. H. Gillingwater (2010). "Review: neuromuscular synaptic vulnerability in motor neurone disease: amyotrophic lateral sclerosis and spinal muscular atrophy." *Neuropathol Appl Neurobiol* 36(2): 133-156.
176. Nadeau, J. H. (2001). "Modifier genes in mice and humans." *Nat Rev Genet* 2(3): 165-174.
177. Nagy, A., L. Mar and G. Watts (2009). "Creation and use of a cre recombinase transgenic database." *Methods Mol Biol* 530: 365-378.
178. Naia, L., I. L. Ferreira, E. Ferreira and A. C. Rego (2016). "Mitochondrial Ca<sup>2+</sup> handling in Huntington's and Alzheimer's diseases - Role of ER-mitochondria crosstalk." *Biochem Biophys Res Commun*.
179. Naryshkin, N. A., M. Weetall, A. Dakka, J. Narasimhan, X. Zhao, Z. Feng, K. K. Ling, G. M. Karp, H. Qi, M. G. Woll, G. Chen, N. Zhang, V. Gabbeta, P. Vazirani, A. Bhattacharyya, B. Furia, N. Risher, J. Sheedy, R. Kong, J. Ma, A. Turpoff, C. S. Lee, X. Zhang, Y. C. Moon, P. Trifillis, E. M. Welch, J. M. Colacino, J. Babiak, N. G. Almstead, S. W. Peltz, L. A. Eng, K. S. Chen, J. L. Mull, M. S. Lynes, L. L. Rubin, P. Fontoura, L. Santarelli, D. Haehnke, K. D. McCarthy, R. Schmucki, M. Ebeling, M. Sivaramakrishnan, C. P. Ko, S. V. Paushkin, H. Ratni, I. Gerlach, A. Ghosh and F. Metzger (2014). "Motor neuron disease. SMN2 splicing modifiers improve motor function and longevity in mice with spinal muscular atrophy." *Science* 345(6197): 688-693.
180. Nicole, S., B. Desforgues, G. Millet, J. Lesbordes, C. Cifuentes-Diaz, D. Vertes, M. L. Cao, F. De Backer, L. Languille, N. Roblot, V. Joshi, J. M. Gillis and J. Melki (2003). "Intact satellite cells lead to remarkable protection against *Smn* gene defect in differentiated skeletal muscle." *J Cell Biol* 161(3): 571-582.
181. Nolle, A., A. Zeug, J. van Bergeijk, L. Tonges, R. Gerhard, H. Brinkmann, S. Al Rayes, N. Hensel, Y. Schill, D. Apkhazava, S. Jablonka, J. O'Mer, R. K. Srivastav, A. Baasner, P. Lingor, B. Wirth, E. Ponimaskin, R. Niedenthal, C. Grothe and P. Claus (2012). "The spinal muscular atrophy disease protein SMN is linked to the Rho-kinase pathway via profilin." *Hum Mol Genet* 20(24): 4865-4878.

182. Nyabi, O., M. Naessens, K. Haigh, A. Gembarska, S. Goossens, M. Maetens, S. De Clercq, B. Drogat, L. Haenebalcke, S. Bartunkova, I. De Vos, B. De Craene, M. Karimi, G. Berx, A. Nagy, P. Hilson, J. C. Marine and J. J. Haigh (2009). "Efficient mouse transgenesis using Gateway-compatible ROSA26 locus targeting vectors and F1 hybrid ES cells." *Nucleic Acids Res* 37(7): e55.
183. Oh, D. Y., J. H. Cho, S. Y. Park, Y. S. Kim, Y. J. Yoon, S. H. Yoon, K. C. Chung, K. S. Lee and J. S. Han (2008). "A novel role of hippocalcin in bFGF-induced neurite outgrowth of H19-7 cells." *J Neurosci Res* 86(7): 1557-1565.
184. Ollion, J., J. Cochennec, F. Loll, C. Escude and T. Boudier (2013). "TANGO: a generic tool for high-throughput 3D image analysis for studying nuclear organization." *Bioinformatics* 29(14): 1840-1841.
185. Oprea, G. E., S. Krober, M. L. McWhorter, W. Rossoll, S. Muller, M. Krawczak, G. J. Bassell, C. E. Beattie and B. Wirth (2008). "Plastin 3 is a protective modifier of autosomal recessive spinal muscular atrophy." *Science* 320(5875): 524-527.
186. Osborne, M., D. Gomez, Z. Feng, C. McEwen, J. Beltran, K. Cirillo, B. El-Khodori, M. Y. Lin, Y. Li, W. M. Knowlton, D. D. McKemy, L. Bogdanik, K. Butts-Dehm, K. Martens, C. Davis, R. Doty, K. Wardwell, A. Ghavami, D. Kobayashi, C. P. Ko, S. Ramboz and C. Lutz (2012). "Characterization of behavioral and neuromuscular junction phenotypes in a novel allelic series of SMA mouse models." *Hum Mol Genet* 21(20): 4431-4447.
187. Oskoui, M., G. Levy, C. J. Garland, J. M. Gray, J. O'Hagen, D. C. De Vivo and P. Kaufmann (2007). "The changing natural history of spinal muscular atrophy type 1." *Neurology* 69(20): 1931-1936.
188. Otsu, N. (1979). "A threshold selection method from gray-level histograms." *IEEE Trans. Sys., Man., Cyber.* 9: 62-66.
189. Palladino, A., L. Passamano, A. Taglia, P. D'Ambrosio, M. Scutifero, M. R. Cecio, E. Picillo, E. Viggiano, V. Torre, F. De Luca, G. Nigro and L. Politano (2011). "Cardiac involvement in patients with spinal muscular atrophies." *Acta Myol* 30(3): 175-178.
190. Palmer, C. L., W. Lim, P. G. Hastie, M. Toward, V. I. Korolchuk, S. A. Burbidge, G. Banting, G. L. Collingridge, J. T. Isaac and J. M. Henley (2005). "Hippocalcin functions as a calcium sensor in hippocampal LTD." *Neuron* 47(4): 487-494.
191. Palop, J. J., J. Chin and L. Mucke (2006). "A network dysfunction perspective on neurodegenerative diseases." *Nature* 443(7113): 768-773.
192. Paquet, D., D. Kwart, A. Chen, A. Sproul, S. Jacob, S. Teo, K. M. Olsen, A. Gregg, S. Noggle and M. Tessier-Lavigne (2016). "Efficient introduction of specific homozygous and heterozygous mutations using CRISPR/Cas9." *Nature* 533(7601): 125-129.
193. Park, G. H., Y. Maeno-Hikichi, T. Awano, L. T. Landmesser and U. R. Monani (2010). "Reduced survival of motor neuron (SMN) protein in motor neuronal progenitors functions cell autonomously to cause spinal muscular atrophy in model mice expressing the human centromeric (SMN2) gene." *J Neurosci* 30(36): 12005-12019.
194. Passini, M. A., J. Bu, A. M. Richards, C. Kinnecom, S. P. Sardi, L. M. Stanek, Y. Hua, F. Rigo, J. Matson, G. Hung, E. M. Kaye, L. S. Shihabuddin, A. R. Krainer, C. F. Bennett and S. H. Cheng (2011). "Antisense oligonucleotides delivered to the mouse CNS ameliorate symptoms of severe spinal muscular atrophy." *Sci Transl Med* 3(72): 72ra18.
195. Pellizzoni, L. (2007). "Chaperoning ribonucleoprotein biogenesis in health and disease." *EMBO Rep* 8(4): 340-345.
196. Pellizzoni, L., N. Kataoka, B. Charroux and G. Dreyfuss (1998). "A novel function for SMN, the spinal muscular atrophy disease gene product, in pre-mRNA splicing." *Cell* 95(5): 615-624.

197. Popugaeva, E., E. Pchitskaya and I. Bezprozvanny (2016). "Dysregulation of neuronal calcium homeostasis in Alzheimer's disease - A therapeutic opportunity?" *Biochem Biophys Res Commun.*
198. Porensky, P. N., C. Mitropant, V. L. McGovern, A. K. Bevan, K. D. Foust, B. K. Kaspar, S. D. Wilton and A. H. Burghes (2012). "A single administration of morpholino antisense oligomer rescues spinal muscular atrophy in mouse." *Hum Mol Genet* 21(7): 1625-1638.
199. Powis, R. A. and T. H. Gillingwater (2016). "Selective loss of alpha motor neurons with sparing of gamma motor neurons and spinal cord cholinergic neurons in a mouse model of spinal muscular atrophy." *J Anat* 228(3): 443-451.
200. Prior, T. W., A. R. Krainer, Y. Hua, K. J. Swoboda, P. C. Snyder, S. J. Bridgeman, A. H. Burghes and J. T. Kissel (2009). "A positive modifier of spinal muscular atrophy in the SMN2 gene." *Am J Hum Genet* 85(3): 408-413.
201. Prior, T. W., K. J. Swoboda, H. D. Scott and A. Q. Hejmanowski (2004). "Homozygous SMN1 deletions in unaffected family members and modification of the phenotype by SMN2." *Am J Med Genet* 130A(3): 307-310.
202. Riessland, M., B. Ackermann, A. Forster, M. Jakubik, J. Hauke, L. Garbes, I. Fritzsche, Y. Mende, I. Blumcke, E. Hahnen and B. Wirth (2010). "SAHA ameliorates the SMA phenotype in two mouse models for spinal muscular atrophy." *Hum Mol Genet* 19(8): 1492-1506.
203. Riessland, M., L. Brichta, E. Hahnen and B. Wirth (2006). "The benzamide M344, a novel histone deacetylase inhibitor, significantly increases SMN2 RNA/protein levels in spinal muscular atrophy cells." *Hum Genet* 120(1): 101-110.
204. Riessland, M., A. Kaczmarek, S. Schneider, K. J. Swoboda, H. Löhr, C. Bradler, V. Grysko, M. Dimitriadi, S. M. Hosseini Barkooie, L. Torres-Benito, M. Peters, A. Upadhyay, N. Biglari, S. Kröber, I. Hölker, L. Garbes, C. Gilissen, A. Hoischen, G. Nürnberg, P. Nürnberg, M. Walter, F. Rigo, F. C. Bennett, M. J. Kye, A. C. Hart, M. Hammerschmidt, P. Kloppenburg and B. Wirth (under review). "Neurocalcin delta suppression rescues spinal muscular atrophy across species." *Nature Medicine* in review.
205. Rigo, F., Y. Hua, A. R. Krainer and C. F. Bennett (2012). "Antisense-based therapy for the treatment of spinal muscular atrophy." *J Cell Biol* 199(1): 21-25.
206. Rodemer, C. and V. Haucke (2008). "Clathrin/AP-2-dependent endocytosis: a novel playground for the pharmacological toolbox?" *Handb Exp Pharmacol*(186): 105-122.
207. Rosen, B., J. Schick and W. Wurst (2015). "Beyond knockouts: the International Knockout Mouse Consortium delivers modular and evolving tools for investigating mammalian genes." *Mamm Genome* 26(9-10): 456-466.
208. Rossoll, W., S. Jablonka, C. Andreassi, A. K. Kroning, K. Karle, U. R. Monani and M. Sendtner (2003). "Smn, the spinal muscular atrophy-determining gene product, modulates axon growth and localization of beta-actin mRNA in growth cones of motoneurons." *J Cell Biol* 163(4): 801-812.
209. Roudier, M. P., B. R. Winters, I. Coleman, H. M. Lam, X. Zhang, R. Coleman, L. Chery, L. D. True, C. S. Higano, B. Montgomery, P. H. Lange, L. A. Snyder, S. Srivastava, E. Corey, R. L. Vessella, P. S. Nelson, A. Uren and C. Morrissey (2016). "Characterizing the molecular features of ERG-positive tumors in primary and castration resistant prostate cancer." *Prostate* 76(9): 810-822.
210. Rudkowska, I., L. Perusse, C. Bellis, J. Blangero, J. P. Despres, C. Bouchard and M. C. Vohl (2015). "Interaction between Common Genetic Variants and Total Fat Intake on Low-Density Lipoprotein Peak Particle Diameter: A Genome-Wide Association Study." *J Nutrigenet Nutrigenomics* 8(1): 44-53.

211. Ruggiu, M., V. L. McGovern, F. Lotti, L. Saieva, D. K. Li, S. Kariya, U. R. Monani, A. H. Burghes and L. Pellizzoni (2012). "A role for SMN exon 7 splicing in the selective vulnerability of motor neurons in spinal muscular atrophy." *Mol Cell Biol* 32(1): 126-138.
212. Ruiz, R., J. J. Casanas, L. Torres-Benito, R. Cano and L. Tabares (2010). "Altered intracellular Ca<sup>2+</sup> homeostasis in nerve terminals of severe spinal muscular atrophy mice." *J Neurosci* 30(3): 849-857.
213. Saal, L., M. Briese, S. Kneitz, M. Glinka and M. Sendtner (2014). "Subcellular transcriptome alterations in a cell culture model of spinal muscular atrophy point to widespread defects in axonal growth and presynaptic differentiation." *RNA* 20(11): 1789-1802.
214. Sahashi, K., K. K. Ling, Y. Hua, J. E. Wilkinson, T. Nomakuchi, F. Rigo, G. Hung, D. Xu, Y. P. Jiang, R. Z. Lin, C. P. Ko, C. F. Bennett and A. R. Krainer (2013). "Pathological impact of SMN2 mis-splicing in adult SMA mice." *EMBO Mol Med* 5(10): 1586-1601.
215. Schick, J. A., C. Seisenberger, J. Beig, A. Burger, V. Iyer, V. Maier, S. Perera, B. Rosen, W. C. Skarnes and W. Wurst (2016). "CRISPR-Cas9 enables conditional mutagenesis of challenging loci." *Sci Rep* 6: 32326.
216. Schmid, A. and C. J. DiDonato (2007). "Animal models of spinal muscular atrophy." *J Child Neurol* 22(8): 1004-1012.
217. Schnurra, I., H. G. Bernstein, P. Riederer and K. H. Braunewell (2001). "The neuronal calcium sensor protein VILIP-1 is associated with amyloid plaques and extracellular tangles in Alzheimer's disease and promotes cell death and tau phosphorylation in vitro: a link between calcium sensors and Alzheimer's disease?" *Neurobiol Dis* 8(5): 900-909.
218. Schrank, B., R. Gotz, J. M. Gunnensen, J. M. Ure, K. V. Toyka, A. G. Smith and M. Sendtner (1997). "Inactivation of the survival motor neuron gene, a candidate gene for human spinal muscular atrophy, leads to massive cell death in early mouse embryos." *Proc Natl Acad Sci U S A* 94(18): 9920-9925.
219. Schreijf, A. M., E. A. Fon and P. S. McPherson (2016). "Endocytic membrane trafficking and neurodegenerative disease." *Cell Mol Life Sci* 73(8): 1529-1545.
220. Schreml, J., M. Riessland, M. Paterno, L. Garbes, K. Rossbach, B. Ackermann, J. Kramer, E. Somers, S. H. Parson, R. Heller, A. Berkessel, A. Sterner-Kock and B. Wirth (2013). "Severe SMA mice show organ impairment that cannot be rescued by therapy with the HDACi JNJ-26481585." *Eur J Hum Genet* 21(6): 643-652.
221. See, K., P. Yadav, M. Giegerich, P. S. Cheong, M. Graf, H. Vyas, S. G. Lee, S. Mathavan, U. Fischer, M. Sendtner and C. Winkler (2014). "SMN deficiency alters Nrnx2 expression and splicing in zebrafish and mouse models of spinal muscular atrophy." *Hum Mol Genet* 23(7): 1754-1770.
222. Sen, A., D. N. Dimlich, K. G. Guruharsha, M. W. Kankel, K. Hori, T. Yokokura, S. Brachat, D. Richardson, J. Loureiro, R. Sivasankaran, D. Curtis, L. S. Davidow, L. L. Rubin, A. C. Hart, D. Van Vactor and S. Artavanis-Tsakonas (2013). "Genetic circuitry of Survival motor neuron, the gene underlying spinal muscular atrophy." *Proc Natl Acad Sci U S A* 110(26): E2371-2380.
223. Shababi, M., C. L. Lorson and S. S. Rudnik-Schoneborn (2014). "Spinal muscular atrophy: a motor neuron disorder or a multi-organ disease?" *J Anat* 224(1): 15-28.
224. Shafey, D., P. D. Cote and R. Kothary (2005). "Hypomorphic Smn knockdown C2C12 myoblasts reveal intrinsic defects in myoblast fusion and myotube morphology." *Exp Cell Res* 311(1): 49-61.
225. Shi, X., C. Ma, Q. Zhu, D. Yuan, M. Sun, X. Gu, G. Wu, T. Lv and Y. Song (2016). "Upregulation of long intergenic noncoding RNA 00673 promotes tumor proliferation via LSD1 interaction and repression of NCALD in non-small-cell lung cancer." *Oncotarget* 7(18): 25558-25575.



226. Simon, C. M., A. M. Janas, F. Lotti, J. C. Tapia, L. Pellizzoni and G. Z. Mentis (2016). "A Stem Cell Model of the Motor Circuit Uncouples Motor Neuron Death from Hyperexcitability Induced by SMN Deficiency." *Cell Rep* 16(5): 1416-1430.
227. Simone, C., A. Ramirez, M. Bucchia, P. Rinchetti, H. Rideout, D. Papadimitriou, D. B. Re and S. Corti (2016). "Is spinal muscular atrophy a disease of the motor neurons only: pathogenesis and therapeutic implications?" *Cell Mol Life Sci* 73(5): 1003-1020.
228. Singh, N. N., M. Shishimorova, L. C. Cao, L. Gangwani and R. N. Singh (2009). "A short antisense oligonucleotide masking a unique intronic motif prevents skipping of a critical exon in spinal muscular atrophy." *RNA Biol* 6(3): 341-350.
229. Sintusek, P., F. Catapano, N. Angkathunkayul, E. Marrosu, S. H. Parson, J. E. Morgan, F. Muntoni and H. Zhou (2016). "Histopathological Defects in Intestine in Severe Spinal Muscular Atrophy Mice Are Improved by Systemic Antisense Oligonucleotide Treatment." *PLoS One* 11(5): e0155032.
230. Sleigh, J. N., A. Barreiro-Iglesias, P. L. Oliver, A. Biba, T. Becker, K. E. Davies, C. G. Becker and K. Talbot (2014). "Chondrolectin affects cell survival and neuronal outgrowth in in vitro and in vivo models of spinal muscular atrophy." *Hum Mol Genet* 23(4): 855-869.
231. Sleigh, J. N., T. H. Gillingwater and K. Talbot (2011). "The contribution of mouse models to understanding the pathogenesis of spinal muscular atrophy." *Dis Model Mech* 4(4): 457-467.
232. Somers, E., R. D. Lees, K. Hoban, J. N. Sleigh, H. Zhou, F. Muntoni, K. Talbot, T. H. Gillingwater and S. H. Parson (2016). "Vascular Defects and Spinal Cord Hypoxia in Spinal Muscular Atrophy." *Ann Neurol* 79(2): 217-230.
233. Somers, E., M. Riessland, J. Schreml, B. Wirth, T. H. Gillingwater and S. H. Parson (2013). "Increasing SMN levels using the histone deacetylase inhibitor SAHA ameliorates defects in skeletal muscle microvasculature in a mouse model of severe spinal muscular atrophy." *Neurosci Lett* 544: 100-104.
234. Soykan, T., T. Maritzen and V. Haucke (2016). "Modes and mechanisms of synaptic vesicle recycling." *Curr Opin Neurobiol* 39: 17-23.
235. Stevens, C. F. (2003). "Neurotransmitter release at central synapses." *Neuron* 40(2): 381-388.
236. Sudhof, T. C. (2012). "Calcium control of neurotransmitter release." *Cold Spring Harb Perspect Biol* 4(1): a011353.
237. Sumner, C. J., T. N. Huynh, J. A. Markowitz, J. S. Perhac, B. Hill, D. D. Coovert, K. Schussler, X. Chen, J. Jarecki, A. H. Burghes, J. P. Taylor and K. H. Fischbeck (2003). "Valproic acid increases SMN levels in spinal muscular atrophy patient cells." *Ann Neurol* 54(5): 647-654.
238. Sun, Y., M. Grimmmler, V. Schwarzer, F. Schoenen, U. Fischer and B. Wirth (2005). "Molecular and functional analysis of intragenic SMN1 mutations in patients with spinal muscular atrophy." *Hum Mutat* 25(1): 64-71.
239. Suszynska-Zajczyk, J., M. Luczak, L. Marczak and H. Jakubowski (2014). "Hyperhomocysteinemia and bleomycin hydrolase modulate the expression of mouse brain proteins involved in neurodegeneration." *J Alzheimers Dis* 40(3): 713-726.
240. Suszynska-Zajczyk, J., M. Luczak, L. Marczak and H. Jakubowski (2014). "Hyperhomocysteinemia and Bleomycin Hydrolase Modulate the Expression of Mouse Brain Proteins Involved in Neurodegeneration." *J Alzheimers Dis*.
241. Suszynska-Zajczyk, J., M. Luczak, L. Marczak and H. Jakubowski (2014). "Inactivation of the paraoxonase 1 gene affects the expression of mouse brain proteins involved in neurodegeneration." *J Alzheimers Dis* 42(1): 247-260.

242. Swoboda, K. J., C. B. Scott, T. O. Crawford, L. R. Simard, S. P. Reyna, K. J. Krosschell, G. Acsadi, B. Elsheik, M. K. Schroth, G. D'Anjou, B. LaSalle, T. W. Prior, S. L. Sorenson, J. A. Maczulski, M. B. Bromberg, G. M. Chan, J. T. Kissel and N. Project Cure Spinal Muscular Atrophy Investigators (2010). "SMA CARNI-VAL trial part I: double-blind, randomized, placebo-controlled trial of L-carnitine and valproic acid in spinal muscular atrophy." *PLoS One* 5(8): e12140.
243. Swoboda, K. J., C. B. Scott, S. P. Reyna, T. W. Prior, B. LaSalle, S. L. Sorenson, J. Wood, G. Acsadi, T. O. Crawford, J. T. Kissel, K. J. Krosschell, G. D'Anjou, M. B. Bromberg, M. K. Schroth, G. M. Chan, B. Elsheikh and L. R. Simard (2009). "Phase II open label study of valproic acid in spinal muscular atrophy." *PLoS One* 4(5): e5268.
244. Takei, K. and V. Haucke (2001). "Clathrin-mediated endocytosis: membrane factors pull the trigger." *Trends Cell Biol* 11(9): 385-391.
245. Tamariz, E. and A. Varela-Echavarria (2015). "The discovery of the growth cone and its influence on the study of axon guidance." *Front Neuroanat* 9: 51.
246. Tapia, J. C., J. D. Wylie, N. Kasthuri, K. J. Hayworth, R. Schalek, D. R. Berger, C. Guatimosim, H. S. Seung and J. W. Lichtman (2012). "Pervasive synaptic branch removal in the mammalian neuromuscular system at birth." *Neuron* 74(5): 816-829.
247. Tejero, R., M. Lopez-Manzaneda, S. Arumugam and L. Tabares (2016). "Synaptotagmin-2, and -1, linked to neurotransmission impairment and vulnerability in Spinal Muscular Atrophy." *Hum Mol Genet*.
248. Thomas, K. R. and M. R. Capecchi (1987). "Site-directed mutagenesis by gene targeting in mouse embryo-derived stem cells." *Cell* 51(3): 503-512.
249. Thyagarajan, B., E. C. Olivares, R. P. Hollis, D. S. Ginsburg and M. P. Calos (2001). "Site-specific genomic integration in mammalian cells mediated by phage phiC31 integrase." *Mol Cell Biol* 21(12): 3926-3934.
250. Tintignac, L. A., H. R. Brenner and M. A. Ruegg (2015). "Mechanisms Regulating Neuromuscular Junction Development and Function and Causes of Muscle Wasting." *Physiol Rev* 95(3): 809-852.
251. Torres-Benito, L., M. F. Neher, R. Cano, R. Ruiz and L. Tabares (2011). "SMN requirement for synaptic vesicle, active zone and microtubule postnatal organization in motor nerve terminals." *PLoS One* 6(10): e26164.
252. Torres, R. M. and R. Kuhn (1997). Laboratory protocols for conditional gene targeting. Oxford ; New York, Oxford University Press.
253. Valenzuela, D. M., A. J. Murphy, D. Frendewey, N. W. Gale, A. N. Economides, W. Auerbach, W. T. Poueymirou, N. C. Adams, J. Rojas, J. Yasenchak, R. Chernomorsky, M. Boucher, A. L. Elsasser, L. Esau, J. Zheng, J. A. Griffiths, X. Wang, H. Su, Y. Xue, M. G. Dominguez, I. Noguera, R. Torres, L. E. Macdonald, A. F. Stewart, T. M. DeChiara and G. D. Yancopoulos (2003). "High-throughput engineering of the mouse genome coupled with high-resolution expression analysis." *Nat Biotechnol* 21(6): 652-659.
254. Venkataraman, V., T. Duda, S. Ravichandran and R. K. Sharma (2008). "Neurocalcin delta modulation of ROS-GC1, a new model of Ca(2+) signaling." *Biochemistry* 47(25): 6590-6601.
255. Vercauteren, F. G., G. Flores, W. Ma, J. G. Chabot, L. Geenen, S. Clerens, A. Fazel, J. J. Bergeron, L. K. Srivastava, L. Arckens and R. Quirion (2007). "An organelle proteomic method to study neurotransmission-related proteins, applied to a neurodevelopmental model of schizophrenia." *Proteomics* 7(19): 3569-3579.
256. Vezain, M., P. Saugier-veber, E. Goina, R. Touraine, V. Manel, A. Toutain, S. Fehrenbach, T. Frebourg, F. Pagani, M. Tosi and A. Martins (2010). "A rare SMN2 variant in a previously

unrecognized composite splicing regulatory element induces exon 7 inclusion and reduces the clinical severity of spinal muscular atrophy." *Hum Mutat* 31(1): E1110-1125.

257. Villalobos, C. and R. Andrade (2010). "Visinin-like neuronal calcium sensor proteins regulate the slow calcium-activated afterhyperpolarizing current in the rat cerebral cortex." *J Neurosci* 30(43): 14361-14365.

258. Vitte, J. M., B. Davoult, N. Roblot, M. Mayer, V. Joshi, S. Courageot, F. Tronche, J. Vadrot, M. H. Moreau, F. Kemeny and J. Melki (2004). "Deletion of murine Smn exon 7 directed to liver leads to severe defect of liver development associated with iron overload." *Am J Pathol* 165(5): 1731-1741.

259. Viviano, J., A. Krishnan, H. Wu and V. Venkataraman (2016). "Data on the calcium-induced mobility shift of myristoylated and non-myristoylated forms of neurocalcin delta." *Data Brief* 7: 630-633.

260. von Kleist, L., W. Stahlschmidt, H. Bulut, K. Gromova, D. Puchkov, M. J. Robertson, K. A. MacGregor, N. Tomilin, A. Pechstein, N. Chau, M. Chircop, J. Sakoff, J. P. von Kries, W. Saenger, H. G. Krausslich, O. Shupliakov, P. J. Robinson, A. McCluskey and V. Haucke (2011). "Role of the clathrin terminal domain in regulating coated pit dynamics revealed by small molecule inhibition." *Cell* 146(3): 471-484.

261. Wang, C. H., J. Xu, T. A. Carter, B. M. Ross, M. K. Dominski, C. A. Bellcross, G. K. Penchaszadeh, T. L. Munsat and T. C. Gilliam (1996). "Characterization of survival motor neuron (SMNT) gene deletions in asymptomatic carriers of spinal muscular atrophy." *Hum Mol Genet* 5(3): 359-365.

262. Weiss, J. L., H. Hui and R. D. Burgoyne (2010). "Neuronal calcium sensor-1 regulation of calcium channels, secretion, and neuronal outgrowth." *Cell Mol Neurobiol* 30(8): 1283-1292.

263. Wen, H. L., C. H. Ting, H. C. Liu, H. Li and S. Lin-Chao (2013). "Decreased stathmin expression ameliorates neuromuscular defects but fails to prolong survival in a mouse model of spinal muscular atrophy." *Neurobiol Dis* 52: 94-103.

264. Werdnig, G. (1891). "Two early infantile hereditary cases of progressive muscular atrophy simulating dystrophy, but on a neural basis. ." *Arch Neurol* 25(3): 276-278.

265. Westerfield, M., J. V. McMurray and J. S. Eisen (1986). "Identified motoneurons and their innervation of axial muscles in the zebrafish." *J Neurosci* 6(8): 2267-2277.

266. Wettenhall, J. M. and G. K. Smyth (2004). "limmaGUI: a graphical user interface for linear modeling of microarray data." *Bioinformatics* 20(18): 3705-3706.

267. Wiederschain, D., S. Wee, L. Chen, A. Loo, G. Yang, A. Huang, Y. Chen, G. Caponigro, Y. M. Yao, C. Lengauer, W. R. Sellers and J. D. Benson (2009). "Single-vector inducible lentiviral RNAi system for oncology target validation." *Cell Cycle* 8(3): 498-504.

268. Wilhelm, B. G., S. Mandad, S. Truckenbrodt, K. Krohnert, C. Schafer, B. Rammner, S. J. Koo, G. A. Classen, M. Krauss, V. Haucke, H. Urlaub and S. O. Rizzoli (2014). "Composition of isolated synaptic boutons reveals the amounts of vesicle trafficking proteins." *Science* 344(6187): 1023-1028.

269. Wirth, B., L. Garbes and M. Riessland (2013). "How genetic modifiers influence the phenotype of spinal muscular atrophy and suggest future therapeutic approaches." *Curr Opin Genet Dev* 23(3): 330-338.

270. Wirth, B., N. Mendoza-Ferreira and L. Torres-Benito (2016). Spinal Muscular Atrophy Disease Modifiers. Spinal Muscular Atrophy. C. J. Sumner, S. Paushkin and C. P. Ko, Academic Press.

271. Wishart, T. M., C. A. Mutsaers, M. Riessland, M. M. Reimer, G. Hunter, M. L. Hannam, S. L. Eaton, H. R. Fuller, S. L. Roche, E. Somers, R. Morse, P. J. Young, D. J. Lamont, M. Hammerschmidt, A. Joshi, P. Hohenstein, G. E. Morris, S. H. Parson, P. A. Skehel, T. Becker, I. M. Robinson, C. G. Becker, B. Wirth and T. H. Gillingwater (2014). "Dysregulation of ubiquitin homeostasis and beta-catenin signaling promote spinal muscular atrophy." *J Clin Invest* 124(4): 1821-1834.
272. Xu, W., S. Cohen-Woods, Q. Chen, A. Noor, J. Knight, G. Hosang, S. V. Parikh, V. De Luca, F. Tozzi, P. Muglia, J. Forte, A. McQuillin, P. Hu, H. M. Gurling, J. L. Kennedy, P. McGuffin, A. Farmer, J. Strauss and J. B. Vincent (2014). "Genome-wide association study of bipolar disorder in Canadian and UK populations corroborates disease loci including SYNE1 and CSMD1." *BMC Med Genet* 15: 2.
273. Yamatani, H., T. Kawasaki, S. Mita, N. Inagaki and T. Hirata (2010). "Proteomics analysis of the temporal changes in axonal proteins during maturation." *Dev Neurobiol* 70(7): 523-537.
274. Yang, X., S. Arber, C. William, L. Li, Y. Tanabe, T. M. Jessell, C. Birchmeier and S. J. Burden (2001). "Patterning of muscle acetylcholine receptor gene expression in the absence of motor innervation." *Neuron* 30(2): 399-410.
275. Yoshida, M., S. Kitaoka, N. Egawa, M. Yamane, R. Ikeda, K. Tsukita, N. Amano, A. Watanabe, M. Morimoto, J. Takahashi, H. Hosoi, T. Nakahata, H. Inoue and M. K. Saito (2015). "Modeling the early phenotype at the neuromuscular junction of spinal muscular atrophy using patient-derived iPSCs." *Stem Cell Reports* 4(4): 561-568.
276. Zerres, K., S. Rudnik-Schoneborn, R. Forkert and B. Wirth (1995). "Genetic basis of adult-onset spinal muscular atrophy." *Lancet* 346(8983): 1162.
277. Zerres, K., B. Wirth and S. Rudnik-Schoneborn (1997). "Spinal muscular atrophy--clinical and genetic correlations." *Neuromuscul Disord* 7(3): 202-207.
278. Zhang, Z., F. Lotti, K. Dittmar, I. Younis, L. Wan, M. Kasim and G. Dreyfuss (2008). "SMN deficiency causes tissue-specific perturbations in the repertoire of snRNAs and widespread defects in splicing." *Cell* 133(4): 585-600.
279. Zhang, Z., A. M. Pinto, L. Wan, W. Wang, M. G. Berg, I. Oliva, L. N. Singh, C. Dengler, Z. Wei and G. Dreyfuss (2013). "Dysregulation of synaptogenesis genes antecedes motor neuron pathology in spinal muscular atrophy." *Proc Natl Acad Sci U S A* 110(48): 19348-19353.
280. Zhou, C., Z. Feng and C. P. Ko (2016). "Defects in Motoneuron-Astrocyte Interactions in Spinal Muscular Atrophy." *J Neurosci* 36(8): 2543-2553.
281. Zhou, H., N. Janghra, C. Mitropant, R. L. Dickinson, K. Anthony, L. Price, I. C. Eperon, S. D. Wilton, J. Morgan and F. Muntoni (2013). "A novel morpholino oligomer targeting ISS-N1 improves rescue of severe spinal muscular atrophy transgenic mice." *Hum Gene Ther* 24(3): 331-342.
282. Zong, Y., B. Zhang, S. Gu, K. Lee, J. Zhou, G. Yao, D. Figueiredo, K. Perry, L. Mei and R. Jin (2012). "Structural basis of agrin-LRP4-MuSK signaling." *Genes Dev* 26(3): 247-258.

## 8 Appendix

The manuscript “Neurocalcin delta suppression rescues spinal muscular atrophy across species”, under review in Nature Medicine (for reference purposes)

### Neurocalcin delta suppression rescues spinal muscular atrophy across species

Markus Riessland,<sup>1,2,3,13,14</sup> Anna Kaczmarek,<sup>1,2,3,13</sup> Svenja Schneider,<sup>1,2,3,13</sup> Kathryn J. Swoboda,<sup>4</sup> Heiko Löhr,<sup>5,7</sup> Cathleen Bradler,<sup>6,7</sup> Vanessa Grysko,<sup>1,2,3</sup> Maria Dimitriadi,<sup>8,15</sup> Seyyedmohsen Hosseinibarkooie,<sup>1,2,3</sup> Laura Torres-Benito,<sup>1,2,3</sup> Miriam Peters,<sup>1,2,3</sup> Aaradhita Upadhyay,<sup>1,2,3</sup> Nasim Biglari,<sup>1,2,3</sup> Sandra Kröber,<sup>1,2,3</sup> Irmgard Hölker,<sup>1,2,3</sup> Lutz Garbes,<sup>1,2,3</sup> Christian Gilissen,<sup>9</sup> Alexander Hoischen,<sup>9</sup> Gudrun Nürnberg,<sup>7,10</sup> Peter Nürnberg,<sup>7,10</sup> Michael Walter,<sup>11</sup> Frank Rigo,<sup>12</sup> C. Frank Bennett,<sup>12</sup> Min Jeong Kye,<sup>1,2</sup> Anne C. Hart,<sup>8</sup> Matthias Hammerschmidt,<sup>5,7</sup> Peter Kloppenburg,<sup>6,7</sup> and Brunhilde Wirth<sup>1,2,3,\*</sup>

<sup>1</sup>Institute of Human Genetics, University of Cologne, 50931 Cologne, Germany

<sup>2</sup>Center for Molecular Medicine Cologne, University of Cologne, 50931 Cologne, Germany

<sup>3</sup>Institute for Genetics, University of Cologne, 50674 Cologne, Germany

<sup>4</sup>MassGeneral Hospital for Children, Boston, MA 02115, USA

<sup>5</sup>Institute for Zoology - Developmental Biology, University of Cologne, 50674 Cologne, Germany

<sup>6</sup>Institute for Zoology - Neurophysiology University of Cologne, 50674 Cologne, Germany

<sup>7</sup>Excellence Cluster on Cellular Stress Responses in Aging Associated Diseases (CECAD), University of Cologne, 50931 Cologne, Germany

<sup>8</sup>Department of Neuroscience, Brown University, Providence, Rhode Island, USA

<sup>9</sup>Department of Human Genetics, Donders Centre for Neuroscience, Radboud University Medical Center, 6525 Nijmegen, The Netherlands

<sup>10</sup>Center for Genomics Cologne, University of Cologne, 50931 Cologne, Germany

<sup>11</sup>Institute of Medical Genetics, University of Tübingen, 72076 Tübingen, Germany

<sup>12</sup>IONIS Pharmaceuticals, Carlsbad, California, CA 92008, USA

<sup>13</sup>These authors contributed equally to this work

#### Present address:

<sup>14</sup>Laboratory of Molecular and Cellular Neuroscience, The Rockefeller University, New York, NY 10065, USA

<sup>15</sup>Department of Biological and Environmental Sciences, University of Hertfordshire, Hatfield, AL10 9AB, UK

\*Correspondence: brunhilde.wirth@uk-koeln.de

**ABSTRACT**

Homozygous *SMN1* gene loss causes spinal muscular atrophy (SMA), the most common lethal genetic childhood motor neuron disease. SMA patients harbor low SMN expression from *SMN2* copy genes, insufficient to functionally compensate for *SMN1* loss. Here, we identify that the neuronal calcium sensor Neurocalcin delta (NCALD) functions as a protective SMA modifier in humans and acts as a  $\text{Ca}^{2+}$ -dependent negative regulator of endocytosis. Indeed, SMN deficiency impairs endocytosis, which is restored by NCALD depletion. NCALD depletion also restores pharmacologically induced endocytosis impairment in zebrafish and effectively ameliorates SMA pathology in severe SMA models of worm, zebrafish and mouse. Notably, a combinatorial treatment combining antisense oligonucleotide-mediated SMN elevation and NCALD depletion improves survival rate and motoric disabilities of severe SMA mice, resembling asymptomatic condition. Thus, our study identifies a previously unknown protective mechanism against SMA and suggests a potential therapeutic strategy that might efficiently treat SMA, regardless of severity.

## INTRODUCTION

Genetic modifiers can influence disease-causing mechanisms resulting in incomplete penetrance (Wirth et al. 2013). Identification of such modifiers is of utmost relevance since they can uncover novel regulatory networks and pathological mechanisms, and allow identification of therapeutic pathways. For recessive disorders, the full protection through modifiers is very rare, making their identification highly challenging.

Spinal muscular atrophy (SMA), a motor neuron disease, is one of the most common and devastating autosomal recessive disorders, for which no treatment is available yet. However, various clinical trials using antisense oligonucleotides (ASOs), small molecules or gene therapy show highly promising ameliorations (Kaczmarek et al. 2015). Most SMA patients show homozygous absence of exon 7 of the survival motor neuron 1 (*SMN1*) gene (Lefebvre et al. 1995), allowing an easy and efficient genetic testing. SMN is an housekeeping protein involved in snRNP biogenesis (Fischer et al. 1997); full absence causes embryonic lethality (Hsieh-Li et al. 2000). Only humans have an almost identical gene copy, *SMN2*, which, however, produces only 10% correctly spliced full-length transcript and protein, due to a single silent mutation affecting an exonic splicing enhancer (Lorson et al. 1999). In SMA patients, *SMN2* is the only source of SMN, thus its copy number (between 1-6) determines SMA severity (Feldkotter et al. 2002). In SMA-I, the severe and most common form (60%), the majority of patients carry two *SMN2* copies and die within the first two years of life. Most SMA-II patients carry three *SMN2* copies and are never able to walk. In SMA-III, the mild form, most patients carry four *SMN2* copies, are able to walk, but often become wheel-chair bound (Lunn and Wang 2008). Reduced SMN levels cause spinal motor neuron (MN) dysfunction in all types of SMA (Lunn and Wang 2008). In SMA mouse models impaired maturation and maintenance of neuromuscular junctions (NMJs) and decreased proprioceptive inputs on MN soma are hallmarks of SMA (Kariya et al. 2008, Mentis et al. 2011). Additionally, non-neuronal cells and tissues can also be affected in the severe form (Hamilton and Gillingwater 2013).

Rare SMA-discordant families exist, in which relatives of SMA patients carry a homozygous *SMN1*-deletion together with three or four *SMN2* copies, but are clinically asymptomatic (Cobben et al. 1995, Hahnen et al. 1995, Wang et al. 1996, Prior et al. 2004). In seven of these families, we identified the  $\text{Ca}^{2+}$ -dependent protein Plastin 3 (PLS3) as a protective modifier (Oprea et al. 2008, Heesen et al. 2016). PLS3 overexpression (OE) rescues SMA across species and is specifically upregulated in MNs of asymptomatic individuals (Oprea et al. 2008, Dimitriadi et al. 2010, Lotti et al. 2012, Ackermann et al. 2013, Hosseinibarkooie et al. 2016).

Here, we identified Neurocalcin delta (NCALD), a neuronal  $\text{Ca}^{2+}$  sensor protein, as a SMA protective modifier in humans. Based on the function and interacting partners of both SMA modifiers (PLS3 (Hosseinibarkooie et al. 2016) and NCALD), we identified endocytosis as a main impaired cellular mechanism in SMA. NCALD acts as a negative regulator of endocytosis. We demonstrate that NCALD knockdown (KD) in various SMA animal models rescues the major functional SMA disturbances. Most importantly, a combined therapy using a low suboptimal SMN-ASO dose and NCALD KD rescues severe SMA in mice, defining a novel powerful strategy to efficiently treat patients with SMA.

## RESULTS

### Identification of NCALD as a potential SMA modifier

In a four-generation Mormon family from Utah, we identified seven individuals carrying homozygous *SMN1* deletions, two affected by SMA-I and five fully asymptomatic, except an increased photosensitivity (**Fig. 1a**) (Online Methods for clinical pictures).

Haplotype analysis of SMA regions showed a co-segregation of three different SMA alleles (**Fig. 1a**). The two SMA-I patients carried no *SMN1* and two *SMN2* copies. By contrast, all five asymptomatic individuals showed homozygous absence of *SMN1* and four *SMN2* copies, resembling a genotype associated with SMA-III (Feldkotter et al. 2002) (**Fig. 1a**). *SMN2* sequencing excluded any further variant affecting expression. In lymphoblastoid cells (LBs), SMN RNA and protein levels were similar to those in typical SMA-III patients, thus excluding *cis* and *trans*-acting factors regulating *SMN2*. Increased *PLS3* levels were not found (**Fig. 1a**, GEO: GSE58316). Thus, we conclude that a previously unknown SMA modifier potentially protects these individuals.

To identify the SMA modifier, we combined linkage with transcriptome-wide differential expression analysis followed by targeted resequencing. Assuming a dominant mode of inheritance, a parametric linkage analysis with 14 family members revealed eight positive peaks with a maximum LOD score of 1.5 (**Fig. 1b**). In parallel, a transcriptome-wide differential expression analysis with 12 RNA samples was performed (GEO: GSE58316) and revealed 17 transcripts significantly differentially regulated in asymptomatic individuals (**Supplementary Table 1**). Most importantly, *NCALD* was the only transcript localized in one of the eight linked regions on chromosome 8q22.3 (between rs28144 and rs958381), making it a highly likely candidate. Microarray data were confirmed by RT-qPCR and Western blot (**Fig. 1c,d**).

Targeted resequencing of ~3 Mb genomic DNA encompassing *NCALD* in five family members and detailed genetic analysis (**Supplementary Table 2**) revealed various polymorphisms in *NCALD* non-coding sequence; these may impact *NCALD* expression in protected individuals.

*NCALD* is a highly conserved neuronal calcium sensor (NCS), primarily involved in neuronal  $\text{Ca}^{2+}$  signaling (Burgoyne and Haynes 2012, Di Sole et al. 2012). *NCALD* encodes a small protein containing two pairs of EF-hand domains and an N-terminal myristoyl anchor that enables a switching from cytosolic to membrane-bound forms in a  $\text{Ca}^{2+}$ -dependent manner (Hidaka and Okazaki 1993, Ladant 1995). Both myristoylated and non-myristoylated forms show  $\text{Ca}^{2+}$ -dependent mobility shifts (Viviano et al. 2016). *NCALD* is highly expressed in cerebral neurons, spinal MNs, and in axonal growth cones (Iino et al. 1998). *NCALD* overexpression inhibits neurite outgrowth (Yamatani et al. 2010). *NCALD* is important in phototransduction (Venkataraman et al. 2008), which may explain photosensitivity in asymptomatic individuals. Importantly, *NCALD* interacts with clathrin and actin, both of which are involved in endocytosis and synaptic vesicle recycling (Ivings et al. 2002, Haucke et al. 2011).

### NCALD knockdown triggers MN differentiation and restores neurite and axonal growth in SMA



First, we analyzed NCALD expression levels during MN differentiation and maturation in NSC34 cells treated with retinoic acid (RA) (Cashman et al. 1992) and we observed a steady increase in NCALD amount over time under RA treatment (**Fig. 2a**). siRNA-mediated *Ncald* reduction induced MN differentiation (indicated by HB9-positive staining) and triggered neurite outgrowth even without RA (**Fig. 2b**). In contrast, NCALD overexpression in RA-treated NSC34 cells impaired neurite outgrowth (**Supplementary Fig. 2b,c**).

NCALD is highly abundant in axonal growth cones of spinal MNs (lino et al. 1998). In addition, we show that it localizes at the presynaptic terminals of NMJs, suggesting a potential role at the NMJ (**Fig. 2c,d**).

We found that *Ncald* KD in *Smn* deficient NSC34 cells restored impaired neurite outgrowth to controls levels (**Supplementary Fig. 2a**). Similar results were obtained in cultured primary MNs from SMA (*Smn*<sup>ko/ko</sup>; *SMN2*<sup>tg/0</sup>) versus heterozygous (*Smn*<sup>ko/wt</sup>; *SMN2*<sup>tg/0</sup>) embryos, where reduced axon length was fully restored by siRNA-mediated *Ncald* KD (**Fig. 2e**). These findings indicate that reduced NCALD levels counteract the impaired axonal development of SMN-deficient MNs.

### ***ncald* knockdown restores axonal growth and NMJ functionality in zebrafish *smn* morphants**

We investigated the modifying effect of *ncald* *in vivo* in zebrafish (Flanagan-Steet et al. 2005) by morpholino (MO)-mediated KD of either *smn*, *ncald* or both. Consistent with previous results, *smn* depletion resulted in motor axon-specific outgrowth defects such as truncations and ectopic branches (McWhorter et al. 2003, Oprea et al. 2008) (**Fig. 3a**). KD of *ncald* led to enhanced motor axons branching, whereas double *smn+ncald* KD fully rescued the truncated motor axon defect associated with *Smn* deficiency (**Fig. 3a,c; Supplementary 3a**). KD efficiency was confirmed by Western blot (**Fig. 3b**). We also found that OE of human NCALD mRNA in zebrafish caused truncation and branching of motor axons (**Supplementary Fig. 3b**), resembling the phenotype of *smn* morphant zebrafish (**Fig. 3a**) similar to NSC34 cells (**Supplementary Fig. 2c**).

During NMJ maturation the width of the synaptic cleft, which is essential in neurotransmission (Drapeau et al. 2001) increases. Ultrastructural analysis of synaptic clefts revealed an impaired NMJ maturation in *smn* morphants (**Fig. 3d,e**). The synaptic cleft of *smn* morphants was significantly smaller than in controls or *ncald* morphants, but fully restored to control level in double *smn+ncald* KD embryos (**Fig. 3d,e**).

To test the functionality of neuromuscular synapses between caudal primary MNs and ventral fast muscle cells (Westerfield et al. 1986), we performed whole-cell patch clamp recordings from muscle cells during MN stimulation in morphants. We recorded spontaneous endplate potentials at rest (without stimulation) and during MN stimulation by NMDA (**Supplementary Fig. 3c**). In controls, we recorded at rest small endplate potentials that were primarily not tetrodotoxin (TTX) sensitive (**Supplementary Fig. 3d,e**). Most resembled miniature endplate potentials (mEPPs) (Fatt and Katz 1951). During NMDA stimulation, the mEPP frequency did not significantly increase, but large TTX-sensitive endplate potentials and muscle action potentials were induced by MN spike evoked transmission. In *smn* morphants, a significantly lower spontaneous mEPP frequency and only occasional action potentials during NMDA stimulation were observed (**Fig. 3f**). In the

*smn+ncald* morphants, the spontaneous mEPP frequency was slightly increased and the frequency of large NMDA-induced EPP was restored to control levels (**Fig. 3f,g**). In line with these data, induced swimming velocity was reduced in *smn* morphants, but rescued in *smn+ncald* morphants (**Supplementary Fig. 3f**). Together, these results show that Ncald KD rescues neural circuit function at NMJs of *smn* morphants.

### **NCALD loss suppresses defects of *C. elegans* SMN loss of function animals**

*C. elegans* lacking the SMN ortholog *smn-1*, referred to here as *Cesmn-1*, have neuromuscular defects, including decreased pharyngeal pumping rate (**Fig. 3h**) (Briese et al. 2009, Dimitriadis et al. 2010). The *C. elegans* ortholog of NCALD is encoded by neuronal calcium sensor-1 (*ncs-1*) (Gomez et al. 2001). Either *ncs-1* KD by RNA interference or introduction of the *ncs-1(qa401)* loss of function allele in *Cesmn-1* animals, significantly ameliorated pumping defects (**Fig. 3i,j**), confirming that NCALD loss ameliorates the SMN loss-of-function-induced neuromuscular defects across species.

### **Heterozygous *Ncald* KO ameliorates motor neuron development in severe SMA mice**

Heterozygous *Ncald*<sup>ko/wt</sup> mice are asymptomatic and show >50% reduction of NCALD expression in spinal cord and brain (**Fig. 4a**). Homozygous *Ncald*<sup>ko/ko</sup> mice are fertile; however, preliminary reported data ([www.mousephenotype.org](http://www.mousephenotype.org)) and our data show behavioral abnormalities, vision defects and metabolic impairment. Since asymptomatic individuals have reduced NCALD levels, we used the heterozygous *Ncald*<sup>ko/wt</sup> animals for experiments herein.

The *Ncald*<sup>ko/wt</sup> allele was bred into a severe SMA mouse model (Hsieh-Li et al. 2000) on a C57BL/6N background. Severe SMA mice show multi-organ failure (Riessland et al. 2010, Ackermann et al. 2013, Somers et al. 2013) due to very low SMN expression, which could not be rescued by *Ncald* KD alone. Both SMA and SMA-*Ncald*<sup>ko/wt</sup> mice die at a mean age of 13 days (**Supplementary Fig. 4a**). Nonetheless, we found larger NMJs in the *Transversus abdominis* muscle (TVA) and elevated proprioceptive inputs on MN soma in SMA-*Ncald*<sup>ko/wt</sup> versus SMA mice (P10) (**Fig. 4b,c**). Moreover, SMA-*Ncald*<sup>ko/wt</sup> mice show more inputs per MN than SMA mice independent of cell size (**Supplementary Fig. 4c**). A comparison of axonal development in cultured primary MNs revealed a large impact of *Ncald* reduction on axonal growth and arborization (**Fig. 4d**), confirming our initial results with NCALD knockdown (**Fig. 2e**). Therefore, NCALD reduction counteracts impaired axonal development and restores NMJ size in SMN-deficient mice.

### **Combinatorial therapy with a suboptimal low-dose SMN-ASO and reduced *Ncald* expression rescues SMA pathogenesis in a severe SMA mouse model**

In our study, we combined suboptimal low-dose SMN-ASOs with heterozygous *Ncald* KD mice: for three reasons: firstly, asymptomatic individuals carry four *SMN2* copies similar to typical SMA-III patients, but not two *SMN2* copies as most SMA-I patients or severe SMA mice. Secondly, SMA-I patients, currently treated with SMN-ASOs, show only a moderate SMN elevation and thirdly, genetic modifiers efficiently protect against SMA only

if a certain SMN level is present (Hosseiniabarkooie et al. 2016). Since presymptomatic subcutaneous (s.c.) injection of high dose SMN-ASO in severely-affected SMA mice fully rescues SMA (Hua et al. 2011), we opted for a suboptimal dose to ameliorate SMA. We crossed C57BL/6N *Ncald*<sup>ko/wt</sup>; *Smn*<sup>ko/wt</sup> males with FVB/N *Smn*<sup>ko/ko</sup>; *SMN*<sup>tg</sup> females to produce 50% C57BL/6N:50% FVB/N (mixed<sub>50</sub>) offspring (Fig. 5a). Untreated mixed<sub>50</sub> SMA and SMA-*Ncald*<sup>ko/wt</sup> mice live 16.5 and 17.0 days, respectively (Fig. 5b). Mixed<sub>50</sub> offspring were injected s.c. with a single suboptimal dose of SMN-ASO at P1. Elevated SMN levels were obtained in liver, but not in spinal cord or brain (Supplementary Fig. 5a). Survival of SMA+ASO mice was rescued (Fig. 5b), but their motoric abilities were visibly impaired as determined by righting reflex and grip strength test (Fig. 5c,d). This suggests that slightly elevated SMN expression achieved by systemic ASO-treatment rescued non-neuronal multi-organ impairment (Hosseiniabarkooie et al. 2016), but not MN function. In contrast, *Ncald* KD in addition to low dose SMN-ASO treatment significantly improved also motoric abilities (Fig. 5c,d). Analysis of NMJs maturation score at P21 (Bogdanik et al. 2015), showed that both NMJ size and maturation were markedly restored by *Ncald* KD as compared to SMA+ASO mice (Fig. 5e). *Ncald* KD did not rescue tail necrosis and impacted slightly weight progression in male mice (Supplementary Fig. 5b-d). Our data provide clear evidence of the beneficial effect of reduced NCALD on the neuromuscular system and motoric function in SMA+ASO mice.

### Low SMN decreases Ca<sup>2+</sup> influx in NSC34 and PC12 cells

Since impaired Ca<sup>2+</sup> homeostasis has been reported in SMA (Ruiz et al. 2010), we tested if lowering SMN levels can modulate voltage-dependent Ca<sup>2+</sup> currents (*I*<sub>Ca</sub>) in MN-like cells. We performed whole-cell patch-clamp recordings and ratiometric Ca<sup>2+</sup> imaging with fura-2. We recorded *I*<sub>Ca</sub> of RA-differentiated NSC34 cells that were treated with siRNAs specific to *Smn*, *Ncald*, or *Smn+Ncald* and analyzed the *I*<sub>Ca</sub> tail currents with a series of increasing voltage pulses. In NSC34 cells, *Smn* depletion significantly reduced the voltage-dependent Ca<sup>2+</sup> influx, which was not restored by additional *Ncald* reduction (Fig. 6a). Ratiometric Ca<sup>2+</sup> imaging with fura-2 revealed a reduced voltage-dependent Ca<sup>2+</sup> influx in SMN-depleted PC12 cells compared to controls (Supplementary Fig. 6a). These data show that low SMN levels impair Ca<sup>2+</sup> influx, which is not restored by NCALD KD and that NCALD depletion rescues synaptic transmission by a different mechanism.

### Disturbed endocytosis and synaptic vesicle recycling is rescued by NCALD depletion

We next sought for a common pathway in which both SMA modifiers, NCALD and PLS3, might operate. Since NCALD binds clathrin (Ivings et al. 2002) directly and PLS3 knockout in yeast impairs endocytosis (Kubler and Riezman 1993, Ivings et al. 2002), we hypothesized that low SMN levels may impair endocytosis, which in turn is rescued by NCALD KD or PLS3 OE. Indeed, we recently identified impaired endocytosis as a disturbed cellular mechanism affected in SMA, which is rescued by PLS3 OE (Hosseiniabarkooie et al. 2016). Impaired endocytosis and endocytic trafficking have also been demonstrated in a *C. elegans* SMA model (Dimitriadi et al. 2016).

Co-immunoprecipitation studies in NSC34 revealed NCALD interaction with clathrin only in the absence of Ca<sup>2+</sup> (Fig. 6b) or at low Ca<sup>2+</sup> levels (data not shown). TEM analyses after

immunogold staining of wt zebrafish sections showed co-localization of Ncald and clathrin in the presynaptic sites of NMJs (**Supplementary Fig. 6b**).

To study the effect of NCALD on endocytosis, we applied FITC-dextran internalization assays in various cell culture systems. In primary fibroblast cell lines derived from SMA patients, endocytosis rates were strongly reduced compared to controls but restored in fibroblasts of asymptomatic individuals (**Fig. 6c**; **Supplementary 6c**). Moreover, *Smn* KD in NSC34 cells significantly reduced FITC-dextran uptake, which was rescued by concomitant *Ncald* KD. *Ncald* KD alone increased the rate of endocytosis by 1.3-fold, demonstrating that low NCALD levels already facilitate endocytosis (**Supplementary Fig. 6f**).

Moreover, we analyzed endocytic uptake of FM1-43 in mouse NMJs under stimulation at 5 and 20 Hz as described (Hosseinibarkooie et al. 2016). FM1-43 uptake was markedly decreased in SMA mice at 5 Hz stimulation (triggering clathrin-dependent endocytosis), but *Ncald* reduction fully restored the levels similar to heterozygous mice (**Fig. 6d**; **Supplementary Fig. 6d**). *Ncald* reduction had no impact at 20 Hz stimulation (triggering bulk endocytosis), further strengthening the role of NCALD in clathrin-dependent endocytosis in NMJs (**Supplementary Fig. 6e**).

Lastly, we investigated *in vivo* whether endocytosis and the *Smn*-*Ncald*-clathrin network is relevant for SMA using pharmacological inhibition of endocytosis in zebrafish. Using sub-phenotypical concentrations of *smn* MO in combination with Pitstop2, an inhibitor of clathrin (von Kleist et al. 2011), resulted in more truncated motor axons than in *smn* MO alone (**Fig. 6e**) and a phenotype similar to severe *smn* KD (4 ng) (**Fig. 3a,c**). Moreover, treatment with Dynasore, an inhibitor of the endocytosis-driving GTPase dynamin (Macia et al. 2006), either alone or in combination with low *smn* MO resulted in an SMA-like axonal truncation (**Fig. 6e**). These defects were rescued by additional treatment with *ncald* MO (**Fig. 6e**; **Supplementary 6g**). Together, these findings suggest that SMN and clathrin interact genetically to promote endocytosis and MN axogenesis, whereas NCALD negatively interferes with an SMN-dependent function of clathrin.

## DISCUSSION

Here, we describe NCALD as a novel genetic SMA modifier in humans. Reduced NCALD expression fully protects individuals from developing SMA, despite lacking *SMN1* and carrying only four *SMN2* copies, usually causing SMA-III (Feldkotter et al. 2002). NCALD reduction acts as genetic suppressor of SMA. We analyzed the impact of NCALD KD on SMA models across species and found that it ameliorates SMA pathology, counteracting the disruptive impact of SMN loss on a conserved cellular mechanism in MNs and NMJs.

Clinical trials using ASOs correcting *SMN2* splicing are highly promising and close to FDA-approval (Kaczmarek et al. 2015). However, for SMA-I children, with only two *SMN2* copies, these approaches are likely insufficient to fully counteract SMA symptoms. A combinatorial therapy, elevating SMN and decreasing NCALD (e.g. by ASO treatment), might bring additional benefit to SMA patients and likely provide a full protection as in asymptomatic individuals.

In SMA, impaired neurotransmission, disturbed  $\text{Ca}^{2+}$  homeostasis, decreased synaptic vesicle number and reduced F-actin caging of reserve pool synaptic vesicles have been

reported (Kariya et al. 2008, Murray et al. 2008, Kong et al. 2009, Ruiz et al. 2010). For repeated neurotransmitter release, subsequent endocytosis is important (Stevens 2003); furthermore, endo- and exocytosis are regulated by the  $\text{Ca}^{2+}$  dynamics within the presynaptic terminals (Sudhof 2012).

We found that low SMN levels cause reduction of voltage activated  $\text{Ca}^{2+}$  influx, in accordance with recent studies in a zebrafish SMA model and mislocalization of calcium channels in SMA (Jablonka et al. 2007, See et al. 2014). However, unlike SMA pathology,  $\text{Ca}^{2+}$  influx was not restored by reduced NCALD, suggesting a different counteraction. Since NCALD binds clathrin and actin, two major players in endocytosis (Ivings et al. 2002, Haucke et al. 2011), we propose that reduced SMN may disturb endocytosis, possibly due to decreased  $\text{Ca}^{2+}$ , whereas NCALD KD subsequently compensates for SMN loss. We demonstrate *in vitro* and *in ex vivo* mouse NMJs that NCALD KD restores impaired clathrin-dependent endocytosis. Furthermore, chemical endocytosis-inhibition in zebrafish caused MN axogenesis defects that were reversed upon Ncald suppression. Importantly, NCALD binds clathrin only at low  $\text{Ca}^{2+}$  levels (mimicking unstimulated MNs) but not at high  $\text{Ca}^{2+}$  levels mimicking action potentials in MNs). For SMA MNs, with low  $\text{Ca}^{2+}$  levels even during action potential, we predict that NCALD constantly binds clathrin, thereby inhibiting its function in recycling. However, low NCALD levels, as in asymptomatic individuals, may allow free clathrin to act in endocytosis even at reduced  $\text{Ca}^{2+}$  levels (**Fig. 6f**).

Moreover, reduced NCALD amount might be beneficial for other MN or neurodegenerative disorders with impaired endocytosis and  $\text{Ca}^{2+}$ -homeostasis, as was shown for Alzheimer's, where NCALD is highly upregulated (Suszynska-Zajczyk et al. 2014) or Parkinson's, hereditary spastic paraplegia and ALS where impaired endocytic trafficking was found (Schreij et al. 2016). Therefore, NCALD downregulation might become an efficient strategy against SMA and other neurodegenerative diseases.

## **METHODS**

Methods and any associated references are available in the online version of the paper.

### **Accession codes.**

Gene Expression Omnibus: all microarray data are available in GSE58316.

## **ACKNOWLEDGMENT**

We thank SMA families, Jay Gopalakrishnan for critical reading of the manuscript and CECAD for help with imaging. This work was supported by grants from the Deutsche Forschungsgemeinschaft Wi-945/13-1, Wi-945/14-1, RTG 1970 (BW), SMA Europe (MR), EU FP7 NEUROMICS (BW), CMMC (BW), IGSDHD (AK) AFM-Telethon (LTB) and NIH PO1NS066888 (ACH).

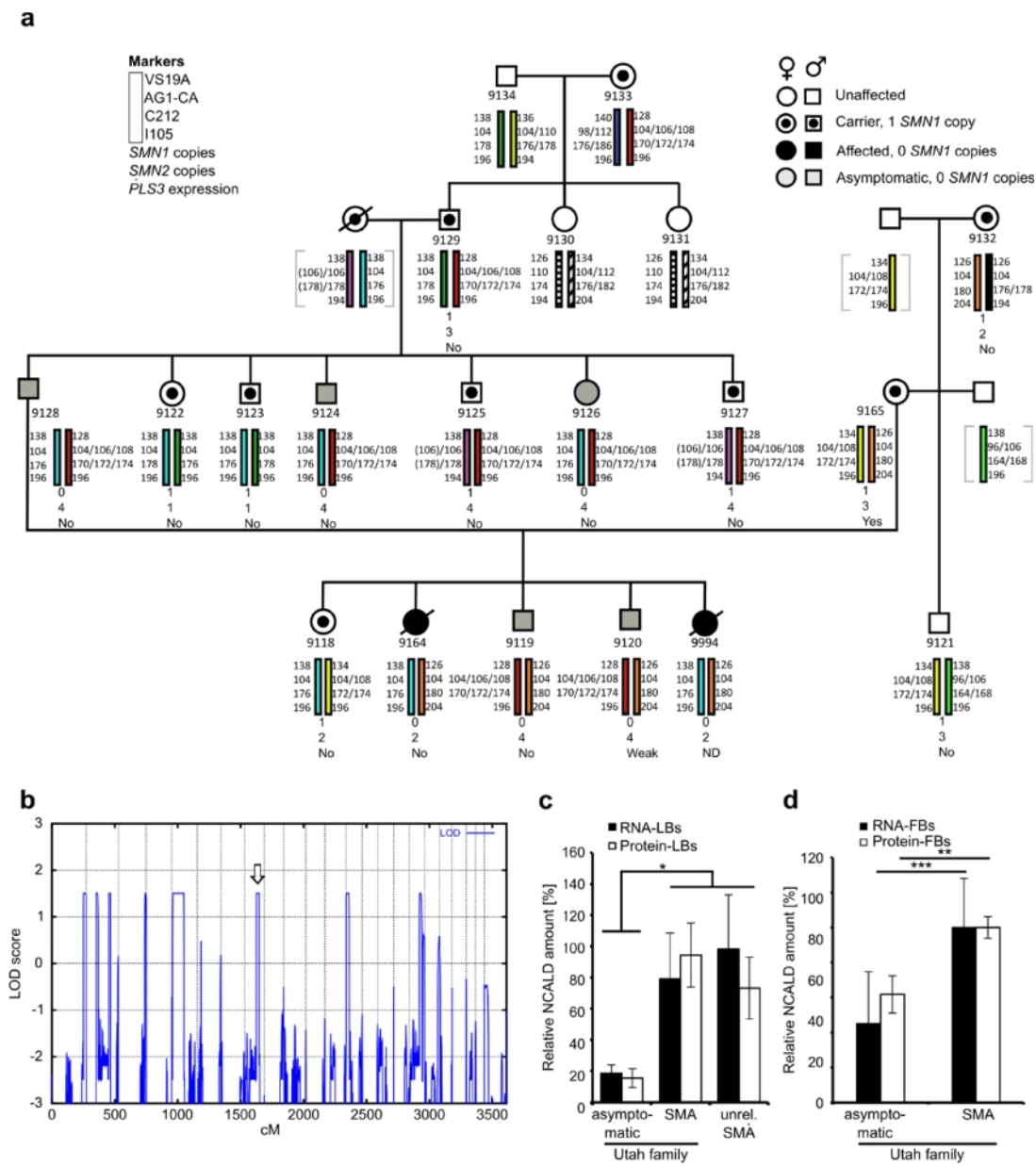
## **AUTHORS CONTRIBUTIONS**

BW, MR, AK and SS conceived and designed the project; KJS diagnosed and collected samples of the Utah family. MR, AK and SS performed and analyzed most experiments in patients, cell culture, zebrafish and mice with help of MSBH, MP, NB, VG, SK, IH, MJK, HL, AU, LTB and MH. CR, LTB & PK performed the electrophysiology and calcium imaging experiments, MR & SK the electron microscopy experiments, MD and ACH the experiments in worm, LG, CG and AH the targeted re-sequencing, GN & PN the linkage analysis and MW the transcriptome analysis. CFB and FR provided the SMN-ASOs. BW, MR, AK and SS wrote the paper with the contribution and comments from all co-authors.

## **COMPETING FINANCIAL INTERESTS**

C. Frank Bennett and Frank Rigo are employees of IONIS Pharmaceuticals. Brunhilde Wirth and Markus Riessland hold an US PCT/EP2014/066276 entitled “Neurocalcin delta inhibitors and therapeutic and non-therapeutic uses there of” with the international publication number WO/2015/014838 A1.

Fig. 1



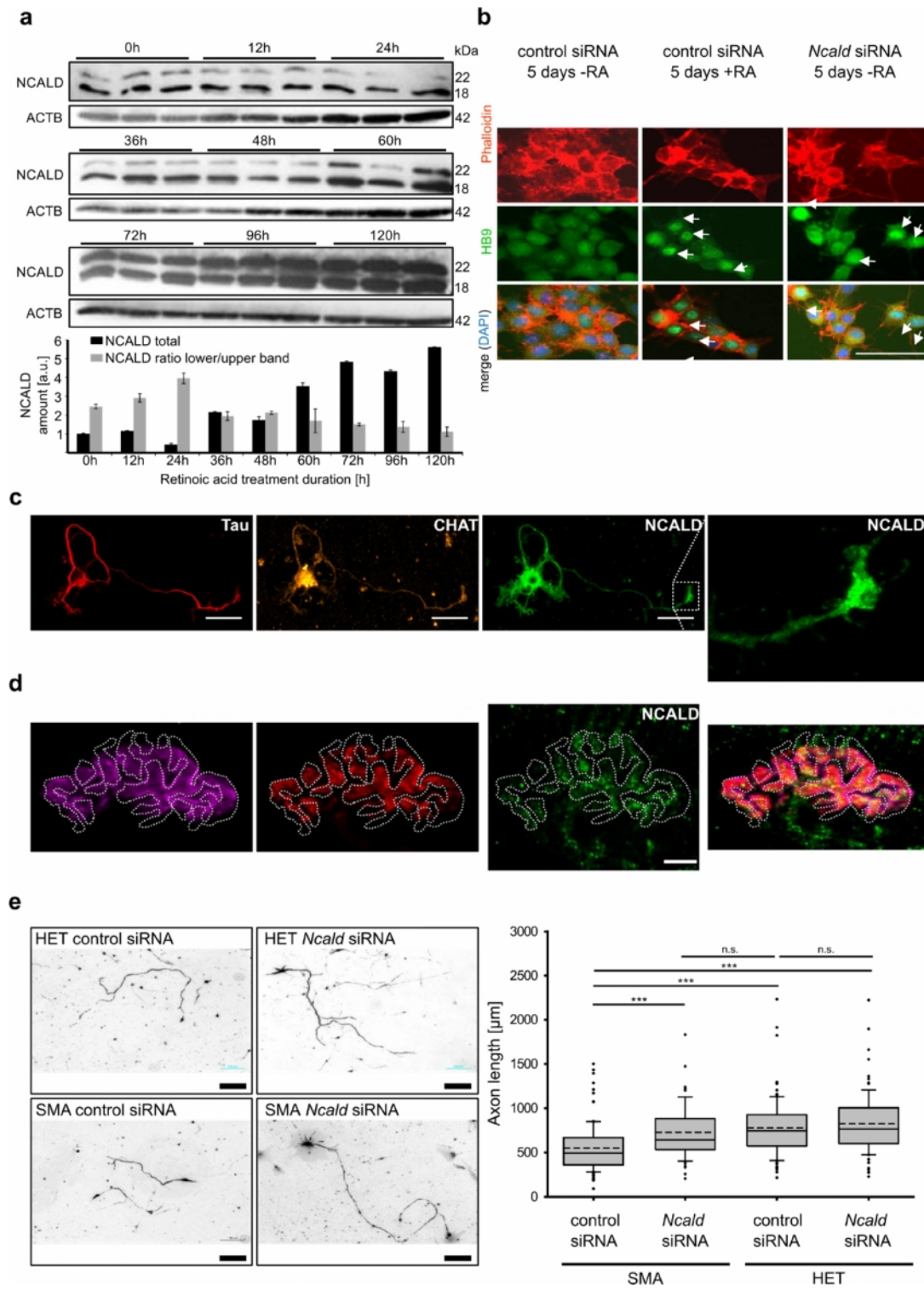
**Fig. 2**



Fig. 3

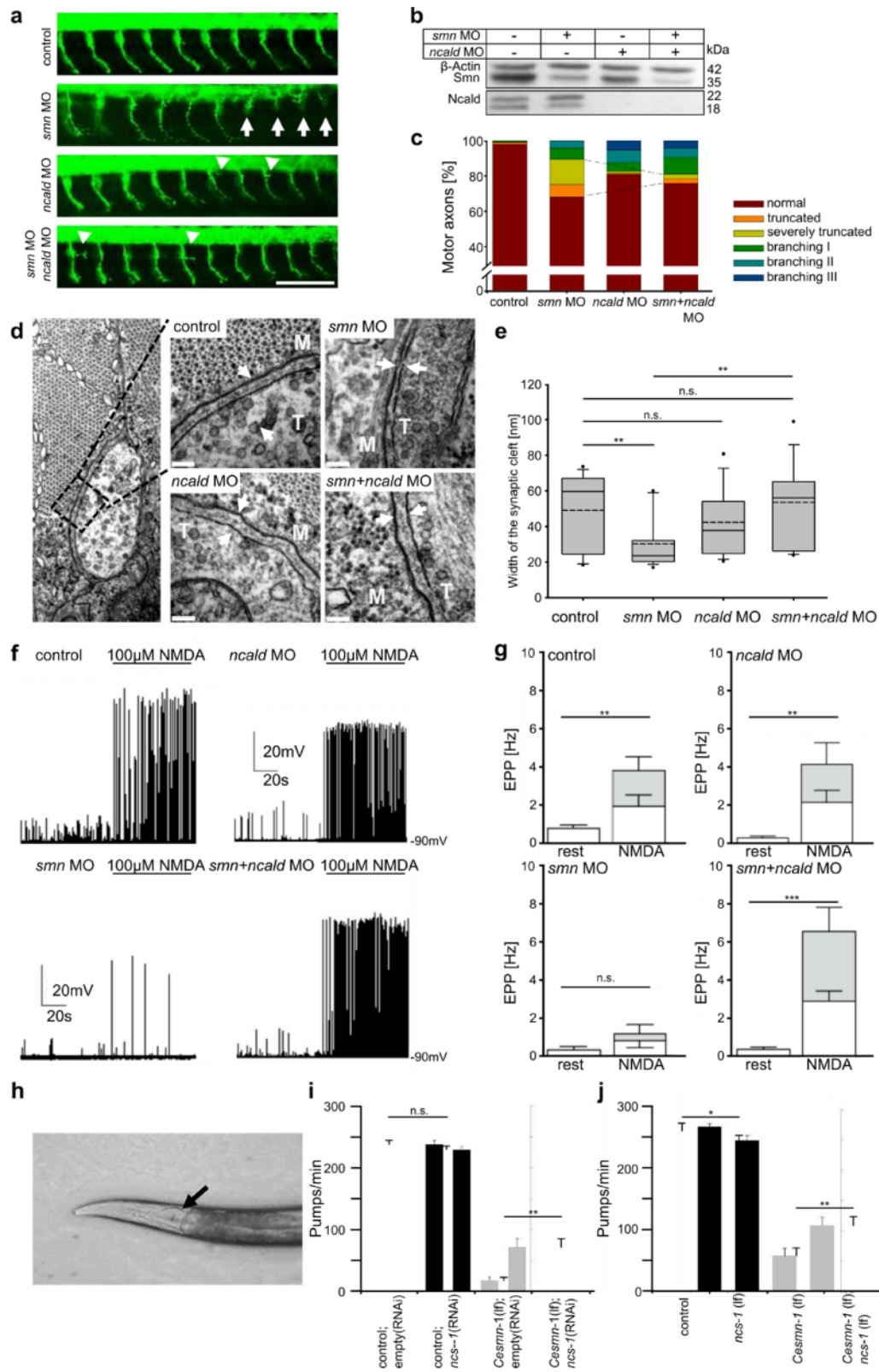


Fig. 4

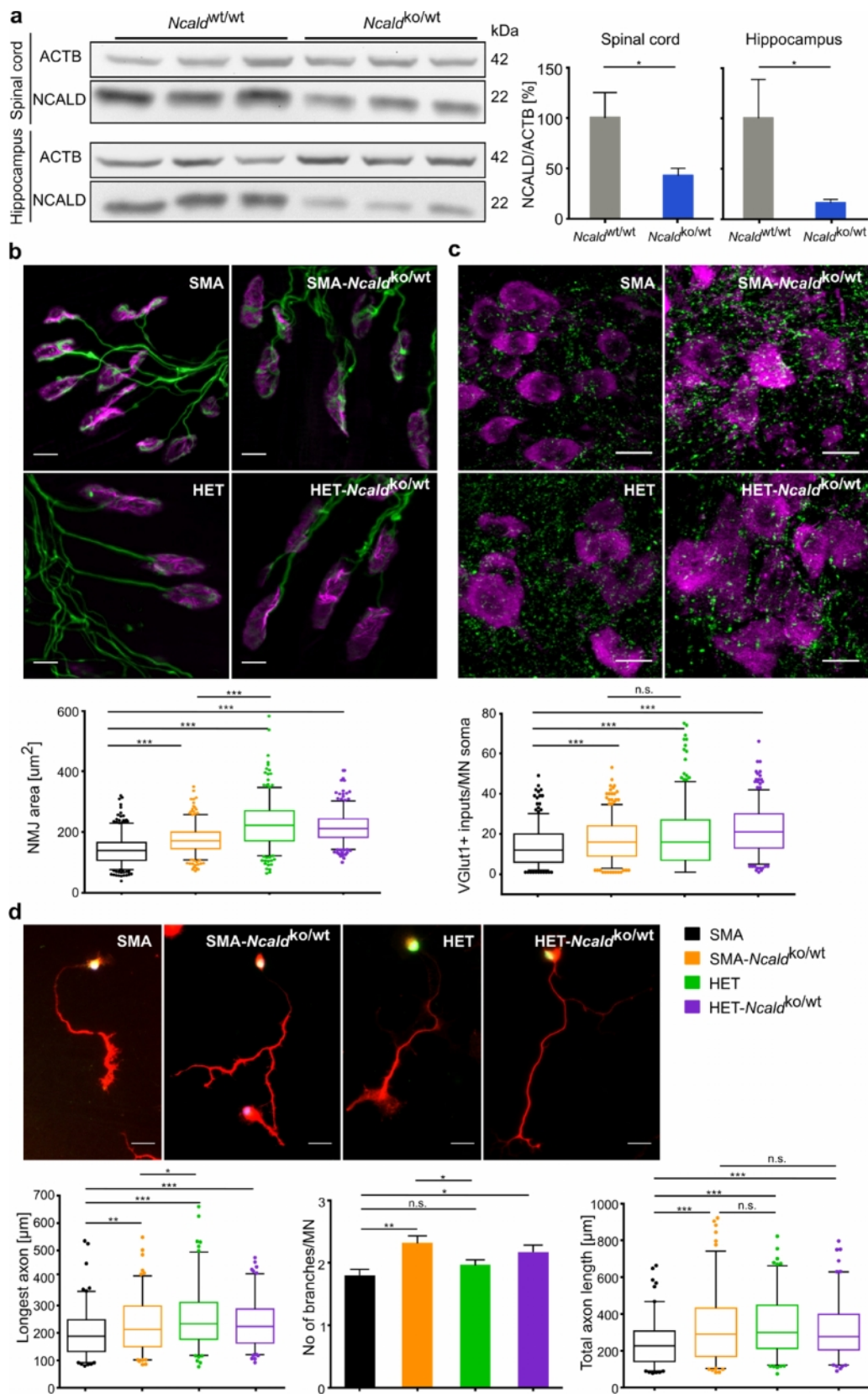


Fig. 5

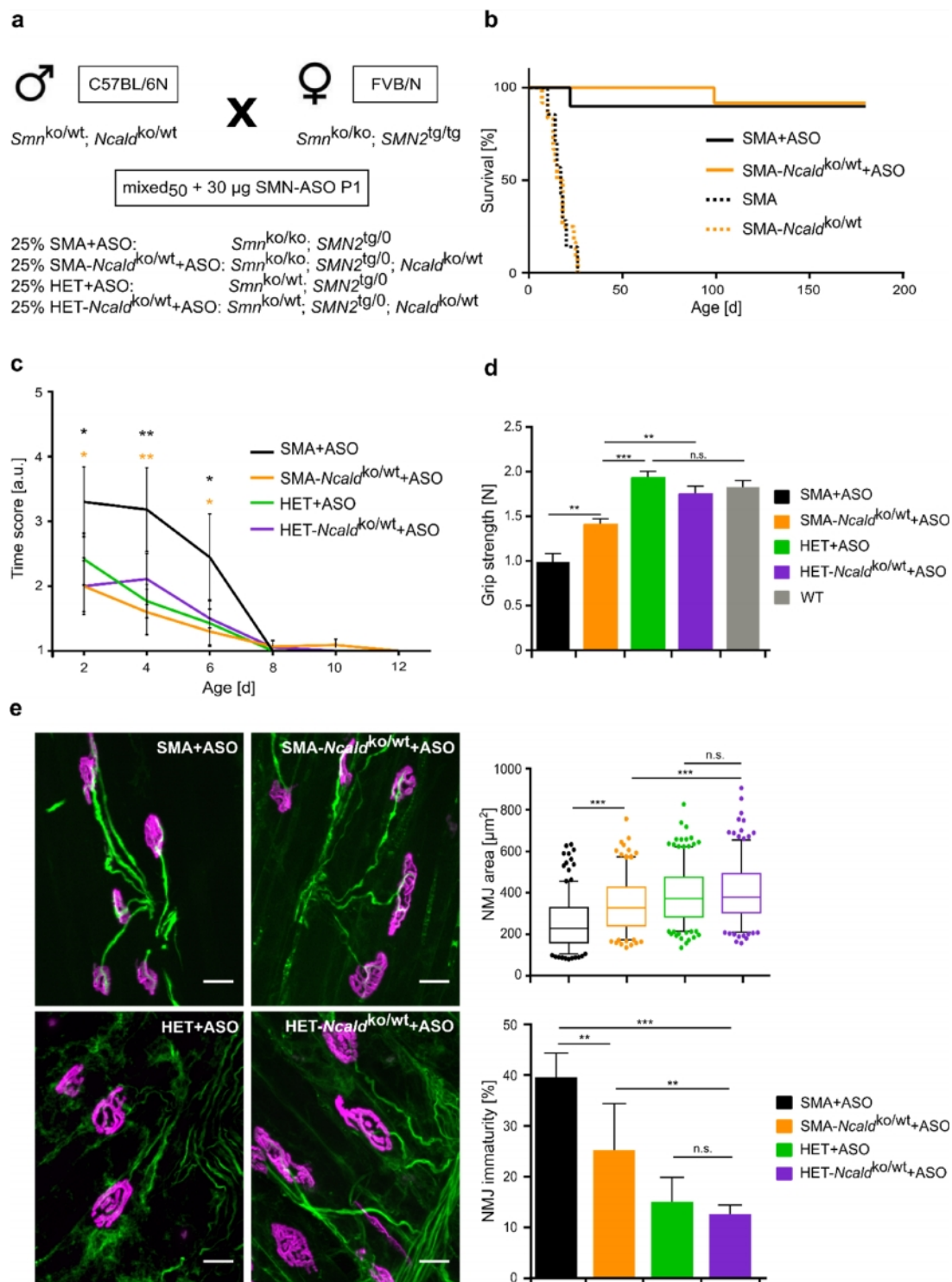
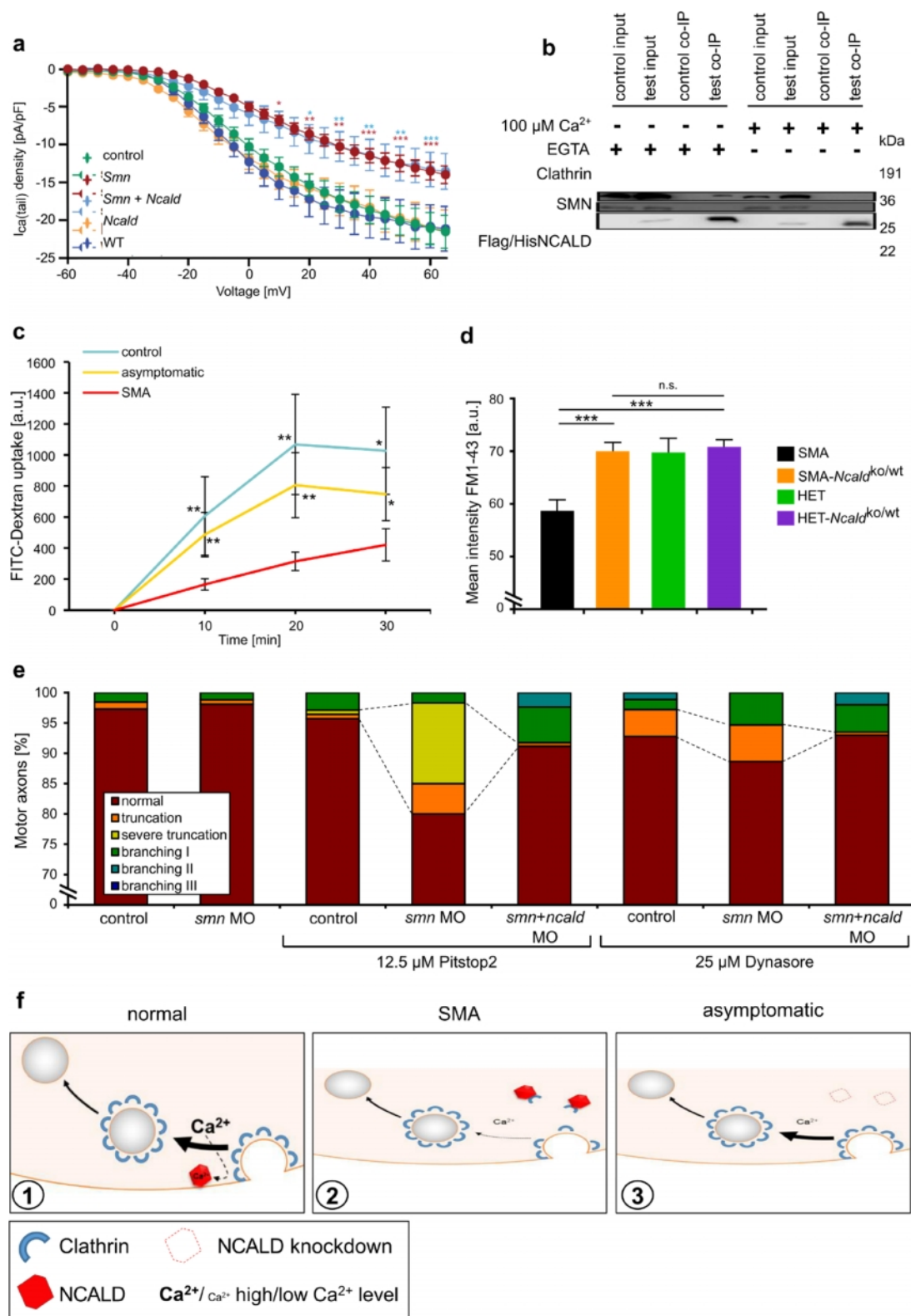


Fig. 6



## REFERENCES

1. Ackermann, B., et al. Plastin 3 ameliorates spinal muscular atrophy via delayed axon pruning and improves neuromuscular junction functionality. *Hum Mol Genet* 22, 1328-1347 (2013).
2. Bogdanik, L.P., et al. Systemic, postsymptomatic antisense oligonucleotide rescues motor unit maturation delay in a new mouse model for type II/III spinal muscular atrophy. *Proc Natl Acad Sci U S A* 112, E5863-5872 (2015).
3. Briese, M., et al. Deletion of *smn-1*, the *Caenorhabditis elegans* ortholog of the spinal muscular atrophy gene, results in locomotor dysfunction and reduced lifespan. *Hum Mol Genet* 18, 97-104 (2009).
4. Burgoyne, R.D. & Haynes, L.P. Understanding the physiological roles of the neuronal calcium sensor proteins. *Mol Brain* 5, 2 (2012).
5. Cashman, N.R., et al. Neuroblastoma x spinal cord (NSC) hybrid cell lines resemble developing motor neurons. *Dev Dyn* 194, 209-221 (1992).
6. Cobben, J.M., et al. Deletions of the survival motor neuron gene in unaffected siblings of patients with spinal muscular atrophy. *Am J Hum Genet* 57, 805-808 (1995).
7. Di Sole, F., Vадnagara, K., Moe, O.W. & Babich, V. Calcineurin homologous protein: a multifunctional  $\text{Ca}^{2+}$ -binding protein family. *Am J Physiol Renal Physiol* 303, F165-179 (2012).
8. Dimitriadi, M., et al. Conserved genes act as modifiers of invertebrate SMN loss of function defects. *PLoS Genet* 6, e1001172 (2010).
9. Dimitriadi, M., et al. Decreased function of survival motor neuron protein impairs endocytic pathways. *Proc Natl Acad Sci U S A* (2016).
10. Drapeau, P., Buss, R.R., Ali, D.W., Legendre, P. & Rotundo, R.L. Limits to the development of fast neuromuscular transmission in zebrafish. *J Neurophysiol* 86, 2951-2956 (2001).
11. Fatt, P. & Katz, B. An analysis of the end-plate potential recorded with an intracellular electrode. *J Physiol* 115, 320-370 (1951).
12. Feldkotter, M., Schwarzer, V., Wirth, R., Wienker, T.F. & Wirth, B. Quantitative analyses of SMN1 and SMN2 based on real-time lightCycler PCR: fast and highly reliable carrier testing and prediction of severity of spinal muscular atrophy. *Am J Hum Genet* 70, 358-368 (2002).
13. Flanagan-Steet, H., Fox, M.A., Meyer, D. & Sanes, J.R. Neuromuscular synapses can form in vivo by incorporation of initially aneural postsynaptic specializations. *Development* 132, 4471-4481 (2005).

14. Fischer, U., Liu, Q. & Dreyfuss, G. The SMN-SIP1 complex has an essential role in spliceosomal snRNP biogenesis. *Cell* 90, 1023-1029 (1997).
15. Gomez, M., et al. Ca<sup>2+</sup> signaling via the neuronal calcium sensor-1 regulates associative learning and memory in *C. elegans*. *Neuron* 30, 241-248 (2001).
16. Hahnen, E., et al. Molecular analysis of candidate genes on chromosome 5q13 in autosomal recessive spinal muscular atrophy: evidence of homozygous deletions of the SMN gene in unaffected individuals. *Hum Mol Genet* 4, 1927-1933 (1995).
17. Hamilton, G. & Gillingwater, T.H. Spinal muscular atrophy: going beyond the motor neuron. *Trends Mol Med* 19, 40-50 (2013).
18. Haucke, V., Neher, E. & Sigrist, S.J. Protein scaffolds in the coupling of synaptic exocytosis and endocytosis. *Nat Rev Neurosci* 12, 127-138 (2011).
19. Heesen, L., et al. Plastin 3 is upregulated in iPSC-derived motoneurons from asymptomatic SMN1-deleted individuals. *Cell Mol Life Sci* 73, 2089-2104 (2016).
20. Hidaka, H. & Okazaki, K. Neurocalcin family: a novel calcium-binding protein abundant in bovine central nervous system. *Neurosci Res* 16, 73-77 (1993).
21. Hosseinibarkooie, S., et al. The Power of Human Protective Modifiers: PLS3 and CORO1C Unravel Impaired Endocytosis in Spinal Muscular Atrophy and Rescue SMA Phenotype. *Am J Hum Genet* 99, 647-665 (2016).
22. Hsieh-Li, H.M., et al. A mouse model for spinal muscular atrophy. *Nat Genet* 24, 66-70 (2000).
23. Hua, Y., et al. Peripheral SMN restoration is essential for long-term rescue of a severe spinal muscular atrophy mouse model. *Nature* 478, 123-126 (2011).
24. Iino, S., Kobayashi, S. & Hidaka, H. Neurocalcin-immunopositive nerve terminals in the muscle spindle, Golgi tendon organ and motor endplate. *Brain Res* 808, 294-299 (1998).
25. Ivings, L., Pennington, S.R., Jenkins, R., Weiss, J.L. & Burgoyne, R.D. Identification of Ca<sup>2+</sup>-dependent binding partners for the neuronal calcium sensor protein neurocalcin delta: interaction with actin, clathrin and tubulin. *Biochem J* 363, 599-608 (2002).
26. Jablonka, S., Beck, M., Lechner, B.D., Mayer, C. & Sendtner, M. Defective Ca<sup>2+</sup> channel clustering in axon terminals disturbs excitability in motoneurons in spinal muscular atrophy. *J Cell Biol* 179, 139-149 (2007).
27. Kaczmarek, A., Schneider, S., Wirth, B. & Riessland, M. Investigational therapies for the treatment of spinal muscular atrophy. *Expert Opin Investig Drugs* 24, 867-881 (2015).
28. Kariya, S., et al. Reduced SMN protein impairs maturation of the neuromuscular junctions in mouse models of spinal muscular atrophy. *Hum Mol Genet* 17, 2552-2569 (2008).

29. Kong, L., et al. Impaired synaptic vesicle release and immaturity of neuromuscular junctions in spinal muscular atrophy mice. *J Neurosci* 29, 842-851 (2009).
30. Kubler, E. & Riezman, H. Actin and fimbrin are required for the internalization step of endocytosis in yeast. *Embo J* 12, 2855-2862 (1993).
31. Ladant, D. Calcium and membrane binding properties of bovine neurocalcin delta expressed in *Escherichia coli*. *J Biol Chem* 270, 3179-3185 (1995).
32. Lefebvre, S., et al. Identification and characterization of a spinal muscular atrophy-determining gene. *Cell* 80, 155-165 (1995).
33. Lorson, C.L., Hahnen, E., Androphy, E.J. & Wirth, B. A single nucleotide in the SMN gene regulates splicing and is responsible for spinal muscular atrophy. *Proc Natl Acad Sci U S A* 96, 6307-6311 (1999).
34. Lotti, F., et al. An SMN-Dependent U12 Splicing Event Essential for Motor Circuit Function. *Cell* 151, 440-454 (2012).
35. Lunn, M.R. & Wang, C.H. Spinal muscular atrophy. *Lancet* 371, 2120-2133 (2008).
36. Macia, E., et al. Dynasore, a cell-permeable inhibitor of dynamin. *Dev Cell* 10, 839-850 (2006).
37. McWhorter, M.L., Monani, U.R., Burghes, A.H. & Beattie, C.E. Knockdown of the survival motor neuron (Smn) protein in zebrafish causes defects in motor axon outgrowth and pathfinding. *J Cell Biol* 162, 919-931 (2003).
38. Mentis, G.Z., et al. Early functional impairment of sensory-motor connectivity in a mouse model of spinal muscular atrophy. *Neuron* 69, 453-467 (2011).
39. Murray, L.M., et al. Selective vulnerability of motor neurons and dissociation of pre- and post-synaptic pathology at the neuromuscular junction in mouse models of spinal muscular atrophy. *Hum Mol Genet* 17, 949-962 (2008).
40. Oprea, G.E., et al. Plastin 3 is a protective modifier of autosomal recessive spinal muscular atrophy. *Science* 320, 524-527 (2008).
41. Prior, T.W., Swoboda, K.J., Scott, H.D. & Hejmanowski, A.Q. Homozygous SMN1 deletions in unaffected family members and modification of the phenotype by SMN2. *Am J Med Genet* 130A, 307-310 (2004).
42. Riessland, M., et al. SAHA ameliorates the SMA phenotype in two mouse models for spinal muscular atrophy. *Hum Mol Genet* 19, 1492-1506 (2010).
43. Ruiz, R., Casanas, J.J., Torres-Benito, L., Cano, R. & Tabares, L. Altered intracellular Ca<sup>2+</sup> homeostasis in nerve terminals of severe spinal muscular atrophy mice. *J Neurosci* 30, 849-857 (2010).



44. Schreij, A.M., Fon, E.A. & McPherson, P.S. Endocytic membrane trafficking and neurodegenerative disease. *Cell Mol Life Sci* 73, 1529-1545 (2016).
45. See, K., et al. SMN deficiency alters Nrnx2 expression and splicing in zebrafish and mouse models of spinal muscular atrophy. *Hum Mol Genet* 23, 1754-1770 (2014).
46. Somers, E., et al. Increasing SMN levels using the histone deacetylase inhibitor SAHA ameliorates defects in skeletal muscle microvasculature in a mouse model of severe spinal muscular atrophy. *Neurosci Lett* 544, 100-104 (2013).
47. Stevens, C.F. Neurotransmitter release at central synapses. *Neuron* 40, 381-388 (2003).
48. Sudhof, T.C. Calcium control of neurotransmitter release. *Cold Spring Harb Perspect Biol* 4, a011353 (2012).
49. Suszynska-Zajczyk, J., Luczak, M., Marczak, L. & Jakubowski, H. Hyperhomocysteinemia and Bleomycin Hydrolase Modulate the Expression of Mouse Brain Proteins Involved in Neurodegeneration. *J Alzheimers Dis* (2014).
50. Venkataraman, V., Duda, T., Ravichandran, S. & Sharma, R.K. Neurocalcin delta modulation of ROS-GC1, a new model of Ca(2+) signaling. *Biochemistry* 47, 6590-6601 (2008).
51. Viviano, J., Krishnan, A., Wu, H. & Venkataraman, V. Data on the calcium-induced mobility shift of myristoylated and non-myristoylated forms of neurocalcin delta. *Data Brief* 7, 630-633 (2016).
52. von Kleist, L., et al. Role of the clathrin terminal domain in regulating coated pit dynamics revealed by small molecule inhibition. *Cell* 146, 471-484 (2011).
53. Wang, C.H., et al. Characterization of survival motor neuron (SMNT) gene deletions in asymptomatic carriers of spinal muscular atrophy. *Hum Mol Genet* 5, 359-365 (1996).
54. Westerfield, M., McMurray, J.V. & Eisen, J.S. Identified motoneurons and their innervation of axial muscles in the zebrafish. *J Neurosci* 6, 2267-2277 (1986).
55. Wirth, B., Garbes, L. & Riessland, M. How genetic modifiers influence the phenotype of spinal muscular atrophy and suggest future therapeutic approaches. *Curr Opin Genet Dev* 23, 330-338 (2013).
56. Yamatani, H., Kawasaki, T., Mita, S., Inagaki, N. & Hirata, T. Proteomics analysis of the temporal changes in axonal proteins during maturation. *Dev Neurobiol* 70, 523-537 (2010).



## FIG. LEGENDS

**Fig. 1** Genome-wide linkage and transcriptome analysis uncovered NCALD as candidate modifier of SMA. **(a)** Pedigree of the Utah family: haplotype analysis of microsatellite markers in the 5q13 SMA region and *SMN1* and *SMN2* copies are indicated. Black filled symbols: SMA-affected individuals, grey filled symbols: asymptomatic *SMN1*-deleted individuals and symbols with a dot: SMA carriers. **(b)** Genome-wide linkage analysis identified eight regions with positive LOD scores. Black arrow marks 8q22.3 region containing *NCALD*. **(c)** Verification of microarray results (Table S1) of *NCALD* RNA and protein in lymphoblastoid (LB) cells. *NCALD* is represented by two independent probes, showing a 4-to-5 fold downregulation in the asymptomatic group versus familial SMA-I or an independent SMA-III group. Three independent experiments including all 17 cell lines (asymptomatic, N = 5; symptomatic, N = 2; independent SMA-III, N = 10) were performed. \* P 0.05. **(d)** Expression analysis of *NCALD* RNA and proteins in fibroblasts (FB) derived from the Utah family (asymptomatic, N = 5; symptomatic, N = 2). Three independent experiments including all seven cell lines were performed. \*\* P 0.01; \*\*\* P 0.001. See also **Supplementary Fig. 1 and Table 1**.

**Fig. 2** NCALD downregulation restores neurite outgrowth defect in SMN-deficient neuronal cells. **(a)** Western blot of NSC34 cells treated with 1 $\mu$ M retinoic acid (RA) for 0-120h as a model of MN differentiation and maturation (n = 3 biological replicates). **(b)** *Ncald* siRNA-treated NSC34 cells show signs of MN differentiation (HB9-positive staining, marked with white arrows) even in absence of RA (right panel). As positive control, cells were differentiated with RA and treated with control siRNA (middle panel). Negative control was treated only with control siRNA (left panel). Scale bar, 100  $\mu$ m. **(c)** Representative images of primary murine MNs cultured 6 days *in vitro* (DIV) stained with antibodies against NCALD, tau and CHAT. Note the high expression of NCALD in soma and growth cones (inset). Scale bar, 50  $\mu$ m. **(d)** Exemplary NCALD staining of NMJ in TVA of 3-week-old wt mice. Postsynaptic terminals stained with Bungarotoxin (magenta) and presynaptic terminals with SV2 (red, delineated by the dashed line). NCALD (green) localizes to presynaptic region, based on overlap between SV2 and NCALD, by Pearson's correlation of  $0.72 \pm 0.082$  (Z stack, 0.5  $\mu$ m per stack; n = 4). Scale bar, 5  $\mu$ m. **(e)** Primary MNs from SMA or heterozygous murine embryos were fixed at 8 DIV and stained with anti-neurofilament. Quantitative analysis of axon length of MNs. SMA: N = 7, control heterozygotes (HET): N = 6, n = 100 per measurement; \*\*\* P 0.001; dashed line = mean; straight line = median. Scale bar, 100  $\mu$ m. See also **Supplementary Fig. 2**.

**Fig. 3** *Ncald* reduction corrects the phenotype in *Smn*-deficient zebrafish and *C. elegans*. **(a)** First 10 motor axons posterior to the yolk globule of 34 hpf zebrafish embryos injected with respective morpholinos (MO). White arrows mark truncated motor axons. Arrowheads mark extensive branching in *ncald* or *smn+ncald* morphants; green = Znp1 staining. Scale bar, 100  $\mu$ m. **(b)** Western blot of lysates of zebrafish embryos injected with indicated MO. **(c)** Quantification of motor axon phenotype. Dashed lines mark the rescue of the truncation phenotype (\*\*P 0.01). *smn+ncald* and *ncald* morphants showed increased branching. n >500 motor axons per MO injection. **(d)** TEM images of NMJs of 48 hpf zebrafish embryos injected with respective MO. White arrows mark synaptic clefts including basal lamina. M = muscle fiber, T = nerve terminal. Scale bar, 100 nm. **(e)** Quantification of synaptic cleft

width of MO-injected 48 hpf fish ( $n = 15$  per treatment). \*\* $P < 0.01$ , dashed line=mean; straight line=median. (f) Whole-cell current clamp recordings EPPs and (g) quantification of mean EPP frequencies in ventral fast muscle cells of control ( $n = 12$ ), *smn* ( $n = 10$ ), *ncald* ( $n = 11$ ) and *smn+ncald* ( $n = 12$ ) morphants under control conditions or NMDA induction. White bar parts reflect the mEPP frequencies, grey bar parts reflect the frequency of the TTX-sensitive large EPPs. \*\* $P < 0.01$ ; \*\*\* $P < 0.001$ . (h) *C. elegans* neuromuscular function was assessed based on pharyngeal pumping rates during feeding. Arrow indicates the pharyngeal grinder, which moves during each pumping event. (i, j) Quantification of pharyngeal pumping in wt or mutant *smn-1* worms fed with control or *ncs-1* RNAi KD (i) or with an *ncs-1(qa401)* mutant allele (j). For every determination  $n \geq 25$ . Mean  $\pm$  SEM is shown; \*  $P < 0.05$ , \*\*  $P < 0.01$ . See also **Supplementary Fig. 3**.

**Fig. 4** Heterozygous *Ncald* KO improves axonal outgrowth, proprioceptive input and NMJ size in severe SMA mice. (a) Western blot and quantification of NCALD and ACTB (loading control) in spinal cord and hippocampus of P10-old wt and *Ncald*<sup>ko/wt</sup> mice. \* $P < 0.05$ . (b) Representative images and quantification of NMJ area [ $\mu\text{m}^2$ ] in TVA muscle from P10-old mice stained with antibodies against NF and SV2 (green) and Bungarotoxin (magenta). NMJ area was analyzed with ImageJ software ( $n = 3$ , 100-120 NMJs/mouse). \*\*\* $P < 0.001$ . Scale bar, 10  $\mu\text{m}$ . (c) Representative images and quantification of proprioceptive inputs (VGLUT1, green) on MN soma (CHAT, magenta) in lumbar spinal cord sections from P10-old mice. Mean input number within 5  $\mu\text{m}$  of MN soma was analyzed ( $n = 3$ , 100-120 MNs/mouse). \*\*\* $P < 0.001$ . Scale bar, 25  $\mu\text{m}$ . (d) Representative merged images of 6 DIV MNs isolated from E13.5 embryos and stained with DAPI (blue) and antibodies against HB9 (green) and Tau (red). The longest axon and axonal branches were quantified with ImageJ ( $n = 3-5$ , 20-40 axons per mouse). Scale bar, 25  $\mu\text{m}$ . Each box plot covers values from 25-75% with line at median and dotted outliers at <5% and >95% CI. For each experiment, image analysis was double-blinded. n.s. not significant; \* $P < 0.05$ ; \*\* $P < 0.01$ ; \*\*\* $P < 0.001$ . See also **Supplementary Fig. 4**.

**Fig. 5** NCALD reduction improves motoric function, NMJ size, and NMJ architecture in SMA+ASO mice. (a) Breeding scheme to produce mixed<sub>50</sub> SMA and HET mice. All mixed<sub>50</sub> offspring were injected with 30  $\mu\text{g}$  SMN-ASO at P1. (b) Kaplan-Meier curves of uninjected mixed<sub>50</sub> mice show no differences in survival between SMA (17 days,  $n = 7$ ) and SMA-*Ncald*<sup>ko/wt</sup> (16.5 days,  $n = 12$ ). Injection of 30  $\mu\text{g}$  SMN-ASO on P1 increases survival to >180 days for both SMA+ASO ( $n = 10$ ) and SMA-*Ncald*<sup>ko/wt</sup>+ASO ( $n = 12$ ) mice. (c) Righting reflex test shows improvement in SMA-*Ncald*<sup>ko/wt</sup>+ASO, but not SMA+ASO mice during P2-P6 ( $n \geq 12$  per genotype). Error bars represent SEM. n.s. not significant, \*\* $P < 0.01$ , \*\*\* $P < 0.001$ . (d) Grip strength test performance at P73 reveals enhanced strength for SMA-*Ncald*<sup>ko/wt</sup>+ASO mice compared to SMA+ASO mice ( $n \geq 12$  per genotype). Error bars indicate SEM. \* $P < 0.05$ , \*\* $P < 0.01$ , \*\*\* $P < 0.001$ . (e) Representative images of NMJs of ASO-treated mixed<sub>50</sub> mice at P21 stained with the antibody against NF (green, for presynaptic terminal) and Bungarotoxin (magenta, for postsynaptic terminal). Scale bar, 20  $\mu\text{m}$ . Box plot shows quantification of NMJ area in  $\mu\text{m}^2$  in TVA muscle which was analyzed and represented as in Fig. 4 (b). Bar graph shows percentage of immature NMJs in TVA muscle (mean  $\pm$  SD).  $N = 3$  mice per genotype;  $n = 60-100$  NMJs per mouse. n.s. not significant, \* $P < 0.05$ , \*\* $P < 0.01$ , \*\*\* $P < 0.001$ . See also **Supplementary Fig. 5**.

**Fig. 6** Interconnection between SMN, NCALD, voltage-dependent  $\text{Ca}^{2+}$  influx, endocytosis and SMA. **(a)** Measurement of *I*-*V* relations of  $\text{Ca}^{2+}$  tail currents in differentiated NSC34 cells treated with respective siRNAs and depolarized for 5 ms to 60 mV, in 5 mV increments, at holding potential -80 mV. Currents were not different between wildtype (*n* = 7), control siRNA (*n* = 33) and *Ncald* KD (*n* = 13) and were significantly reduced upon *Smn* KD (*n* = 15) and *Smn+Ncald* KD (*n* = 12) at current pulses above -35 mV. \**P* 0.05; \*\**P* 0.01; \*\*\**P* 0.001. **(b)** Western blot of co-immunoprecipitation experiment. NCALD interacts with clathrin in the absence of  $\text{Ca}^{2+}$  (EGTA addition) but not in presence of  $\text{Ca}^{2+}$ . Interaction between NCALD and SMN was not observed. **(c)** Quantification of endocytosis by FITC-dextran uptake in fibroblasts from SMA (*N* = 10), controls (*N* = 3) and asymptomatic individuals (*N* = 5); *n* = 50 per cell line and time point. Mean  $\pm$ SD. \**P* 0.05, \*\**P* 0.01. **(d)** Quantification of FM1-43 intensity at presynaptic terminals in TVA muscles under low frequency stimulation (5 Hz, 1s). *N* = 3 per genotype, *n* 100 per mouse. Mean  $\pm$ SEM. n.s. not significant; \*\*\**P* 0.001. **(e)** Quantification of MN axon phenotype of zebrafish embryos treated with sub-phenotypical doses of *smn* MO (2 ng), *ncald* MO (2 ng) and the endocytosis inhibitors Pitstop2 and Dynasore, respectively. Dashed lines highlight the synergistic effect of *smn* MO and Pitstop2 and the effect of Dynasore on axon truncation. Additional *ncald* MO injection ameliorates the truncation defect. \*\*\**P* 0.001. Motor axons per treatment: Pitstop2: *n* 100, Dynasore: *n* 150. **(f)** Proposed mode of action of NCALD in synaptic vesicle recycling in normal, SMA, and asymptomatic presynaptic terminals. See also **Supplementary Fig. 6**.

## ONLINE MATERIAL

**Patient DNA, fibroblast cell lines and lymphoblastoid cell lines.** Informed written consent was obtained from each subject or their legal guardians for all biological samples according to the Declaration of Helsinki. The study has been approved by the Ethical Committee of University of Cologne (04-138). Human fibroblast and EBV-transformed lymphoblastoid cell lines (LCL) from SMA patients, carriers and asymptomatic individuals used in this work are listed in **Supplementary Table 3**. DNA was extracted from EDTA blood samples, primary fibroblast cell lines and LCL using standard protocols. *SMN1* and *SMN2* copy number were determined by qRT-PCR or MLPA analysis (MRC Holland) as described (Arkblad et al. 2009). For haplotype analysis, polymorphic markers Ag1-CA (D5S1556), C212 (D5F149S1/S2), VS19A (D5S435) and MIT-1105 (D5S351) were analyzed as described (Zerres et al. 1997). *SMN2* coding region was sequenced in qRT-PCR products obtained from LCL-isolated RNA as described (Sun et al. 2005). *PLS3* RNA expression was analyzed as described (Oprea et al. 2008). All cell lines used were tested for mycoplasma contamination.

**Genome-wide linkage analysis.** Genome-wide scan was performed in 14 individuals of the Utah family using Affymetrix GeneChip Human Mapping 10K Array 2.0, which comprises total 10,024 SNPs with a mean intermarker distance of 258kb, equivalent to 0.36cM (Affymetrix). Parametric linkage analysis was performed by ALLEGRO program assuming autosomal dominant inheritance with full penetrance and 0.0001 disease allele frequency. Haplotypes were reconstructed with ALLEGRO and presented graphically with HaploPainter. All data handling was performed with ALOHOMORA user interface.

**Transcriptome analysis.** For expression profiling, 400ng total RNA were amplified and biotinylated using Illumina® TotalPrepTMRNA Amplification Kits (Ambion) according to manufacturer's protocol. Human HT-12v3 bead arrays (Illumina) were hybridized with 750ng cRNA for 18h at 58°C according to Illumina® Whole-Genome Gene Expression with IntelliHyb SealSystem Manual. Arrays were washed with E1BC buffer, High-Temp Wash Buffer and 100% ethanol, stained with streptavidine-Cy3 and washed with E1BC buffer. Fluorescence intensities were recorded on BeadArray Reader GX (Illumina). Average signal intensities without background correction (Dunning et al. 2008) were performed with BeadStudio3.1 (Illumina). All data analysis steps were performed in the statistical environment R (version 2.10.0; www.r-project.org) with several bioconductor packages (version 2.6.1; www.bioconductor.org). Signal intensities were normalized with VSN and non-informative probes were removed based on p-values. Signals were averaged for individual subgroups and a linear model was designed capturing the influence of the patient group on gene expression levels (Wettenhall and Smyth 2004). Differences between subgroups were extracted as contrasts and analyzed with the moderated F-test (empirical Bayes method) including a correction step for multiple testing with 5%-FDR-based method (Benjamini and Hochberg 1995). To attribute significant regulations to individual contrasts, a decision matrix was generated based on the function “*decide tests*” within the “*limma*” package, where significant up- or downregulations are represented by values of 1 or -1, respectively.

**Targeted resequencing.** To identify a potential variant regulating differential *NCALD* expression, complete *NCALD* locus ±1Mb (chr8:101,505,353-104,404,346) was deep-

sequenced from gDNA of family members 9129, 9124, 9128, 9119, 9165 at Radboud University Medical Center Nijmegen using a 5500xl sequencing instrument (Life Technologies). ~3Mb genomic DNA from chromosome 8 were captured using a 385K NimbleGen SequenceCapture Array (Roche).

On average, we obtained 2.7Gb of mappable sequence data/individual. Reads were mapped to the hg19 reference genome with LifeTechnologies BioScope software 1.3. On average, 94% of bases originated from the target region (mean 544-fold coverage). 99.8% of the targeted region was covered 20 times. Single-nucleotide variants were subsequently high-stringency called by the DiBayes algorithm. Small insertions and deletions were detected using the Small IndelTool. Variants were annotated using an in-house analysis pipeline.

On average 2,723 variants were called per sample. Based on previous haplotype data, we filtered for heterozygous variants shared between individuals 9129, 9124, 9128, 9119 but absent in 9165. This yielded 43 variants (21 previously annotated SNPs), none of which were in *NCALD* coding region. Only the SNP rs147264092 in intron1 with a minor allele frequency=0.1079 (1000Genome database) was located in *NCALD* UTR (**Supplementary Table 2**). Subsequent Sanger sequencing of potential variants in 50 unrelated SMA patients identified several symptomatic individuals carrying the same alleles, thus refuting a protective role of the respective variant (**Supplementary Fig. 1**). ~600kb upstream of *NCALD* we identified a 17bp deletion (nt103783522-38, rs150254064; MAF=0.056 in 1000Genome database) linked to the modifier haplotype, adjacent to an H3K27AC block (<http://genome.ucsc.edu/ENCODE>). Sanger sequencing of this variant in the family showed co-segregation with the modifier haplotype. As the 17bp deletion was present in 8/50 independent SMA patients, we excluded it as a sole cause.

**Microscopy.** Unless indicated otherwise, all microscopic experiments were performed with a fully motorized fluorescence microscope AxioImager M2 (Zeiss) equipped with an ApoTome. All quantitative measurements were performed using Zen software (Zeiss) and ImageJ and evaluated with indicated statistical packages.

### Cell culture

**Quantitative RT-PCR.** RNA was extracted from cell lines using RNeasy kit (Qiagen). 150ng RNA was reversely transcribed to cDNA (Quantitect Reverse Transcription Kit, Qiagen). For *NCALD* cDNA measurements, 9ng cDNA was used for RT-PCR (LightCycler, Roche). RT-PCR was performed in triplicates according to manufacturer's protocol (annealing temperature 68°C, *NCALD* cDNA primers: 5'-GGAATGCCAGAGCCCCAGTGT-3'; 5'-GCCCCAACCCCCGAGTCTTACG-3'). Standard curve-based absolute transcript quantification was performed using Excel (Microsoft). For statistical evaluation, the Student's t-test was applied. For quantitative measurements of *SMN* and *PLS3*, previously described protocols were used (Oprea et al. 2008).

**Western blot analysis.** Cells were lysed on ice in RIPA buffer (Sigma) containing protease inhibitors (Complete Mini, Roche). Following primary antibodies were used: anti-beta-actin (A5316, Sigma), anti-SMN (MANSMA7, Hybridoma Bank; 610646, BD Biosciences), anti-*NCALD* (12925-1-AP, Proteintech) and clathrin heavy chain (C1860, Sigma). Signal was detected with HRP conjugated-secondary antibodies and Chemiluminescence reagent (Thermo Scientific) according to manufacturer's protocol.

**siRNA-mediated RNA knockdown.** For all siRNA experiments NSC34 (CLU140)<sup>32</sup> and PC12(Greene and Tischler 1976) cells were transfected with Dharmafect1 (Thermo Scientific) according to manufacturer's protocol. siTOX (Dharmacon) and AllStars Negative Control (Qiagen) siRNA were used as controls. siRNAs sequences: mmu-*Smn*: 5'-AAGAAGGAAAGTGCTCACATA-3'; mmu-*Ncald* 5'-CAGGTGATTCACCCATTATAA-3'; rn-*Smn* 5'-CCCGACCTGTGAAGTAGCTAA-3'; rn-*Ncald* 5'-AGAGACTTCCTAGCAATTAA-3. After incubation, cells were harvested for protein isolation or imaging. Every experiment was performed at least in triplicates.

**Transient overexpression.** Human *NCALD* cDNA was cloned into pcDNA<sup>TM</sup>3.1/CT-GFP TOPO using primers NCALD-FWD 5'-ATGGGGAAACAGAACAGCAAG-3' and NCALD-REV 5'-GAACTGGCCGGCACTGCTC-3' (IDT) and manufacturer's protocol (Invitrogen). To overexpress human NCALD-GFP, NSC34 cells were transfected with Dharmafect1 according to manufacturer's protocol.

**NCALD co-immunoprecipitation.** NSC34 cells transiently transfected with pcDNA<sup>TM</sup>6/FLAG-His-NCALD or control vector were lysed in the following buffer: 50mM Tris/HCl, 5% (w/v) glycerol, 270mM sucrose, 0.5%(v/v) Tween 20, 0.1%(v/v) -mercaptoethanol, pH7.5, with protease inhibitor cocktail (Complete Mini, EDTA-free, Roche). Immunoprecipitations were performed in 1mM EGTA/1mM EDTA or in the presence of 100μM free Ca<sup>2+</sup>. Cell lysates were immunoprecipitated with FLAG-M2 affinity beads (Sigma) under gentle agitation overnight at 4°C. Bound proteins were eluted in laemmli buffer (240mM Tris-HCl, pH6.8, 6% SDS, 30% (v/v) glycerol, 0.06% bromophenol blue (w/v), 16%(v/v) -mercaptoethanol) and analyzed by Western blots were performed as described above.

**Primary motor neuron culture.** Spinal cords were dissected from E13.5 mouse embryos(Hsieh-Li et al. 2000). Neurons were singularized with trypsin (Worthington) and DNase (Sigma), sieved, plated on poly-D-lysine/laminin (Sigma) coated coverslips and cultured in neurobasal medium with B27 supplement, 2mM L-glutamine, 1x pen-strep (Invitrogen) containing 50ng/μl, BDNF, 50ng/μl GDNF and 50ng/μl CNTF (Peprotech) at 37°C in a humidified incubator with 5%CO<sub>2</sub>.

**Immunocytochemistry.** Cells were cultured on laminin-coated coverslips, washed with PBS, fixed in 4%PFA/4%sucrose (AppliChem), permeabilized in PBS-T (PBS/0.2%Tween20 (AppliChem)) and blocked in blocking solution (PBS-T/5%BSA (Sigma)/5%FCS (Biochrom)). Cells were incubated with blocking solution containing primary antibodies ( -HB9 (1:100), AB2145209, Hybridoma Bank; -Synaptic vesicle 2, AB2315387, (SV2-c), Hybridoma Bank; -Neurofilament, AB2314897, (2H3-c), Hybridoma Bank; -Choline Acetyltransferase (CHAT), AB144P, Millipore; -Tau, sc-390476, Santa Cruz; -NCALD) overnight at 4°C. After washing in PBS, cells were incubated with secondary antibodies labelled with AlexaFluor488, AlexaFluor647 or AlexaFluor568 (Invitrogen) in PBS, optionally with phalloidin-AlexaFluor568 (Invitrogen). Cells were washed and mounted on objects slides with Mowiol (Sigma) for imaging.

**Endocytosis Assay.** Fibroblasts were plated in DMEM (Invitrogen) and starved for 10min in starvation media (DMEM transparent (HEPES), 2%FKS) prior to FITC-Dextran

treatment (5mg/ml, Sigma) for respective time periods at 37°C. Subsequently, cells were washed with ice-cold PBS and fixed in 4%PFA for 10min. After washing, cells were stained with phalloidin-AlexaFluor568 and DAPI (Invitrogen) and mounted with Mowiol for imaging.

**Flow Cytometry Analysis.** NSC34 cells were transfected with indicated siRNAs for 48h prior to 6h starvation and incubation with 5mg/ml FITC-Dextran (Sigma) for 20min at 37°C. Cells were trypsinized (Trypsin, Sigma) on ice and washed with PBS. Uptake of FITC-Dextran was measured with FACS Calibur (BD Biosciences) and analyzed with Cyflogic software ([www.cyflogic.com](http://www.cyflogic.com)). Dead cells were excluded by propidium iodide staining (10µg/ml, Sigma).

**Ca<sup>2+</sup> current recordings in NSC34 and PC12.** Whole-cell recordings were performed at 24°C. Electrodes (tip resistance 2.5-3 M $\Omega$ ) were made of borosilicate glass (0.86mm OD, 1.5mm ID, Science Products) with a temperature-controlled pipette puller (PIP5, HEKA Elektronik) and filled with solution containing (in mM) 133 CsCl, 1 CaCl<sub>2</sub>, 2 MgCl<sub>2</sub>, 10 HEPES and 10 EGTA, adjusted to pH7.2 and osmolarity of 415mOsm. During experiments, cells were constantly superfused with saline solution containing (in mM) 84 NaCl, 20 CsCl, 2.5 KCl, 10 CaCl<sub>2</sub>, 2 MgCl<sub>2</sub>, 10 HEPES and 30 glucose, adjusted to pH7.3 and osmolarity of 310mOsm. To isolate Ca<sup>2+</sup> currents, a combination of pharmacological blockers and ion substitution were used. Transient voltage-gated Na<sup>+</sup> currents were blocked by tetrodotoxin (10<sup>-6</sup>M TTX, T-550, Alomone). 4-Aminopyridine (4AP, 4×10<sup>-3</sup>M, A78403, Sigma) blocked transient K<sup>+</sup> currents (*I<sub>A</sub>*) and tetraethylammonium (TEA, 2×10<sup>-3</sup>, Sigma) blocked sustained K<sup>+</sup> currents (*I<sub>K(V)</sub>*) and Ca<sup>2+</sup>-activated K<sup>+</sup> currents (*I<sub>K(Ca)</sub>*). The pipette solution did not contain potassium. Whole-cell voltage-clamp recordings were made with EPC10 patch-clamp amplifier (HEKA Elektronik) controlled by Patchmaster program (V2x53, HEKA-Elektronik). Electrophysiological signals were low-pass filtered at 2.9kHz (3pole Bessel filter). Data were sampled at 50µs intervals (20kHz). The offset-potential and capacitance were compensated using 'automatic mode' of EPC10 and liquid-junction potential between intracellular and extracellular solution of 2.5mV (calculated with Patcher's PowerTools plug-in, <http://www.mpibpc.gwdg.de/abteilungen/140/software/index.html> (WaveMetrics)) was compensated. Whole-cell capacitance was determined using EPC10 capacitance compensation (C-slow). To remove uncompensated leakage and capacitive currents, p/6 protocol was used (Armstrong and Bezanilla 1974). Voltage errors due to series resistance (RS) were minimized using RS compensation of EPC10 to 70-80% with 100µs time constant ( ).

## Animal models

**Zebrafish experiments.** All experiments were performed with the transgenic line *tg(mnx1-GFP)<sup>ml2TG</sup>* (Flanagan-Steet et al. 2005) and approved by the local animal protection committee (LANUV NRW; reference number 84-02.04.2012.A251).

**Zebrafish injection and analysis.** Morpholinos (MO) were designed against the translational start codons of respective genes (Gene Tools, LLC). *smn*-MO: 5'-CGACATCTTCTGCACCATTTGGC-3'; *ncaldb*-MO: 5'-GGAGCTTGCTGTTTTGTTTCCCAT-3'; control-MO: 5'-CCTCTTACCTCAGTTACAATTATA-3'. For *NCALD* mRNA injections, human *NCALD* cDNA was cloned into pCS2+ mRNA expression vector and transcribed *in vitro* using

mMESSAGE mMACHINE® SP6 Transcription Kit (Ambion) according to manufacturer's protocol. Embryos from TL/EK wildtype and TL/EK-*hb9-GFP* (Flanagan-Steet et al. 2005) crossings were used to visualize the MN phenotype. Embryos were injected with the respective dose of MOs or mRNA in aqueous solution containing 0.05% PhenolRed and 0.05% Rhodamine-Dextran (Sigma). 6h after injection embryos were sorted according to homogeneity of the rhodamine fluorescence signal.

**Immunohistochemistry for motor axon quantification.** 34hpf zebrafish were manually dechorionated, fixed in 4% PFA-PBS and permeabilized by collagenase digest of the whole animal. To visualize the primary motor axons, zebrafish were incubated at 4°C overnight in PBS-T/1%DMSO/10%FCS containing znp-1 antibody (AB2315626, Hybridoma Bank) and stained in PBS-T/1%DMSO/10%FCS containing donkey anti-mouse secondary antibody labelled with AlexaFluor488 (Invitrogen) after all-day washing in PBS-T/1%FCS/1%BSA (changing solution hourly) and stored in 80% glycerol/20% PBS in the dark at 4°C or embedded in low-melting agarose microslides for microscopy analysis. The structure of first ten motor axons posterior to the yolk was analyzed, rated as: 1) normal, 2) truncated (truncation ventral from midline), 3) severely truncated (shorter than midline), 4) branched I (branching ventral from midline), 5) branched II (branching at midline), or 6) branched III (branching dorsal from midline).

**Western blot analysis of zebrafish.** 48hpf dechorionated embryos were gently spinned-down, sacrificed by incubation on ice and lysed in RIPA buffer (Sigma) containing protease inhibitors (Complete Mini, Roche). Following primary antibodies were used for overnight incubation: anti-beta-actin (zebrafish) (553399, Anaspec), anti-SMN and anti-NCALD. Signal detection was performed as described above.

**Transmission electron microscopy of zebrafish.** 48hpf zebrafish were fixed in 4%PFA for 30min and postfixed in 0.6% glutaraldehyde for another day. Samples were prepared and embedded in resin as previously described (Ackermann et al. 2013). The thickness of semi-thin and ultra-thin sections was 0.5 and 0.1mm, respectively. For immunogold stainings, pre-stained sections were blocked, incubated with primary antibodies (anti-clathrin, anti-NCALD), washed in PBS and stained with gold-labelled secondary antibodies (donkey-anti-mouse 6nm gold, ab39616, goat-anti-rabbit 20nm gold, ab27237; Abcam). Image acquisition was performed with TEM CM10 (Philips) microscope, Orius SC200W 1 Gatan camera and the Digital Micrograph software.

**Motor behaviour analysis of zebrafish.** 30 zebrafish treated with respective MOs were placed in 10cm petri dish containing embryo medium. To trigger a swimming response, zebrafish were stimulated with an electrical impulse (60V; delay: 60ms, duration: 4ms, frequency: 6pps (SD9 Stimulator)). Swimming behaviour was recorded with 120 frames/second using a high-speed camera (FC-100, Casio). Swimming velocity and distance were analyzed using LoliTrack software (Loligo Systems).

**Endocytosis inhibitor treatment.** Dynasore (dynamin inhibitor) and Pitstop2 (clathrin inhibitor) (Abcam) were dissolved as stock solutions (50mM) in DMSO. Zebrafish were dechorionated and incubated with the respective inhibitors in the medium starting at 16hpf at 28°C on a rocking platform (20rpm) until fixed in 4%PBS-PFA at 34hpf. Subsequent zebrafish immunohistochemistry was performed as described above.



**Electrophysiology.** 72hpf zebrafish (control, *smn*<sup>-</sup>, *ncald*<sup>-</sup>, and *smn*+*ncald*-morphants) were anesthetized with 0.02% tricaine (in saline; Sigma) for 1-2min and rinsed with saline containing (in mM): 134 NaCl, 2.9 KCl, 2.1 CaCl<sub>2</sub>, 1.2 MgCl<sub>2</sub>, 10 HEPES, 10 glucose adjusted to pH7.8. Zebrafish were decapitated and pinned under saline in a Sylgard-coated (Dow Corning) recording chamber (~3ml volume). Skin was removed using a tungsten pin and forceps; preparation was incubated in 3M formamide (in saline; Carl Roth) for 2min to prevent muscle contractions. After rinsing the preparation, the superficial layer of ventral slow muscle cells was removed by scratching with a tungsten pin to expose deeper fast skeletal muscle cells and remaining superficial slow muscles were removed with a low resistance pipette (~2 M $\Omega$ ). The preparation was continuously superfused with saline at a flow rate of ~2ml/min<sup>1</sup>. Experiments were carried out at ~24°C. Muscle cells were visualized with a fixed-stage upright microscope (Zeiss Axio Examiner, Zeiss), using a 40x water immersion objective (Zeiss) with infrared-differential interference contrast and fluorescence optics. Fast muscle cells were identified by their orientation to the spinal cord and ability to generate action potentials.

***Caenorhabditis elegans* experiments.** *Caenorhabditis elegans* strains. LM99 *smn-1(ok355)/hT2(I;III)*(Briese et al. 2009), HA1981 *+hT2(I;III)*, HA2530 *+hT2(I;III);ncs-1(qa401)X*, HA2531 *smn-1(ok355)/hT2(I;III);ncs-1(qa401)X*, HA2599 *+hT2(I;III);uls72*, HA2623 *smn-1(ok355)/hT2(I;III);uls72*, were maintained at 20°C under standard conditions. *+hT2* strains used as control for genetic background; RNAi studies were undertaken in a sensitized background (transgene *uls72*) expressing the SID-1 dsRNA channel in neurons (Calixto et al. 2010).

**C. *elegans* pharyngeal pumping.** Pharyngeal grinder movement in any axis was scored as a pumping event. Average pumping rates ( $\pm$ SEM) were combined from at least three independent trials (n = 25 animals in total). For RNAi knockdown, animals were reared for two generations (F2) on either control vector L4440 or C44C1.3/*ncs-1(RNAi)* in HT115. *ncs-1* RNAi clone contains genomic DNA amplified by primers 5'-AAATCGTCTAGCTGTAGTGTGCGC-3' and 5'-TTGTGCTCCCTACACTTTGTTTT-3' inserted into L4440. Clone was verified by sequencing.

**Mouse experiments.** All mouse experiments were approved by LANUV NRW (reference number 9.93.2.10.31.07.186 and 84-02.04.2014.A 126). The Taiwanese SMA mice (FVB.Cg-Tg(SMN2)2Hung *Smn1tm1Hung/J*, Stock Number:005058) and heterozygous *Ncald*<sup>ko/wt</sup> (B6N(Cg)-*Ncald*<sup>tm1.1(KOMP)Vlclg/J</sup>, Stock Number:018575) were purchased from Jackson Laboratory. The severe SMA (SMA) mouse model and the corresponding heterozygous (HET) mice were produced as previously described (Hsieh-Li et al. 2000, Riessland et al. 2010). The breeding scheme and genotypes for SMA-*Ncald*<sup>ko/wt</sup> and HET-*Ncald*<sup>ko/wt</sup> are similar to SMA+ASO treated mice (Fig. 5a), except that all animals were on congenic C57Bl/6N and untreated.

Primers used for mouse genotyping: mmu *Smn*KOfw: ATAACACCACCACTCTTACTC; mmu *Smn*KOrev1: 5'-AGCCTGAAGAACGAGATCAGC-3'; mmu *Smn*KOrev2: 5'-TAGCCGTGATGCCATTGTCA-3'; hsa *SMN2*fw: 5'-CGAATCACTTGAGGGCAGGAGTTTG-3'; hsa *SMN2*rev: 5'-AACTGGTGGACATGGCTGTTCATTG-3'; mmu *Ncald*KOfw: 5'-CGGTCGCTACCATTAC-3'; mmu *Ncald*KOrev: 5'-GCATGTGTGACAACAG-3'.

A mild SMA mouse model was produced by suboptimal subcutaneous injection of severe SMA mice (50% FVB/N: 50% C57BL6/N) on P1 with 30µg of SMN-ASO (IONIS Pharmaceuticals) using a MICROLITER syringe (Hamilton). The SMN-ASO was diluted as previously described<sup>19</sup>. SMA-*Ncal*<sup>ko/wt</sup>+ASO and HET-*Ncal*<sup>ko/wt</sup>+ASO were produced using the breeding scheme in **Fig. 5a**. Unless stated otherwise, all mouse experiments were performed double-blinded.

**Mouse motoric tests.** Righting reflex test was performed as previously described (El-Khodor et al. 2008). Righting time scores were evaluated as followed: 0-2s=1; 3-4s=2; 5-6s=3; 7-8s=4; 9-10s=5; 11s=6. Muscle strength was assessed in P73 SMN-ASO injected mixed<sub>50</sub> background mice by the animal's grasp of a horizontal metal bar mounted to a high-precision force sensor (Grip strength meter, TSE Systems). Muscle force was recorded in pounds and converted to Newton [N].

**Quantification of proprioceptive inputs.** Analysis of proprioceptive input on MN soma was performed as described (HosseiniBarkoie et al. 2016). The spinal cord was dissected from euthanized mice and fixed in 4% PFA overnight. The lumbar L4-L5 region was rinsed in PBS, embedded in tissue freezing medium (Jung) after cryoprotection (first day: 20% sucrose, second day: 30% sucrose) and sliced into 100µm sections (cryostat, Leica). Samples were permeabilized, blocked in PBS/4% BSA/1% Triton/PBS for 1h and incubated with anti-CHAT and anti-VGLUT1 (135303, Synaptic Systems) antibodies overnight. Samples were washed and incubated with secondary antibodies (donkey anti-rabbit AlexaFluor488, donkey anti-goat AlexaFluor568) and mounted in Mowiol. Images were taken in Z-stacks of 30-60 slices of 0.3µm interval. Proprioceptive input numbers on MN and MN soma size were quantified using the ImageJ software.

**Quantification of NMJ size and maturity.** The TVA muscle was prepared at the indicated time points, fixed in 4%PFA for 20min and stained with anti-Neurofilament M (Hybridoma-Bank), secondary goat-anti mouse AlexaFluor488 and Bungarotoxin (Invitrogen, labeled with AlexaFluor555). Surface area of Bungarotoxin-positive post-synapse was measured by ImageJ with threshold set to the method established by Li. NMJ immaturity index was analyzed as described previously (Bogdanik et al. 2015): NMJs exhibiting 3 perforations were evaluated as mature, NMJs with < 3 perforations as immature.

**FM1-43 endocytic uptake at NMJ under electrical stimulation.** FM1-43 endocytic uptake at NMJ under electrical stimulation was undertaken as recently described (HosseiniBarkoie et al. 2016). Three animals per genotype and stimulation set were used. Imaging was performed as described above. All imaging processes and analyses were performed double-blinded. Images were analyzed with ImageJ using a macro setting and Li threshold method applied to the postsynaptic terminals to delineate the area of interest in the presynaptic site.

**Statistical analysis.** If not mentioned otherwise, all statistical analyses were performed using software programs Excel 2013 (Microsoft), GraphPad Prism 6 (GraphPad Software) and Sigma Plot 11 (Systat Software); ANOVA, Mann-Whitney U-test, Fisher's exact test or unpaired two-tailed Student's t-tests were applied. All data are represented as mean±SEM/SD. Significance of RNA expression and protein levels was tested using a directional student's t-test for uncorrelated samples. For experiments performed in

*C.elegans*, Mann-Whitney-U test analysis was performed. Significance in the differences of mouse behavioral analyses, NMJ and muscle fiber surface area size, motor axon length, proprioceptive inputs on MNs, NSC34 neurite length and width of the synaptic cleft was determined by the use of 1-way ANOVA or directional student's t-test for uncorrelated samples. Survival was analyzed using Kaplan-Meier method by log rank test.

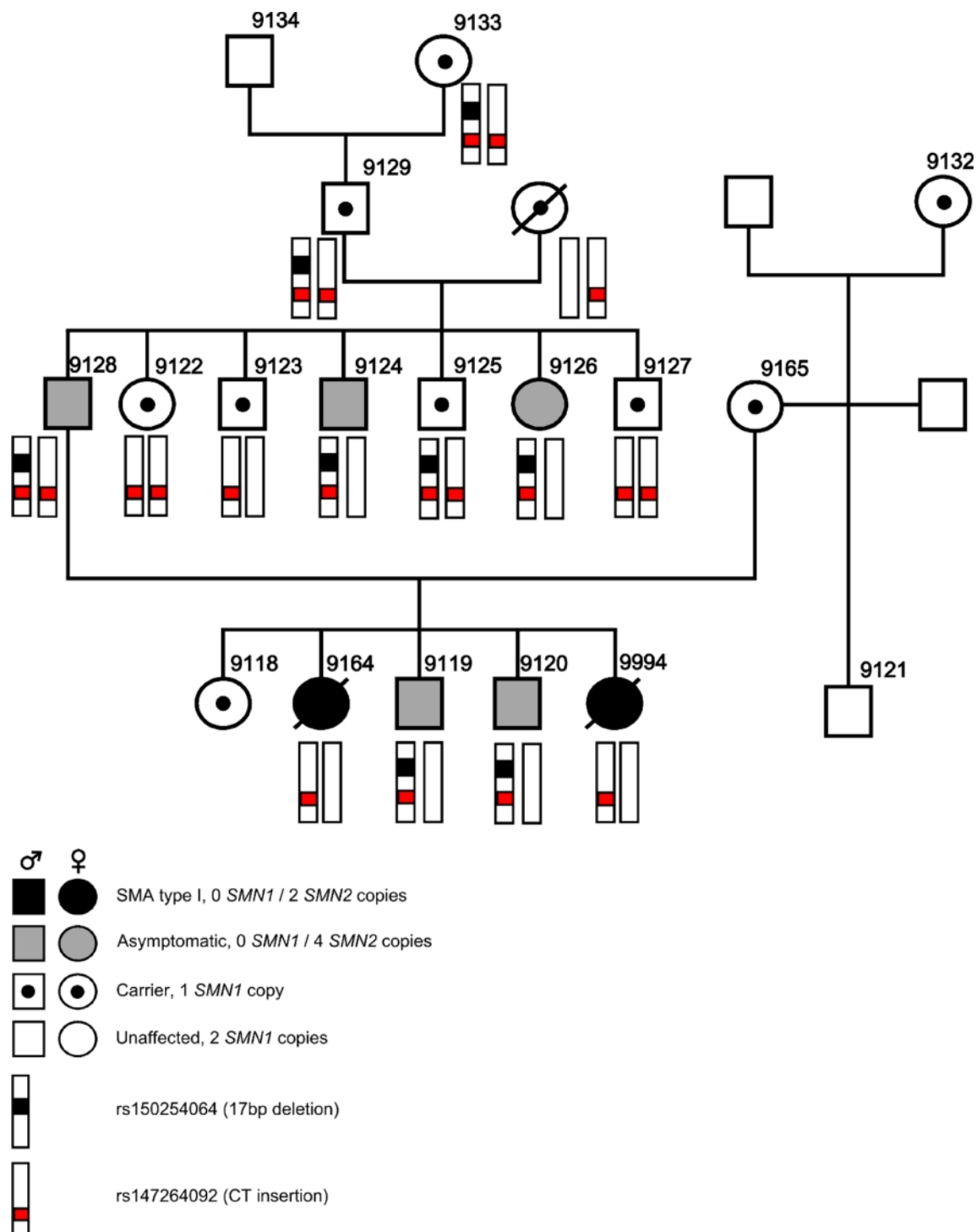
For all studies using mice, animals numbers were calculated prior to experiments by power calculation using the G\*Power 3.1.7 software (Power=0.8 and alpha-error=0.05). Endpoint criteria for mouse experiments were defined in animal application prior to experiments. Animal samples were processed equally and allocated to experimental groups post-analysis. For all other experiments, sample size was estimated based on the known variability of the assay.

Values of  $P < 0.05$  were considered significant. In all cases, three levels of statistical significance were distinguished: \* $P < 0.05$ , \*\* $P < 0.01$  and \*\*\* $P < 0.001$ .

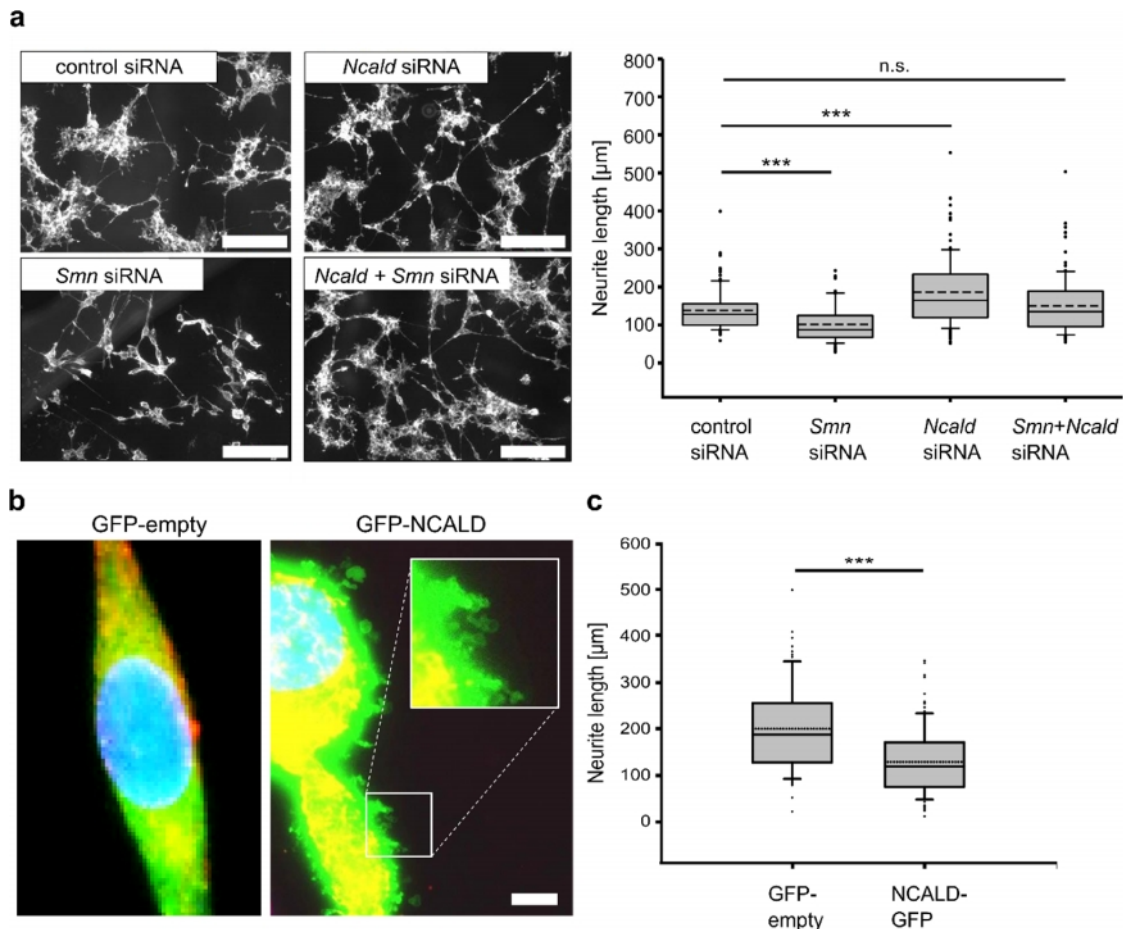
Specific statistical tests, sample size and P-values are indicated in the Fig. legends.

**Statistical analysis of electrophysiology.** Data were analyzed using Spike2 and statistical analysis was performed in GraphPad Prism 5.05 (GraphPad Software). All calculated values are expressed as mean $\pm$ SEM. The EEP frequencies for each cell were measured as mean frequencies over 30s intervals. Frequencies before and during NMDA application were compared by a paired t-test for each group. A Kruskal-Wallis test followed by Dunns multiple comparisons was used to compare EPP frequencies in different groups. A significance level of  $P < 0.05$  was accepted for all tests.

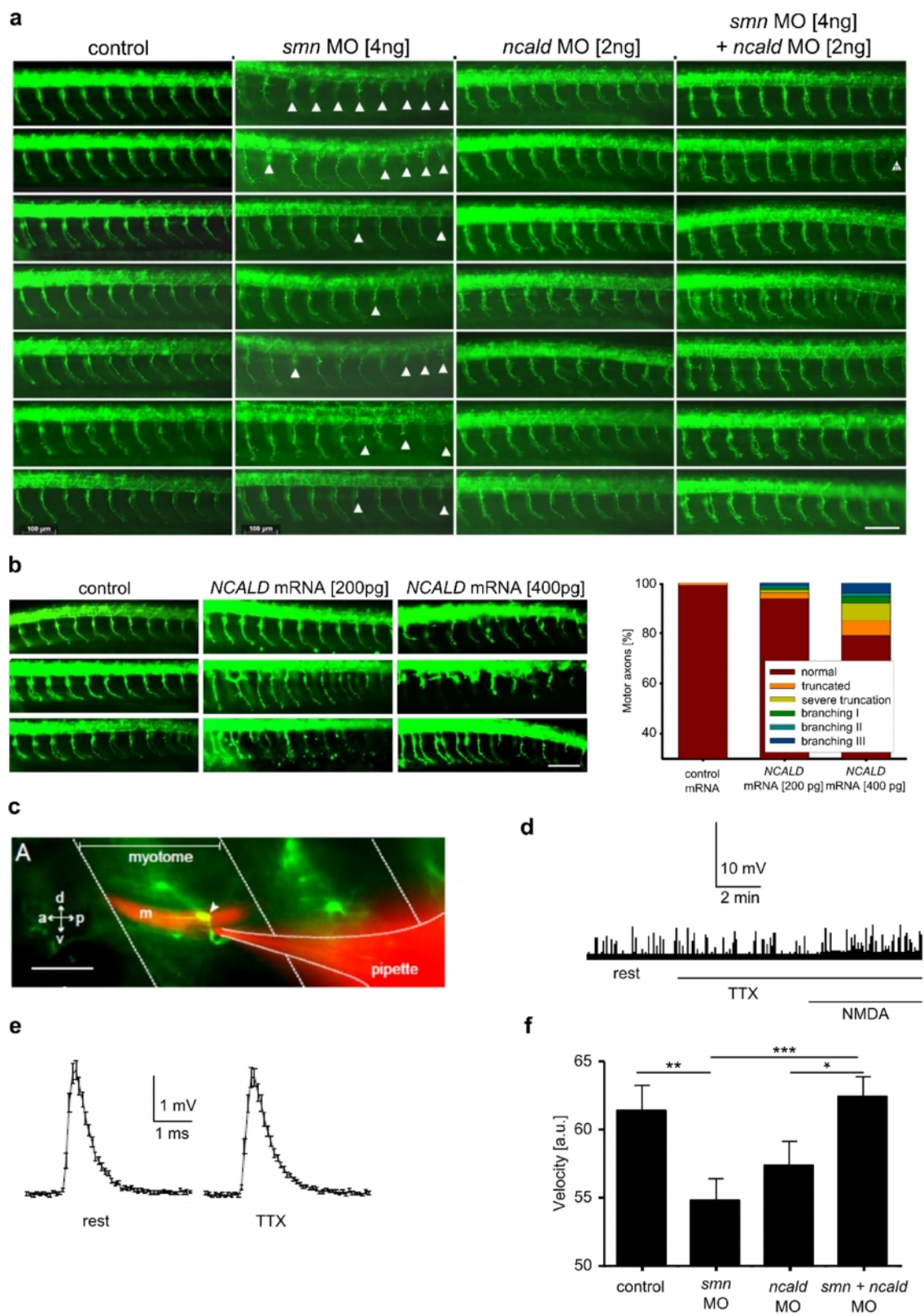
## SUPPLEMENTAL FIGURES AND LEGENDS



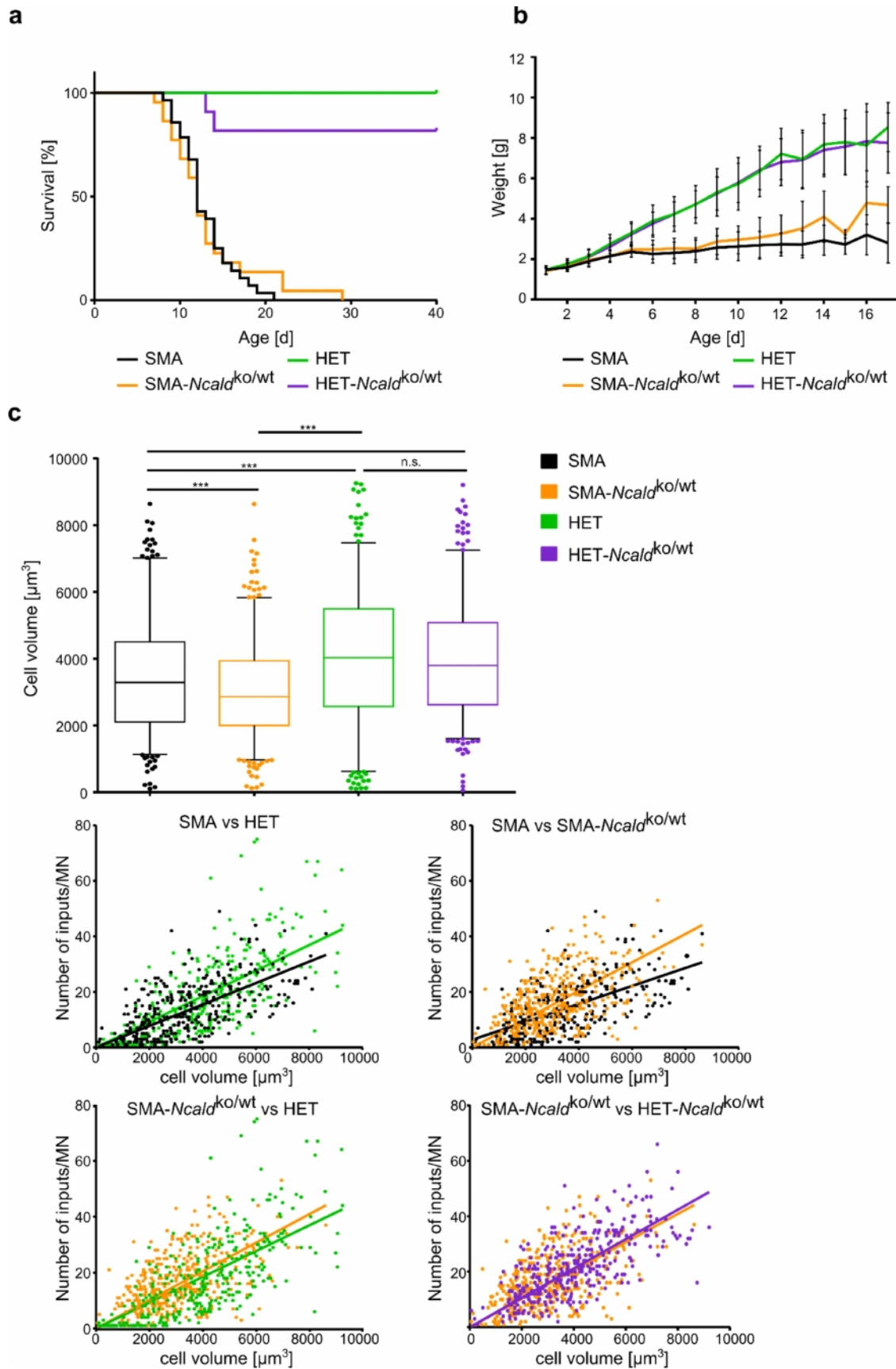
**Supplementary Figure 1** Pedigree showing of Utah family segregation of identified variants. (CT insertion in intron1 of *NCALD* and 17 bp deletion upstream of *NCALD*) on chromosome 8.



**Supplementary Figure 2.** NCALD downregulation restores neurite outgrowth in SMN-deficient neuronal cells, NCALD overexpression induces membrane blebbing. **(a)** Representative images and quantification of neurite outgrowth of NSC34 cells treated with respective siRNAs (50nm) and differentiated with retinoic acid (1 $\mu$ m RA). 4 days after siRNA transfection and 3 days after RA treatment *Smn* siRNA cells showed neurite outgrowth defects. *Smn+Ncald* siRNA cells showed a phenotype rescue and an outgrowth comparable to control siRNA cells. Cells were stained with Phalloidin-Alexa Fluor 568. Scale bar, 200  $\mu$ m. N = 100 cells per treatment; \*\*\*P < 0.001; dashed line = mean (control siRNA: 138.32  $\mu$ m; *Smn* siRNA: 101.35 $\mu$ m; *Ncald* siRNA: 185.9  $\mu$ m; *Smn+Ncald* siRNA: 150.36  $\mu$ m), line=median (control siRNA: 122.5  $\mu$ m; *Smn* siRNA: 87.5  $\mu$ m; *Ncald* siRNA: 165  $\mu$ m; *Smn+Ncald* siRNA: 135  $\mu$ m). **(b)** Representative image of an NSC34 cell overexpressing GFP or NCALD-GFP. Significant membrane blebbing is present only in the NCALD-GFP overexpressing cell. Inset shows detail of membrane blebbing. Scale bar, 10  $\mu$ m. **(c)** Quantification of neurite outgrowth length of NSC34 cells transfected either with GFP or NCALD-GFP and treated with 1 $\mu$ m RA for 3 days and stained with Phalloidin-rhodamine. NCALD-GFP cells showed reduced neurite length. N = 100; \*\*\*P < 0.001.

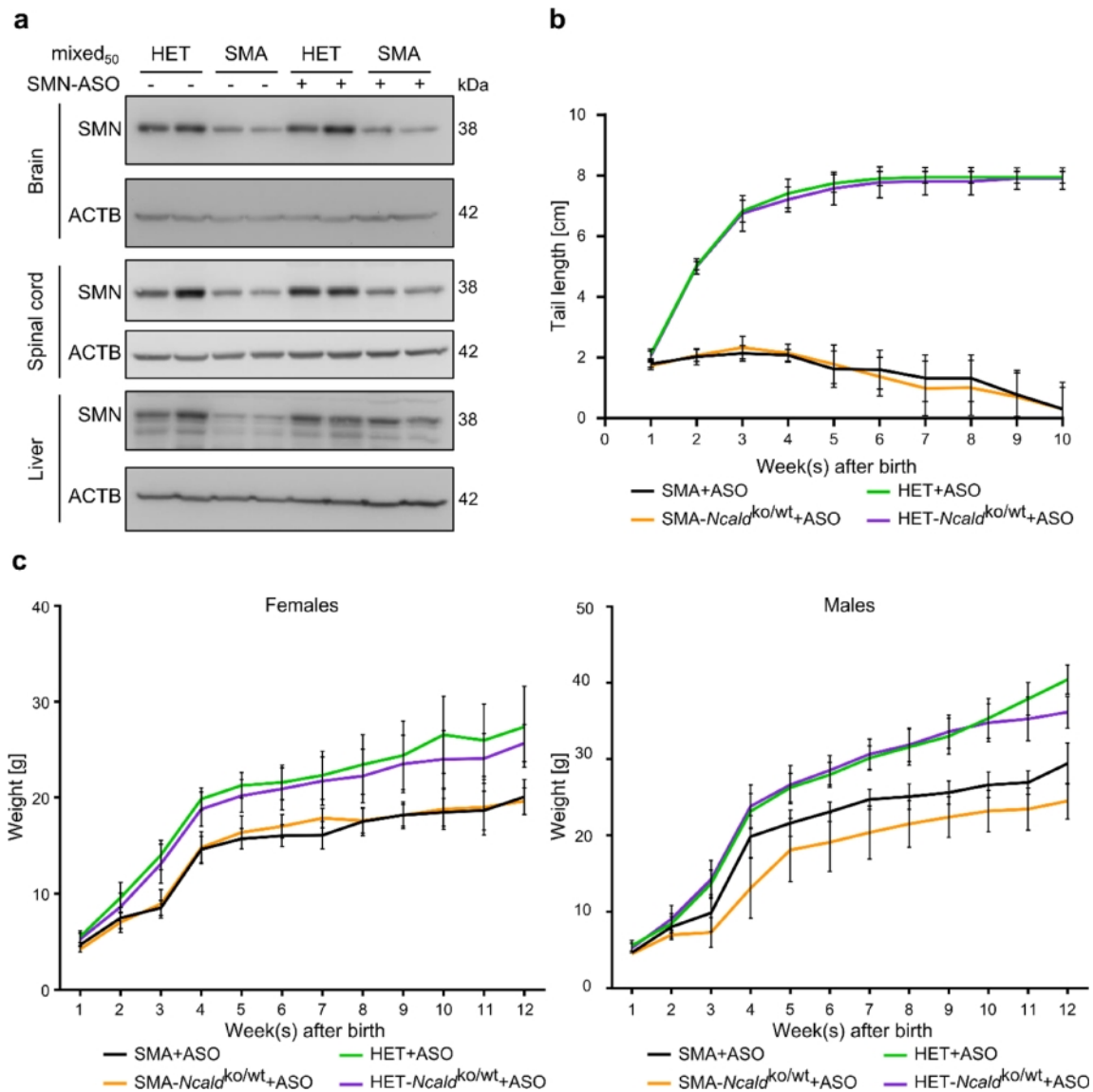


**Supplementary Figure 3.** Overview of motor neuron phenotype after downregulation or overexpression of NCALD and characterization of electrophysiological properties of zebrafish muscles and swimming behavior of zebrafish. **(a)** Representative overview of motor axon outgrowth phenotype of 34 hpf morphants (including pictures from main Figure 3). Significant truncation phenotype of *smn* morphants is corrected by additional *ncald* KD. Scale bar, 100  $\mu$ m. **(b)** Representative overview of motor axon outgrowth phenotype of 34 hpf zebrafish after human *NCALD* mRNA injection. Quantification shows the dose-dependent truncation phenotype of zebrafish overexpressing NCALD. Scale bar, 100  $\mu$ m. First 10 motor axons posterior to the yolk were evaluated in every fish.  $n = 200$  motor axons per mRNA injection. **(c)** Fluorescence image of the recording situation. A wild-type ventral fast muscle cell was filled with rhodamine dextran (red) during a whole-cell patch-clamp recording. The muscle cell (m) is innervated by GFP-labeled motor neurons (green) indicated by the arrowhead. The muscle cell spans one myotome. Scale bar, 20  $\mu$ m. **(d)** Whole-cell current clamp recordings of zebrafish muscles. Diagram shows original whole-cell current clamp recordings of mEPPs: at rest, during 1  $\mu$ M TTX, -and during simultaneous TTX- and 100  $\mu$ M NMDA-application. NMDA application failed to increase muscle action potentials in the presence of TTX. mEPP amplitude and frequency are not TTX-sensitive. **(e)** Means of 30 EPPs in the absence or presence of 1  $\mu$ M TTX. **(f)** Bar graph of high-speed camera swimming velocity measurement of 48 hpf zebrafish embryos ( $N = 30$  per treatment). After LoLitracker software evaluation, mean swimming velocity is given in arbitrary units.

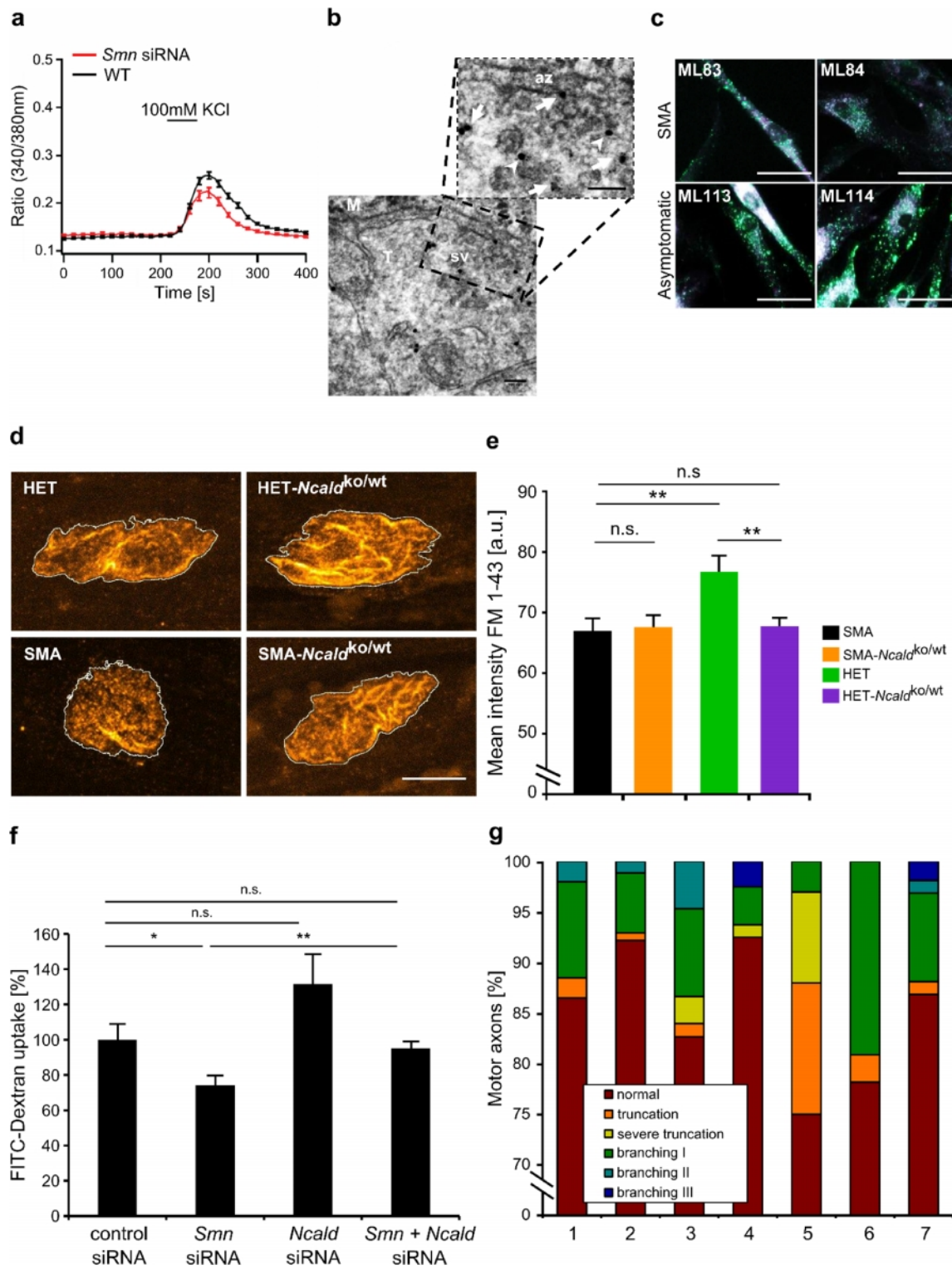




**Supplementary Figure 4.** Characterization of NCALD KD in SMA mice: survival, weight progression and proprioceptive inputs on motor neurons: NCALD KD ameliorates the input number but not cell size. **(a)** Mean survival of SMA mice on pure C57BL/6N: SMA =  $12.9 \pm 3.2$  days, N = 28, SMA-*Ncald*<sup>ko/wt</sup> =  $13.1 \pm 5.3$  days, N = 22. **(b)** The weight of SMA and SMA-*Ncald*<sup>ko/wt</sup> mice is reduced significantly from P5 onwards when compared to HET and HET-*Ncald*<sup>ko/wt</sup>. Error bars indicate SD. N >20 for each genotype. **(c)** The MN cell volume [ $\mu\text{m}^3$ ] of SMA and SMA-*Ncald*<sup>ko/wt</sup> is significantly smaller in comparison to HET. **(d)** Analysis of proprioceptive inputs on spinal MN relative to cell volume: individual values of input number were plotted against cell volume and linear regression was drawn. The number of proprioceptive inputs in SMA-*Ncald*<sup>ko/wt</sup> MN is increased independently of cell volume and input number/cell volume ratio was similar in SMA-*Ncald*<sup>ko/wt</sup> and HET-*Ncald*<sup>ko/wt</sup> MN. N = 3/genotype, n = 100-120 MN/animal. \*\*\*P < 0.001. Box plots defined in Figure 5.



**Supplementary Figure 5** SMN-ASO functionality testing, tail length and weight progression in the SMA+ASO mouse model. **(a)** Western blot of spinal cord, brain and liver lysates of P4-old control-ASO or SMN-ASO injected mixed<sub>50</sub> HET or SMA mice. SMN levels were increased in the liver, but not in the brain or spinal cord after SMN-ASO injection. Beta-Actin (ACTB) was used as loading control. **(b)** Tail length of SMN-ASO injected mixed<sub>50</sub> mice was measured weekly; tail necrosis in SMA+ASO (N = 7) and SMA-*Ncal*<sup>ko/wt</sup>+ASO (N = 9) mice started between the 6<sup>th</sup> and 8<sup>th</sup> week after birth. Control mice: HET+ASO (N = 9); HET-*Ncal*<sup>ko/wt</sup>+ASO (N = 10). Error bars indicate SD. **(c)** Weight of female (F) and male (M) of SMN-ASO injected mixed<sub>50</sub> mice was measured weekly. SMA+ASO (F = 7, M = 5), SMA-*Ncal*<sup>ko/wt</sup>+ASO (F = 4, M = 9), HET+ASO (F = 7, M = 9), HET-*Ncal*<sup>ko/wt</sup>+ASO (F = 8, M = 9). Error bars indicate SD.



**Supplementary Figure 6** Voltage induced  $\text{Ca}^{2+}$  dynamics of cells treated with *Smn* siRNA or *Smn+Ncald* siRNA; impact of  $\text{Ca}^{2+}$  on endocytosis. **(a)** Ratiometric  $\text{Ca}^{2+}$  imaging with fura-2 in differentiated PC12 cells showed that the increase in cytosolic  $\text{Ca}^{2+}$ , which is triggered by KCl-induced, is reduced in SMN depleted cells ( $N = 3$ ,  $n = 41$ ) compared to control cells ( $N = 3$ ,  $n = 38$ );  $P < 0.001$ . **(b)** Immunogold staining of NMJs of 48 hpf control zebrafish embryos. *Ncald* is visualized by secondary antibody labelled with 20 nm gold particle (big black dots) and clathrin with 6 nm gold particle (small black dots). *Ncald* (white arrows) is localized to synaptic vesicles and the active zone (az) of the presynapse and clathrin is localized to some synaptic vesicles (black arrows); white arrowheads mark the colocalization of *Ncald* and clathrin at synaptic vesicles. M = muscle fiber, T = nerve terminal, scale bar, 100 nm. **(c)** Representative images of fibroblasts derived from Utah family members, SMA patients and controls after endocytosis assay. After starvation cells were incubated for 20 min with FITC-dextran (green), fixed and counterstained with phalloidin-AlexaFluor 568 (red). The FITC signal is higher in asymptomatic cells. Scale bar, 50  $\mu\text{m}$ . For quantification see also **Figure 6c**. **(d)** Representative images of endocytic FM1-43 uptake at the presynaptic terminals on P10 in TVA muscles under low frequency stimulation (5 Hz, 1s). Postsynaptic receptors staining (BTX-Alexa647) was used to define the area to analyze the FM1-43 uptake (orange) at the presynaptic terminals. Scale bar, 10  $\mu\text{m}$ . For quantification see also **Figure 6d**. **(e)** Quantification of the FM1-43 mean intensity at the presynaptic terminals on P10 in TVA muscles under high frequency stimulation (20 Hz, 1s). For each genotype 3 animals and ~100 NMJs were analysed. Error bars represent SEM. n.s. non-significant; \*\*\* $P < 0.001$ . **(f)** FACS-based quantification of FITC signal in NSC34 cells treated with respective siRNA. *Ncald* KD resulted in elevated FITC-dextran endocytosis. *Smn* KD decreased endocytosis (\* $P < 0.05$ ), which was fully restored by additional *Ncald* KD (*Smn* siRNA vs. *Smn+Ncald* siRNA: \*\* $P < 0.01$  control siRNA vs. *Smn+Ncald* siRNA: n.s.).  $N=6$  biological replicates per siRNA treatment, individual sample  $n=50,000$  cells. **(g)** Quantitative analysis of motor axon phenotype of 34 hpf zebrafish, subjected to the respective treatment: 1 = *ncald* MO (2 ng), 2 = *smn+ncald* MO (2 ng), 3 = *ncald* MO + Pitstop2 (12.5  $\mu\text{M}$ ), 4 = control + Pitstop2 (25  $\mu\text{M}$ ), 5 = *smn* MO + Pitstop2 (25  $\mu\text{M}$ ), 6 = *smn* MO + *ncald* MO + Pitstop2 (25  $\mu\text{M}$ ), 7 = *ncald* MO + Dynasore (25  $\mu\text{M}$ ). Note the rescue effect of *ncald* MO injection on the truncation phenotype of *smn* MO and 25  $\mu\text{M}$  Pitstop2 treated zebrafish (bars 5 and 6).

**SUPPLEMENTAL REFERENCES**

57. Arkblad, E., Tulinius, M., Kroksmark, A.K., Henricsson, M. & Darin, N. A population-based study of genotypic and phenotypic variability in children with spinal muscular atrophy. *Acta Paediatr* 98, 865-872 (2009).
58. Armstrong, C.M. & Bezanilla, F. Charge movement associated with the opening and closing of the activation gates of the Na channels. *The Journal of general physiology* 63, 533-552 (1974).
59. Benjamini, Y. & Hochberg, Y. Controlling the False Discovery Rate: A Practical and Powerful Approach to Multiple Testing [Royal Statistical Society, Wiley] 57, 289-300 (1995).
60. Calixto, A., Chelur, D., Topalidou, I., Chen, X. & Chalfie, M. Enhanced neuronal RNAi in *C. elegans* using SID-1. *Nat Methods* 7, 554-559 (2010).
61. Dunning, M.J., Barbosa-Morais, N.L., Lynch, A.G., Tavare, S. & Ritchie, M.E. Statistical issues in the analysis of Illumina data. *BMC Bioinformatics* 9, 85 (2008).
62. El-Khodori, B.F., et al. Identification of a battery of tests for drug candidate evaluation in the SMNDelta7 neonate model of spinal muscular atrophy. *Exp Neurol* 212, 29-43 (2008).
63. Greene, L.A. & Tischler, A.S. Establishment of a noradrenergic clonal line of rat adrenal pheochromocytoma cells which respond to nerve growth factor. *Proc Natl Acad Sci U S A* 73, 2424-2428 (1976).
64. Sun, Y., et al. Molecular and functional analysis of intragenic SMN1 mutations in patients with spinal muscular atrophy. *Hum Mutat* 25, 64-71 (2005).
65. Wettenhall, J.M. & Smyth, G.K. limmaGUI: a graphical user interface for linear modeling of microarray data. *Bioinformatics* 20, 3705-3706 (2004).
66. Zerres, K., Wirth, B. & Rudnik-Schoneborn, S. Spinal muscular atrophy--clinical and genetic correlations. *Neuromuscul Disord* 7, 202-207 (1997).

## 9 Publications, talks, poster presentations and scholarships

### Publications:

**\*Kaczmarek A**, \*Schneider S, Wirth B, Riessland M

Investigational therapies for the treatment of spinal muscular atrophy. **2015, Expert Opinion on Investigational Drugs 24, 867-881.** \*authors contributed equally to this work

Hosseiniabarkooie SM, Peters M, Torres-Benito L, Rastetter RH, Hupperich K, Hoffmann A, Mendoza-Ferreira N, **Kaczmarek A**, Janzen E, Milbradt J, Lamkemeyer T, Rigo F, Bennett CF, Guschlbauer C, Büschges A, Hammerschmidt M, Riessland M, Jeong MK, Clemen CS, Wirth B

The power of human protective modifiers: PLS3 and CORO1C unravel impaired endocytosis in spinal muscular atrophy and rescue SMA phenotype. **2016, American Journal of Human Genetics 99, 647-665.**

\*Riessland M, **\*Kaczmarek A**, \*Schneider S, Swoboda KJ, Löhr H, Bradler C, Grysko V, Dimitriadi M, Hosseiniabarkooie SM, Torres-Benito L, Peters M, Upadhyay A, Biglari N, Kröber S, Hölker I, Garbes L, Gilissen C, Hoischen A, Nürnberg G, Nürnberg P, Walter M, Rigo F, Bennett FC, Kye MJ, Hart AH, Hammerschmidt M, Kloppenburg P, Wirth B  
Neurocalcin delta suppression rescues spinal muscular atrophy species. **Nature Medicine, under review.** \*authors contributed equally to this work

### Talks:

24.09.2014 Symposium Shaping cells and Organisms, Universität zu Köln, Cologne, Germany

**Kaczmarek A**, Schneider S, Grysko V, Swoboda KJ, Riessland M, Wirth B

Investigation of ASO-mediated protective effect of modifier genes in mouse models of spinal muscular atrophy (SMA)

23.06.2016 10<sup>th</sup> International Motoneuron Meeting, Koc University, Istanbul, Turkey

**Kaczmarek A**, Schneider S, Torres-Benito L, Grysko V, Upadhyay A, Riessland M, Swoboda KJ, Wirth B

SMA modifier MOD2 improves motor neuron length and neuromuscular junction size

06.10.2016 6<sup>th</sup> Annual Human Genetics Meeting, Universität zu Köln, Cologne, Germany

**Kaczmarek A**, Schneider S, Torres-Benito L, Grysko V, Riessland M, Swoboda K, Wirth B

Reduction of potential SMA modifier NCALD improves axonal length *in vitro* and proprioceptive inputs on motoneuron soma and neuromuscular junction size *in vivo*

#### Poster presentations:

13.05.2011 3<sup>rd</sup> Annual Human Genetics Meeting, Universität zu Köln, Cologne, Germany

**Kaczmarek A**, Riessland M, Förster A, Swoboda KJ, Wirth B

Genetic studies of NCALD as a potential modifier in SMA

12.07.2012 1<sup>st</sup> GSfBS Alumni Day, Universität zu Köln, Cologne, Germany

**Kaczmarek A**, Riessland M, Swoboda KJ, Wirth B

Genetic and functional studies of MOD2 as potential modifier for SMA

29.11.2012 4<sup>th</sup> Annual Human Genetics Meeting, Universität zu Köln, Cologne, Germany

**Kaczmarek A**, Riessland M, Förster A, Swoboda K, Wirth B

Genetic and functional studies of neurocalcin delta (NCALD) as potential modifier for SMA

14.06.2013 17<sup>th</sup> Annual SMA Conference, Anaheim, California, USA

**Kaczmarek A**, Riessland M, Garbes L, Hölker I, Gilissen C, Hoischen A, Swoboda KJ, Wirth B

Generation of a Doxycycline inducible shRNA-mediated Mod2 knockdown mouse to analyze the protection effect on SMA

24.05.2014 5<sup>th</sup> Annual Human Genetics Meeting, Universität zu Köln, Cologne, Germany

**Kaczmarek A**, Riessland M, Schneider S, Wirth B

Investigation of the protective effect of NCALD downregulation on the SMA phenotype in mice

#### Scholarships:

Sep 2010 - Aug 2013

Graduate scholarship from the International Graduate School "Disease, Health and Development"

12 - 14.06.2013

Scholarship from the Initiative SMA to participate in the 17<sup>th</sup> Annual SMA Conference, Anaheim, California, USA

29.06 – 04.07.2014

Elke-Fresenius-Scholarship to participate in the 64<sup>th</sup> Lindau Nobel Laureate Meeting

19.-23.06.2016

Scholarship from FAZIT Stiftung to participate in the 10<sup>th</sup> International Motoneuron Meeting, Istanbul, Turkey





## Acknowledgements

My first words of gratitude go to Prof. Brunhilde Wirth for giving me the opportunity to work in her group on this interesting and challenging project and for generously supporting me to learn and grow as a scientist; I am especially grateful for her help during the final stage of this thesis.

I thank Prof. Aleksandra Trifunovic for kindly agreeing to review my thesis and Prof. Peter Kloppenburg for taking the chair of the exam committee.

I would like to first thank Dr. Markus Rießland, the initiator of the NCALD project, for being the best teacher, colleague and a real friend. I also thank Dr. Min Jeong Kye for motivating me in the end phase of my thesis and keeping up my faith in science. I am very grateful to my “older” colleagues who welcomed me in the Wirth lab: Bastian Ackermann, Anja Förster, Lutz Garbes, Mohsen Hosseini, Irmgard Hölker, Kristina Hupperich, Miriam Jakubik, Sandra Kröber, Lilian Martinez Carrera and Markus Storbeck – you have been great role models and someone to look up to. Many thanks to my “younger” colleagues: Eva Janzen, Miriam Peters, Natalia Mendoza-Ferreira, Janine Milbradt and Andrea Delle Vedove – I have truly enjoyed working next to all of you. My special thanks go to the “NCALD group”: Vanessa Grysko, who I was honoured to call “my” technician, and Svenja Schneider (this would not be possible without you two), Laura Torres-Benito and Aaradhita Upadhyay – you all are my favourite people and have a very special place in my heart.

I would also like to thank all the colleagues from other groups at the Institute of Human Genetics, Cologne: AG Kye, AG Wollnik, AG Beck, AG Schreml and AG Netzer, as well as our wonderful Dr. Uwe Becker.

I would like to acknowledge our numerous collaborators on the NCALD project at the University of Cologne and beyond: Prof. Kathryn Swoboda, Prof. Peter Kloppenburg and his group, Prof. Matthias Hammerschmidt and his group, and especially our collaborators from Ionis Pharmaceuticals, who have always generously provided me with ASOs. I thank Dr. Ralf Kühn for providing me the ES cells and plasmids for mouse generation. My gratitude goes to Peter Zentis and Dr. Astrid Schauss for their assistance with image analysis. My work has also been greatly supported by the animal caretakers at the Centre for Mouse Genetics at the Institute of Genetics, University of Cologne.

The following words go to my family who have supported me throughout all these not so easy years with their love and faith: Mimo e byli cie daleko, sercem byli cie zawsze ze mn i Wasze wsparcie było dla mnie bezcenne. Dzi kuj Wam za to i bardzo Was kocham. Finally, my deepest gratitude goes to my dear Bartosz “Pablo” Kaczmarek, who has been there for me every step of the way. You are my beloved husband and my best friend and I am looking forward to the rest of our lives together.

## Erklärung

Ich versichere, dass ich die von mir vorgelegte Dissertation selbstständig angefertigt, die benutzten Quellen und Hilfsmittel vollständig angegeben und die Stellen der Arbeit – einschließlich Tabellen, Karten und Abbildungen – die anderen Werken im Wortlaut oder im Sinn nach entnommen sind, in jedem Einzelfall als Entlehnung kenntlich gemacht habe; dass diese Dissertation noch an keiner anderen Fakultät oder Universität zur Prüfung vorgelegen hat; dass sie noch nicht veröffentlicht worden ist sowie, dass ich eine solche Veröffentlichung vor Abschluss des Promotionsverfahrens nicht vornehmen werde. Die Bestimmungen dieser Promotionsordnung sind mir bekannt. Die von mir vorgelegte Dissertation ist von Prof. Dr. Brunhilde Wirth und Prof. Dr. Peter Kloppenburg betreut und in der Arbeitsgruppe von Prof. Dr. Brunhilde Wirth durchgeführt worden.

Teilpublikationen liegen nicht vor.

Ich versichere, dass ich alle Angaben wahrheitsgemäß nach bestem Wissen und Gewissen gemacht haben und verpflichte mich, jedmögliche, die obigen Angaben betreffenden Veränderungen, dem Promotionsausschuss unverzüglich mitzuteilen.

.....

Datum

.....

Unterschrift

## Lebenslauf

### • Persönliche Daten

Name	Kaczmarek
Familienname	Koper
Vorname	Anna
Geburtsdatum	17.06.1985
Geburtsort	Sucha Beskidzka, Polen
Nationalität	Polnisch

### • Schulausbildung

1991 – 1999	Henryk-Sienkiewicz-Grundschule Nr. 1, Makow Podhalanski, Polen
1999 – 2003	Bartlomiej-Nowodworski-Lyzeum Nr. 1, Krakow, Polen, mit dem Abschluss des Abiturs (Mai 2003)

### • Akademische Ausbildung

Okt 2003 – Juli 2009	Studium der Angewandten Linguistik an der Adam-Mickiewicz-Universität, Poznan, Polen
Akademischer Abschluss:	Master of Arts
Masterarbeit:	Institut für Angewandte Linguistik, unter Anleitung von Prof. Dr. Alicja Sakaguchi
Titel:	Analyse der Bezeichnungen und Attributen Gottes in deutschen und polnischen religiösen Texten
Okt 2004 – Juli 2009	Studium der Biotechnologie an der Naturwissenschaftlichen Universität, Poznan, Polen
Akademischer Abschluss:	Master of Science
Masterarbeit:	Department of Genetics and Animal Breeding, unter Anleitung von Dr. Ewelina Warzych-Plejer
Titel:	Evaluation of the developmental competence of swine oocytes based on the transcript analysis of genes <i>ATP5A1</i> and <i>EEF1A1</i>

- **Praktikum**

August 2009 – Mai 2010

DAAD-Stipendium am Institut für  
Humangenetik, Universität Leipzig, unter  
Anleitung von Prof. Dr. med. Ursula Froster

Forschungsprojekt:

Evaluierung der HRMA (High Resolution  
Melting Analysis) als Verfahren zur Mutation-  
Screening bei *APC*- und *BRCA 2*-Genen

- **Dissertation**

Sep 2010 – Aug 2013

Stipendium der International Graduate  
School for Disease, Health and Development

Sep 2013 – Okt 2016

Wissenschaftlicher Mitarbeiter an der  
Uniklinik Köln

Dissertation

Institut für Humangenetik, unter der  
Anleitung von Prof.Dr.rer.nat. Brunhilde Wirth

Titel

Analysis of reduced Neurocalcin delta  
(NCALD) as a protective modifier in mouse  
models of Spinal Muscular Atrophy (SMA)